The Synthesis of Rationally Designed Donor-Acceptor Dyads Incorporating the Boron Dipyrromethene Fluorophore

A PhD thesis for the title of Doctor of Philosophy submitted to:
Newcastle University

Sophie Clift

September 2012

Abstract

This thesis is concerned with the design, synthesis, characterisation and subsequent photophysical examination of dyads incorporating the boron dipyrromethane (bodipy) framework.

Photodriven processes such as electron-, energy- and charge-transfer reactions are of the utmost importance in nature, with photosynthesis as a key example. Energy capturing arrays composed of intricate building blocks trap, transfer and store energy within a cell, employing a complex series of cascade-type reactions to channel this energy to the desired acceptor. Within this thesis, the theme of charge-transfer in particular is of principal focus and systems designed to investigate this phenomenon are examined.

Chapter one presents an introduction to the bodipy fluorophore and the ever-expanding field of artificial photosynthesis. In addition to this, the methods involved in analysing the distribution and movement of charge are discussed, as are the thought processes behind the rational design of molecules for specific functions. The second chapter serves as a detailed account of all the synthetic procedures undertaken. The chapter covers all the bodipy derivatives prepared, in addition to the precursors to these compounds and all additional materials synthesised.

In chapters three to six, the rationale behind the design of each purpose built system is discussed, along with any preparative difficulties encountered and modifications to traditional synthetic protocol. Finally, the electrochemical properties of the compounds are analysed by cyclic voltammetry and their photophysics investigated by absorption and fluorescence spectroscopy. The data obtained is complimented by both appropriate NMR spectra and a discussion of crystal structural information obtained.

In the case of the novel push-pull chromophore, **JULBD**, which is the principal focus of chapters three and four, the charge transfer capabilities of the dyad are analysed by correlating ^{13}C chemical shift values with solvent polarity. This polarity dependence is further explored and analysed by solvent dependent absorption spectroscopy. In

order to study the emissive properties, a temperature dependent fluorescence experiment was undertaken.

Chapter five discusses the use of current catalytic methods to prepare a series of novel donor acceptor dyads and their precursor building blocks, introducing novel methodology for the synthesis of boronic esters including iridium and palladium catalysis.

Finally, chapter six addresses the design rationale, synthesis and characterisation of a binaphthalene-spaced dyad incorporating the N,N-dimethylaniline moiety. This chapter also serves to introduce novel methodology which can be employed to execute bodipy sythesis employing the commonly used organic reagent formamide.

Acknowledgments

I would like to thank Professor Andy Benniston and Professor Tony Harriman for welcoming me into the Molecular Photonics Laboratory and for their dedicated advice and guidance throughout my PhD. Their technical assistance and supervision of my projects has been invaluable.

I would also like to acknowledge the support of all past and present members of the Molecular Photonics Laboratory who have assisted in the smooth running of the lab, helped with technical aspects of my work and enhanced the lab atmosphere with their valued presence. This includes Dr Ruth Ryan, Dr Graeme Copley, Tommy Winstanley, Xiao Yan He, Dan Bai, Dr Songjie Yang and David Howgego, in addition to previous MPL members for their warm welcome to the group.

I would like to acknowledge the advice and support of Dr Simon Doherty and the NMR expertise of both Professor William MacFarlane and Dr Corrine Wills. I would also like to thank Dr Ross Harrington for recording the X-ray crystal data of my compounds.

Finally I must thank my amazing family for supporting and encouraging me throughout my Masters degree, Year abroad and PhD studies. I feel very lucky to have experienced such love, care and generosity.

Contents

Chapter 1

Introduction

1.1 An overview

Within this thesis, diverse research topics are addressed, which incorporate a number of significant themes, the most important of which resurface in multiple chapters. In Chapters 3 and 4, the synthesis, photophysical characteristics and charge transfer capabilities of a novel dyad incorporating both an electron donating julolidine unit and the difluoroboradiaza-s-indacene (bodipy) fluorophore are discussed. The charge transfer properties associated with the system are investigated via a series of polarity dependent NMR experiments, a study which allowed us to break the mould in terms of investigating a photophysical phenomenon employing atypical spectroscopic tools.

In Chapter 5, the use of current catalytic methods to prepare a donor-acceptor dyad series is addressed. It is envisaged that the methodology researched and developed will be incorporated by current and future MPL members into their synthetic protocols. Chapter 6 is divided into two discrete topics, the first being the preparation of a *N,N*-dimethylaniline binaphthalene-spaced dyad. This involved a convergent synthesis employing knowledge and techniques developed and discussed within previous chapters. The second topic is focussed upon the alternative methods available of synthesising the bodipy fluorophore. It must be mentioned here that this framework is the common photoactive unit within all the dyads explored in this work. Background information to present the bodipy chromophore, discussing its undeniably favourable chemical, photophysical and synthetic properties and vast range of uses will be given within this introductory chapter. An addition to this, an overview of energy driven processes observed in organic systems will also be summarized here. Included are key electron-, energy- and charge-transfer mechanisms. An introduction to artificial photosynthesis is also given, as this is a pivotal topic of discussion within the field of molecular photonics.

In recent years, with an advanced knowledge base and range of synthetic and analytical tools at their disposal, scientists' attempts to replicate photosynthetic processes have yielded increasingly fruitful results. The preparation of vast arrays, capable of channelling energy to accepting species via a connected series of complex cascade reactions, has revolutionized the field. At the forefront of such developments, are chromophores capable of accepting or donating energy. They are typically either

metal based or highly conjugated organic residues with extended series of π orbitals, or sometimes, encompass both of these features. Equally, on a synthetic and a photophysical level, it is now possible to achieve what could only be imagined one to two decades ago. The constant evolution of the field due to developments in the fundamental knowledge base, technological and material resources and facilities, provides an extremely positive and prosperous outlook for the future.

1.2 The bodipy fluorophore

For some time, the boron dipyrromethane fluorophore has resided at the forefront of the field of molecular photonics. This can be attributed to the excellent photophysical and synthetic properties exhibited, inherent to most derivatives. These include high fluorescence quantum yields (Φ_f ca. 0.2-1.0), a small Stokes Shift and high molar absorption co-efficients (>70,000 M^{-1} cm^{-1}). Additionally, rapid and efficient synthetic procedures have been established which generate workable quantities of material in high yield. This ensures that the fluorophore remains a favourite with synthetic chemists. Finally, the ability of bodipy to act as either an electron donor or acceptor, depending on the nature of the system, is an additional significant attribute. This is somewhat due to its ability to undertake both the donation and the acceptance of electrons with an undeniable efficiency, in addition to the various other remarkable properties it possesses. Since its initial synthesis by Triebs *et al.* in 1968, the popularity of bodipy in the literature had soared. Due to the robust and adaptable nature of the indacene core, meso position and boron atom which comprise the system, vast bodipy libraries can be generated, capable of functioning across an extensive wavelength range. Applications of the fluorophore vary dramatically from chemosensors[1,2,3,4,5,6,7,8,9,10,11,12] biological labelling[13,14,15,16,17] and imaging[18,19,20,21] viscosity probes[22,23,24] and molecular rotors[25,26,27,28,29,30,31] to vast light harvesting arrays[32,33,34,35,36] molecular photonic wires[37], electroluminescent materials[38,39,40,41] and T-Gate systems[42].

Recently, interestingly substituted pyrrole and aldehyde units have been generated, to yield attractive bodipy molecules with remarkable photophysical properties. Examples include the bodipy appended cone-calix[4]arene complex[43] synthesised from the corresponding diformylcalixarene. The molecular system was found to

display remarkable fluorescence quenching upon Ca^{2+} binding (at the ester carbonyl oxygen atoms and the proximal hydroxyl groups[44]) due to the reverse Photoinduced Electron Transfer (PET) mechanism[45] taking place. PET is a well-known mechanism through which the fluorescence is quenched by electron transfer from the donor molecule to the acceptor fluorophore[46]. The properties of this fluorogenic ionophore make it suitable for use as a selective[47] chemosensing device and numerous publications exist[48,49,50] describing rational design strategies for fluorescence PET probes.

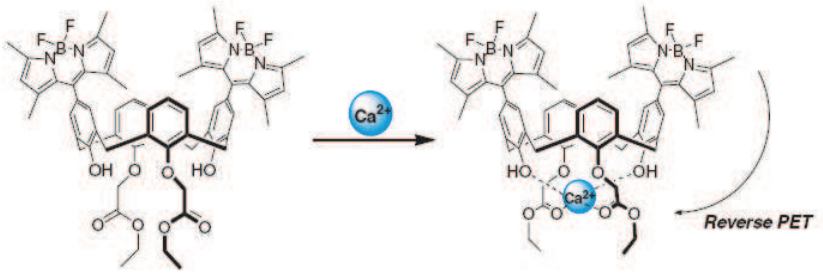

Figure 1 - Upon interaction of Ca^{2+} with the lone pair of the carbonyl oxygen atoms, the bodipy unit acts as a PET donor to the electron deficient carbonyl group facilitating electron transfer.

The system over the page (*Figure 2*)[51] is a borondi(iso)indomethene based conjugated polymer with a narrow emission band. These light emitting polymers lend themselves towards applications in telecommunications[52], photovoltaic cells[53], ionic lasers[54] and light emitting devices[55]. The diisoindomethene ligand series was prepared by stirring the corresponding aryl functionalised α,β-diketones in a solution of methanol and acetic acid, followed by addition of concentrated ammonium hydroxide and a subsequent 48 hour stir. The ligands were then reacted with base and boron trifluoride diethyletherate, typical of standard bodipy forming conditions. Sonogashira coupling was then affected at the indole iodine to achieve polymerization and generate the series of systems pictured in *Figure 2*.

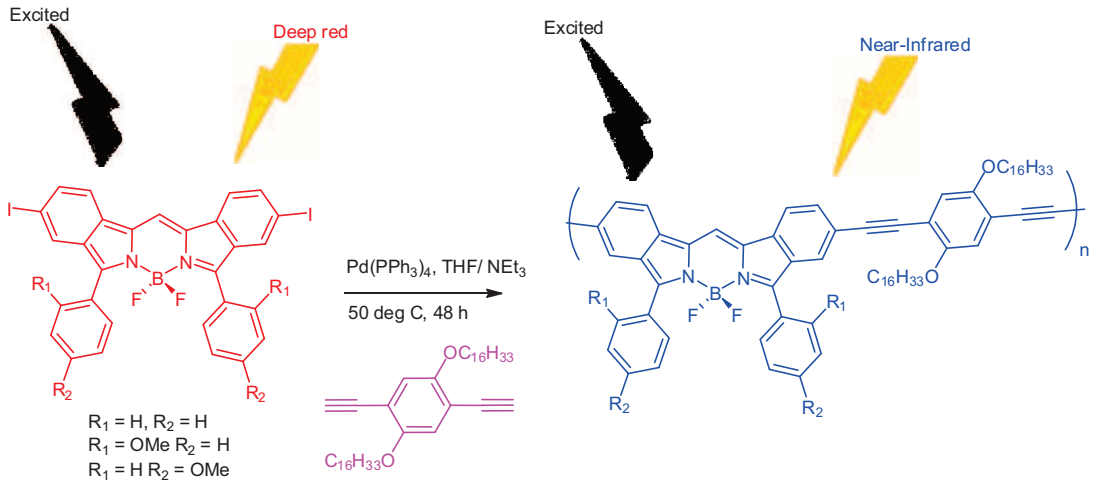

Figure 2 - The incorporation of various aromatic fused bodipy monomers into the poly(p-phenylene-ethynylene) backbone to generate a series of high NIR emissive π-conjugated polymers.

These elegant systems reinforce the versatility of the bodipy fluorophore towards substitution and modification of the dipyrrin core and extended units. Furthermore, the wide range of unusual aldehydes that can be used to synthesise novel and exciting systems, also reinforces the constant and ever increasing popularity of this probe.

The next system to be discussed serves to link the theme of the bodipy fluorophore with that of artificial photosynthesis. The energy transfer dynamics of both the T-shaped optoelectronic gate system[42], detailed below in *Figure 3* and its linear counterpart, were probed in their neutral and oxidised forms. Energy transfer has been shown to occur on a rapid timescale from a zinc to a magnesium-based porphyrin connected via a diphenylethyne linker[56]. Therefore, most of the energy in the neutral T-gate initially flows to the switching site rather than to the output unit. However, further studies on the trimers indicate that super-exchange mediated transfer from the magnesium porphyrin will occur rapidly to the distant free base (fb) porphyrin in the T-gate. This means that the same efficiency is maintained of the ON state as in the linear gate.

Similarly, via an efficient super-exchange mechanism, the Mg-porphyrin π-cation radical in the oxidised T-gate, quenches the energy arriving at the distant free base porphyrin. This means that the same efficiency of the OFF state can be observed as in the linear gate. It also reveals that non-pair-wise interactions involving distant neutral porphyrins or a neutral porphyrin and a distant π-cation radical are imperative to the function of the T-gate system.

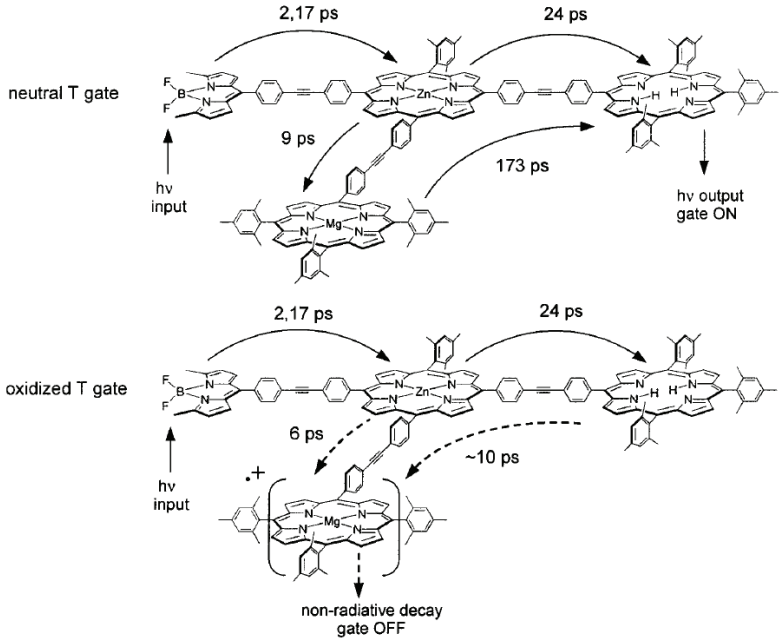

Figure 3 – The neutral and oxidised T-shaped optoelectronic gate systems designed by Lindsey et al.[56]

1.3 Artificial Photosynthesis – system design and preparation.

Global energy need will approximately double by mid-century and triple by 2100[57]. Most of that demand is driven by 3 billion low energy users in the non-legacy world and by 3 billion people yet to inhabit the planet over the next half century[58]. In order to provide a solution for a sustainable and carbon neutral energy future, it is imperative that research effort is concentrated into meeting and fulfilling the energy requirements of these 6 billion energy users. One of the principal themes addressed within this work, is that of energy capture via replication of photosynthetic processes, i.e., the conversion of sunlight into biologically useful energy such as electrochemical potential. It can then be stored in fuels such as carbohydrates, lipids or even hydrogen gas[59].

Photosynthesis is carried out by pigments and electron donor and acceptor moieties such as chlorophylls, quinones and carotenoid polyenes situated within proteins[60]. They interact via three basic photochemical processes: singlet-singlet energy transfer[61,62,63] triplet-triplet energy transfer and photo-initiated electron transfer. In green plants and cyanobacteria, photosystem I (PSI)[64] generates NADPH which reduces carbon dioxide during the Calvin cycle, whilst photosystem II (PSII)[65] catalyses the conversion of light energy into water oxidizing agents[66]. Photosynthetic bacteria possess simpler photoconversion pathways and the electron transfer processes involved have inspired numerous biomimetic studies. *Figure 4*[67] below details the redox co-factors and the primary charge separation in the photosynthetic reaction centre of purple bacteria.

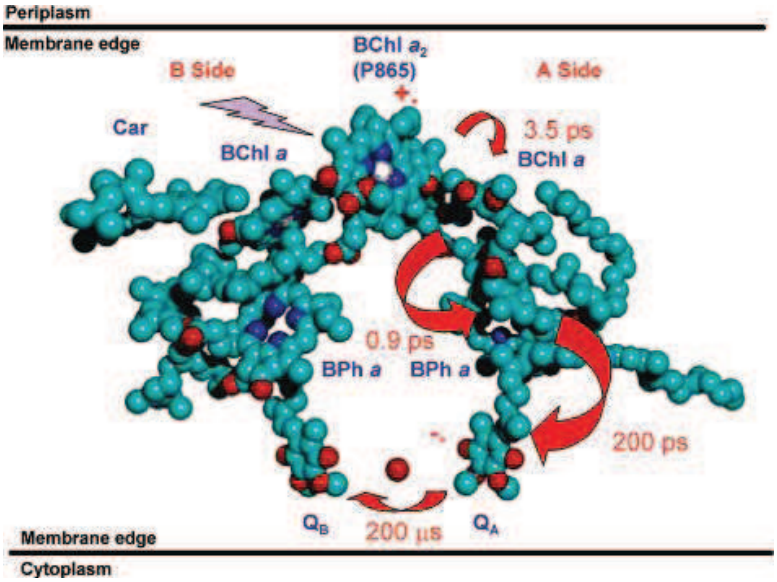

Figure 4 – The redox co-factors of the photosynthetic RC found in purple bacteria.

Thousands of artificial photosynthetic constructs have been developed over the past thirty years and a number of reviews are available on the topic[68,69,70,71,72,73,74,75,76]. In order to design and synthesise systems capable of mimicking natural photosynthetic process, there are a number of factors to consider and components which are necessary for efficient functioning of the device. As its basic operation is PET, a model reaction centre must at minimum be composed of an electron donor moiety and an organisational principle that controls their electronic interactions.[77] The choice of

pigments and electron donors and acceptors must be carefully considered and excited state energy levels and photophysical parameters are especially critical.

Artificial photosynthesis can be considered to encompass several topics to include light driven CO_2 reduction (replicating natural carbon fixation) and water splitting. The four-electron oxidation of water is a kinetically challenging process which occurs on a millisecond timescale within the oxygen evolving complex (OEC) of Photosystem II as well as in a number of synthetic catalysts[78,79,80,81,82,83,84].

Water oxidation is of pivotal importance and in recent years numerous systems[85,86,87,88] have been developed, capable of carrying out this process. A typical artificial photosynthetic design for water splitting consists of the following four integral components:

- Antenna – collection of chromophores which absorb light throughout the portion of the solar spectrum used by photosynthesis and transfer excitation energy towards the reaction centre. They are also involved in photoprotection and photoregulation.
- Reaction Centre (RC) – here, excitation energy drives photoinduced electron transfer to an electron acceptor, generating a charge separated state. They must be designed in such a manner that the charge separated states live long enough that their oxidising and reducing power can be transferred to fuel generating catalysts.
- Fuel production catalyst – inexpensive and efficient catalysts must be devised for generating hydrocarbons, hydrogen or other fuels. The reducing equivalents from the reaction centre are ultimately used to power the organism and to store energy as carbohydrate, lipid, hydrogen or some other reduced material.
- Water oxidation catalyst – oxidising equivalents from the reaction centre must be used to generate oxygen gas and hydrogen ions from water, whilst simultaneously rejuvenating the oxidising side of the RC.

Unfortunately, there is still a long way to go before the shortfalls associated with artificial photosynthetic devices can be rectified. Upon closer inspection of the components involved in water splitting, complications can instantly be highlighted. For example, iridium dioxide is a stable and efficient catalyst for the oxidation of

water[89], however iridium is the least abundant element on earth and significant overpotential is required. Secondly, the ruthenium complexes commonly incorporated into these systems do not absorb light efficiently at wavelengths longer than 500-550 nm, meaning that much of the solar spectrum is wasted. They are also prone to decomposition under irradiation. Thirdly, the reaction centre faces kinetic and thermodynamic issues. The former can be attributed to rapid charge recombination via electron migration back to the oxidised ruthenium complex from TiO_2. This is very quick when compared to the rate of electron transfer from IrO_2 to the oxidised complex. The thermodynamic issue arises from ineffective positioning of the conduction band of TiO_2, resulting in inefficient reduction of hydrogen ions. Finally, the most commonly used platinum based proton reduction catalysts are expensive and, like iridium, platinum is a rare element. Due to the immense scale of human energy usage, more abundant catalysts must be identified.

Some systems in recent years have effectively addressed some of these issues. However, to date, regaling in the success that all of the problems aforementioned have been rectified appears to be rather premature. Increasingly robust water oxidation catalysts containing more abundant and inexpensive manganese[90,91,92] or cobalt[93,94,95,96] oxides are increasing in popularity, being far more suitable for large scale use. Dinuclear ruthenium[97,98,99] catalysts in addition to those which are iron[100,101] based have also enjoyed a surge in popularity. Proton reduction catalysts employing hydrogenases directly for catalytic functions[102] or analogues of the hydrogenase active site are known, but exhibit variable activity[103]. Photoprotective effects to provide resistance to singlet oxygen damage have also been put in place in several artificial photosynthetic devices[104,105,106,107,108,109,110,111].

In natural photosynthesis, photoinduced charge separation is proceeded by a cascade of thermal electron transfer steps in order to increase charge separation lifetimes. This has been demonstrated by numerous systems[112]. Within the novel molecular arrays developed, the charge separation and storage characteristics must be tailored to specific applications. An example is the system[113] illustrated in *Figure 5* below, which features a molecular triad composed of a carotenoid, a porphyrin and fullerene (C_{60})[114]. Fullerenes have been found to possess numerous favourable properties

which make them excellent electron accepting components in supramolecular species of the type depicted below and are able to take on as many as six electrons[115,116,117]. Furthermore, they have been found to minimise the associated reorganisation energy (λ), allowing efficient performance in the solid state. For example, electron transfer events in this carotenoporphyrin-fullerene triad have been found to occur even in a glass at 77K. The porphyrin behaves as a chromophore, absorbing energy and transferring an electron to the fullerene. The beta-carotene does the same and a charge separated state with a huge dipole moment of over 150 debye is generated.

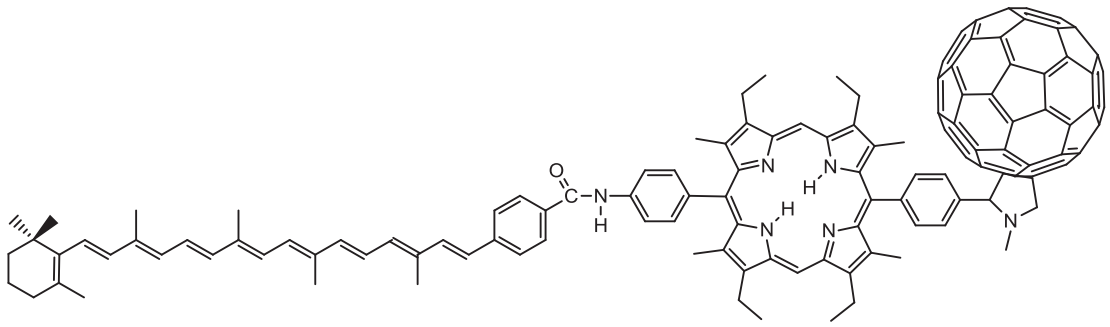

Figure 5 – The C-P-C_{60} molecular triad designed by Gust, Moore and Moore[113].

Self-assembled light harvesting antennae which vastly increase the cross section for solar energy absorption, without actually undergoing charge separation themselves have been successfully generated[118,119,120]. Photosynthetic organisms universally exploit antennae systems to absorb light and funnel the excitation energy to the RCs where the charge separation occurs. Within such systems, the use of antenna proteins serves to limit the need for the organism to produce large quantities of the complex charge separation apparatus, whilst still continuing to maintain an excellent efficiency for light collection by regulating their response to varying light intensity[121]. Following photoexcitation, a series of energy-transfer steps takes place to channel excitation energy to the site of charge separation.

An example of such a system is that in *Figure 6* below, an elaborate and elegant system composed of metalloporphyrins connected via readily constructed[122] and semi-rigid[123] diarylethyne units. These units enable rotation of the porphyrin planes about the ethyne in solution. The individual porphyrins are weakly coupled electronically, which means that the desired properties rationally designed into either the individual

chromophores or the small assemblies, are retained when the units are joined. Thus, predicting the properties of such complex architectures can become more straightforward. Selective photoexcitation of the zinc porphyrins results in rapid energy transfer in approximately 24 ps to the central non-metallated (free-base) porphyrin[124].

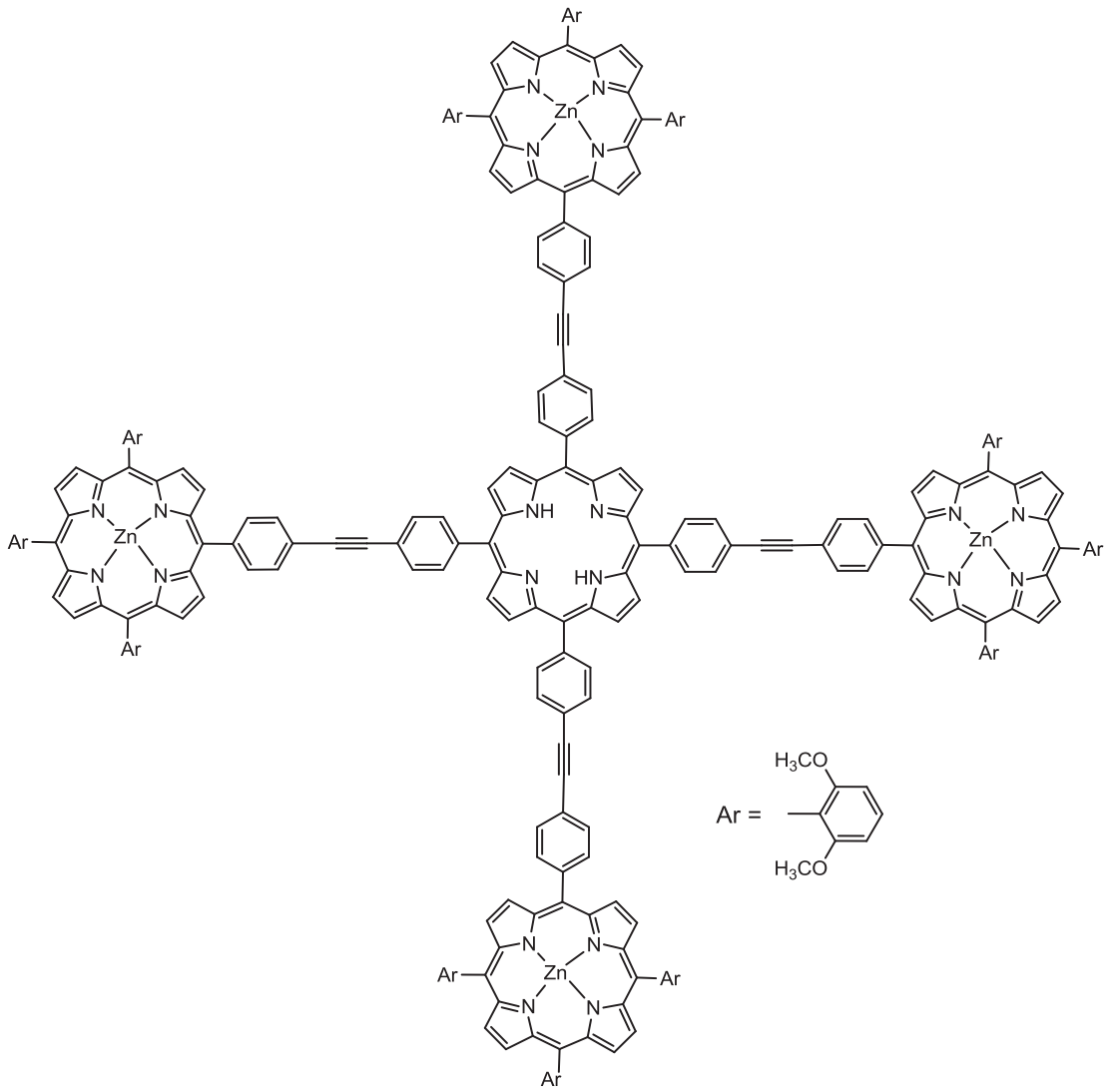

Figure 6 – The covalent light-harvesting chromophoric array[125] designed by Lindsey, Prathapan and Johnson.

Semisynthetic chlorophyll-based systems have been previously shown to undergo efficient PET.[126] Chlorophylls absorb light across a broad wavelength range and can behave as both electron and energy donors and acceptors. Additionally, they can naturally generate supramolecular assemblies using metal-ligand co-ordination, π-π

interactions[127] and hydrophobic effects within the protein environment[128]. Earlier this year, Wasielewski *et al.* generated a series of donor acceptor triads incorporating functionalised zinc methyl 3-ethylpyrochlorophyllide *a* (Chl) modified at its 20 position. This allowed covalent attachment of a pyromellitimide acceptor bearing a pyridine ligand, in addition to either one or two NDI (naphthalene-1,8:4,5-bis(dicarboximide)) or PDI (perylene-3,4:9,10-bis-(dicarboximide)) electron acceptors[129]. In this system, shown below in *Figure 7*, the pyridine ligand within each triad enables intermolecular Chl metal-ligand co-ordination, generating cyclic tetramers in solution, which can be observed by X-ray scattering. The self-assembly modifies their structures in a manner which results in prolonged charge separation lifetimes. For example, charge recombination in the Chl-PI-NDI_2 cyclic tetramer (τ_{CR} = 30 ± 1 ns in toluene) is three times slower relative to the monomeric building blocks (τ_{CR} = 10 ± 1 ns in toluene-1% pyridine).

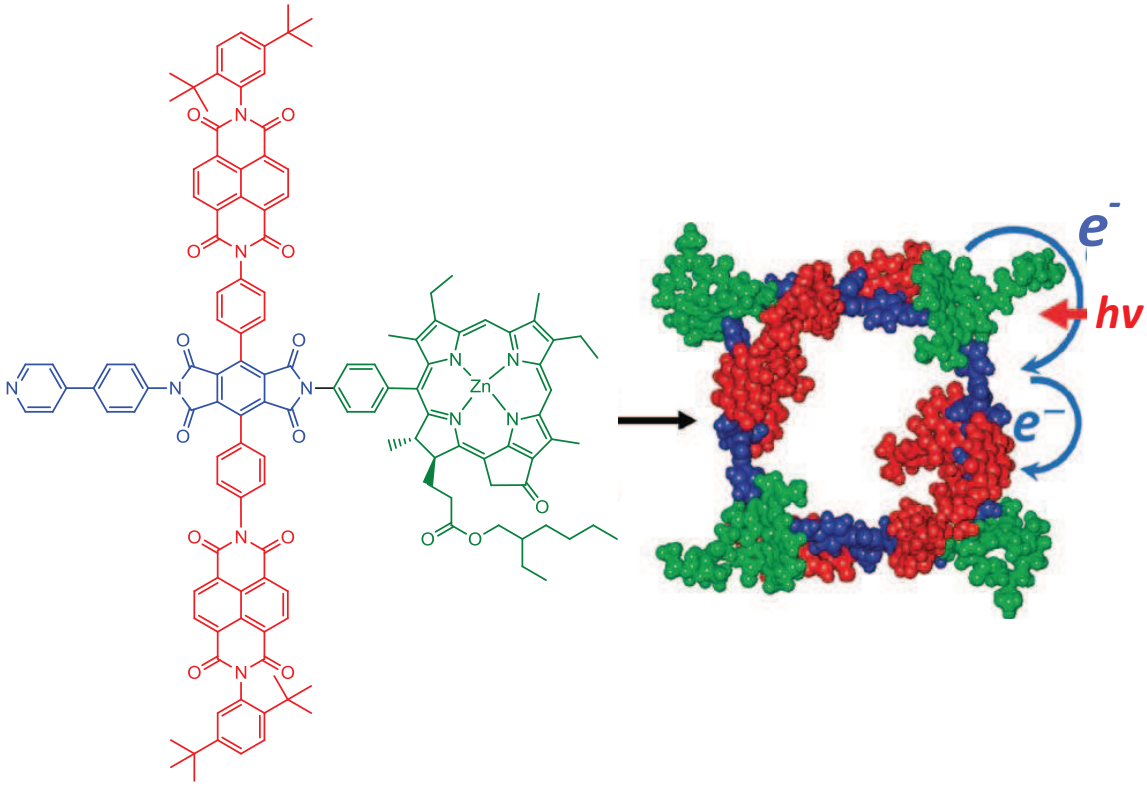

Figure 7 – The cyclic tetramer designed by Wasielewski et al. formed via self-assembly of Chl-based donor-acceptor triad building blocks. The system shows how supramolecular assembly can influence photoinduced charge transfer dynamics.

This system (*Figure 8*)[130] self-assembles into stacked dimers in toluene as revealed by Small Angle X-ray Scattering (SAXS). Wasielewski *et al.* synthesised the chlorophyll-a mimic[131] 1,7-bis(pyrrolidin-1'-yl)perylene-3,4:9,10-bis(dicarboximide) (also known as 5PDI)[132], a green chromophore which exhibits an intense absorption at 686 nm. Their system demonstrates that self-assembly of a robust PDI-based artificial light harvesting antenna promotes the formation of a functional special pair of 5PDI molecules, which undergoes ultrafast quantitative charge separation. Femtosecond transient absorption spectroscopy indicates that energy transfer from $(PDI)_2$ to $(5PDI)_2$ takes place with τ = 21 ps. This is followed by excited-state symmetry breaking of singlet excited $(5PDI)_2$ to quantitatively generate $5PDI^{+\bullet}$-$5PDI^{-\bullet}$ with a charge separation lifetime of 7 picoseconds. The ion pair recombines with τ_{CR} = 420 ps and it is in the dimeric system uniquely that electron transfer takes place. This serves as a mimic for special pair formation - so called due to the fact that they are excitonically coupled through proximity to each other with electronic orbital overlap.

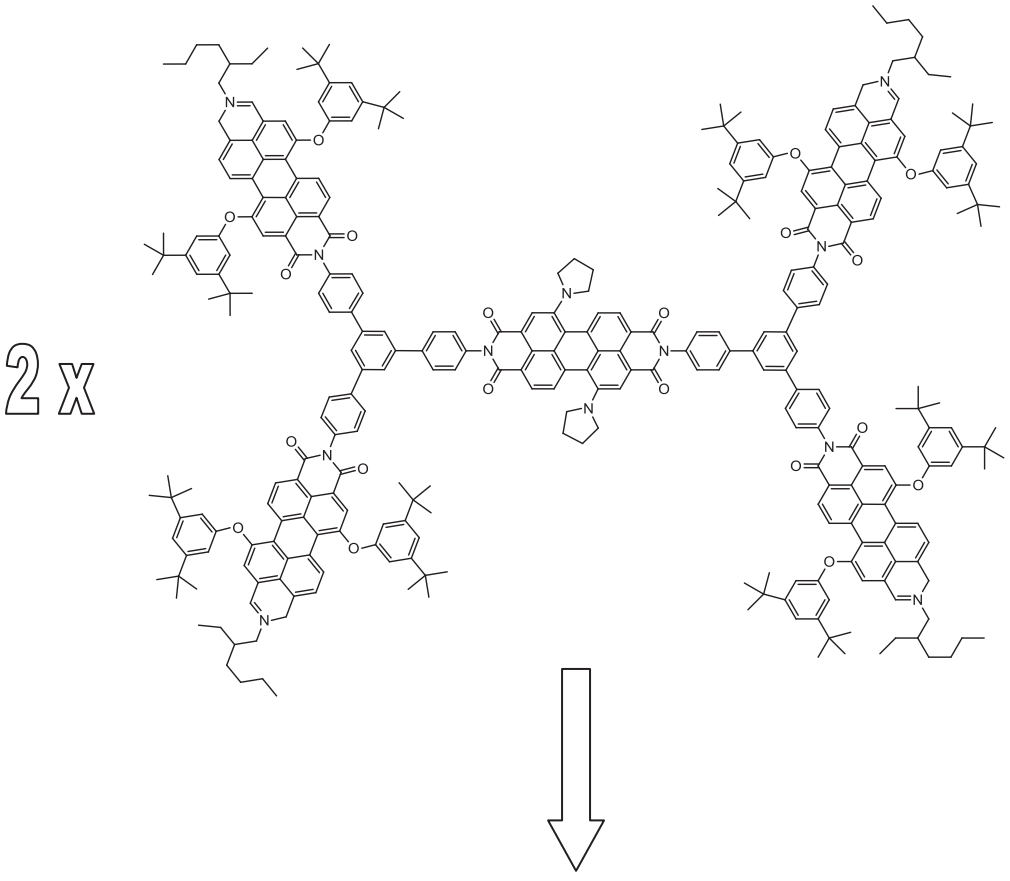

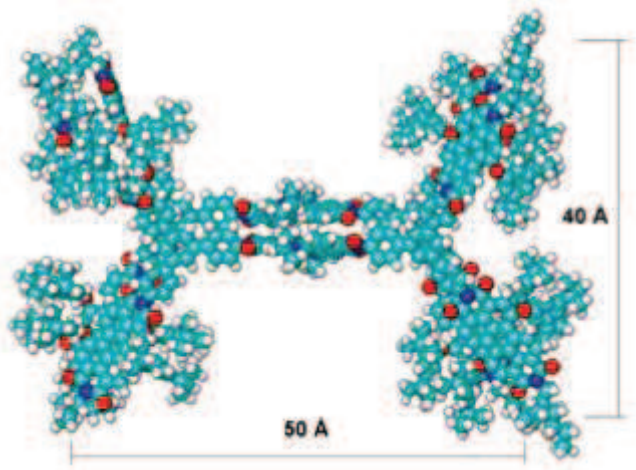

Figure 8 – The self-assembling array synthesised by Rybtchinski, Sinks and Wasielewski – the chemical structure is shown (top) and the best fit structure of the dimer from modelling the SAXS data (bottom).

It can be seen from the systems described above, that designing and building such intricate and powerful arrays involves a complex thought process. Numerous factors must be taken into consideration. These are dependent upon the purpose of the molecule, the synthetic tools and materials at the disposal of the chemist and the environment in which the system must function, to name but a few. In the case of the latter, it must be decided if the molecule will be used in the solid state or in solution and if solvent will be employed, the polarity range in which the system will function must also be considered. The subunits must be carefully selected, the fluorophores tuned to absorb light of the desired wavelength and finally, stringent purification measures adhered to, in order to ensure effects are not diminished by factors such as background fluorescence or phosphorescence. Due to the synthetic nature of the projects discussed within this thesis, another hugely important factor is therefore how the subunits incorporated can be prepared, connected and tuned to ensure optimum efficiency of the photoactive processes occurring in the system.

The favourable properties of the bodipy fluorophore aforementioned can also be extended to include a high synthetic robustness and an excellent solubility in a range of common laboratory solvents. These features allow much functionalisation and modification as the framework can be solubilised and subsequently adapted in the

chemist's solvent of choice. In addition to this, stability to light and acceptance of even relatively harsh coupling conditions including extreme heating/ cooling, high loading of catalyst and ligand and a remarkable resistivity to acid and base is displayed. An additional important factor to consider is the purity of the final compound which is of utmost importance in this field. Residual emission due to contamination by unwanted side products / starting materials or un-pure solvent or reagents must be omitted. Strict purification protocols including column chromatography, preparative thin-layer chromatography and recrystallisation/ slow diffusion crystallisation are in place to ensure the utmost purity of the final compounds. Compound identification is further confirmed by mass spectrometry, melting point analysis, and a full and complimentary range of NMR spectroscopic tools.

1.4 Light Induced Charge Transfer

A prominent subject within this thesis which is addressed within multiple chapters is that of light-induced charge transfer, one of the most fundamental chemical processes and that which can be considered to be one of the principal driving forces behind photosynthesis. There are numerous ways by which charge transfer can be measured, depending on the nature of the system involved. For example much work[133,134,135,136,137,138] has been completed on the study of charge transfer within DNA. Strong evidence of its occurrence through base-base hopping via π–π overlap was given by measurements, which served to probe changes in oxidized guanine damage yield with response perturbations in the bases[139,140]. The efficiency of charge transfer through the mismatch was found to be linked to the stacking efficiency of the bases in the mismatch providing strong evidence that charges are transferred through the π–π stack[141].

Charge transfer can also be related to solvent polarity, a topic which is discussed at length in Chapter 4. Daub and co-workers[142,143,144,145,146] have described the solvent dependent variation of the optical properties of some bodipy derivatives. The meso substituent varied from a crown-ether or thio-aza crown to a phenyl ring or the *N,N*'dimethylaniline unit. The latter substituent will be discussed in much greater detail in a subsequent chapter. In the *N,N*'dimethylaniline substituted bodipy and its

crown-ether analogue shown (*Figure 9)*, Daub *et al* examined and compared the polarity dependent charge transfer emission. Extensive studies involving molecules consisting of aromatic amine donor groups directly and covalently bound to fluorophores has been carried out. Amines including anthracene[147,148,149,150,151,152] pyrene[153,154] phenanthrene[155], or acridine/ium[156,157] have been extensively and successfully studied to elucidate mechanistic processes associated with charge transfer.

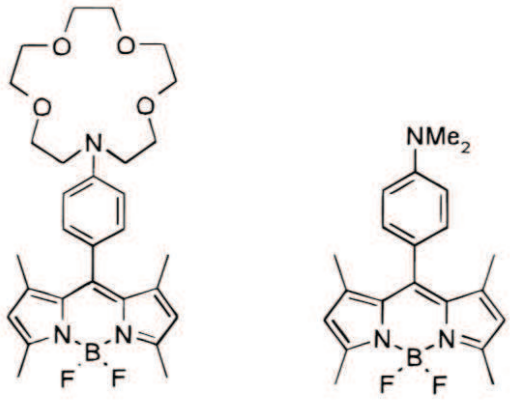

Figure 9 - The dimethylanilinobodipy (right) and crown-ether aniline analogue (left) studied by Daub et al.

Upon comparing the solvent dependent absorption and emission properties of amino-substituted bodipy dyes, it was seen that in low polarity solvent systems, emission occurred solely from a locally excited state. However, in higher polarity solvents, an ultrafast excited state charge transfer reaction from the amino donor to the basic fluorophore occurs. Strong quenching of the locally excited emission is observed. Furthermore, a bathochromically shifted emission from a lower lying CT state can also be seen. The efficient non-radiative deactivation process can be utilized to construct a very efficient molecular switch as complexation/ protonation is found to block the CT pathway and switch on emission from the locally excited state.

More recently, Nagano *et al.*[158] investigated the mechanisms of the solvent dependent polarity changes in the fluorescence on/off threshold of aryl substituted bodipy derivatives. PET-dependent fluorescence quenching was found to occur more easily with increasing polarity of the medium and the group generated a library of environment-sensitive fluorescent probes to detect local polarity changes in

membranes, receptors and proteins. In addition to measuring polarity dependent charge transfer using photophysical techniques, NMR can also be used to probe the electronic environment over the carbon atoms of choice and deduce CT effects in this way. This is discussed in much greater detail in Chapter 4.

Much attention has also been focused upon Metal-Ligand-Charge-Transfer (MLCT) over the past few decades[159,160,161,162,163,164,165] and numerous CT sensitizers have been developed. These possess favourable properties including visible light absorption across a broad wavelength range and long excited state lifetimes and can often be used in both homogenous and heterogenous redox reactions. One of the best known MLCT lumophores is tris(2,2'-bipyridyl)-ruthenium(II). A derivative of this is *cis*-di(thiocyanato)bis(2,2-bipyridyl-4,4'-dicarboxylate ruthenium(II) shown below in *Figure 10,* (alongside alternatively substituted examples). The series are generated by photosubstitution of $Ru(bipy)_3$ by X[166,167,168] where X can be a halide, cyanide or thiocyanide anion.

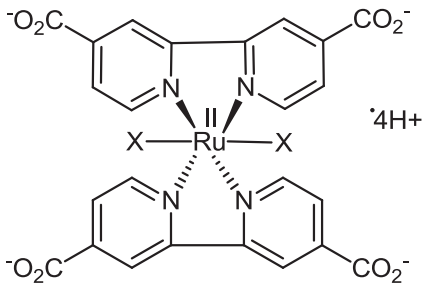

Figure 10 – The much studied cis-X_2 bis(2,2'-bipyridyl-4-4'-dicarboxylate)ruthenium(II) charge transfer sensitizer series (X = Cl^-, Br^-, I^-, CN^-, SCN^-).

The series of systems portrayed in *Figure 10* are able to adsorb strongly to the surface of oxides such as TiO_2, to generate strong electronic coupling between the CT excited state and the conduction band of the semiconductor. As a result, ultra-fast electron injection into the semiconductor occurs from the excited state complex with a quantum yield close to 100%[159].

Intramolecular charge transfer is also known to generate heteroatom containing σ-electron systems[169] with very different dipole moments in their ground and lowest

energy singlet excited states. Most common examples have enlarged dipoles [170,171,172], however this is not the case for betaines, such as the popular solvatochromic but non-fluorescent dye E_T (30)[173] (2,6-di-phenyl-4(2,4,6-triphenyl-1-pyridino)phenolate). E_T (30) is an example of a system showing strong solvent dependent ground and excited state properties. In the ground state, the molecule is characterised by a charge separated electronic structure and its conformation is highly dependent upon the environment[174,175]. However, upon excitation to the first excited state through a CT mechanism, the molecule's geometry changes[176]. Back electron transfer to the ground state is also an ultrafast solvent and temperature dependent process[177,178]. These observations collectively indicate a strong interaction of the system with the solvent. The solvent sensitivity of the CT absorption band maximum has been used to define the empirical E_T(30) polarity scale.

It can be seen from this brief insight into charge transfer mechanisms that there are numerous ways by which this phenomenon can be investigated within organic systems. Furthermore, there are various recognisable characteristics of molecules possessing these charge transfer properties, which allow further elucidation and understanding of the topic. The applications of such systems vary dramatically from molecular sensing and probing devices and photosynthetic constructs, to data storage and superconductors. The use of advanced photophysical tools and spectroscopic measurements now provides us with a wealth of data on the topic and has vastly increased our understanding of important and fundamental processes.

1.5 Conclusion

Overall, it can be seen that there are an abundance of fascinating and inspiring devices which have been synthesised in recent years. These molecular systems are enabling the research community to get closer each day to realising the goal of sustaining the planet with renewable energy. Using a range of meticulously developed synthetic techniques and chromatographic and crystallization methods, vast arrays can be assembled and purified. In addition to this, novel, clean and efficient catalysts are also being produced for the generation of hydrogen using water-splitting. Effective and robust components for photosynthetic mimics are constantly being developed to create workable systems.

In the meantime, bodipy continues to retain its place very much as the fluorophore of choice for a vast range of applications, due to its favourable synthetic and photochemical properties and the ease of functionalisation. Much research has been affected on developing novel techniques and expanding current ideas, both in terms of synthesising bodipy compounds and investigating and improving coupling conditions for appendage of spacer units and donor molecules. In addition to this, photophysical studies on the dyads prepared have provided much insight into charge-, electron- and energy-transfer mechanisms. It is hoped that the topics discussed herein will pave the way for future researchers undertaking similar projects and provide a thorough grounding for subsequent studies.

1.6 References

[1] Rurack, K.; Kollmannsberger, M.; Resch-Genger, U.; Daub, J. *J. Am. Chem. Soc*. **2000**, *122*, 968
[2] Rurack, K.; Kollmannsberger, M.; Daub, J. *Angew. Chem., Int. Ed.* **2001**, *40*, 385
[3] Turfan, B.; Akkaya, E. U. *Org. Lett*. **2002**, *4*, 2857
[4] Gee, K. R.; Rukavishnikov, A.; Rothe, A. *Comb. Chem. High Throughput Screening.* **2003**, *6*, 363.
[5] Goze, C.; Ulrich,G.; Charbonnière, L.; Cesario, M.; Prangé, T.; Ziessel, R. *Chem.-Eur. J.* **2003**, *9*, 3748.
[6] Cha, N. R.; Moon, S. Y.; Chang, S.-K. *Tetrahedron Lett*. **2003**, *44*, 8265.
[7] Moon, S. Y.; Cha, N. R.; Kim, Y. H.; Chang, S.-K. *J. Org. Chem.* **2004**, *69*, 181.
[8] Gabe, Y.; Urano, Y.; Kikuchi, K.; Kojima,H.; Nagano, T. *J. Am. Chem. Soc.* **2004**, *126*, 3357
[9] Coskun, A.; Akkaya, E. U. *Tetrahedron Lett.* **2004**, *45*, 4947.
[10] Baruah, M.; Qin, W.; Basariæ,N.; De Borggaeve, W. M.; Boens, N. *J. Org. Chem.* **2005**, *70*, 4152
[11] Yamada, K.; Nomura, Y.; Citterio, D.; Iwasawa, N.; Suzuki, K. *J. Am. Chem. Soc.* **2005**, *127*, 6956.
[12] Coskun, A.; Akkaya, E. U. *J. Am. Chem. Soc.* **2005**, *127*, 10464
[13] Katayama, M.; Nakane, R.; Matsuda, Y.; Kaneko, S.; Hara, I.; Sato, H. *Analyst.* **1998**, *123*, 2339
[14] Drummen, G, P, C.; van Liebergen, L, C, M.; Op den Kamp, J, A, F.; Post, J, A. *Free Radical Biol. Med.* **2002**, *33*, 473
[15] Kurata, S.; Kanagawa, T.; Yamada, K.; Torimura, M.; Yokomaku, T.; Kamagata, Y.; Kurane, R.; *Nucleic Acids Res.* **2001**, *29*, e34/1
[16] Yamada, K.; Toyota, T.; Takakura, K.; Ishimaru, M.; Sugawara, T. *New. J. Chem.* **2001**, *25*, 667.
[17] Merino, E, J.; Weeks, K, M. *J. Am. Chem. Soc.* **2005**, *127*, 12766
[18] Hendricks, J. A.; Keliher, E. J.; Wan, D.; Hilderbrand, S. A.; Weissleder, R.; Mazitschek, R. *Angewandte.Chemie. Int. Ed*. **2012**, *51*, 4603.
[19] Chorrell, E.; Pinkner, J. S.; Bengtsson, C.; Cusumano, C. K.; Rosenbaum, E.; Johansson, L. B.; Hultgren, S. J.; Almqvist, F. *Chem. Eur. J*. **2012**, *18*, 4522.
[20] Shao, J.; Guo, H.; Ji, S.; Zhao, J. *Biosensors and Bioelectronics*. **2011**, *26*, 3012.
[21] Deniz, E.; Ray, S.; Tomasulo, M.; Impellizzeri, S.; Sortino, S.; Raymo, F. M. *J. Phys. Chem. A*. **2010**, *114*, 11567.
[22] Yin, X.; Li, Y.; Zhu, Y.; Jing, X.; Li, Y.; Zhu, D. *Dalton Trans*, **2010**, *39*, 9929.
[23] Alamiry, M. A. H.; Benniston, A. C.; Copley, G.; Elliott, K. J.; Harriman, A.; Stewart, B.; Zi, Y. G. *Chem. Mater*. **2008**, *20*, 4024.
[24] Levitt, J.; Chung, H.-P.; Kuimova, M. K.; Yahioglu, G.; Wang, Y.; Qu, J.; Suhling, K. *ChemPhysChem*. **2011**, *12*, 662.
[25] Hungerford, G.; Allison, A.; McLoskey, D.; Kuimova, M. K.; Yahioglu, G.; Suhling, K. *J. Phys. Chem. B.* **2009**, *113*, 12067.

[26] Yin, X. D.; Li, Y. J.; Zhu, Y. L.; Jing, X. A.; Li, Y. L.; Zhu, D. B. *Dalton Trans*. **2010**, *39*, 9929.
[27] Benniston, A. C.; Harriman, A.; Whittle, V. L.; Zelzer, M.; *Eur. J. Org. Chem*. **2010**, *3*, 523.
[28] Kee, H. L.; Kirmaier, C.; Yu, L. H.; Thamyongkit, P.; Youngblood, W. J.; Calder, M. E.; Ramos, L.; Noll, B. C.; Bocian, D. F.; Scheidt, W. R.; Birge, R. R.; Lindsey, J. S.; Holten, D. *J. Phys. Chem. B* **2005**, *109*, 20433.
[29] Kuimova, M. K.; Yahioglu, G.; Levitt, J. A.; Suhling, K. *J. Am. Chem. Soc*. **2008**, *130*, 6672.
[30] Levitt, J. A.; Kuimova, M. K.; Yahioglu, G.; Chung, P. H.; Suhling, K.; Phillips, D. *J. Phys. Chem. C*. **2009**, *113*, 11634.
[31] Ulrich, G.; Ziessel, R.; Harriman, A.; *Angew. Chem*. **2008**, *120*, 1202; *Angew. Chem. Int. Ed*. **2008**, *47*, 1184
[32] Shiragami, T.; Tanaka, K.; Andou, Y.; Tsunami, S-I.; Matsumoto, J.; Luo, H.; Araki, Y.; Ito, O.; Inoue, H.; Yasuda, M. J. *Photochem. Photobiol*. A. **2005**, *170*, 287.
[33] Koepf, M.; Trabolsi, A.; Elhabiri, M.; Wytko, J. A.; Paul, D.; Albrechet-Gary, A. M.; Weiss, *J. Org. Lett*. **2005**, *7*, 1279.
[34] Harriman, A.; Mallon, L, J.; Ziessel, R.; *Chem. Eur. J*. **2008**, *14*, 11461.
[35] Yilmaz, M.D.; Bozdemir, O. A.; Akkaya, E. U. *Org. Lett*. **2006**, *8*, 2871.
[36] Li, F.; Yang, S. I.; Ciringh, Y.; Seth, J.; Martin, C. H, III.; Singh, D. L.; Kim, D.; Birge, R. R.; Bocian, D. F.; Holten, D.; Lindsay, J. S. *J. Am. Chem. Soc*. **1998**, *120*, 10001.
[37] Holten, D.; Bocian, D. F.; Lindsay, J. S. *Acc. Chem. Res*. **2002**, *35*, 57.
[38] Lai, R, Y.; Bard, A, J. *J. Phys. Chem. B.* **2003**, *107*, 5036
[39] Hepp, A.; Ulrich, G.; Schmechel, R.; von Seggern, H.; Ziessel, R. *Synth. Met.* **2004**, *146*, 11
[40] Bonardi, L.; Kanaan, H.; Camerel, F.; Jolinat, P.; Retailleau, P.; Ziessel, R. *Adv. Funct. Mater.* **2008**, *18*, 401
[41] Trieflinger, C.; Röhr, H.; Rurack, K.; Daub, J. *Angew. Chem. Int. Ed.* **2005**, 44, 6943
[42] Lammi, R. K.; Wagner, R. W.; Ambroise, A.; Diers, J. R.; Bocian, D. F.; Holten, D.; Lindsey, J. S.; *J. Phys. Chem. B*, **2001**, *105*, 5341.
[43] Kim, H. J.; Kim, J. S. *Tetrahedron. Lett*, **2006**, *47*, 7051.
[44] Choi, J. K.; Lee, A.; Kim, S.; Ham, S.; No, K.; Kim, J. S. *Org. Lett*. **2006**, *8*, 1601.
[45] Lee, S. H.; Kim, J. Y.; Kim, S. K.; Lee, J. H.; Kim, J. S. *Tetrahedron*, **2004**, *60*, 5171.
[46] deSilva, A. P.; Gunaratne, H. Q. N.; Gunnlaugsson, T.; Huxley, A. J. M.; McCoy, C. P.; Rademacher, J. T.; Rice, T. E. *Chem. Rev.* **1997**, *97*, 1515.
[47] Calix arenes functionalised in this manner often display a high selectivity towards specific cations: see (a) Beer, P. D.; Timoshenko, V.; Passaniti, P.; Balzani, V. *J. Chem. Soc., Chem. Commun*. **1995**, 1755; (b) Kim, S. K.; Bok, J. H.; Bartsch, R. A.; Lee, J. Y.; Kim, J. S. *Org. Lett*. **2005**, *7*, 4839; (c) Peng, X.; Wu, Y.; Fan, J.; Tian, M.; Han, K. *J. Org. Chem*. **2005**, *70*, 10524.
[48] Tanaka, K.; Miura, T.; Umezawa, N.; Urano, Y.; Kikuchi, K.; Higuchi, T.; Nagano, T. *J. Am. Chem. Soc.* **2001**, *123*, 2530.
[49] Miura, T.; Urano, Y.; Tanaka, K.; Nagano, T.; Ohkubo, K.; Fukuzumi, S. *J. Am. Chem. Soc.* **2003**, *125*, 8666.
[50] Urano, Y.; Kamiya, M.; Kanda, K.; Ueno, T.; Hirose, K.; Nagano, T. *J. Am. Chem. Soc.* **2005**, *127*, 4888.
[51] Atsushi, N.; Yoshiki, C. *Macromolecules*. **2010**, *43*, 193.
[52] (a) Yang, C.; Cho, S.; Chiechi, R. C.; Walker, W.; Coates, N. E.; Moses, D.; Heeger, A. J.; Wudl, F. J. Am. Chem. Soc. **2008**, *130*, 16524. (b) Duncan, T. V.; Ghoroghchian, P. P.; Rubtsov, I. V.; Hammer, D. A.; Therien,M. J. *J. Am. Chem. Soc*. **2008**, *130*, 9773. (c) Zhang, F.; Bijleveld, J.; Perzon, E.; Tvingstedt, K.; Barrau, S.; Ingañas, O.; Andersson, M. R. *J. Mater. Chem*. **2008**, *18*, 5468. (d) Walker, W.; Veldman, B.; Chiechi, R.; Patil, S.; Bendikov, M.; Wudl, F. *Macromolecules.***2008**, *41*, 7278. (e) Peet, J.; Kim, J. Y.; Coates, N. E.; Ma, W. L.; Moese, D.; Heeger, A. J.; Bazan, G. *C. Nature,* **2007**, *6*, 497. (f) Cheng, K.-F.; Liu, C.-L.; Chen,W.-C. *J. Polym. Sci., Part A: Polym. Chem*. **2007**, *45*, 5872. (g) Sonmez, G.; Sonmez, H. B.; Shen, C. K. F.; Jost, R. W.; Rubin, Y.; Wudl, F. *Macromolecules*. **2005**, *38*, 669. (h) Wang, F.; Lai, T.-H.; Han, M.-Y. *Macromolecules,* **2004**, *37*, 3222. (i) Eldo, J.; Ajayaghosh, A. *Chem. Mater*. **2002**, *14*, 410. (j) Ajayaghosh, A.; Eldo, *J. Org. Lett*. **2001**, *3*, 2595
[53] (a) Morana, M.; Wegscheider, M.; Bonanni, A.; Kopidakis, N.; Shaheen, S.; Scharber, M.; Zhu, Z.; Waller, S.; Caudiana, R.; Brabec, C. *Adv. Funct. Mater*. **2008**, *18*, 1757. (b) Hebbink, G. A.; Stouwdam, J.W.; Reinhoudt, D. N.; van Veggel, F. C. J. M. *Adv. Mater*. **2002**, *14*, 1147. (c) Slooff, L. H.; Polman, A.; Cacialli, F.; Friend, R. H.; Hebbink, G. A.; van Veggel, F. C. J. M.; Reinhoudt, D. N.

Appl. Phys. Lett. **2001**, *78*, 2122. (d) Tessler, N.; Medvedev, V.; Kazes, M.; Kan, S.; Banin, U. *Science.* **2002**, *185*, 1906.
[54] Suzuki, H. *Appl. Phys. Lett*. **2000**, *76*, 1543.
[55] (a) Perzon, E.; Zhang, F.; Andersson, M.; Mammo, W.; Inganäs, O.; Andersson, M. R. Adv. Mater. **2007**, *19*, 3308. (b) Ostrowski, J. K.; Susumu, K.; Robinson, M. R.; Therien, M. J.; Bazan, G. C. *Adv. Mater*. **2003**, *15*, 1296.
[56] Hascoat, P.; Yang, S. I.; Lammi, R. K.; Alley, J.; Bocian, D. F.; Lindsey, J. S.; Holten, D. *Inorg. Chem*. **1999**, *38*, 4849.
[57] Dincă, M.; Surendranath, Y.; Nocera, D. G, *PNAS Inaugural article- Sustainability Sciences*, **2010**, p1-5. www.pnas.org/cgi/doi/10.1073/pnas.1001859107
[58] Lewis N.S.; Nocera D.G, *Proc Natl Acad Sci USA*, **2006**, *103*, 15729.
[59] Gust, D.; Moore, T. A.; Moore, A. L. *Faraday Discuss*. **2012**, *155*, 9.
[60] Gust, D.; Moore, T. A.; Moore, A. L. *Acc. Chem. Res*. **1993**, *26*, 198.
[61] Scheer, H.; Schneider, S. *Photosynthetic Light Harvesting Systems*. Walter de Gruyter, New York, 1988**.**
[62] Sauer, K. *Acc. Chem. Res*. **1978**, *11*, 257.
[63] Cogdell, R. J.; Frank, H. A. *Biochim. Biophys. Acta*, **1987**, *895*, 63.
[64] Oevering, H.; Paddon-Row, M. N.; Heppener, M.; Oliver, A. M.; Cotsaris, E.; Verhoeven, J. W.; Hush, N. S. *J. Am. Chem. Soc*. **1987**, *109*, 3258.
[65] Imahori, H. *J. Phys. Chem. B*. **2004**, *108*, 6130.
[66] Ferreira, K. N.; Iverson, T. M.; Maghlaoui, K.; Barber, J.; Iwata, S. *Science*, **2004**, *303*, 1831.
[67] Wasielewski, M. R. *J. Org. Chem*. **2006**, *71*, 5051.
[68] Gust, D.; Moore, T. A, in The Porphyrin Handbook, ed. Kadish, K. M, Smith, K. M and Guilard, R. Academic Press, New York, **2000**, *vol. 8*, ch 57, pp 153-190.
[69] Redmore, N. P.; Rubtsov, I. V.; Therien, M. J. *J. Am. Chem. Soc*. **2003**, 125, 8769.
[70] Meyer, T. *J. Acc. Chem. Res*. **1989**, *22*, 163
[71] Wasielewski, M. R. *Chem. Rev*. **1992**, *92*, 435.
[72] Gust, D.; Moore, T. A.; Moore, A. L. *Acc. Chem. Res*. **2001**, *34*, 40.
[73] Falkenstrom, M.; Johansson, O.; Hammarström, L. *Inorg. Chim. Acta*. **2007**, *360*, 741.
[74] Fukuzumi, S.; Imahori, H. *Electron Transfer in Chemistry*. **2001**, *2*, 927.
[75] Flamigni, L.; Armaroli, N.; Barigelletti, F.; Balzani, V.; Collin, J. –P.; Dalbavie, J. –O.; Heitz, V.; Sauvage, J. –P. *J. Phys. Chem. B*. **1997**, *101*, 5936.
[76] Gust, D.; Moore, T. A.; Moore, A. L. *Acc. Chem. Res*. **2009**, *42*, 1890.
[77] Gust, D.; Moore, T. A.; Moore, A. L. *Acc. Chem. Res*. **2001**, *34*, 40.
[78] Yin, Q et al, *Science*. **2010**, *328*, 342.
[79] Blakemore, J. D. et al. *J. Am. Chem. Soc*, **2010**, *132*, 16017.
[80] Jiao, F.; Frei, H. *Chem. Commun*. **2010**, *46*, 2920.
[81] Kanan, M. W.; Nocera, D. G, *Science*. **2008**, *321*, 1072.
[82] Conception, J.J.; Jurss, J. W.; Templeton, J. L.; Meyer, T. J. *Proc. Natl. Acad. Sci,. USA*. **2008**, *105*, 17632.
[83] Gust, D.; Moore, T. A.; Moore, A. L. *Acc. Chem. Res*, **2009**, *42*, 1890.
[84] Sala, X.; Romerco, I.; Rodriguez, M.; Escriche, L.; Llobet, A. *Angew. Chem. Int. Ed*. **2009**, *48*, 2842.
[85] Youngblood, W. J.; Lee, S. –H. A.; Kobayashi, E. A.; Hemandez-Pagan.; Hoertz, P. G.; Moore, T. A.; Moore, A. L.; Gust, D.; Mallouk, T. E. *J. Am. Chem. Soc*. **2009**, *131*, 926.
[86] Duan, L.; Bozoglian, F.; Mandal, S.; Stewart, B.; Privalov, T.; Llobet, A.; Sun, L. *Nature Chemistry*. **2012***, 4*, 418.
[87] Alstrum-Acevedo, J. H., Brennaman, M. K. & Meyer, T. J. *Inorg. Chem***. 2005**, *44*, 6802.
[88] Sun, L.; Hammarström, L.; Akermark, B.; Styring, S. *Chem. Soc. Rev*. **2001**, *30*, 36.
[89] Harriman, A.; Pickering, I. J.; Thomas, J. M.; Christensen, P. A. *J. Chem. Soc., Faraday Trans. 1*, **1988***, 84*, 2795.
[90] Jiao, F.; Frei, H. *Chem. Commun.* **2010**, *46*, 2920
[91] Gorlin, Y.; Jaramillo, T. F. *J. Am. Chem. Soc.* **2010**, *132*, 13612.
[92] Hocking, R. K.; Brimblecombe, R.; Chang, L-Y.; Singh, A.; Cheah, M. H.; Glover, C.; Casey, W. H.; Spiccia, L. *Nature Chemistry*. **2011**, *3*, 461.
[93] Kanan, M. W.; Nocera, D. G. *Science*. **2008**, *321*, 1072.
[94] Jiao, F.; Frei, H. *Angew. Chem. Int. Ed*. **2009**, *48*, 1841.
[95] Surendranath, Y.; Dincă, M.; Nocera, D. G. *J. Am. Chem. Soc*. **2009**, *131*, 2615.

[96] Huang, Z. Q.; Luo, Z.; Geletii, Y. V.; Vickers, J. W.; Yin, Q. S.; Wu, D.; Hou, Y.; Ding, Y.; Song, J.; Musaev, D. G.; Hill, C. L.; Lian, T. Q. *J. Am. Chem. Soc*. **2011**, *133*, 2068.
[97] Meyer, T. J. *Acc. Chem. Res*. **1989**, *22*, 163
[98] Romain, S., Vigara, L. & Llobet, A.. *Acc. Chem. Res.* **2009**, *42*, 1944.
[99] Dau, H. *ChemCatChem*. **2010**, *2*, 724
[100] Ellis, W. C., McDaniel, N. D., Bernhard, S. & Collins, T. J. *J. Am. Chem. Soc*. **2010**, *132*, 10990.
[101] Fillol, J. L.; Codolà, Z.; Garcia-Bosch, I.; Gómez, L.; Pla, J. J.; Costas, M. *Nature Chem*. **2011**, *3*, 807.
[102] Hambourger, M.; Gervaldo, M.; Svedruzic, D.; King, P. W.; Gust, D.; Ghirardi, M.; Moore, A. L.; Moore, T. A. *J. Am. Chem. Soc*., **2008**, *130*, 2015.
[103] Barton, B. E.; Olsen, M. T.; Rauchfuss, T. B.; *Curr. Opin. Biotechnol*, **2010**, *21*, 292.
[104] Moore, A. L.; Joy, A.; Tom, R.; Gust, D.; Moore, T. A.; Benasson, R. V.; Land, E. J. *Science*. **1982**, *216*, 982.
[105]Gust, D.; Moore, T. A.; Benasson, R. V.; Mathis, P.; Land, E. J.; Chachaty, C.; Moore, A. L.; Liddell, . A.; Nemeth, G. A. *J. Am. Chem. Soc*. **1985**, *107*, 3631.
[106] Bensasson, R. V.; Land, E. J.; Moore, A. L.; Crouch, R. L.; Dirks, G.; Moore, T. A.; Gust, D. *Nature*. **1981**, *290*, 329.
[107] Moore, A. L.; Joy, A. M.; Tom, R.; Gust, D.; Moore, T. A.; Bensasson, R. V.; Land, E. J. *Science*. **1982**, *216*, 982.
[108] Gust, D.; Moore, T. A.; Moore, A. L.; Devadoss, C.; Liddell, P. A.; Hermant, R. M.; Nieman, R. A.; Demanche, L. J.; DeGraziano, J. M.; Gouni, I. *J. Am. Chem. Soc*., **1992**, *114*, 3590.
[109] Gust, D.; Moore, T. A.; Moore, A. L.; Kuciauskas, D.; Liddell, P. A.; Halbert, B. D. *J. Photochem. Photobiol. B*. **1998**, *43*, 209.
[110] Kodis, G.; Herrero, C.; Palacios, R.; Mariño-Ochoa, E.; Gould, S. L.; de la Garza, L.; van Grondelle, R.; Gust, D.; Moore, T. A.; Moore, A. L.; Kennis, J. T. M. *J. Phys. Chem. B*. **2004**, *108*, 414.
[111] Kloz, M.; Pillai, S.; Kodis, G.; Gust, D.; Moore, T. A.; Moore, A. L.; van Grondelle, R.; Kennis, J. T. M. *J. Am. Chem. Soc*. **2011**, *133*, 7007.
[112] Reviews of these systems can be found within the following publications: (a) Maruyama, K.; Osuka, A. *Pure Appl. Chem.* **1990**, *62*, 1511 (b) Wasielewski, M. R. *Chem. Rev*. **1992**, *92*, 435 (c) Gust, D.; Moore, T. A.; Moore, A. L. *Acc. Chem. Res.* **1993**, *26*, 198. (d) Gust, D.; Moore, T. A. In *The Porphyrin Handbook*; Kadish, K. M., Smith, K. M., Guilard, R., Eds.; Academic Press: San Diego, 2000; Vol. 8, pp 153-190 (e) Guldi, D. M.; Imahori, H. *J. Porphyrins Phthalocyanines*. **2004**, *8*, 976-983. (f) Imahori, H. *J. Phys. Chem. B.* **2004**, *108*, 6130.
[113] Kuciauskas, D.; Liddell, P. A.; Lin, S.; Stone, S. G.; Moore, A. L.; Moore, T. A.; Gust, D. *J. Phys. Chem. B.* **2000**, *104*, 4307.
[114] A significant number of chromophore-fullerene dyads have been reported in the literature, see the following example references: (a) Kuciauskas, D.; Liddell, P. A.; Lin, S.; Johnson, T. E.; Weghorn; S. J.; Lindsey, J. S.; Moore, A. L.; Moore, T. A.; Gust, D. *J. Am. Chem. Soc*. **1999**, *121*, 8604-8614. (b) Imahori, H.; Hagiwara, K.; Akiyama, T.; Aoki, M.; Taniguchi, S.; Okada, T.; Shirakawa, M.; Sakata, Y. *Chem. Phys. Lett*. **1996**, *263*, 545. (c) Carbonera, D.; Di Valentin, M.; Corvaja, C.; Agostini, G.;Giacometti, G.; Liddell, P. A.; Kuciauskas, D.; Moore, A. L.; Moore, T. A.; Gust, D. *J. Am. Chem. Soc*. **1998**, *120*, 4398. (d) Guldi, D. M.; Maggini, M.; Scorrano, G.; Prato, M. J. *Am. Chem. Soc.* **1997**, *119*, 974. (e) Higashida, S.; Imahori, H.; Kaneda, T.; Sakata, Y. *Chem. Lett*. **1998**, 605. (f) Kuciauskas, D.; Liddell, P. A.; Moore, A. L.; Moore, T. A.; Gust, D. *J. Am. Chem. Soc*. **1998**, *120*, 10880. (g) Nierengarten, J.-F.; Schall, C.; Nicoud, J.-F. *Angew. Chem. Int*. *Ed. Engl.* **1998**, *37*, 1934.
[115] Kroto, H. W.; Heath, J. R.; O'Brien, S. C.; Curl, R. F.; Smalley, R. E. *Nature*, **1985**, *318*, 162.
[116] Kratschmer, W.; Lamb, L. D.; Fostriopoulos, D.; Huffman, R. *ibid*. **1990**, *347*, 354.
[117] Kroto, H. W.; Allaf, A. W.; Balm, S. P. *Chem.Rev*. **1991**, *91*, 1213.
[118] Seth, J.; Palaniappan, V.; Wagner, R. W.; Johnson, T. E.; Lindsey, J. S.; Bocian, D. F. *J. Am. Chem. Soc.* **1996**, *118*, 11194.
[119] Aratani, N.; Osuka, A. *Bull. Chem. Soc. Jpn.* **2001**, *74*, 1361.
[120] Kim, D.; Osuka, A. *Acc. Chem. Res.* **2004**, *37*, 735.
[121] Sunstrom, V.; Pullerits, T.; van Grondelle, R. *J. Phys. Chem. B*. **1999**, *103*, 2327.
[122] Wagner, R. W.; Johnson, T. E.; Lindsey, J. S. *J. Am. Chem. Soc*. **1996**, *118*, 11166.
[123] Bothner-By, A. A.; Dadok, J.; Johnson, T. E.; Lindsey, J. S. *J. Phys. Chem*. **1996**, *100,* 17551.

[124] Seth, J.; Palaniappan, V.; Wagner, R.W.; Johnson, T. E.; Lindsey, J. S.; Bocian, D. F. *J. Am. Chem. Soc*. **1996**, *118*, 11194.
[125] Prathapan, S.; Johnson, T. E.; Lindsey, J. S. *J. Am. Chem. Soc*. **1993**, *115*, 7519.
[126] (a) Wasielewski, M. R. In *Chlorophylls*; Scheer, H., Ed.; CRC Press: Boca Raton, FL, 1991; pp 269−286; (b) Regehly, M.; Ermilov, E. A.; Helmreich, M.; Hirsch, A.; Jux, N.; Roeder, B. *J. Phys. Chem. B.* **2007**, *111*, 998. (c) Shinoda, S.; Tsukube, H.; Nishimura, Y.; Yamazaki, I.; Osuka, A. *Tetrahedron*. **1997**, *53*, 13657.
[127] For examples of molecules that contain redox active chromophores and use π-π interactions to generate supramolecular arrays see: (a) Beckers, E. H. A.; Jonkheijm, P.; Schenning, A. P. H. J.; Meskers, S. C. J.; Janssen, R. A. J. *ChemPhysChem* **2005**, *6*, 2029 (b) Ahrens, M. J.; Sinks, L. E.; Rybtchinski, B.; Liu, W.; Jones, B. A.; Giaimo, J. M.; Gusev, A. V.; Goshe, A. J.; Tiede, D. M.; Wasielewski, M. R. *J. Am. Chem. Soc.* **2004**, *126*, 8284 (c) Herrikhuyzen, J. V.; Syamakumari, A.; Schenning, A. P. H. J.; Meijer, E. W. *J. Am. Chem. Soc.* **2004**, *126*, 10021 (d) Ramos, A. M.; Meskers, S. C. J.; Beckers, E. H. A.; Prince, R. B.; Brunsveld, L.; Janssen, R. A. J. *J. Am. Chem. Soc.* **2004**, *126*, 9630 (e) Hayes, R. T.; Walsh, C. J.; Wasielewski, M. R. *J. Phys. Chem. A* **2004**, *108*, 3253.
[128] Balaban, T.; Tamiaki, H.; Holzwarth, A. In *Supramolecular Dye Chemistry*; Würthner, F., Ed.; Spinger: Berlin/ Heidelberg, 2005; Vol. 258, pp 585.
[129] Kelley, R. F.; Tauber, M. J.; Wasielewski, M. R. *J. Am. Chem. Soc*. **2006**, *128*, 4779.
[130] Rybtchinski, B.; Sinks, L. E.; Wasielewski, M. R. *J. Am. Chem. Soc.* **2004**, *126*, 12268
[131] Lukas, A. S.; Bushard, P.; Wasielewski, M. R. *J. Phys. Chem. A.* **2002**, *106*, 2074.
[132] Zhao, Y.; Wasielewski, M. R. *Tetrahedron Lett.* **1999**, *40*, 7047
[133] Dekker, C.; Ratner, M. *Physics World*, **2001**, *14*, 29.
[134] Eley, D. D.; Spivey, D. I. *Trans. Faraday Soc*, **1962**, *58*, 411
[135] Murphy, C. J.; Arkin, M. R.; Jenkins, Y.; Ghatlia, N. D.; Bossmann, S. H.; Turro, N. J.; Barton, J. K, *Science*. **1993**, *262*, 1025
[136] Yoo *et al*., *Phys. Rev. Lett*. **2002**, *87*, 198102
[137] Bruinsma, R.; Gruner, G.; Orsogna, M. R. D.; Rudnik, J.; *Phys. Rev. Lett*, **2000**, *85*, 4393
[138] Lewis, F. D.; Wu, T.; Zhang, Y.; Letsinger, R. L.; Greeneld, S. R.; Wasielewski, M. R. *Science*, **1997**, *277*, 673.
[139] Bhattacharyaa, P. K and Barton, J. K. *J. Am. Chem. Soc*. **2001,** *123*, 8649.
[140] Rosen, M. A.; Shapiro, L.; Patel, D. J. *Biochemistry.* **1992***, 31*, 4015.
[141] Armitage, N. P.; Briman, M.; Grüner, G.; *Phys. Stat. Sol (b)*, **2004**, *1*, 69.
[142] Kollmannsberger, M.; Rurack, K.; Resch-Genger, U.; Daub, J. *J. Phys. Chem. A.*. **1998**, *102*, 10211.
[143] Kollmannsberger, M.; Rurack, K.; Resch-Genger, U.; Rettig, W.; Daub, J. *Chem. Phys. Lett.* **2000**, *329*, 363.
[144] Rurack, K.; Kollmannsberger, M.; Resch-Genger, U.; Daub, J. *J. Am. Chem. Soc.* **2000**, *122*, 968.
[145] Rurack, K.; Kollmannsberger, M.; Daub, J. *Angew. Chem., Int. Ed.* **2001**, *40*, 385.
[146] Rurack, K.; Kollmannsberger, M.; Daub, J. *New J. Chem.* **2001**, *25*, 289.
[147] Siemiarczuk, A.; Grabowski, Z. R.; Krowczinski, A.; Asher, M.; Ottolenghi, M. *Chem. Phys. Lett.* **1977**, *51*, 315.
[148] Siemiarczuk, A.; Ware, W. R. *J. Phys. Chem.* **1987**, *91*, 3677
[149] Siemiarczuk, A.; Koput, J.; Pohorille, A. *Z. Naturforsch.* **1982**, *37a*, 598
[150] Okada, T.; Mataga, N.; Baumann, W.; Siemiarczuk, A. *J. Phys. Chem.* **1987**, *91*, 4490
[151] Mataga, N.; Nishikawa, S.; Asahi, T.; Okada, T. *J. Phys. Chem.* **1988**, *92*, 6233.
[152] Lee, S.; Arita, K.; Kajimoto, O.; Tamao, K. *J. Phys. Chem. A* **1997**, *101*, 5228.
[153] Wiessner, A.; Hüttmann, G.; Ku¨hnle, W.; Staerk, H. *J. Phys. Chem.* **1995**, *99*, 14923
[154] Herbich, J.; Kapturkiewicz, A. *Chem. Phys.* **1993**, *170*, 221.
[155] Onkelinx, A.; De Schryver, F. C.; Viaene, L.; van der Auweraer, M.; Iwai, K.; Yamamoto, M.; Ichikawa, M.; Masuhara, M.; Maus, M.; Rettig, W. *J. Am Chem. Soc.* **1996**, *118*, 2892.
[156] (a) Jonker, S. A.; Ariese, F.; Verhoeven, J. W. *Recl. Trav. Chim. Pays-Bas* **1989**, *108*, 109. (b) Jonker, S. A.; van Dijk, S. I.; Goubitz, K.; Reiss, C. A.; Schuddeboom, W.; Verhoeven, J. W. *Mol. Cryst. Liq. Cryst.* **1990**, *183*, 273. (c) Jonker, S. A.; Verhoeven, J. W.; Reiss, C. A.; Goubitz, K.; Heijdenrijk, D. *Recl. Trav. Chim. Pays-Bas* **1990**, *109*, 154.
[157] Herbich, J.; Kapturkiewicz, A. *J. Am Chem. Soc.* **1998**, *120*, 1014
[158] Sunahara, H.; Urano, Y.; Kojima, H.; Nagano. T. *J. Am. Chem. Soc*. **2007**, *129*, 5597.

[159] Nateeruddin, M. K.; Kay, A.; Rodicio, I.; Humphry-Baker, R.; Müller, E.; Liska, P.; Vlachopoulos, N.; Gräzel, M. *J. Am. Chem. Soc*. **1993**, *115*, 6382
[160] Seneviratne, D. S.; Uddin, M. J.; Swayambunathan, V.; Bernhard Schlegel, H.; Endicott, J. F. *Inorg Chem.* **2002**, *41*, 1502
[161] Higgins, S. L.; Tucker, A. J.; Winkel, B. S. J.; Brewer, K. J. *Chem. Commun***. 2012,** *41*, 67
[162] Litke, S. V.; Ershov, A. Y.; Meyer, T. J. *J. Phys. Chem. A*. **2011**, *115*, 14235
[163] Verma, S.; Kar, P.; Das, A.; Ghosh, H. N. *Dalton Trans.* **2011**, *40*, 9765
[164] Thompson, D. W.; Fleming, C. N.; Myron, B. D.; Meyer, T. J. *J. Phys. Chem. B.* **2007**, *111*, 6930
[165] Koike, K.; Okoshi, N.; Hori, H.; Takeuchi, K.; Ishitano, O.; Tsubaki, H.; Clark, I. P.; George, M. W.; Johnson, F. P.; Turner, J. T. *J. Am. Chem. Soc*. **2002**, *124*, 11448
[166] Gleria, M.; Minto, F.;Beggiato, G.; Bortulus, P. *J. Chem. Soc, Chem Commun*, **1978**, *285*.
[167] Durham, B.; Caspar, J.; Nagle, J. K.; Meyer, T. J. *J. Am. Chem. Soc*. **1982**, *104*, 4803.
[168] Hoggard, P. E.; Porter, G. B. *J. Am. Chem. Soc*, **1978**, *100*, 1457.
[169] Krasovitskii, B. M.; Bolotin, B. M. *Organic Luminescent Materials*. VCH: Weinheim, 1989
[170] Werner, T. C, *Modern Fluorescence Spectroscopy*. Wehry, E. L., Ed.; Plenum: New York, 1976-81; Vol 2, p277.
[171] Langhals, H. *Z. Phys. Chem. Neue Folge.* **1981**, *127*, 45
[172] Langhals, H. *Angew. Chem., Int. Ed. Engl.* **1982**, *21*, 724.
[173] Reichardt, C. *Chem. Rev.* **1994**, *94*, 2319.
[174] Bartkowiak, W.; Lipinski, J. *J. Phys. Chem. A*. **1998,** *102*, 5236.
[175] Labaugh, J.; Rossky, P. J. *J. Phys. Chem. A.* **1999**, *103,* 9432.
[176] Higiu, S.; Dreyer, J.; Pfeiffer, M.; Brzezinka, K. W.; Wevneke, W. *J. Raman Spectrosc*. **2000**, *31*, 797
[177] Kesson, E.; Walker, G. C.; Barbara, P. F. *J. Chem. Phys*. **1991**, *95*, 4188
[178] Jhonson, A. E.; Levinger, N. E.; Jarzebe, W.; Schlief, R.; Kliner, D. A. V.; Barbara, P. F. *Chem. Phys*. **1993**, *176,* 555.

Chapter 2

Experimental and Synthetic Protocols

2.1 General Experimental

Nuclear Magnetic Resonance spectroscopy

^{1}H and ^{13}C NMR spectra were recorded with either Bruker AVANCE 300 MHz, JEOL 400 MHz, or JEOL Lambda 500 MHz spectrometers. ^{11}B and ^{19}F NMR spectra were recorded using the 400 MHz spectrometer. Chemical shifts for ^{1}H and ^{13}C NMR spectra are referenced relative to the residual protiated solvent. The ^{11}B NMR chemical shift is referenced relative to $BF_3.Et_2O$ (δ = 0ppm), and the ^{19}F NMR chemical shift is given relative to $CFCl_3$ (δ = 0ppm). Simulated ^{19}F NMR spectra were created using the program NUMARIT.

Mass spectrometry and elemental analysis

Routine mass spectra and elemental analyses were obtained using in-house facilities. MALDI mass spectra were recorded at the EPSRC sponsored Mass Spectrometry Service at Swansea. Absorption spectra were recorded using a Hitachi U3310 spectrophotometer and corrected fluorescence spectra were recorded using a Lambda Advanced F 4500 spectrometer. Uncorrected melting points were measured using a Stuart SMP11 apparatus and typically carried out twice to check for consistency in the readings.

Absorption spectra

Absorption spectra were recorded on a Hitachi U3310 UV/Visible dual-beam spectrophotometer. A baseline was recorded prior to making the measurement using spectroscopic grade solvent in a cuvette of 1cm path placed in each beam. Spectra were recorded with a solvent cuvette in the reference beam. Spectroscopic grade solvents were used in all fast kinetic experiments and fluorescence/absorption spectroscopy measurements.

Emission spectra

Emission spectra were recorded in quartz cuvettes using a Hitachi F4500 spectrofluorimeter. Solutions used were optically dilute, with an absorbance at the excitation wavelength of <0.1, and were purged with nitrogen. Spectra were corrected by reference to a standard lamp.

Fluorescence lifetime measurements

Ultrafast fluorescence decays were measured by an up-conversion method as described previously.[1] The instrument (FOG100, CDP, Moscow, Russia) utilizes the second harmonic (420 nm) of a 50 fs Ti:sapphire laser (TiF50, CDP, Moscow, Russia) pumped by an Ar ion laser (Innova 316P, Coherent). The samples were placed in a rotating disk-shaped 1mm cuvette. A typical resolution for the instrument was 150 fs (fwhm). Fluorescence decays in the sub-nanosecond region were recorded using a PTI EasyLife LS fluorescence lifetime apparatus. The instrument response function was collected using a ludox solution, and the decay data processed using the en-suite fitting program associated with the equipment. The typical resolution of the instrument was 50 ps. These measurements were made by other members of the MPL.

Infrared spectra

Infrared spectra were recorded using an Avatar 370 DGTS spectrometer. The sample was run in the solid phase after dispersing on a diamond tip.

Cyclic voltammetry

Cyclic voltammetry experiments were performed using a fully automated HCH Instruments Electrochemical Analyzer and a three electrode set-up consisting of a platinum working electrode, a platinum wire counter electrode and an Ag/AgCl reference electrode. Ferrocene was used an internal standard. All studies were performed in deoxygenated solvent (typically CH_3CN or DCM) containing TBATFB (0.2 M) as background electrolyte. Solvents were distilled immediately before making the measurement and were purged thoroughly with dried N_2. The solute concentrations were typically 0.1 mM. Redox potentials were reproducible to within ± 15 mV.

Time-resolved absorption measurements

Femto- to pico-second time-resolved absorption spectra were collected using a pump-probe technique described previously[1]. The femtosecond pulses of a Ti-sapphire generator were amplified by using a multipass amplifier (CDP-Avesta, Moscow,

[1] Tkachenko, N. V.; Rantala, L.; Tuaber, A. Y.; Helaja, J.; Hynninen, P. H.; Lemmetyinen, H. *J. Am. Chem. Soc.* **1999**, *121*, 9378-9387.

Russia) pumped by a second harmonic of the Nd:YAG Q-switched laser (model LF114, Solar TII, Minsk, Belorussia). The amplified pulses were used to generate second harmonic (420 nm) for sample excitation (pump beam) and the white light continuum for a time-resolved spectrum detection (probe beam). The samples were placed in 1 mm rotating cuvettes, and averaging of 100 pulses at a 10 Hz repetition rate was used to improve the signal-to-noise ratio. The typical response time of the instrument was 150 fs (fwhm). Absorption spectra were recorded prior to and after all experiments to check for compound degradation. These measurements were made by other members of the MPL.

Data analysis

Time–resolved transient absorption data were manipulated using a freely available software package. In a typical analysis the whole collection of differential absorption spectra were inspected over the full time scale, and decay kinetics obtained at two specifically chosen wavelengths using an appropriate number of exponentials and instrument response function. Lifetimes obtained by a least-squares fit to the kinetic model were also checked by a global analysis at several different wavelengths. Up-conversion fluorescence lifetimes were obtained by fitting the single-photon-counting data to different kinetic models using a variable Gaussian instrument response function. Analysis was attempted using mono- to tri-exponentials and the stretched exponential function. Best fits were judged by the usual methods of remaining residuals and sigma value.

2.2 Chemicals Used

All chemicals employed in synthetic procedures, together with their supplier and stated purity are presented in *Table 1*.

Chemical name	Supplier	Purity
1-bromonaphthalene	Sigma-Aldrich	97%
1-bromo-4-methyl naphthalene	Sigma-Aldrich	98%
1-butyl-3-methylimidazolium tetrafluoroborate	Sigma-Aldrich	97%
1,4-dibromonaphthalene	Accros Organics	99%
(1,5-cyclooctadiene) (methoxy)iridium(I)dimer	Sigma-Aldrich	Not stated
1-naphthol	Sigma-Aldrich	99%
1,5,6,7-tetrahydro-4H-indol-4-one	Sigma-Aldrich	98%
(2-dicyclohexylphosphino-2',6'-dimethoxyphenyl) (S-PHOS)	Sigma- Aldrich	97%
2,2'-bipyridine	GFS Chemicals	99%
2,3-dichloro-5,6-dicyano-p-benzoquinone	Sigma-Aldrich	98%
2,4-dimethyl-3-ethylpyrrole	Sigma-Aldrich	97%
2,4-dimethylpyrrole	Sigma-Aldrich	97%
4-bromo-1-naphthalene boronic acid	Sigma-Aldrich	Not stated
4-bromobenzalaldehyde	Sigma-Aldrich	99%
4-methoxybenzyl chloride	Sigma-Aldrich	98%
4-nitrobenzaldehyde	Sigma-Aldrich	98%
4,4-di-tertbutyl-2,2dipyridyl	Sigma-Aldrich	98%
α,α,α-trifluorotoluene	Sigma-Aldrich	≥99%
Acetone $-d_6$	Cambridge Laboratory supplies	99.9% atom D
Acetonitrile-d_3	Sigma-Aldrich	99.8% atom D
Barium hydroxide	AnalaR	98%
Bis(1,5-cyclooctadiene)diiridium(I)	Sigma-Aldrich	97%

dichloride		
Bispinacolatodiboron	Fluorochem Sigma-Aldrich	97% 99%
Bistriphenylphosphine palladium (II) dichloride	Sigma-Aldrich	>99%
Boron trifluoride diethyl etherate	Sigma-Aldrich	Purified by redistillation
Caesium fluoride	Alfa-Aesar	99%
Calcium hydride	Sigma-Aldrich	95%
Carbon tetrachloride	Sigma-Aldrich	99%
Chloroform-d_3	Cambridge Laboratory supplies Sigma-Aldrich	99.8% atom D 99.8 atom % D
Dimethyl sulfoxide–d_6	Sigma-Aldrich	99.9 atom % D
Dimethyl formamide	Sigma-Aldrich	99.8%
Ethylmagnesium bromide	Sigma-Aldrich	1.0M solution in THF
Formamide	Sigma-Aldrich	99.5%
Hydrochloric acid, ACS reagent 37%	Sigma-Aldrich	-
Iodine	Sigma-Aldrich	99.8%
Julolidine	Sigma-Aldrich	97%
Magnesium Sulphate (anhydrous)	Sigma-Aldrich	99.5%
Magnesium turnings	Sigma-Aldrich	Not stated
Methanol-d_4	Cambridge Laboratory supplies	99.8% atom D
Methylene chloride-d_2	Cambridge Laboratory supplies	99.96% atom D
Naphthalene-1-boronic acid	Sigma-Aldrich	≥ 95%
n-Butyllithium solution	Sigma-Aldrich	2.5 M in hexanes
N-methyliminodiacetic acid	Sigma-Aldrich	99%
Palladium (II) acetate	Sigma-Aldrich	98%
Phosphorus (V) oxychloride	Sigma-Aldrich	99%
Potassium carbonate (anhydrous)	Sigma-Aldrich	≥99%
Potassium hydrogen difluoride	Sigma-Aldrich	≥99%

Potassium iodide	Sigma-Aldrich	≥99%
Potassium phosphate tribasic	Sigma-Aldrich	99%
Pyrrole	Sigma-Aldrich	98%
Pyrrole-2-carbonitrile	Sigma-Aldrich	96%
Pyrrole-2-carboxaldehyde	Sigma-Aldrich	98%
Pyrrole-2-carboxaldoxime	Alfa Aesar	97%
Sodium acetate (anhydrous)	Fluka	≥99%
Sodium bicarbonate	Sigma-Aldrich	99.7%
Sodium borohydride	Sigma-Aldrich	99.99%
Sodium chloride	Sigma-Aldrich	99.8%
Sodium hydride	Sigma-Aldrich	60% dispersion in mineral oil
Sodium hydroxide pellets	Sigma-Aldrich	99%
Sodium hydrogen carbonate	Sigma-Aldrich	99.5%
Sodium nitrite	Sigma-Aldrich	97%
Sodium sulphate (anhydrous)	Fischer	Not stated
Sulphuric acid	Fluka	95-97%
Tetra-N-butyl ammonium tribromide	Alfa-Aesar	98%
Tetrakis(triphenylphosphine)palladium(0) / $Pd(PPh_3)_4$	Sigma-Aldrich	99%
Tetrahydrofuran-d_8	Cambridge Laboratory supplies	99.95% atom D
Triethylamine	Fluka	≥99.5%
Triisopropyl borate	Sigma-Aldrich	≥98%
Trifluoroacetic acid	Sigma-Aldrich	99%
Trimethylborate	Lancaster	99%
Tert-Butyllithium solution	Sigma-Aldrich	1.7 M in pentane
Toluene-d_8	Cambridge Laboratory supplies	99.94% atom D

Table 1 - Chemicals employed in preparative work.

2.3 Solvents

All solvents used in preparative work are given in *Table* 2, in addition to the method of purification.

Solvent	**Purification**
α,α,α-trifluorotoluene	Used as received from Sigma-Aldrich (anhydrous, sure seal)
Acetonitrile	Used as received from Sigma-Aldrich (anhydrous, sure seal)
2-Butanol	Distilled from calcium hydride under nitrogen
Carbon tetrachloride	Used as received from Sigma-Aldrich
Dichloromethane	Distilled from calcium hydride under nitrogen
Diethyl ether	Distilled from sodium/ benzophenone under nitrogen
1,4-Dioxane	Used as received from Sigma-Aldrich
Ethanol	Used as received from Sigma-Aldrich (anhydrous, sure seal)
Ethyl acetate	Used as received from Riedel-de-Haën
Hexane	Distilled from calcium hydride under nitrogen
Methanol	Used as received from Sigma-Aldrich (anhydrous, sure seal)
Methyl sulfoxide	Used as received from SAFC
N,N-dimethylformamide	Used as received from Sigma-Aldrich (anhydrous, sure seal)
Petroleum ether	Used as received from Riedel-de-Haën
Propanol	Used as received from Sigma-Aldrich (anhydrous, sure seal)
Tertiary-butyl methyl ether	Distilled from calcium hydride under nitrogen
Tetrahydrofuran	Distilled from sodium/ benzophenone under nitrogen
Toluene	Distilled from sodium under nitrogen

Table 2 – The solvents employed in the synthetic protocols detailed within this thesis, along with their method of purification.

2.4 Experimental Protocol

The following section of the thesis details the synthetic procedures carried out in order to synthesise the desired compounds which are discussed and studied within this work. All glassware was checked for staining, residues and overall cleanliness prior to use and was again washed with water and acetone and thoroughly dried in the oven overnight. Reaction vessels were also degassed prior to use. A stirrer bar was added to every reaction with the exception of those conducted under microwave (CEM Discover) irradiation.

2,3,6,7-Tetrahydro-1H, 5H, benzo[i,j]quinolizine- 9-carboxaldehyde[2]

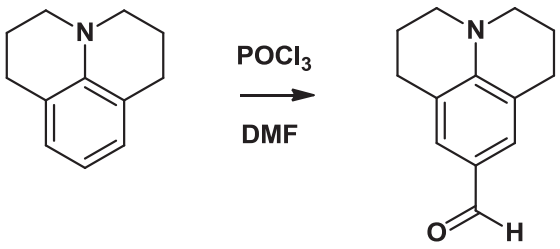

A 100 mL 2-necked flask charged with anhydrous DMF (10 mL, 129 mmol, 7.5 eq) was cooled in an ice bath. Phosphorus oxychloride (1.61 mL, 17.3 mmol, 1 eq) was then added dropwise with stirring to generate a yellow solution. After 30 minutes, julolidine (3g, 17.3 mmol, 1 eq) in DMF (10 mL, 129 mmol, 7.5 eq) was added and the solution heated at 90˚C for 3 hours over which time it became yellow/ pale brown in colour.

The reaction mixture was then cooled, poured onto crushed ice and neutralized to pH 6-8 by an addition of saturated aqueous sodium acetate solution (~20 mL). The precipitate was collected by filtration and the crude material was then purified by column chromatography on silica gel, with DCM: petrol (6:1) as eluent. This afforded **julolidine 9-carboxaldehyde**, a yellow crystalline solid (2.62g, 75% yield), Mp = 80-81˚C. (Lit. 82-83˚C)

^{1}H NMR ($CDCl_3$, 300 MHz): δ (ppm) = 9.49 (s, 1H), 7.18 (s, 2H), 3.19 (t, J = 6.0 Hz, 4H), 2.66 (t, J = 6.0 Hz, 4H), 1.87 (m, 4H).

All chemical shift values were consistent with those stated in the literature[2].

[2] Smith, P. A. S.; Yu, T. Y. *Journal of Organic Chemistry*, **1952**, *17*, 1281.

5-2,3,6,7-Tetrahydro-1H, 5H, benzo[i,j]quinolizine dipyrromethane

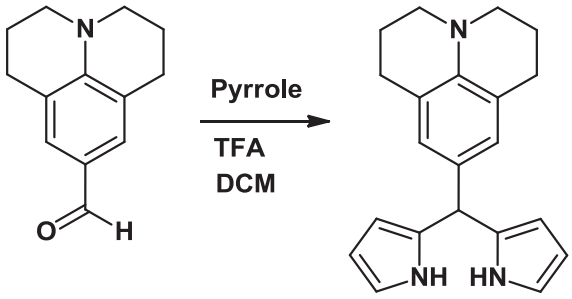

To a degassed solution of julolidine 9-carboxaldehyde (1.74g, 8.6 mmol, 1 eq) in redistilled pyrrole (41.78 mL, 602 mmol, 70 eq), was added a catalytic quantity of trifluoroacetic acid (0.064 mL, 0.86 mmol, 0.1 eq) which turned the yellow solution red/ purple. The reaction mixture was then protected from light and left to stir overnight. The following day, the reaction was heated to 40˚C for 4 hours and then left stirring overnight again at room temperature. The next day, the pyrrole was removed under reduced pressure and the reaction mixture diluted with DCM (50 mL) then washed with 0.1 M NaOH (3 x 100 mL), water (3 x 50 mL) before being separated and dried over sodium sulphate. Removal of the solvent under reduced pressure afforded a brown oily residue which was purified by column chromatography on basic alumina, using DCM / petrol (1:2) as eluent. This gave **julolidine dipyrromethane**, as a pale orange crystalline solid (0.81g, 30% yield), Mp = 118-119˚C.

^{1}H NMR ($CDCl_3$, 300 MHz): δ (ppm) = 7.90 (s, 2H), 6.68 (s, 4H), 6.20 (s, 2H), 6.00 (s, 2H), 5.28 (s, 1H), 3.18 (t, J = 6.0 Hz, 4H), 2.76 (t, J = 6.0 Hz, 4H), 2.02 (m, 4H).

^{13}C NMR ($CDCl_3$, 75 MHz): δ (ppm) = 141.9, 133.5, 129.1, 126.8, 121.8, 116.6, 108.3, 106.7, 50.1, 43.3, 27.7, 22.2.

Acc Mass calculated for $C_{21}H_{23}N_3$: 318.1964 Found 318.1970.

4,4'-Difluoro-8-(julolidinyl)-4-bora-3a,4a-diaza-s-indacene

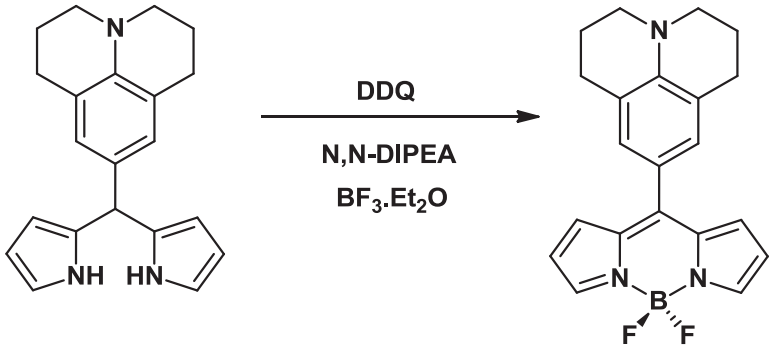

To a 3-necked flask, containing DCM (100 mL) was added julolidine dipyrromethane (0.81g, 2.55 mmol, 1eq) and the solution stirred for 5 minutes prior to the addition of DDQ (1.16g, 5.1 mmol, 2 eq). This caused the solution to turn from yellow to dark blue/ purple. The solution was then stirred at room temperature for 18 hours. N,N-diisopropylethylamine (2.53 mL, 14.54 mmol, 5.7 eq) and boron trifluoride diethyletherate (2.59 mL, 20.4 mmol, 8 eq) were added and the reaction was stirred overnight at room temperature. The solution (which was deep brown with an orange tint) was then washed with water (3 x 100 mL) and brine (3 x 100 mL). The separated organic fractions were dried with magnesium sulphate, filtered and the solvent removed under rotary evaporation to afford a deep blue solid. The crude material was then purified using column chromatography on silica gel. DCM / petrol (2:1) was used as eluent to afford a deep blue crystalline solid, **JULBD** (0.167g, 18% yield), Mp = 209-210˚C.

^{1}H NMR ($CDCl_3$, 300 MHz): δ (ppm) = 7.83 (s, 2H), 7.14 (s, 2H), 7.06 (d, *J* = 4.0 Hz, 2H), 6.52 (dd, *J* = 4.0, *J*'= 1.9, 2H), 3.32 (t, *J* = 6.0 Hz, 4H), 2.81 (t, *J* = 6.0 Hz, 4H), 2.01 (m, 4H).

^{13}C NMR ($CDCl_3$, 75 MHz): δ (ppm) = 148.6, 146.1, 140.7, 134.2, 131.1, 130.3, 121.1, 120.9, 117.1, 50.0, 27.7, 21.4.

^{11}B NMR (160 MHz, $CDCl_3$) δ = -0.61 (t, *Jav* = 29.5 Hz).

^{19}F NMR (470 MHz, $CDCl_3$) δ = -145.07 (q, *Jav* = 36.6 Hz).

MS (EI): m/z: 363 $[M]^+$ for $C_{21}H_{20}N_3F_2B$.

Elemental analysis calcd (%) for $C_{21}H_{20}N_3F_2B$: C 69.44, H 5.55, N 11.56 found C 68.95, H 5.68, N 10.99.

IR (neat): cm^{-1} = 1523, 1475 (C=C, C=N), 1190 (B-F)

5-Phenyldipyrromethane[3]

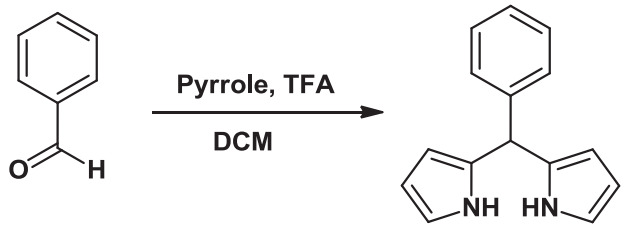

To a degassed solution of benzaldehyde (1.02 mL, 10 mmol, 1eq) in redistilled pyrrole (48.57 mL, 700 mmol, 70 eq), a catalytic quantity of trifluoroacetic acid (0.074 mL, 1 mmol, 0.1 eq) was added. This turned the yellow solution red/ purple. The flask was then protected from light and the reaction mixture left to stir overnight. The following day, a further portion of TFA (0.074 mL, 1 mmol, 0.1 eq) was added and the reaction heated for 4h then left stirring overnight until TLC indicated complete consumption of the aldehyde. The following day, the pyrrole was removed under reduced pressure and the reaction mixture diluted with DCM (50 mL), which was washed with 0.1M NaOH (3 x 100 mL), water (3 x 50 mL) before being separated and dried over sodium sulphate. The solvent was then removed under reduced pressure to give a brown oily residue. The crude product was purified by column chromatography on basic alumina using DCM and petrol (1:2) as eluent to afford **phenyl dipyrromethane**, a yellow/ pale brown solid (1.734g, 78% yield.) M.pt = 97-98˚C (lit. 100-101 ˚C)[3].

^{1}H NMR ($CDCl_3$, 300 MHz): δ (ppm) = 7.85 (br s, 2H), 7.25 (m, 5H), 6.66 (ddd, *J* = 2.6 Hz, *J'* = 2.4 Hz, *J"* = 1.5 Hz, 2H), 6.16 (dd, *J* = 6.0 Hz, *J'* = 2.7 Hz, 2H), 5.91 (m, 2H), 5.44 (s, 1H).

All chemical shifts are consistent with literature values.[3]

[3] Wilson, R. M.; Hengge, A. *J. Org Chem*., **1987**, *52*, 2706.

4,4'-Difluoro-8-(phenyl)-4-bora-3a,4a-diaza-s-indacene[4,5]

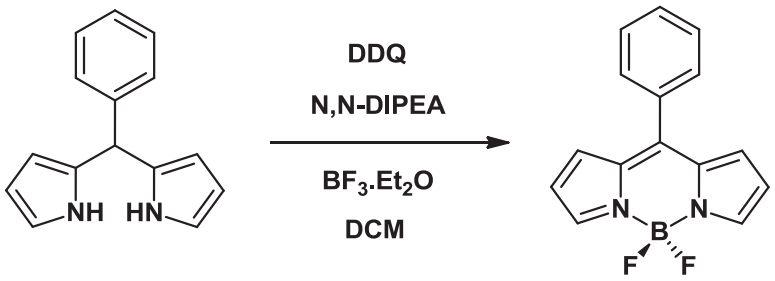

To 3-necked flask was added phenyl dipyrromethane (1.65g, 7.43 mmol, 1 eq) and DCM (200 mL) and the grey/ brown solution stirred for 5 minutes prior to the addition of DDQ (3.38g, 15 mmol, 2 eq). This turned the reaction mixture deep blue. The solution was then left stirring overnight at room temperature. N,N-diisopropylethylamine (7.37 mL, 42 mmol, 5.7 eq) and boron trifluoride diethyletherate (7.53 mL, 59 mmol, 8 eq) were added and the reaction stirred at room temperature overnight. The solution (which was deep brown with an orange tint) was then washed with water (3 x 150 mL) and brine (3 x 150 mL). The separated organic fractions were dried with magnesium sulphate, filtered and the solvent removed under rotary evaporation to afford a brown/ orange solid residue. The crude material was then purified using column chromatography on silica gel. DCM / petrol (2:1) was used as eluent and this gave **PHBD**, a red / orange crystalline solid. (1.33 g, 67% yield). M.pt = 102-103˚C. Lit. = 99-100˚C[4].

^{1}H NMR ($CDCl_3$, 300 MHz): δ (ppm) = 7.94 (s, 2H), 7.54 (m, 5H), 6.93 (d, *J* = 3.7 Hz, 2H), 6.54 (d, *J* = 3.7 Hz, 2H).

^{13}C NMR ($CDCl_3$, 75 MHz): δ (ppm) = 147.3, 144.0, 134.8, 133.6, 131.5, 130,7, 130.4, 128.4, 118.5.

^{11}B NMR (160 MHz, $CDCl_3$) δ = -0.79 (t, *Jav* = 28.3 Hz).

^{19}F NMR (470 MHz, $CDCl_3$) δ = -141.42 (q, *Jav* = 31.4 Hz).

IR (neat): cm^{-1} = 1530, 1474 (C=C, C=N), 1183 (B-F).

[4] Wagner, R. W.; Lindsey, J. S. *Pure & Appl. Chem*. **1996**, *68*, 1373.
[5] Schmidt, E. Y.; Trofimov, B. A.; Mikhaleva, A. I.; Zorina, N. V.; Protzuk, N. I.; Petruchenko, K. B.; Ushakov, I. A.; Dvorko, M. Y.; Méallet-Renault, R.; Clavier, G.; Vu, T. T.; Tran, H. T. T.; Pansu, R. B., *Chem. Eur. J*. **2009**, *15*, 5823.

5-(4-Nitrophenyl) dipyrromethane[6]

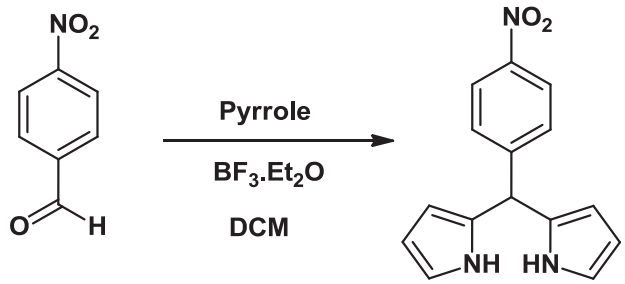

To a degassed solution of 4-nitro-benzaldehyde (1.25g, 8.29 mmol, 1 eq) in redistilled pyrrole (40 mL, 580 mmol, 70 eq) was added a catalytic quantity of boron trifluoride diethyletherate (4 drops). The flask was then protected from light and the reaction mixture stirred at room temperature overnight. The following day, TLC analysis indicated complete consumption of 4-nitro-benzaldehyde. Therefore, the reaction was quenched by the addition of an excess of crushed sodium hydroxide pellets, followed by a 30 minute stir. The pyrrole solvent was then removed by vacuum distillation and the mixture filtered to omit any residual sodium hydroxide pellets. This gave the crude dipyrromethane, which was then purified by column chromatography on basic alumina using ethyl acetate and petrol (2:5) as eluent. This gave **nitrophenyl dipyrromethane**, a red/orange crystalline solid (0.46g, 18% yield). M.pt = 158-159˚C (Lit = 159-160˚C)[6].

^{1}H NMR ($CDCl_3$, 300 MHz): δ (ppm) = 8.16 (d, *J* = 8.7 Hz, 2H), 8.00 (br s, 2H), 7.37 (d, *J* = 8.7 Hz, 2H), 6.74 (m, 2H), 6.18 (q, *J* = 3.0 Hz, 2H), 5.87 (s, 2H), 5.58 (s, 1H).

All chemical shift values were consistent with those stated in the literature.[6]

[6] Litter, B. J.; Miller, M. A.; Hung, C-J.; Wagner, R. W.; O'Shea, D. F. *J. Org. Chem*., **1999**, *64*, 4.

4,4'-Difluoro-8-(nitrophenyl)-4-bora-3a,4a-diaza-s-indacene

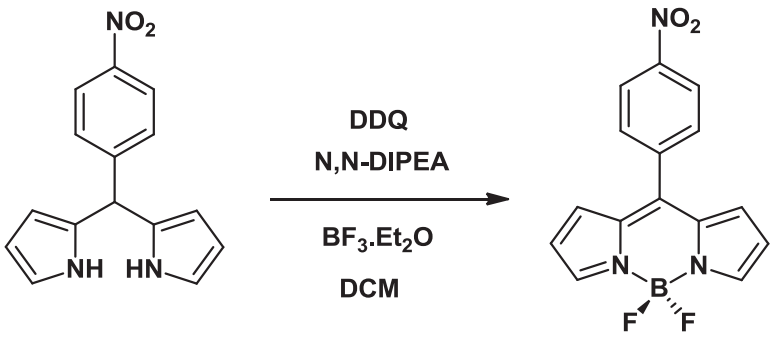

To a 3-necked flask containing DCM (100 mL) was added nitrophenyl dipyrromethane (0.455g, 1.7 mmol, 1 eq) and the orange solution was left to stir for 5 minutes. To this solution was added DDQ (0.77g, 3.4 mmol, 2 eq), which generated a dark blue/ purple solution. This was then stirred at room temperature for 18 hours. N,N-diisopropylethylamine (1.68 mL, 9.67 mmol, 5.7 eq) and boron trifluoride diethyletherate were added and the reaction was stirred overnight at room temperature. The brown solution was then washed with water (3 x 100 mL) and brine (3 x 100 mL). The separated organic fractions were dried with magnesium sulphate, filtered and the solvent removed under rotary evaporation to afford a deep blue solid. The crude material was purified using column chromatography on silica gel with DCM/ petrol (2:1) as eluent to afford a red crystalline solid, **NITBD** (0.256g, 48.1 % yield), M.pt = 277-278˚C.

^{1}H NMR ($CDCl_3$, 300 MHz): δ (ppm) = 8.41 (d, *J* = 8.8, 2H), 8.00 (s, 2H), 7.76 (d, *J* = 8.8, 2H), 6.85 (d, *J* = 4.0, 2H), 6.59 (d, *J* = 4.0, 2H).

^{13}C NMR ($CDCl_3$): 149.1, 145.6, 143.8, 139.8, 134.5, 131.2, 131.2, 123.7, 119.4.

^{11}B NMR (160 MHz, $CDCl_3$) δ = -0.71 (t, *Jav* = 28.3 Hz).

^{19}F NMR (470 MHz, $CDCl_3$) δ = -144.86 (q, *Jav* = 28.0 Hz).

IR (neat): cm^{-1} = 1525 (NO_2), 1544, 1479 (C=C, C=N), 1171 (B-F).

MS (EI): *m/z* 313 $[M]^+$ for $C_{15}H_{10}N_3O_2BF_2$.

Elemental analysis calcd (%) for $C_{15}H_{10}BF_2N_3O_2$ C 57.55, H 3.22, N, 13.42 found C, 58.65, H 3.30, N 12.33. (Note: a partial solvate of THF (e.g., 0.25) is probably associated with the crystal sample which accounts for the high carbon content).

4,4'-Difluoro-8-(julolidinyl)-1,3,5,7-tetramethyl-2,6-diethyl-4-bora-3a,4a-diaza-s-indacene

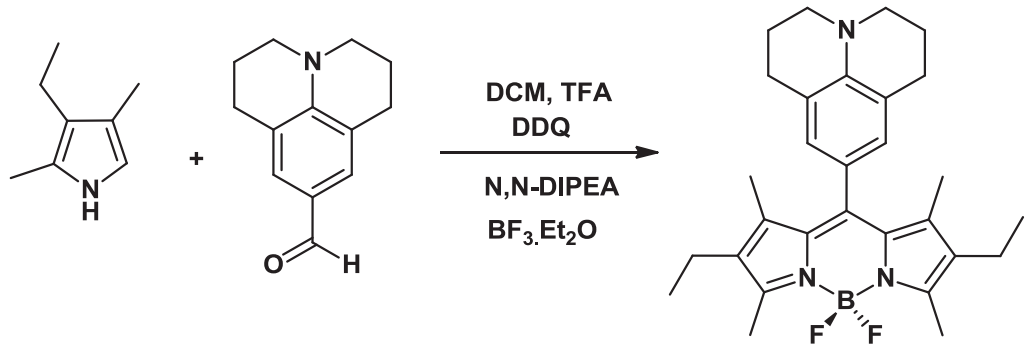

To a stirred solution of 2,4-dimethyl-3-ethylpyrrole (1.75 mL, 12.9 mmol, 2.1 eq) and julolidine 9-carboxaldehyde (1.25g, 6.16 mmol, 1 eq) in DCM (300 mL) was added a catalytic quantity of TFA (3 drops). This turned the solution from pale yellow to purple. The reaction mixture was then stirred at room temperature until TLC showed complete consumption of the aldehyde (18 hours). DDQ (1.47g, 6.47 mmol, 1.05 eq) was then added in a single portion (this turned the mixture deep blue) and the reaction was left to stir at room temperature for 18 hours. N,N-diisopropylethylamine (12.88 mL, 73.9 mmol, 12 eq) and boron trifluoride diethyletherate (13.11 mL, 103 mmol, 16.8 eq) were added and the reaction was stirred overnight at room temperature. The solution was then washed with water (3 × 200 mL) and brine (3 × 200 mL). The separated organic fractions were dried over magnesium sulphate, filtered and the solvent removed under rotary evaporation to afford a dark violet residue with a green tint. The crude material was purified using column chromatography on silica gel with toluene as eluent to afford a green crystalline solid with a purple tint. This solid was then recrystallized by slow diffusion from DCM and petrol to give **JULBD2** (0.30g, 10% yield). The colour of the crystals did not alter upon recrystallisation. M.pt = 240-241˚ C.

^{1}H NMR ($CDCl_3$, 300 MHz): δ (ppm) = 6.59 (s, 2H), 3.20 (t, *J* = 6.0, 4H), 2.74 (t, *J* = 6.0 Hz, 4H), 2.51 (s, 6H), 2.31 (q, *J* = 7.5 Hz, 4H), 1.99 (m, 4H), 1.47 (s, 6H), 0.99 (t, *J* = 7.5, 6H).

^{13}C NMR ($CDCl_3$, 75 MHz): δ (ppm) = 152.53, 142.82, 142.29, 138.49, 132.09, 131.45, 126.47, 122.15, 121.75, 49.99, 27.53, 22.04, 17.09, 14.64, 12.39, 12.21.

^{11}B NMR (160 MHz, $CDCl_3$) δ = -0.12 (t, *Jav* = 33.2 Hz).

^{19}F NMR (470 MHz, $CDCl_3$) δ = -145.68 (q, *Jav* = 32.7 Hz).

IR (neat): cm^{-1} = 2966, 2930, 2871 (C-H), 1536, 1472 (C=C, C=N), 1184 (B-F).

1-Bromo-4-(bromomethyl)naphthalene[7]

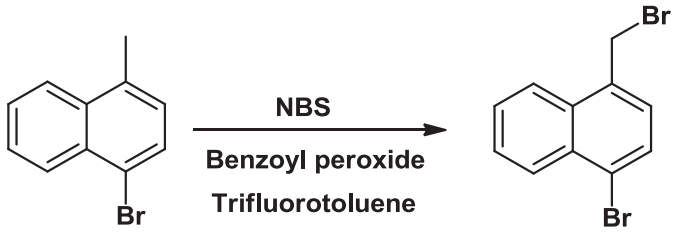

In a 2-necked 250 mL round bottomed flask fitted with a reflux condenser, a solution of 1-bromo-4-methyl naphthalene (4.3 mL, 27.6 mmol, 1 eq), in α,α,α-trifluorotoluene (100 mL) was purged with nitrogen for one hour. NBS (5.40g, 30.36 mmol, 1.1 eq) and benzoyl peroxide (0.267g, 1.10 mmol, 0.04 eq) were then added under a stream of nitrogen and the mixture was refluxed overnight. The reaction mixture was then left to cool to room temperature and filtered. The filtrate was concentrated to dryness in vacuo and the crude material purified by column chromatography on silica gel with hexane / ethyl acetate (11:1) as eluent. The pure product was isolated as a pale yellow fluffy solid, (8.0g, 97% yield). M.pt = 103-105 ºC (Lit = 102-104ºC)[7].

^{1}H NMR ($CDCl_3$): δ = 8.14-8.34 (2m, 2H, aromatic), 7.64-7.70 (m, 2H, aromatic), 7.73 (d, *J* = 8 Hz, 1H, aromatic), 7.39 (d, *J* = 8 Hz, 1H, aromatic), 4.92 (s, 2H, CH_2) ppm.

The spectroscopic data was in accordance with the literature[7].

[7] Carreno, M. C.; Hernandez-Sanchez, R.; Mahugo, J.; Urbano, A.; *J. Org. Chem.* **1999**, *64,* 1387.

4-Bromonaphthaldehyde[8]

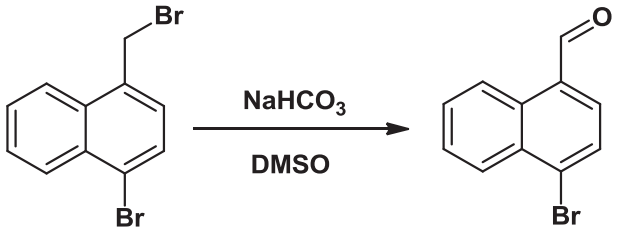

To a 250 mL round bottomed flask equipped with a stirrer bar was added previously synthesized 1-bromo-4-bromomethylnaphthalene (8.0g, 27 mmol, 1 eq) and DMSO (90 mL). The reaction mixture was purged with nitrogen for one hour prior to the addition of $NaHCO_3$ (4.54g, 54 mmol, 2 eq). The solution was then stirred at 95˚C for 3 hours, by which time TLC analysis of the reaction mixture showed complete consumption of the starting material. The brown solution was then washed with water and the separated organic fractions were then dried over sodium sulphate, filtered and the solvent removed *in vacuo* to leave a pale brown residue. This material was purified by column chromatography on silica gel using hexane/ ethyl acetate (9:1) as eluent to give the pure product as a fluffy white solid, (5.6g, 90% yield.) M.pt = 119-120ºC (Lit = 120-122ºC)[8].

^{1}H NMR ($CDCl_3$): δ = 7.66-7.82 (m, 2H, aromatic), 7.81 (d, *J* = 8.0 Hz, 1H, aromatic), 7.97 (d, *J* = 8.0 Hz, 1H, aromatic), 8.36 (d, *J* = 8.0 Hz, 1H, aromatic), 9.26 (d, *J* = 8.0 Hz, 1H), 10.35 (s, 1H, CHO) ppm.

The spectroscopic data was in accordance with the literature[8].

[8] Chen, H.; Luzy, J-P.; Gresh, N.; Garbay, C. *Eur. J. Org. Chem*. **2006**, *10*, 2329.

4,4'-Difluoro-8-(para-bromonaphthyl-)1,3,5,7-tetramethyl-2,6-diethyl-4-bora-3a,4a-diaza-s-indacene

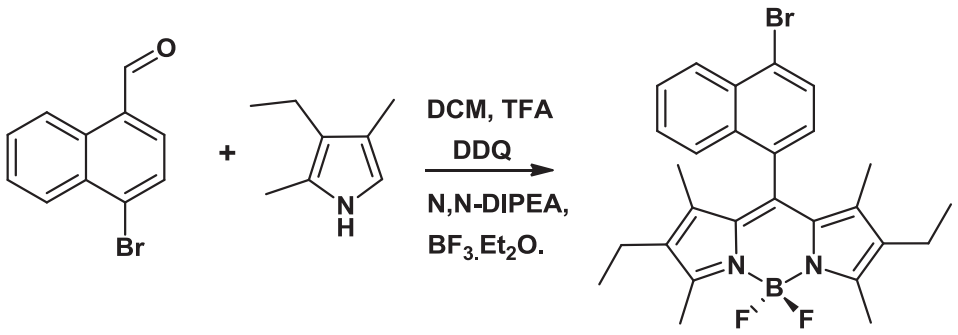

To a nitrogen purged solution of 2,4-dimethyl-3-ethylpyrrole (1.46 mL, 10.84 mmol, 2.1 eq.) and para-bromonaphthaldehyde (1.21g, 5.16 mmol, 1.0 eq.) in DCM (200 mL) was added dropwise a catalytic quantity of TFA (2 drops). The reaction was allowed to stir at room temperature for 18 hours, by which time TLC analysis showed complete consumption of the aldehyde. To this solution was added DDQ (1.23 g, 5.4 mmol, 1.05 eq.) which turned the solution dark blue/ purple. The solution was then stirred overnight at room temperature. N,N-diisopropylethylamine (10.79 mL, 61.92 mmol, 12.0 eq.) and boron trifluoride diethyletherate (10.99 ml, 86.69 mmol, 16.8 eq.) were added, and again the reaction was left to stir overnight at room temperature. The mixture was then washed with water (3 x 150 mL) and brine (3 x 150 mL) and the separated organic fractions were dried over magnesium sulphate and filtered. The solvent was removed in vacuo to afford a pink/ purple residue with a greenish tint. The crude material was then purified by column chromatography on silica gel using toluene as eluent to afford a purple/ green crystalline solid, **BRNBD** (1.55g, 59% yield). This solid was then frozen in ether and the solvent removed at the pump and finally washed with petrol. M.pt = 197-198˚C.

^{1}H NMR ($CDCl_3$): δ = 8.34 (d, *J* = 8.2 Hz, 1H, aromatic), 7.91 (d, *J* = 7.3 Hz, 1H, aromatic), 7.89 (d, *J* = 8.2 Hz, 1H, aromatic), 7.64 (t, *J* = 7.1 Hz, 1H, aromatic), 7.51 (t, *J* = 7.1 Hz, 1H, aromatic), 7.29 (d, *J* = 7.3 Hz, 1H, aromatic), 2.61 (s, 6H, CH_3), 2.27 (q, *J* = 7.5 Hz, 4H, $C\underline{H_2}CH_3$), 1.02 (s, 6H, CH_3), 0.96 (t, *J* = 7.5 Hz, 6H, $CH_2C\underline{H_3}$) ppm.

^{13}C NMR ($CDCl_3$, 75 MHz): δ (ppm) = 154.07, 137.81, 136.94, 133.24, 133.03, 132.76, 131.86, 130.97, 129.75, 127.89, 127.83, 127.23, 126.42, 125.57, 123.72, 16.85, 14.42, 12.41, 11.14.

^{11}B NMR (160 MHz, $CDCl_3$) δ = -0.00 (t, *Jav* = 32.0 Hz).

^{19}F NMR (470 MHz, $CDCl_3$) δ = -145.6 (m)

EI-MS : m/z calc. for $C_{27}H_{28}BBr_2F_2N_2$ = 509 found 509 $[MH]^+$.

IR (neat): cm^{-1} = 2963, 2928, 2870 (C-H), 1534, 1474 (C=C, C=N), 1182 (B-F)

9-Bromo-(2,3,6,7-Tetrahydro-1H, 5H, benzo[i,j]quinolizine)[9]

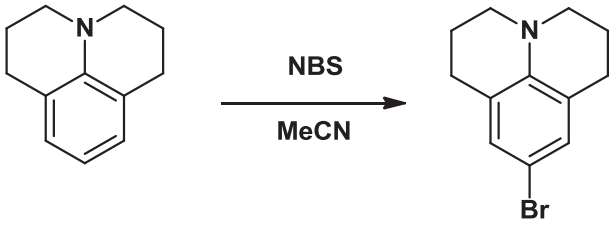

To a 2-necked round bottomed flask was added julolidine (2.50g, 14.43 mmol, 1eq) in freshly distilled acetonitrile (200 mL). This was purged with nitrogen for one hour prior to the addition of N-bromosuccinimide (2.54g, 14.43 mmol, 1 eq) which turned the mixture deep yellow from red/orange. The reaction was stirred overnight at room temperature. The crude product was then taken up in dichloromethane and washed with water. The separated organic fractions were then reduced *in vacuo* to leave a deep red, oily material. This was then purified using column chromatography on silica gel with DCM/ petrol (1:3) as eluent to afford a red oily solid (2.25g, 62% yield.)

^{1}H NMR (300 MHz, $CDCl_3$): δ = 7.11 (s, 2H), 3.33 (t, J = 6.0 Hz, 4H), 2.92 (t, J = 6.0 Hz, 4H), 2.17 (m, 4H).

The spectroscopic data was in accordance with the literature[9].

[9] Zysman-Colman, E.; Arias, K.; Siegel, J. S. *Canadian Journal of Chemistry*, **2009**, *87*, 440.

9-(4,4,5,5-Tetramethyl-1, 3, 2-dioxaborolan-2-yl)-2,3,6,7-Tetrahydro-1H, 5H, benzo[i,j]quinolizine

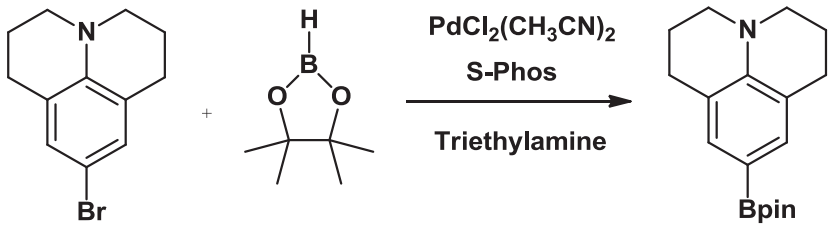

A flame dried Schlenk flask was charged with $PdCl_2(CH_3CN)_2$ (0.02g, 0.08 mmol, 4 mol %), S-Phos (0.131g, 0.32 mmol,16 mol%) and 9-bromojulolidine (0.504g, 2 mmol, 1eq). The Schlenk tube was then capped with a rubber septum and thoroughly degassed. Triethylamine (2 mL) and pinacolborane (0.384g, 3 mmol, 1.5 eq) were then added, followed by dioxane (8 mL). The Schlenk tube was sealed and the reaction stirred at 80ºC for 24 hours. The reaction solution was then filtered through a thin pad of celite and fully eluted with ethyl acetate. The eluent was then concentrated under reduced pressure and the crude material obtained purified by column chromatography on silica gel (DCM/ Petrol) (1:1) to give a very pale yellow slightly oily solid (0.24g, 40 % yield).

^{1}H NMR (300 MHz, $CDCl_3$): δ = 7.17 (s, 2H), 3.09 (t, 4H, *J* = 6.0 Hz), 2.66 (t, 4H, *J* = 6.0 Hz), 1.86 (m, 4H), 1.23 (s, 12H).

^{13}C NMR (300 MHz, $CDCl_3$): δ = 145.45, 133.79, 126.90, 120.34, 82.99, 50.14, 27.64, 24.85, 22.12.

^{11}B (400 MHz, $CDCl_3$): δ 29.91 (s)

4,4'-Difluoro-8-(para-julolidine-naphthyl-)-1,3,5,7-tetramethyl-2,6-diethyl-4-bora-3a,4a-diaza-s-indacene

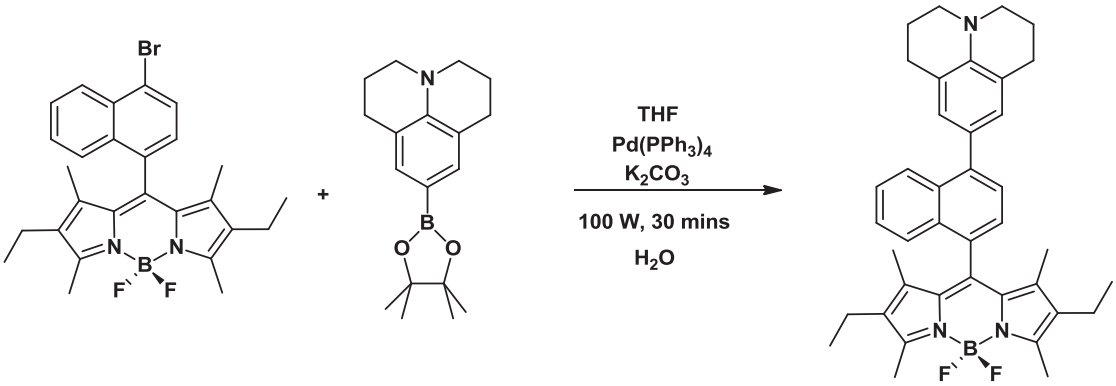

To a 3-necked round bottomed flask was added julolidine boronic ester (0.05g, 0.167 mmol, 2eq) in freshly distilled THF (5 ml). This was degassed for 30 minutes prior to the addition of BRNBD (0.043g, 0.084 mmol, 1eq) and potassium carbonate (0.0008g, 0.006 mmol, 0.07 eq) solubilized in water (0.5 mL). This mixture was then degassed for a further 45 minutes, before the flask was transferred to the microwave, a degassed condenser inserted and the stirrer bar removed. Tetrakis(triphenylphosphine)palladium(0) (0.0097g, 0.008 mmol, 10 mol %) was rapidly added, the flask stoppered and the reaction heated (μW, 30 min, 100 Watt). The reaction mixture was then filtered through a silica plug and the solvent removed *in vacuo*. The crude material was then taken up in dichloromethane (50 mL), washed with sodium bicarbonate solution (0.6M, 50 mL) and the combined organic fractions dried over magnesium sulphate. The crude material was then filtered and again the solvent removed under reduced pressure. Purification was achieved by flash column chromatography (DCM/ petrol 2:1) to give the product, **JULNBD** as a pink solid, (0.084g, 50.2% yield).

^{1}H ($CDCl_3$, 300 MHz): δ = 8.08 (d, *J* = 8.3 Hz, 1H), 7.77 (d, *J* = 8.3 Hz, 1H), 7.35 (m, 4H), 6.94 (s, 2H), 3.17 (t, *J* = 6.0 Hz, 4H), 2.80 (t, *J* = 6.0 Hz, 4H), 2.50 (s, 6H), 2.19 (q, *J* = 7.5 Hz, 4H), 2.00 (m, 4H), 0.97 (s, 6H), 0.88 (t, *J* = 7.5 Hz, 6H).

^{13}C ($CDCl_3$): δ = 153.60, 142.41, 142.11, 139.14, 138.37, 132.55, 132.40, 131.90, 131.42, 131.41, 128.69, 127.23, 126.75, 126.52, 126.32, 125.98, 125.72, 125.42, 121.30, 50.05, 27.74, 22.10, 17.06, 14.62, 12.56, 11.26.

^{11}B ($CDCl_3$): δ = 0.00 ppm, triplet, *J*av = 33.22.

^{19}F ($CDCl_3$): δ -145.55, triplet, *J*av = 33.23.

1-Bromo-naphthalene-4-MIDA boronate

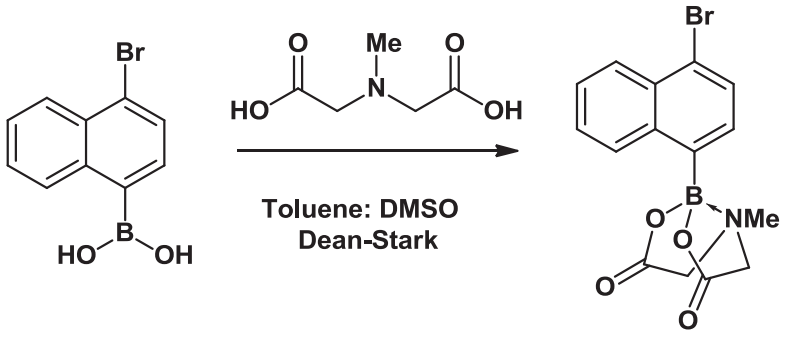

To a 100 mL round bottomed flask was added 4-bromo-1-naphthalene boronic acid (0.3g, 1.20 mmol, 1 eq), N-methyliminodiacetic acid (0.176g, 1.20 mmol, 1eq), toluene (40 mL) and DMSO (4mL). The flask was fitted with a Dean Stark trap and a condenser and the solution was refluxed with stirring overnight. It was then allowed to cool to room temperature before being concentrated under reduced pressure initially on the rotary evaporator to remove excess toluene, then using a kugelrohr to remove residual DMSO. The material was a colourless oil which crystallized upon cooling to room temperature to generate a white crystalline solid (0.36g, 79% yield).

^{1}H ($CDCl_3$, 300 MHz): δ = 8.52 (m, 1H), 8.38 (m, 1H), 7.91 (d, *J* = 7.7 Hz, 2H), 7.68 (t, *J* = 7.7 Hz, 2H), 4.48 (d, *J* = 17.1, 2H,), 4.21 (d, *J* = 17.1, 2H), 2.64 (s, 3H).
^{13}C ($CDCl_3$): δ = 169.84, (C=O) 138.96, 134.59, 132.85, 130.31, 128.49, 127.84, 127.66, 127.24, 126.01, 122.60, 63.06, (NCH_2) 47.82 (NCH_3).
^{11}B ($CDCl_3$): δ = 11.24 ppm (s).

For further information on the MIDA protecting group please refer to the reference below.[10]

[10] Gillis, E. P.; Burke, M. D. *J. Am. Chem. Soc*, **2007**, *129*, 6716.

4,4'-Difluoro-4-bora-(3a,4a)-diazaindacene[11]

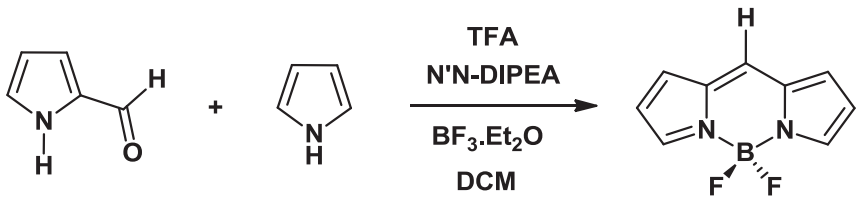

To a 500 mL round bottomed flask was added a solution of pyrrole (0.28 mL, 4mmol, 1 eq) and trifluoroacetic acid (2 drops) in dichloromethane (100 mL). This was degassed and stirred at room temperature for an hour, prior to the dropwise addition of 2-formyl pyrrole (0.456 mL, 4.8 mmol, 1.2 eq) dissolved in dichloromethane (50 mL). The reaction was then stirred until the aldehyde was shown by TLC to be completely consumed. The material was then cooled in an ice bath prior to addition of N'N-diisopropylethylamine (14 mL, 80.4 mmol, 20.1 eq) solubilised in dichloromethane (40 mL). This was followed by the addition of boron trifluoride diethyletherate (20 mL, 157.8 mmol, 39.5eq) in DCM (40 mL). The reaction was then stirred at 25˚C overnight.

It was then washed with water (3 x 100 mL) and brine (3 x 100 mL), dried over magnesium sulphate, filtered and the solvent evaporated to give the crude product. This was then purified by column chromatography using toluene as eluent.

^{1}H ($CDCl_3$, 400 MHz): δ = 7.90 (s, 2H), 7.42 (s, 1H), 7.15 (d, *J* = 3.0 Hz, 2H), 6.55 (d, *J* = 3.0 Hz, 2H)

^{13}C ($CDCl_3$, 500 MHz): δ = 118.89, 131.39, 131.02, 135.26, 145.17.

^{11}B NMR (160 MHz, $CDCl_3$) δ = -0.63 (t, *Jav* = 28.3 Hz).

^{19}F NMR (470 MHz, $CDCl_3$) δ = -145.02 (q, *Jav* = 37.6 Hz).

[11]Schmitt, A.; Hinkeldey, B.; Wild, M.; Jung, G. *Journal of fluorescence*, **2009**, *19*, 755.

4,4'-Difluoro-1,3,5,7-tetramethyl-2,6-diethyl-4-bora-3a,4a-diaza-s-indacene[12,13]

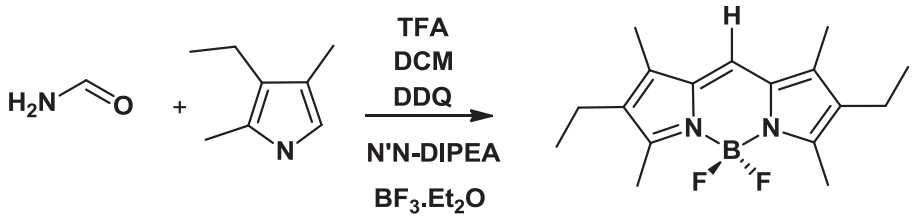

To a 1L round bottomed flask, charged with freshly distilled DCM (500 mL) were added formamide (0.88 mL, 22.2 mmol, 1 eq) and 2,4-dimethyl-3-ethyl pyrrole (6.29 mL, 46.6 mmol, 2.1eq). These reagents were degassed together at room temperature and then a catalytic quantity of trifluoroacetic acid added (2 drops). The reaction was then stirred at room temperature until TLC showed complete consumption of the aldehyde. Next, DDQ (5.29g, 23.3 mmol, 1.05 eq) was added in a single portion, which turned the reaction mixture deep blue and the reaction was left to stir at room temperature overnight. Next, N,N-diisopropylethylamine (26.6 mmol, 46.33 mL, 12 eq) and boron trifluoride diethyl etherate (316 mmol, 40 mL, 14.2 eq) were added. The reaction was then stirred at room temperature overnight. The reaction mixture was then washed with brine (3 x 300mL) and with water (3 x 300 mL), filtered through a sintered funnel then concentrated to dryness on the rotary evaporator. The crude product was purified by column chromatography on silica gel (toluene) to give a green/ purple solid (2.02 g, 30% yield). M.pt = 187-189 ºC (Lit = 187-188ºC).[11]

^{1}H ($CDCl_3$, 300 MHz): δ = 6.94 (s, 1H), 2.50 (s, 6H), 2.38 (q, *J* = 7.5 Hz, 4H), 2.16 (s, 6H), 1.06 (t, *J* = 7.5 Hz, 6H).

The spectroscopic data was in accordance with the literature[12,13].

[12] Wood, T. E.; Berno, B.; Beshara, C. S.; Thompson, A. *J. Org. Chem*, **2006**, *71*, 2964.

[13] Falk, H.; Hofer, O.; Lehner, H. *Monatsh. Chem*., **1974**, *105*, 169.

1-(Ethoxymethyl)-4-methoxybenzene[14]

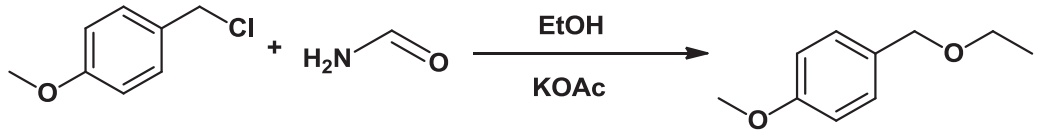

To a 100mL round bottomed flask were added ethanol (50 mL), formamide (1mL, 25.2 mmol, 1 eq) and potassium acetate (0.35g, 2.5 mmol, 0.1eq). This mixture was degassed for 1 hour at room temperature and then 4-methoxybenzyl chloride (5.12 mL, 37.7 mmol, 1.5 eq) added along with a degassed condenser. This mixture was then refluxed with stirring overnight. The following morning, the reaction mixture was filtered to remove unreacted potassium acetate and the organic layer was taken up in DCM and washed with water. The combined organic layers were then dried (sodium sulphate), filtered and evaporated to dryness on the rotary evaporator. This gave a white crystalline solid (3.26g, 78% yield).

^{1}H ($CDCl_3$, 300 MHz): δ = 7.25 (m, 2H), 6.85 (m, 2H), 4.41 (s, 2H), 3.73 (s, 3H), 3.49 (q, J = 6.9 Hz, 2H), 1.22 (t, J = 6.9 Hz, 3H).

All chemical shift values were consistent with those stated in the literature.[14]

[14] Braverman, S.; Reisman, D. *Tetrahedron*, **1974**, *30*, 3891.

4,4'-Difluoro-1,3,5,7-tetramethyl-4-bora-3a,4a-diaza-s-indacene[15,16]

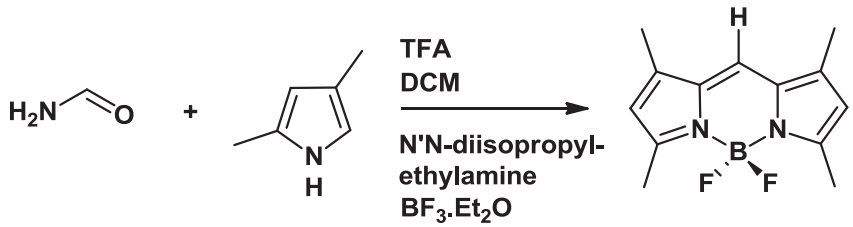

To a stirred solution of 2,4-dimethylpyrrole (1.01 mL, 9.84 mmol, 2.1 eq.) and formamide (0.17 mL, 4.92 mmol, 1 eq.) in DCM (100 mL) was added dropwise a catalytic quantity of TFA (2 drops). The reaction was allowed to stir at room temperature overnight. The following day, DDQ (1.17 g, 5.17 mmol, 1.05 eq.) was added in a single portion, and the reaction was again left stirring overnight at room temperature. N,N-diisopropylethylamine (5.66 mL, 59.04 mmol, 12.0 eq.) and boron trifluoride diethyletherate (8.73 ml, 68.88 mmol, 14 eq.) were added, and the reaction was left to stir overnight once again at room temperature. The reaction mixture was washed with water (3 x 100 mL) and brine (3 x 100 mL). The separated organic fractions were dried ($MgSO_4$), filtered and removed to yield a deep purple residue with a green tint. The residue was chromatographed on silica gel (toluene) to afford a green/ orange solid, (0.36g, 30% yield).

^{1}H NMR ($CDCl_3$, 400 MHz): δ (ppm) = 6.93 (s, 1H), 5.94 (s, 1H), 7.01 (d, J = 8.9 Hz, 1H), 2.44 (s, 6H), 2.13 (s, 6H).

Spectroscopic data was in accordance with literature values[15,16].

[15] Wu, L.; Burgess, K.. *Chem. Commun*. **2008**, *40*, 4933.
[16] Yogo, T.; Urano, Y.; Ishitsuka, Y.; Maniwa, F.; Nagano, T. *J. Am. Chem. Soc*. **2005**, *127*, 12162.

4,4'-Difluoro-8-(N-*para*-methoxyphenyl)-1,3,5,7-tetramethyl-2,6-diethyl-4-bora-3a,4a-diaza-s-indacene

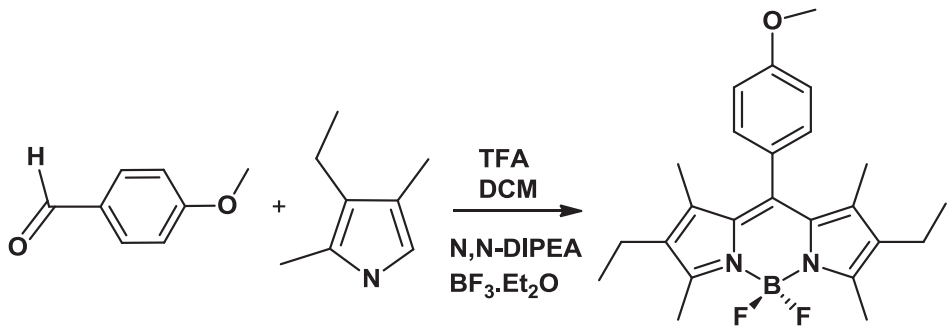

To a stirred solution of 2,4-dimethyl-3-ethylpyrrole (1.19 mL, 8.9 mmol, 2.1 eq.) and anisaldehyde (0.70 g, 4.24 mmol, 1 eq.) in DCM (200 mL) was added a catalytic quantity of TFA (2 drops). The reaction was stirred at room temperature overnight. Next, DDQ (1.01 g, 4.45 mmol, 1.05 eq.) was added in a single portion, and the reaction was again left stirring overnight at room temperature. *N,N*-diisopropylethylamine (8.86 mL, 50.88 mmol, 12.0 eq.) and boron trifluoride diethyletherate (9.03 ml, 71.23 mmol, 16.8 eq.) were added, and the reaction was left to stir for 6 hours. The reaction mixture was washed with water (3 × 150 mL) and brine (3 × 150 mL). The separated organic fractions were dried ($MgSO_4$) and filtered and residual solvent removed to yield a deep violet residue with a green tint. The residue was chromatographed on silica gel (toluene) to afford a red solid with a green tint (0.70g, 40% yield).

^{1}H NMR ($CDCl_3$, 400 MHz): δ (ppm) = 7.14 (d, *J* = 7.5 Hz, 2H), 6.99 (d, *J* = 7.5 Hz, 2H), 3.83 (s, 3H), 2.52 (s, 6H), 2.29 (q, 4H), 1.33 (s, 6H), 0.97 (t, *J* = 4.0 Hz, 6H).
^{13}C NMR ($CDCl_3$, 75 MHz): δ (ppm) = 159.87, 153.27, 140.20, 138.27, 132.46, 131.03, 129.26, 127.59, 114.28, 55.05, 16.88, 14.48, 12.27, 11.65.
^{11}B NMR ($CDCl_3$, 160 MHz): δ (ppm) = -0.12 (t, *Jav* = 33.22 Hz).
^{19}F NMR ($CDCl_3$, 470 MHz): δ (ppm) = -145.49 (q, *J* = 30.82 Hz).

N-Methoxybenzyl formamide[17]

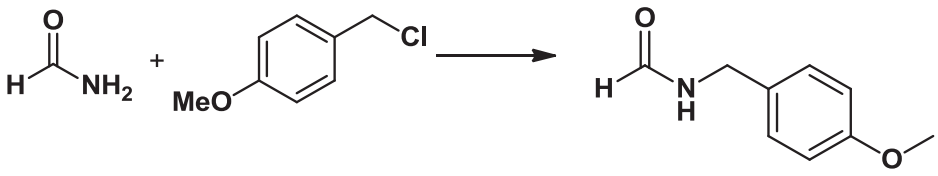

To a 50 mL round bottomed flask were added formamide (25 mL, 0.74 moles, 49 eq) and methoxybenzyl chloride (2 mL, 0.015 moles, 1 eq). The mixture was refluxed at 185˚C for 2 hours and after this time the reaction mixture went yellow. The mixture was then poured over ice water and the organic material extracted with DCM. The product was then recrystallised from ethanol and washed with petrol to give a white powdery solid. Yield = 2.36g, 95%, m.pt = 78-79°C (Lit 79-80°C)[17].

^{1}H NMR ($CDCl_3$, 400 MHz): δ (ppm) = 7.96 (s, 1H, CHO), 7.44 (s, 1H), 7.04 (d, *J* = 8.5 Hz, 2H), 6.71 (d, *J* = 8.5 Hz, 2H), 4.17 (d, *J* = 5.9 Hz, 2H), 3.61 (s, 3H).

[17] Pigge, F. C.; Coniglio, J. J.; Fang, S. *Organometallics,* **2002,** *21,* 4505

4,4'-Difluoro-8-(dimethylamino-phenyl)-1,3,5,7-tetramethyl-2,6-diethyl-4-bora-3a,4a-diaza-s-indacene.

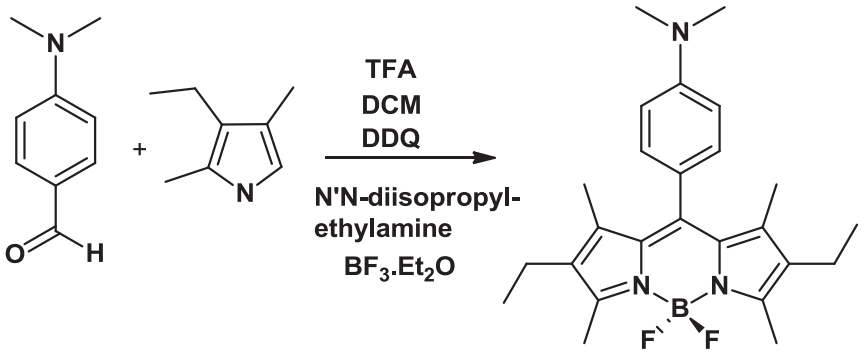

To a stirred solution of 2,4-dimethyl-3-ethylpyrrole (1.88 mL, 14 mmol, 2.1 eq.) and 4-dimethylaminobenzaldehyde (1.0 g, 6.7 mmol, 1.0 eq.) in DCM (250 mL) was added dropwise TFA (2 drops). The reaction was allowed to stir at room temperature until TLC showed complete consumption of the aldehyde. DDQ (1.60 g, 7.0 mmol, 1.05 eq.) was then added in a single portion, and the reaction was left stirring overnight at room temperature. The following day N,N-diisopropylethylamine (14.00 mL, 80.4 mmol, 12.0 eq.) and boron trifluoride diethyletherate (14.26 ml, 113 mmol, 16.8 eq.) were added, and the reaction was left to stir for 6 hours at room temperature. The reaction mixture was washed with water (3 × 200 mL) and brine (3 × 200 mL). The separated organic fractions were dried ($MgSO_4$) and filtered and the solvent removed in vacuo to yield a black/dark violet residue with a green tint. This was chromatographed on silica gel using toluene as eluent to afford a red solid (0.648 g, 22 % yield). This solid was then frozen in ether and the solvent removed at the pump and finally washed with petrol. M.pt. = > 250°C.

^{1}H NMR ($CDCl_3$, 300 MHz): δ (ppm) = 7.06 (d, *J* = 8.7 Hz, 2H), 6.78 (d, *J* = 8.7 Hz, 2H), 3.02, (s, 6H, N-$(CH_3)_2$) 2.53 (s, 6H), 2.31 (q, *J* = 7.4, 4H), 1.26 (s, 6H), 0.99 (t, *J* = 7.4 Hz, 6H).

^{13}C NMR ($CDCl_3$, 75 MHz): δ (ppm) = 152.93, 150.56, 141.55, 138.58, 132.33, 131.48, 128.96, 123.06, 112.33, 40.38, 17.08, 14.64, 12.42, 11.93.

^{11}B NMR ($CDCl_3$, 160 MHz): δ (ppm) = -0.12 (t, *Jav* = 34.45 Hz).

^{19}F NMR ($CDCl_3$, 470 MHz): δ (ppm) = -145.66 (q, *J* = 28.59 Hz)

IR (neat): cm^{-1} = 2958, 2923, 2854 (C-H), 1527, 1473 (C=C, C=N), 1183 (B-F).

EI-MS : m/z calc. for $C_{25}H_{32}BF_2N_3$ = 424.2728 fnd 424.2731 $[MH]^+$.

5-(4-Dimethylaminophenyl)-dipyrromethane[18]

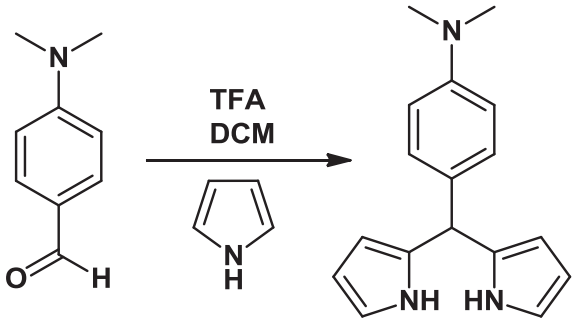

To a degassed solution of *N,N*-dimethylaminobenzaldehyde (2.0 g, 13.4 mmol, 1 eq) in redistilled pyrrole (65.08 mL, 938 mmol, 70 eq), was added a catalytic quantity of trifluoroacetic acid (2 drops) which turned the yellow solution pink/ red. The reaction mixture was then protected from light and left to stir overnight. The following day, 2 further drops of TFA were added to the reaction mixture and the reaction was heated to 40˚C for 4 hours and then left stirring overnight again at room temperature. The next day, the pyrrole was removed under reduced pressure and the reaction mixture diluted with DCM (50 mL) then washed with 0.1 M NaOH (3 x 100 mL), water (3 x 50 mL) before being separated and dried over sodium sulphate. Removal of the solvent under reduced pressure afforded a deep brown oily residue which was purified by column chromatography on basic alumina, using DCM / petrol (1:2) as eluent. This gave *N,N*-dimethylaminophenyldipyrromethane, as a pale brown crystalline solid (1.81g, 51% yield), Mp = 118-119˚C. (No melting point was provided in the literature).

^{1}H NMR ($CDCl_3$, 300 MHz): δ (ppm) = 7.87 (br s, 2H, pyrrole-NH), 7.60 (d, 2H, J = 8.5 Hz), 7.04 (d, *J* = 8.5 Hz, 2H), 6.65 (m, 2H, pyrrole-H), 6.12 (m, 2H, pyrrole-H), 5.89 (m, 2H, pyrrole-H), 5.35 (s, 1H, *meso*-H), 2.89 (s, 6H).

Chemical shifts in accordance with the literature[18].

[18] Durantini, E. N. *Molecules*, **2001**, *6*, 533.

4,4'-Difluoro-8-(4-dimethylaminophenyl)-4-bora-3a,4a-diaza-s-indacene[19]

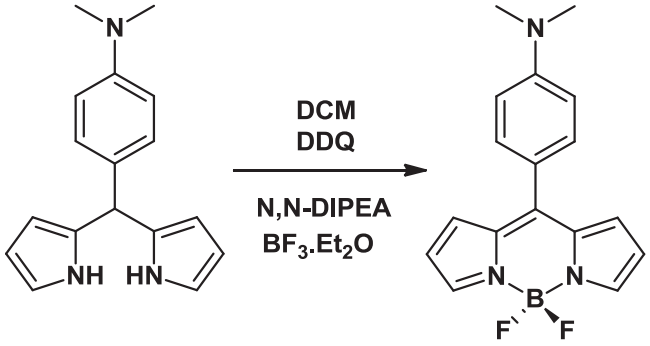

To a 250 mL 2-necked round bottomed flask was added dimethylaminophenyl dipyrromethane (1g, 3.77 mmol, 1.0 eq) in DCM (150 mL). This mixture was degassed with stirring for one hour, prior to the addition of DDQ (1.71g, 7.54 mmol, 2.0 eq). The reaction was stirred overnight at room temperature and the following morning N,N-diisopropylethylamine (3.74 mL, 21.49 mmol, 5.7 eq) was added, followed by boron trifluoride diethyletherate (3.82 mL, 30.16 mmol, 8 eq). The reaction was then stirred overnight at room temperature. The reaction mixture was washed with water (3 × 100 mL) and brine (3 × 100 mL). The separated organic fractions were dried ($MgSO_4$), filtered and the residual solvent removed *in vacuo* to yield a black/dark violet residue with a green tint. The residue was chromatographed on silica gel (toluene) to afford the bright green crystalline solid **DMABD** (0.71g, 61% yield). This solid was then frozen in ether and the solvent removed at the pump and washed with petrol. M.pt > 250 °C (Lit M.pt > 195°C)

^{1}H NMR ($CDCl_3$, 300 MHz): δ (ppm) = 7.87 (s, 2H), 7.56 (d, *J* = 9.0 Hz, 2H), 7.04 (d, *J* = 4.2, 2H), 6.80 (d, *J* = 9.0 Hz, 2H), 6.55-6.53 (m, 2H), 3.11 (s, 6H).

Chemical shifts in-keeping with literature values[19]

[19] Peña-Cabrera, E.; Aguilar-Aguilar, A.; González-Domínguez, M.; Lager, E.; Zamudio-Vázquez, R.; Godoy-Vargas, J.; Villanueva-García, F. *Organic Letters*, **2007,** *9*, 3985.

1,4-Bis(naphthalenylboronic acid)[20]

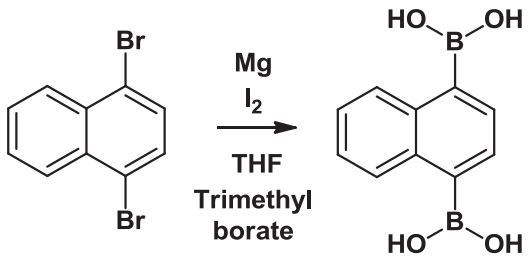

To a 3-necked 250 mL flask equipped with a condenser and dropping funnel was added magnesium turnings (0.51g, 21.0 mmol, 3.0 eq). The flask was thoroughly degassed and a solution of 1,4-dibromonaphthalene (2.0g, 7 mmol, 1.0 eq) in freshly distilled THF (35 mL) was added with stirring in two portions. The first portion (7 mL) was added and the reaction initiated by adding a few crystals of iodine and the solution was then warmed to 45˚C. The remaining portion (28 mL) of the solution was added over 30 minutes and then the solution was warmed to 65˚C and allowed to reflux overnight. In the morning a pale yellow/ cream slurry was present. This was allowed to cool to room temperature and was then immersed in a dry ice/ acetone bath and cooled to -65˚C. Trimethyl borate (3.9 mL, 35 mmol, 5.0 eq) was then added drop-wise as a solution in dry THF (12 mL) over a 60 minute period, then the mixture was slowly warmed to room temperature and stirred overnight. The mixture was then hydrolysed with 2M HCl to decompose the residual Mg turnings and the solution extracted with diethyl ether. The organic layer was washed with brine, dried ($MgSO_4$) and the solvent removed. The residue was then recrystallised from ether to give the product as a white fluffy solid (1.10g, 55% yield) M.pt = >250°C (Lit >300°C[21])

^{1}H NMR ($CDCl_3$, 300 MHz): δ (ppm) = 7.40-7.60 (m, 4H), 7.65 (s, 2H), 8.24-8.50 (m, 4H).

Chemical shifts in-keeping with literature values[20].

[20] Zhang, F-J; Cortez, C.; Harvey, R. G. *J. Org. Chem*, **2000***, 65*, 3952.

4-(4-(4,4'-Difluoro-1,3,5,7-tetramethyl-2,6-diethyl-4-bora-3a,4a-diaza-s-indacen-1-yl)naphthalene-1-yl)-N)N,dimethylaniline

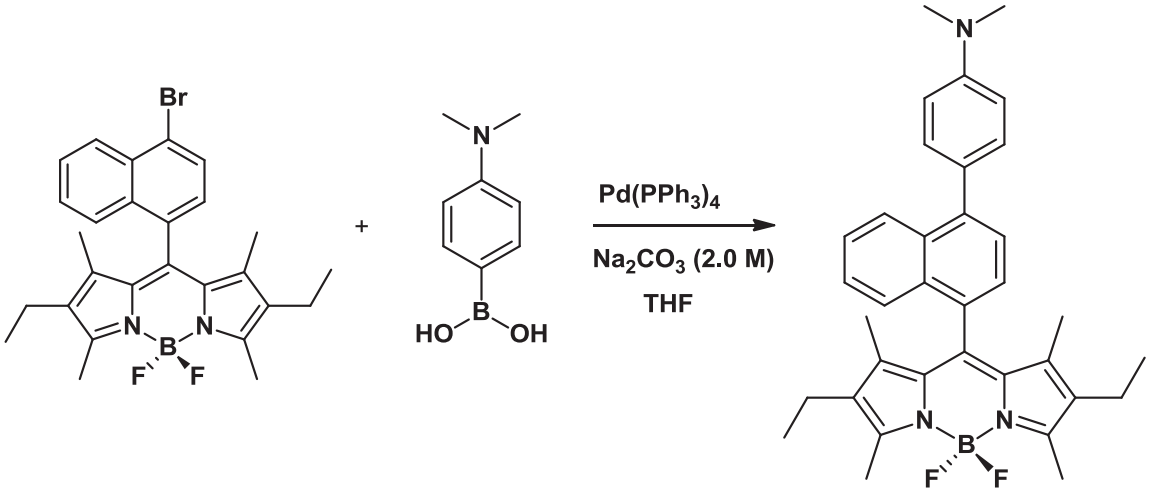

In a flame dried Schlenk flask, a solution in THF (20 mL) of BRNBD (0.15g, 0.295 mmol, 1.0 eq), 4-dimethylaminophenyl boronic acid (0.10g, 0.620 mmol, 2.1 eq) and sodium carbonate (0.093g, 0.885 mmol, 3 eq) in water was degassed for an hour prior to addition of the catalyst, tetrakis (triphenylphosphine) palladium(0) (0.02g, 0.024 mmol, 0.08 eq). The reaction was then heated with continuous stirring overnight at 60˚C. The following morning, the crude reaction mixture was left to cool before being filtered through a silica filled cotton wool plugged glass pipette to remove the unreacted catalyst. The residual solvent was then removed under rotary evaporation and the crude product taken up in DCM and washed with sodium carbonate solution (0.6 M). The combined organic fractions were then dried over sodium sulphate, filtered and the DCM removed *in vacuo* to yield a black/dark violet residue with a green tint. The residue was chromatographed on silica gel (toluene) to afford the red solid **DMANBD** (0.11g, 68% yield). This solid was then frozen in ether and the solvent removed at the pump and washed with petrol. M.pt = > 250°C.

^{1}H NMR ($CDCl_3$, 300 MHz): δ(ppm) = 8.11 (d, *J* = 7.5 Hz, 2H), 7.87 (d, *J* = 7.5 Hz, 2H), 7.46, (m, 4H), 6.91 (d, *J* = 9.0 Hz, 2H), 3.07 (s, 6H, N-$(CH_3)_2$), 2.59 (s, 6H), 2.28 (q, *J* = 7.3, 4H), 1.07 (s, 6H), 0.97 (t, *J* = 7.3 Hz, 6H).

^{13}C NMR ($CDCl_3$, 75 MHz): δ (ppm) = 11.25, 12.56, 14.61, 17.05, 40.56, 112.21, 125.49, 125.76, 125.95, 126.14, 126.27, 126.53, 126.65, 130.94, 131.43, 131.74, 131.93, 132.43, 132.61, 138.34, 138.99, 141.80, 149.95, 153.68.

^{11}B NMR ($CDCl_3$, 160 MHz): δ (ppm) = 0.0192 (t, *Jav* = 33.22 Hz).

^{19}F NMR ($CDCl_3$, 470 MHz): δ (ppm) = -145.39 (multiplet).

EI-MS: m/z calc. for $C_{25}H_{32}BF_2N_3$ = 550 fnd 550 $[MH]^+$.

(4,4,5,5-Tetramethyl-1,3,2-dioxaborolan-2-yl)(trifluoromethyl)benzene[21]

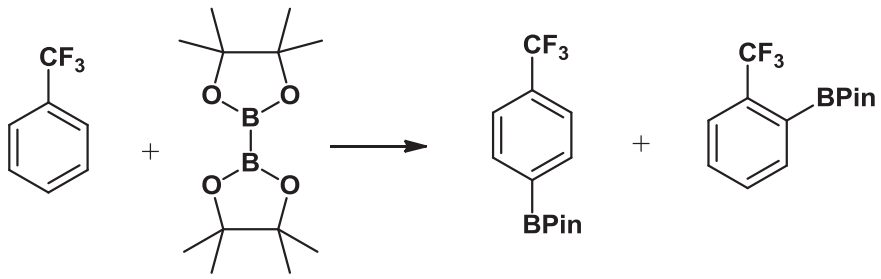

2 : 1

A flame dried Schlenk flask was charged with $[IrCl(COD)]_2$ (10.1 mg, 0.015 mmol, 0.015 eq), 2,2'-bipyridine (4.7 mg, 0.03 mmol, 0.03 eq), bispinacolatodiboron (254 mg, 1 mmol, 1 eq) α,α,α-trifluorotoluene (7.37 mL, 60 mmol, 60 eq) and freshly distilled hexane (6 mL). The resulting mixture was heated with stirring at 80˚C overnight. The following morning, the reaction mixture was allowed to cool to room temperature and the organic layer passed through a short silica plug. The flask was rinsed with a further portion of hexane. The material contained pure *para* and *ortho* products. The material was then diluted with ether and a small portion transferred to a vial for GC analysis. *Para* (major) isomer = 0.29g (66 % yield), *meta* (minor) isomer = 0.15g (33% yield).

^{1}H NMR ($CDCl_3$, 300 MHz): δ(ppm) *meta* isomer = 1.35 (s, 12H), 7.47 (t, *J* = 7.6 Hz, 1H), 7.68 (d, *J* = 7.8 Hz, 1H), 7.97 (d, *J* = 7.6 Hz, 1H), 8.04 (s, 1H), (*para* isomer) 1.34 (s, 12 H), 7.59 (d, *J* = 8.1 Hz, 2H), 7.91 (d, *J* = 7.8 Hz, 2H).

[21] Ishiyama, T, Ahiko, T.; Miyaura, N. *J. Am. Chem. Soc*, **2002**, *124*, 12414.

4,4'-Difluoro-8-(binaphthyl)-1,3,5,7-tetramethyl-2,6-diethyl-4-bora-3a,4a-diaza-s-indacene

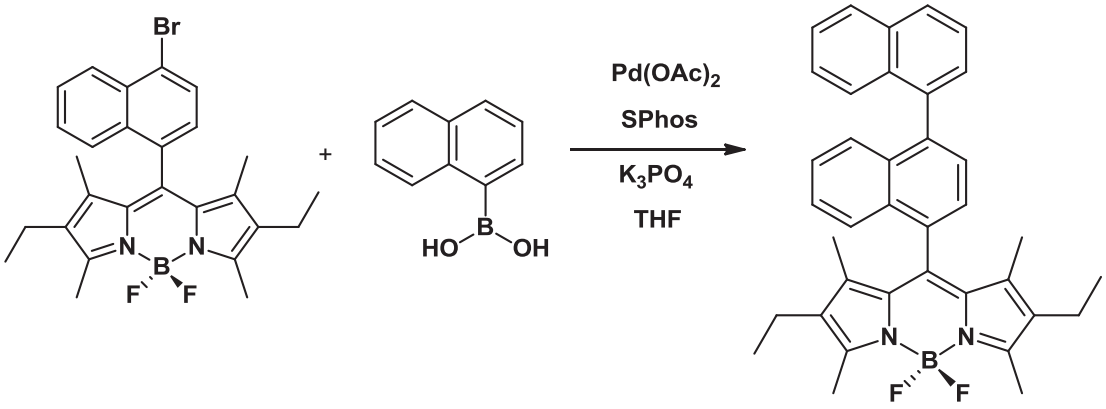

To a flame dried Schlenk flask was added $Pd(OAc)_2$ (4.17 mg, 0.0186 mmol, 4 mol %), S-Phos (0.015g, 0.00372 mmol, 8 mol%), 1-naphthalene boronic acid (0.120g, 0.698 mmol, 1.5 eq) and potassium phosphate (190mg, 1.395mmol, 3eq). BRNBD (80 mg, 0.465 mmol, 1 eq) was added and the system degassed. Freshly distilled toluene was then added (2 mL) and the reaction was then stirred at 105˚C overnight. The following morning, the organic material was taken up in ether and washed with water. The combined organic fractions were then dried over sodium sulphate, filtered and evaporated to dryness. The material was then purified by small scale column chromatography (toluene). This gave the pure product as a red/ purple solid, **BNBD** (0.135g, 52% yield).

^{1}H NMR ($CDCl_3$, 300 MHz): δ(ppm) = 7.93-8.02 (m, 3H), 7.29-7.67, (m, 10H), 2.51 (s, 6H), 2.32 (q,d, *J* = 4.2 Hz, *J*'= 3 Hz, 4H), 1.22, (s, 3H), 1.16 (s, 3H), 0.99 (t, *J* = 6 Hz, *J*'= 4Hz, 6H).

^{13}C NMR ($CDCl_3$, 75 MHz): δ (ppm) = 11.28, 12.60, 14.66, 17.09, 125.37, 125.46, 125.70, 125.90, 125.99, 126.23, 126.59, 126.75, 126.99, 127.68, 127.98, 128.33, 131.38, 132.03, 132.57, 132.80, 132.92, 133.16, 133.54, 137.82, 138.05, 138.31, 138.53, 139.71, 153.89.

^{11}B NMR ($CDCl_3$, 160 MHz): δ (ppm) = 0.0384 (t, *Jav* = 33.23 Hz).

^{19}F NMR ($CDCl_3$, 470 MHz): δ (ppm) = -145.62 (multiplet).

1,1'-Binaphthalene[22]

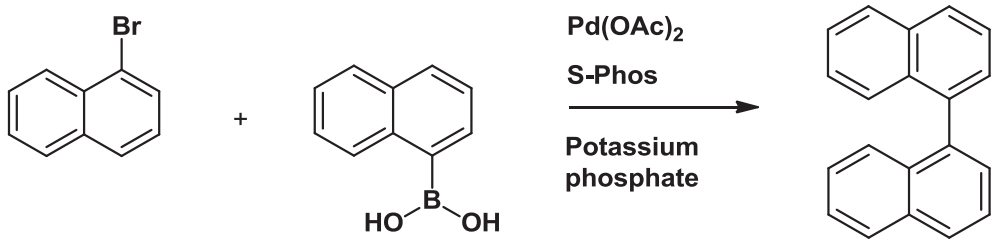

To a flame dried Schlenk flask was added $Pd(OAc)_2$ (4.49 mg, 0.02 mmol, 2 mol %), S-Phos (33mg, 0.08 mmol, 8 mol%), 1-naphthalene boronic acid (258mg, 1.5 mmol, 1.5 eq) and potassium phosphate (636 mg, 3.0 mmol, 3eq). 1-bromonaphthalene (207 mg, 1.0 mmol, 1 eq) was then added and the system degassed. Freshly distilled toluene was then added (2.0 mL). The reaction was then stirred at 105˚C overnight. The following morning the organic material was taken up in ether and washed with water. The combined organic fractions were then dried over sodium sulphate, filtered and evaporated to dryness before being taken up in ether and passed through a silica plug. Upon evaporation of the solvent, a white solid remained, (0.152g, 59% yield). M.pt = 143-147°C (Lit =143-146°C).

^{1}H NMR ($CDCl_3$, 300 MHz): δ(ppm) = 7.85-7.82 (m, 7H), 7.48-7.45, (m, 7H).

[22] Sakellarios, E.; Kyrimis, T. *Chem. Ber*., **1924**, *57*, 324.

(1,5-Cyclooctadiene) (Methoxy)Iridium(I)dimer[23,24]

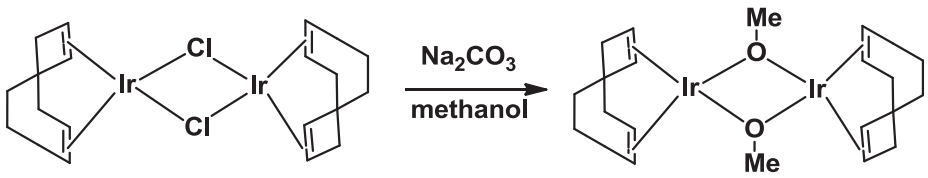

To a flame dried Schlenk flask was added $[Ir(cod)Cl]_2$ (149 mg, 0.222 mmol, 1 eq), anhydrous sodium carbonate (149 mg, 1.41 mmol, 6.35 eq) and methanol (5 mL). These were stirred together at 60˚C for 45 minutes. When the yellow solution began to turn brown, heating was stopped. The reaction mixture was cooled to room temperature and and the yellow solid obtained was filtered and washed with water and methanol. The solid was then dried under vacuum to give a yellow powdery solid (0.14g, 95% yield). M.pt = 155-160 ºC, (Lit = 154-179 ºC) [24,25].

^{1}H NMR ($CDCl_3$, 300 MHz): δ(ppm) = 3.42-3.60 (m, 8H, C<u>H</u>), 3.18 (s, 6H, OC<u>H$_3$</u>), 2.08-2.40 (m, 8H, C<u>H$_2$</u>), 1.24-1.50 (m, 8H, C<u>H$_2$</u>).

Chemical shifts in keeping with the literature.[23,24]

[23] Pannetier, G.; Fourgeroux, P.; Bonnaire, R.; Platzer, N. *J. Less Common Met.* **1971**, *24,* 83.
[24] Maringo, M.; Marsich, N.; Farnetti, E. *Journal of Molecular Catalysis A: Chemical*. **2002**, *187*, 169.

4,4'-Difluoro-8-(naphthyl)-1,3,5,7-tetramethyl-2,6-diethyl-4-bora-3a,4a-diaza-s-indacene

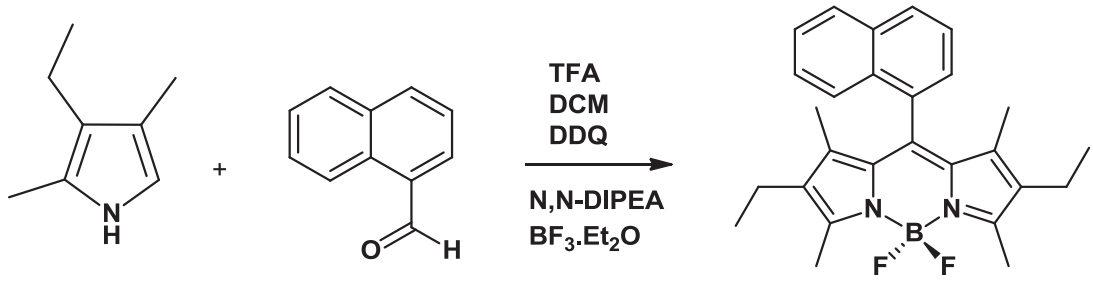

To a stirred, degassed solution of 2,4-dimethyl-3-ethylpyrrole (3.63 mL, 26.9 mmol, 2.1) and 1-naphthaldehyde (2g, 12.8 mmol, 1 eq) in DCM (200 mL) was added TFA (2 drops), which turned the solution red from pale yellow. The reaction was then stirred at room temperature until TLC showed complete consumption of the aldehyde (18 hours). DDQ (3.04g, 13.4 mmol, 1.05 eq) was then added in a single portion (this turned the mixture deep blue) and the reaction was left to stir at room temperature for 16 hours. Next, N,N-diisopropylethylamine (26.76 mL, 153 mmol, 12.0 eq) and boron trifluoride diethyletherate (27.25 mL, 215 mmol, 16.8 eq) were added, the addition of which generated a white gas and a pinkish tint developed in the reaction mixture. After stirring at room temperature overnight, the reaction mixture was washed with water (3 × 150 mL) and brine (3 × 150 mL). The separated organic fractions were dried over $MgSO_4$ and filtered. The solvent was then removed under reduced pressure to yield a deep violet residue with a green tint. The residue was purified by column chromatography on silica gel using toluene as eluent to afford a green crystalline solid (3.0g, 55% yield). This solid was then recrystallized by slow diffusion from DCM and petrol to give **NAPBD**. The colour of the crystals did not alter upon recrystallisation. Mp = 160-163˚ C.

^{1}H NMR ($CDCl_3$, 300 MHz): δ (ppm) = 7.95 (d, *J* = 8.1 Hz, 1H), 7.89 (d, *J* = 8.1 Hz, 1H), 7.82 (d, *J* = 8.1 Hz, 1H), 7.54 (m, 2H), 7.40 (m, 2H), 2.57 (s, 6H), 2.24 (q, *J* = 7.5, 4H), 0.96 (s, 6H), 0.93 (t, *J* = 7.5, 6H).

^{13}C NMR ($CDCl_3$, 75 MHz): δ (ppm) = 153.77, 138.48, 138.18, 133.44, 133.24, 132.65, 131.95, 131.24, 128.98, 128.07, 127.05, 126.47, 126.12, 125.74, 125.18, 17.00, 14.57, 12.53, 11.07.

^{11}B NMR (160 MHz, $CDCl_3$) δ = -0.00 (t, *Jav* = 33.2 Hz).

^{19}F NMR (470 MHz, $CDCl_3$) δ = - 145.46 (m).

N-Ethyl-4-hydroxy-N,N-diisopropyl-4,5,6,7-tetrahydro-1H-indol-4-aminium

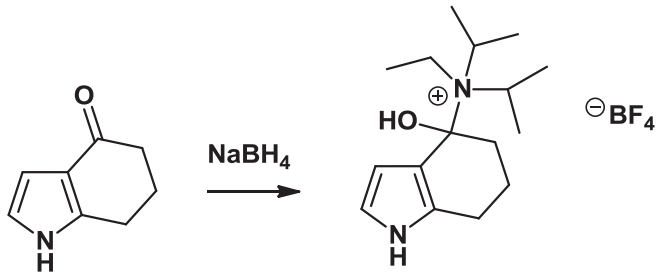

To a stirred solution of 1,5,6,7-tetrahydro-4H-indol-4-one (2.02 g, 15 mmol, 2.1 eq.) and formamide (0.32 mL, 7.14 mmol, 1 eq.) in DCM (150 mL) was added dropwise a catalytic quantity of TFA (3 drops). The reaction was allowed to stir at room temperature overnight. N,N-diisopropylethylamine (14.92 mL, 86 mmol, 12.0 eq.) and boron trifluoride diethyletherate (15.20 ml, 120 mmol, 16.8 eq.) were added, and the reaction was left to stir overnight once again at room temperature. The reaction mixture was washed with water (3 x 100 mL) and brine (3 x 100 mL). The separated organic fractions were dried ($MgSO_4$), filtered and removed to yield a deep red residue. The residue was chromatographed on silica gel (DCM with methanol (2%)) to afford a green/ orange solid, (0.36g, 30% yield).

^{1}H NMR ($CDCl_3$, 400 MHz): δ (ppm) = 9.83 (br s, 1H), 6.88 (br s, 1H), 6.61 (t, *J* = 2.6 Hz, 1H), 6.35 (t, *J* = 2.6 Hz, 1H), 3.63 (m, 1H), 3.11 (m, 1H), 2.91 (s, 1H), 2.80 (s, 1H), 2.76 (t, *J* = 6.4 Hz, 2H), 2.36 (dd, *J'* = 7.1 Hz, *J''* = 5.6 Hz, 2H), 2.05 (pentet, *J* = 6.4 Hz, 2H), 1.35 (m, 15H).

^{11}B NMR (160 MHz, $CDCl_3$) δ = -2.02 (s).

^{19}F NMR (470 MHz, $CDCl_3$) δ = -149.50 (s).

4,5,6,7-Tetrahydro-1*H*-indole[25]

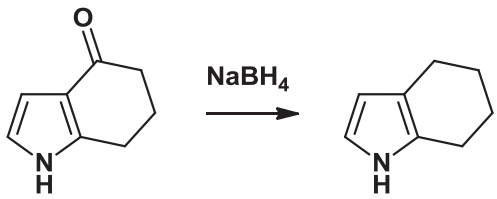

To a 250 mL round-bottomed flask was added 1,5,6,7-tetrahydro-4H-indol-4-one (2g, 14.8 mmol, 1.0 eq) and sodium borohydride (0.84g, 22.2 mmol, 1.5 eq). A reflux condenser was added and the system fully degassed. 2-propanol was added (50 mL) and the mixture refluxed overnight at 90˚C. The material was purified by column chromatography on silica gel (hexane/ ethyl acetate (9 :1)) to give the pure indole as a white solid (1.08g, 60% yield). M.pt = 55-57°C (Lit = 53-57°C)

^{1}H NMR ($CDCl_3$, 300 MHz): δ (ppm) = 7.5-7.7 (br s, 1H, NH), 6.55 (t, *J* = 2.6 Hz, 1H), 6.00 (t, *J* = 2.6 Hz ,1H), 1.80-1.91 (m, 4H), 1.50-1.78 (m, 4H).

[25] Patterson, J.M.; Soedigdo, *S. J. Org. Chem.* **1967**, *32,* 2969.

(*E*)-1-(Benzyloxy)-4-(2-nitroprop-1-en-1-yl)benzene

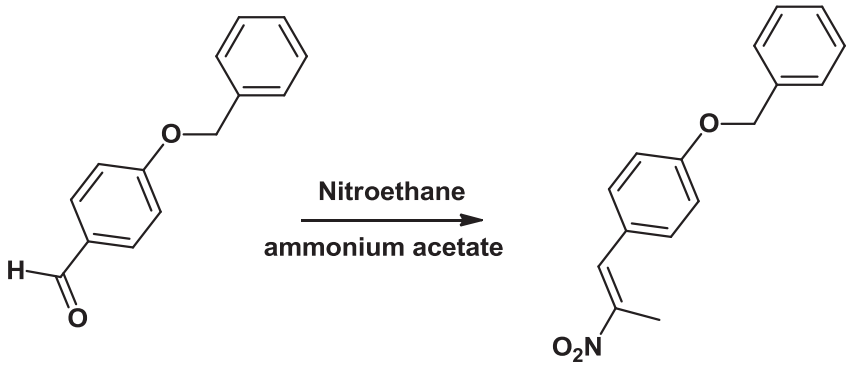

To a round bottomed flask was added 4-benzyloxybenzaldehyde (2.00 g, 9.42 mmol, 1 eq) and ammonium acetate (1.82 g, 23.6 mmol, 2.5 eq). The flask was degassed and nitroethane (150 mL) delivered via a syringe. The reaction mixture was then heated overnight at 60°C. The organic material was taken up in DCM and washed with water. The organic layer was dried ($MgSO_4$) and filtered and the solvent was then removed *in vacuo*. The product was recrystallized from chloroform and ether to give shiny yellow crystals (1.60g, 63% yield).

^{1}H NMR ($CDCl_3$, 300 MHz): δ (ppm) = 7.46 (d, J = 9.0 Hz, 2H), 7.36 (d, J = 9.0 Hz, 2H), 7.25 (m, 3H), 7.04 (d, J = 9.0 Hz, 2H), 2.68 (s, 2H), 2.33 (s, 3H).

^{13}C NMR ($CDCl_3$, 75 MHz): δ (ppm) = 160.02, 146.08, 137.02, 132.99, 128.55, 128.01, 127.71, 125.03, 115.37, 69.82, 13.48.

Ethyl 3-(4-(Benzyloxy)phenyl)-4-methyl-1H-pyrrole-2-carboxylate

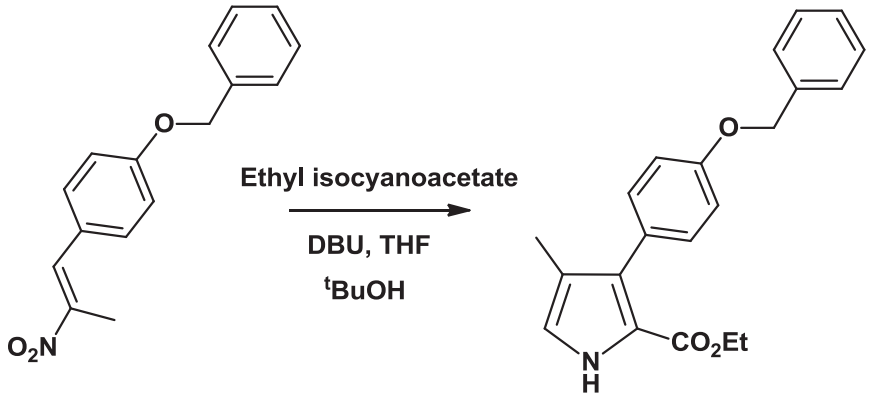

To a 250 mL flask fitted with a reflux condenser was added (E)-1-(benzyloxy)-4-(2-nitroprop-1-en-1-yl)benzene (1.4g, 5.20 mmol, 1eq). The flask was thoroughly degassed prior to the addition of freshly distilled THF (50 mL) and tertiary butyl alcohol (50 mL). DBU (0.87g, 5.72 mmol, 1.1 eq) and ethyl isocyanoacetate (0.37g, 5.2 mmol, 1 eq) were then added. This mixture was stirred at room temperature for 20 minutes and then at 60°C overnight. In the morning the reaction had turned from yellow to deep orange/ red. The solvent was removed *in vacuo* and the remaining orange oil taken up in DCM and washed with water. The combined organic layers were dried ($MgSO_4$), filtered and the solvent removed. This gave an orange solid. Upon recrystallisation from chloroform and ether, orange crystals remained (1.0g, 58% yield).

^{1}H NMR ($CDCl_3$, 300 MHz): δ (ppm) = 9.18 (br s, 1H, N-H of py), 7.45 (m, 5H aromatic benzyl protons), 7.32 (d, *J* = 8.8 Hz, 2H, CH aromatic), 7.02 (d, *J* = 8.8 Hz, 2H, CH aromatic), 6.81 (s, 1H (H-C-NH of pyrrole)), 5.15 (s, CH_2 of benzyloxy, 2H), 4.13 (q, *J* = 7.2 Hz, 2H, CH_2-CH_3), 1.97 (s, 3H (CH_3, on pyrrole backbone)), 1.18 (t, *J* = 7.2 Hz, 3H, CH_3CH_2).

^{13}C NMR ($CDCl_3$, 75 MHz): δ (ppm) = 161.12, 157.68, 137.17, 133.80, 131.40, 130.72, 128.52, 127.88, 127.50, 127.18, 120.36, 118.79, 113.85, 69.95, 59.89, 14.15, 10.57.

1,4-(4,4,5,5-Tetramethyl-1,3,2-dioxaborolan-2-yl)naphthalene

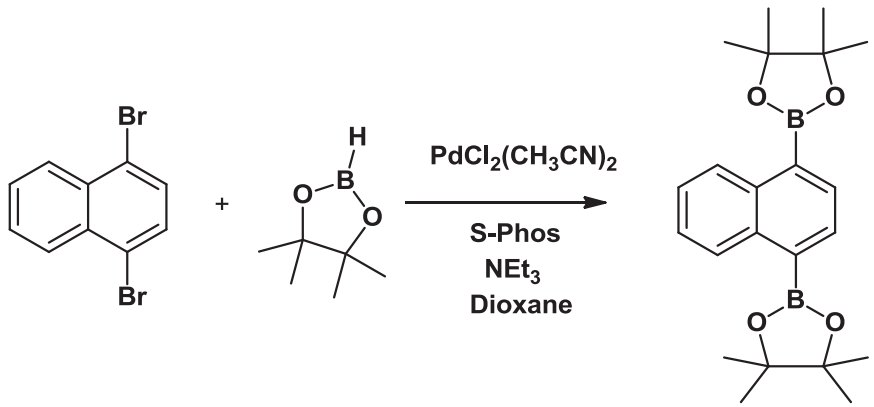

A flame dried Schlenk flask was charged with 1,4-dibromonaphthalene (1.0g, 3.5 mmol, 1 eq), $PdCl_2(CH_3CN)_2$ (0.036g, 0.14 mmol, 4 mol%) and S-Phos (0.23g, 0.56 mmol, 16 mol%). The flask was thoroughly degassed prior to the addition of triethylamine (4 mL), dioxane (20 mL) and pinacolborane (8.75 mmol, 1.12g, 2.5eq). The resulting mixture was then heated at 80˚C for 24 hours with rapid stirring. The reaction mixture, which was deep orange in colour, was then allowed to cool to room temperature and was passed through a short silica plug and eluted with ethyl acetate. The solvent was then removed in vacuo to leave a yellow solid. Recrystallisation from petrol gave white needle-shaped crystals (0.31g, 23% yield).

^{1}H NMR ($C_6D_5CD_3$, 300 MHz): δ (ppm) = 9.27 (dd, *J* = 6.5 Hz ; *J*' = 3.4 Hz, 2H), 8.44 (s, 2H), 7.51 (dd, *J* = 6.5 Hz; *J*' = 3.4 Hz, 2H), 1.18 (s, 24H).
^{13}C NMR ($CDCl_3$, 75 MHz): δ (ppm) = 136.69, 136.44, 134.36, 128.45, 125.14, 82.65, 23.86.
^{11}B NMR (160 MHz, $CDCl_3$) δ = 30.76 (s)

2-Phenyl-*1H*-pyrrole[26,27]

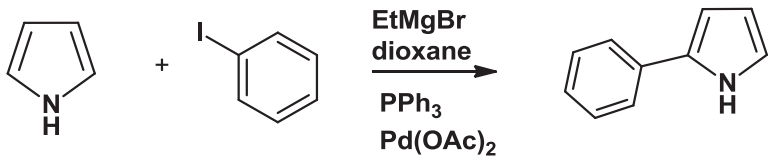

In a flame dried flask, pyrrole (2mL, 28.8 mmol, 1 eq) and ethyl magnesium bromide (11.36 mL, 34.6 mmol, 1.2 eq), were suspended in dry dioxane (12 mL) and stirred at room temperature for ten minutes. This generated a homogenous suspension. The ethyl magnesium bromide was added cautiously to the pyrrole as bubbling was observed. When the dioxane was added, this was also delivered slowly over time and it generated a cloudy solution, which became a homogenous suspension. $Pd(OAc)_2$ (1.44 mmol, 0.32g, 5 mol %) was then added along with PPh_3 (1.51g, 5.76 mmol, 20 mol %) with vigorous stirring. Iodobenzene (3.84 mL, 34.6 mmol, 1.2 eq) was then dissolved in dioxane (6 mL) and added dropwise to the solution and the reaction mixture heated to 150˚C. The reaction mixture became deep turquoise in colour. It was heated at 150˚C for 6 hours and after this time a very deep blue/green viscous material remained. Chloroform was added to the flask and the reaction mixture was filtered through a pad of silica in a sintered funnel into a round bottomed flask. The solvent was then removed *in vacuo* and the crude material dried under vacuum. The material was then purified by column chromatography on silica gel (ethyl acetate: hexane (1:2 then increased over time to 3:1)). This gave pure 2-phenyl-*1H*-pyrrole as a white solid (2.04g, 49% yield).

^{1}H NMR ($CDCl_3$, 300 MHz): δ (ppm) = 8.35 (br s, 1H), 7.16 (t, *J* = 7.5 Hz, 1H), 7.42 (d, *J* = 7.5, 2H), 7.35 (t, *J* = 7.5 Hz, 2H), 6.85 (m, 1H), 6.65 (m, 1H), 6.40-6.38 (m, 1H).

Chemical shifts are in accordance with the literature[26,27].

[26] Burghart, A.; Kim, H.; Welch, M. B.; Thoresen, L. H.; Reibenspies, J.; Burgess, K.; Bergstrom, F.; Johansson, L. B. *J. Org. Chem.* **1999**, *64*, 7813
[27] Sezen, B.; Sames, D. *J. Am. Chem. Soc*, **2003**, *125*, 5274.

4'-Difluoro-8-(phenyl)-1,3-diphenyl-4-bora-3a,4a-diaza-s-indacene

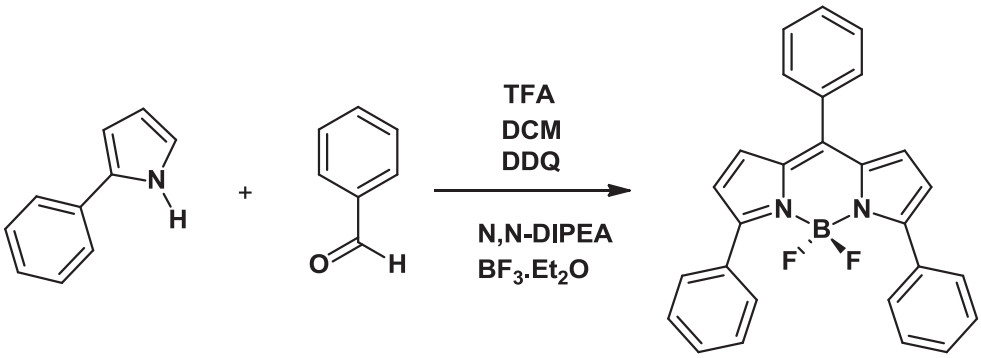

To a stirred solution of phenylpyrrole (0.25g, 1.75 mmol, 2.1 eq) and benzaldehyde (0.09 mL, 0.832 mmol, 1 eq) in DCM (40 mL) was added TFA (2 drops). This turned the solution red from pale pink. The reaction was then stirred at room temperature until TLC showed complete consumption of the aldehyde (18 hours). DDQ (0.2g, 0.087 mmol, 1.05 eq) was then added in a single portion and the reaction was left to stir at room temperature for 16 hours. Next, N,N-diisopropylethylamine (1.74 mL, 9.98 mmol, 12.0 eq) and boron trifluoride diethyl etherate (1.73 mL, 14 mmol, 16.8 eq) were added, the addition of which generated a white gas and a pinkish tint developed in the reaction mixture. After stirring at room temperature overnight, the reaction mixture was washed with water (3 × 100 mL) and brine (3 × 100 mL). The separated organic fractions were dried over $MgSO_4$ and filtered. The solvent was then removed under reduced pressure to yield a deep pink residue. Finally, this material was purified by column chromatography on silica gel using toluene as eluent to afford a pink/ purple crystalline solid (0.44 g, 6% yield).

^{1}H NMR ($CDCl_3$, 300 MHz): δ (ppm) = 7.87 (m, 4H), 7.57 (m, 5H), 7.42, (m, 6H), 6.90 (d, *J* = 6.0 Hz, 2H) 6.64 (d, *J* = 6.0 Hz, 2H).

^{13}C NMR ($CDCl_3$, 75 MHz): δ (ppm) = 159.01, 136.46, 134.48, 132.72, 130.97, 130.66, 130.22, 129.55, 128.83, 128.33, 127.33, 127.25, 120.98.

^{11}B NMR (160 MHz, $CDCl_3$) δ = 0.46 (t), J*av* = 32.06 Hz

^{19}F NMR (470 MHz, $CDCl_3$) δ = 132.41 (q), J*av* = 28.84 Hz.

2-(4-Methylphenyl)pyrrole[28]

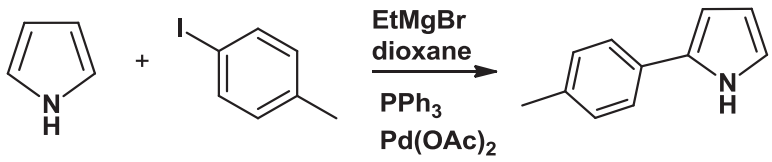

In a flame dried flask, pyrrole (2mL, 28.8 mmol, 1 eq) and ethyl magnesium bromide (11.36 mL, 34.6 mmol, 1.2 eq), were suspended in dry dioxane (12 mL) and stirred at room temperature for ten minutes. This generated a homogenous suspension. The ethyl magnesium bromide was added cautiously to the pyrrole as bubbling was observed. When the dioxane was added, this was also delivered slowly over time and it generated a cloudy solution, which became a homogenous suspension. $Pd(OAc)_2$ (1.44 mmol, 0.32g, 5 mol %) was then added along with PPh_3 (1.51g, 5.76 mmol, 20 mol %) with vigorous stirring. Iodotoluene (7.54g, 34.6 mmol, 1.2 eq) was then dissolved in dioxane (20 mL) and added dropwise to the solution and the reaction mixture heated to 150˚C. The reaction mixture became deep turquoise in colour. It was heated at 150˚C for 4 hours and after this time a very deep blue/green viscous material remained. The material was then stirred for a further 16 hours at 115ºC. Chloroform was added to the flask and the reaction mixture was filtered through a pad of silica in a sintered funnel into a round bottomed flask. The solvent was then removed *in vacuo* and the crude material dried under vacuum. The material was then purified by column chromatography on silica gel (ethyl acetate: hexane (1:2 then increased over time to 3:1)). This gave pure 2-phenyl-*1H*-pyrrole as a white solid (2.04g, 49% yield).

^{1}H NMR ($CDCl_3$, 300 MHz): δ (ppm) = 8.43 (br s, 1H), 7.40 (d, J = 7.2 Hz, 2H), 7.22 (d, J = 7.2, 2H), 6.90-6.86 (m, 1H), 6.58-6.56 (m, 1H), 2.39 (s, 3H).

Chemical shifts are in accordance with the literature[28].

[28] Wen, J.; Qin, S.; Ma, L. F.; Dong, L.; Zhang, J.; Liu, S. S.; Duan, Y. S.; Chen, S. Y.; Hu, C. W.; Yu, X. Q. *Org. Lett.* **2010**, *12*, 2694-2697

4,4'-Difluoro-8-(phenyl)-1,3-ditolyl-4-bora-3a,4a-diaza-s-indacene

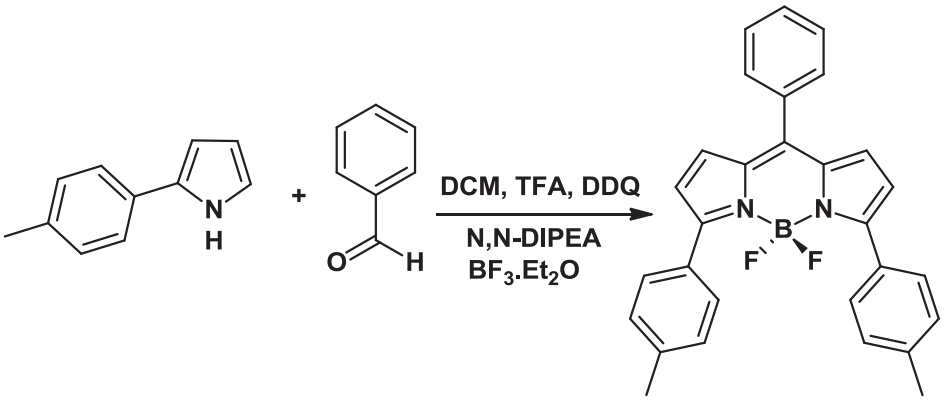

To a stirred solution of 2-tolyl-*1H*-pyrrole (0.25g, 1.75 mmol, 2.1 eq) and benzaldehyde (0.09 mL, 0.832 mmol, 1 eq) in DCM (40 mL) was added TFA (2 drops), which turned the solution red from pale pink. The reaction was then stirred at room temperature until TLC showed complete consumption of the aldehyde (18 hours). DDQ (0.2g, 0.0874 mmol, 1.05 eq) was then added in a single portion (this turned the mixture deep blue) and the reaction was left to stir at room temperature for 16 hours. Next, N,N-diisopropylethylamine (1.74 mL, 9.98 mmol, 12 eq) and boron trifluoride diethyletherate (1.73 mL, 14 mmol, 16.8 eq) were added, the addition of which generated a white gas and a pinkish tint developed in the reaction mixture. After stirring at room temperature overnight, the reaction mixture was washed with water (3 × 100 mL) and brine (3 × 100 mL). The separated organic fractions were dried over $MgSO_4$ and filtered. The solvent was then removed under reduced pressure to yield a deep pink residue. This material was purified by column chromatography on silica gel using toluene as eluent to afford a pink/ purple crystalline solid (0.4g, 9% yield). M.pt = 244-247 ^oC

^1H NMR ($CDCl_3$, 300 MHz): δ (ppm) = 7.87 (d, *J* = 6.0 Hz, 2H), 7.78 (d, *J* = 6.0 Hz, 2H), 7.56, (m, 5H), 7.41 (m, 2H), 7.23 (d, *J* = 6.0 Hz, 2H) 6.86 (m, 2H), 6.61 (m, 2H). 2.39 (s, 6H).

^{13}C NMR ($CDCl_3$, 75 MHz): δ (ppm) = 159.51, 158.51, 131.14, 130.66, 130.12, 129.53, 129.50, 129.44, 129.14, 128.33, 128.27, 121.05, 120.70, 21.56.

^{11}B NMR (160 MHz, $CDCl_3$) δ = -0.46 (t, *Jav* = 32.07 Hz).

^{19}F NMR (470 MHz, $CDCl_3$) δ (ppm) = -132.41 (q, *Jav* = 30.09 Hz

1-(Dimethylaminophenyl)naphthalene

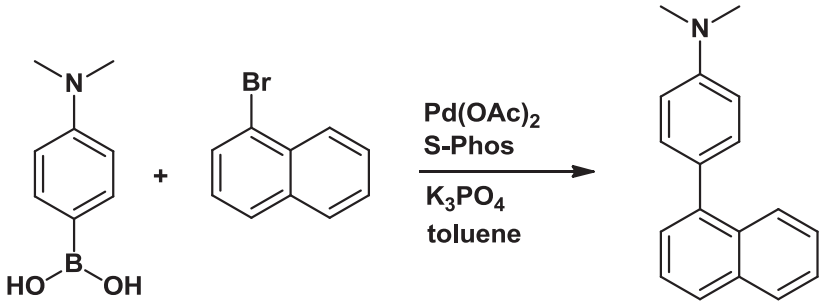

A flame dried Schlenk flask was charged with $Pd(OAc)_2$ (0.04g, 0.19 mmol, 4 mol%), S-Phos (0.16g, 0.39 mmol, 0.08eq), 4-(dimethylamino)phenylboronic acid (0.96g, 5.8 mmol, 1.2eq) and potassium phosphate (1.97g, 14.49 mmol, 3eq). Finally, 1-bromonaphthalene (1g, 4.83 mmol, 1eq) and freshly distilled toluene were added and the resulting mixture was heated at 105˚C for 24 hours with rapid stirring. The reaction mixture, which was pale yellow in colour, was then allowed to cool to room temperature and was passed through a silica plug. The solvent was then removed *in vacuo* to leave a yellow solid. This was purified by column chromatography to give a white crystalline solid, (0.41g, 34% yield).

^{1}H NMR ($CDCl_3$, 300 MHz): δ (ppm) = 8.18 (d, 4H, *J* = 7.5 Hz, 1H), 8.03 (d, *J* = 7.5 Hz, 1H), 7.94, (d, *J* = 7.5 Hz, 1H), 7.58 (m, 6H), 6.99 (d,t, *J* = 9 Hz, *J*'= 3 Hz, 2H), 3.13 (s, 6H).

^{13}C NMR ($CDCl_3$, 75 MHz): δ (ppm) = 149.80, 140.42, 133.88, 132.06, 130.76, 129.01, 128.16, 126.79, 126.69, 126.27, 125.66, 125.52, 125.44, 112.24, 40.55.

1-Iodo-4-bromonaphthalene[29]

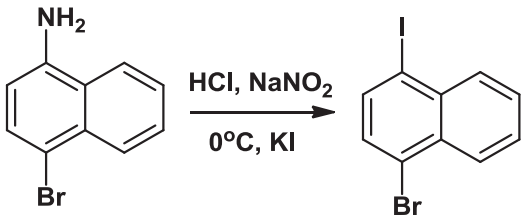

In a 250 mL flask, 4-bromonaphthalen-1-amine (1g, 4.5 mmol, 1.0 eq) was dissolved in HCl (18mL) and distilled water (18mL) with cooling to give a suspension. This suspension was cooled in an ice bath prior to the dropwise addition of a cooled solution of sodium nitrite (0.39g, 5.6 mmol, 1.3 eq) in water (10 mL). The resulting brown mixture was thoroughly stirred for one hour whilst immersed in an ice bath. Finally, potassium iodide (1.08g, 6.5 mmol, 1.4 eq) was dissolved in water (10 mL) in a round bottomed flask equipped with a stirrer bar and to this the diazo solution was added with vigorous stirring. The reaction mixture was then stirred at room temperature overnight. The product was extracted into diethyl ether and the combined organic layers washed with brine, dried ($MgSO_4$) and evaporated to dryness. The residual solid was purified by flash column chromatography on neutral aluminium oxide using hexane as eluent to give the desired product, a fluffy orange solid (0.91g, 61% yield).

^{1}H NMR ($CDCl_3$, 300 MHz): δ (ppm) = 8.19 (m, 1H), 8.08 (m, 1H), 7.90 (d, J = 7.9 Hz, 1H), 7.61 (m, 2H), 7.48 (d, J = 7.9 Hz, 1H).
^{13}C NMR ($CDCl_3$, 75 MHz): δ (ppm) = 137.51 (ArC), 135.30 (ArC), 132.93 (ArC), 132.60 (ArC), 130.86 (ArC), 128.68 (ArC), 128.32 (ArC), 128.02 (Ar-C), 124.22 (Ar-C-Br), 99.07 (ArC-I).

[29] PhD Thesis of Dr Sarah Mitchell, *"Design and construction of naphthalene-based architectures for long distance electron exchange"*, submitted January 2006.

1-(Dimethylaminophenyl)-4-bromonaphthalene

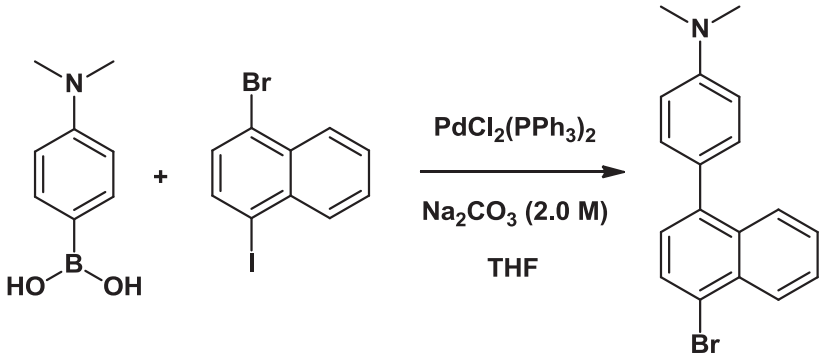

A flame dried Schlenk flask was charged with 1-iodo-4-bromonaphthalene (0.40g, 1.2 mmol, 1.1 eq), dimethylaminophenylboronic acid (0.18g, 1.1 mmol, 1 eq) and $Pd(PPh_3)_4$ (0.05g, 0.044 mmol, 4 mol %). Na_2CO_3 (2.0M) (1mL, 3.0eq) and freshly distilled THF (8mL) were then added and the resulting mixture was heated at 80˚C for 24 hours with rapid stirring. The reaction mixture, which was deep orange in colour, was then allowed to cool to room temperature and was passed through a short silica plug and the solvent removed to leave a very pale yellow solid. (0.36g, 99% yield).

^{1}H NMR ($CDCl_3$, 300 MHz): δ (ppm) = 8.23 (d, *J* = 7.7 Hz, 1H), 7.93 (d, *J* = 7.7 Hz, 1H), 7.73, (d, *J* = 7.7 Hz, 1H), 7.52 (m, 1H), 7.39 (m, 1H), 7.27 (m, 2H), 7.19 (t, *J* = 3.8 Hz, 1H), 6.79 (m, 2H), 3.13 (s, 6H).
^{13}C NMR ($CDCl_3$, 75 MHz): δ (ppm) = 150.19, 140.91, 133.49, 132.35, 130.80, 131.03, 129.60, 128.07, 127.43, 127.07, 126.98, 126.41, 121.40, 112.40, 40.53
Acc mass calculated for $C_{18}H_{16}NBr$: 326.0544. Found 326.0533.

1-(Dimethylaminophenyl)-4-(4,4,5,5-tetramethyl-1, 3, 2-dioxaborolan-2-yl)-naphthalene

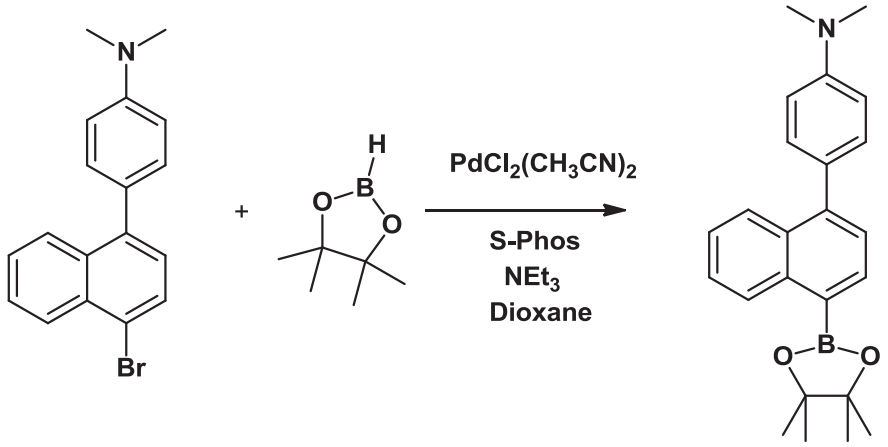

A flame dried Schlenk flask was charged with $PdCl_2(CH_3CN)_2$ (0.015g, 0.06 mmol, 4 mol%), S-Phos (0.099g, 0.024 mmol, 16 mol%) and 1-(dimethylaminophenyl)-4-(bromo)-naphthalene (0.50g, 1.5 mmol, 1eq). The Schlenk tube was then capped with a rubber septum and thoroughly degassed. Triethylamine (2 mL) was then added via a degassed syringe along with pinacolborane (0.28g) and dioxane (10 mL). The Schlenk tube was then sealed and the reaction heated at 80 degrees for 24 hours with rapid stirring. The reaction solution was then passed through a short silica plug and the solvent removed *in vacuo*. The crude material obtained was then purified by column chromatography (DCM: petrol 1:1) to give a white solid (0.18g, 32% yield).

^{1}H NMR ($CDCl_3$, 300 MHz): δ (ppm) = 8.34 (d, *J*= 7.7 Hz, 1H), 8.03 (d, *J* = 7.7 Hz, 1H), 7.83, (d, *J* = 7.7 Hz, 1H), 7.64-7.59 (m, 1H), 7.52-7.47 (m, 1H), 7.38 (d, *J* = 9.0 Hz, 2H), 7.28 (d, *J* = 9.0 Hz, 1H), 6.91-6.85 (m, 2H), 3.07 (s, 6H), 1.28 (s, 12H).
^{13}C NMR ($CDCl_3$, 75 MHz): δ (ppm) = 150.01, 140.79, 133.32, 132.23, 131.03, 130.87, 129.66, 127.45, 127.15, 127.07, 126.53, 126.41, 121.41, 112.32, 82.77, 40.69, 24.64.
^{11}B NMR (160 MHz, $CDCl_3$) δ = 30.05 (s)

4,4'-Difluoro-8-(dimethylaminophenylbinaphthyl)-1,3,5,7-tetramethyl-2,6-diethyl-4-bora-3a,4a-diaza-s-indacene

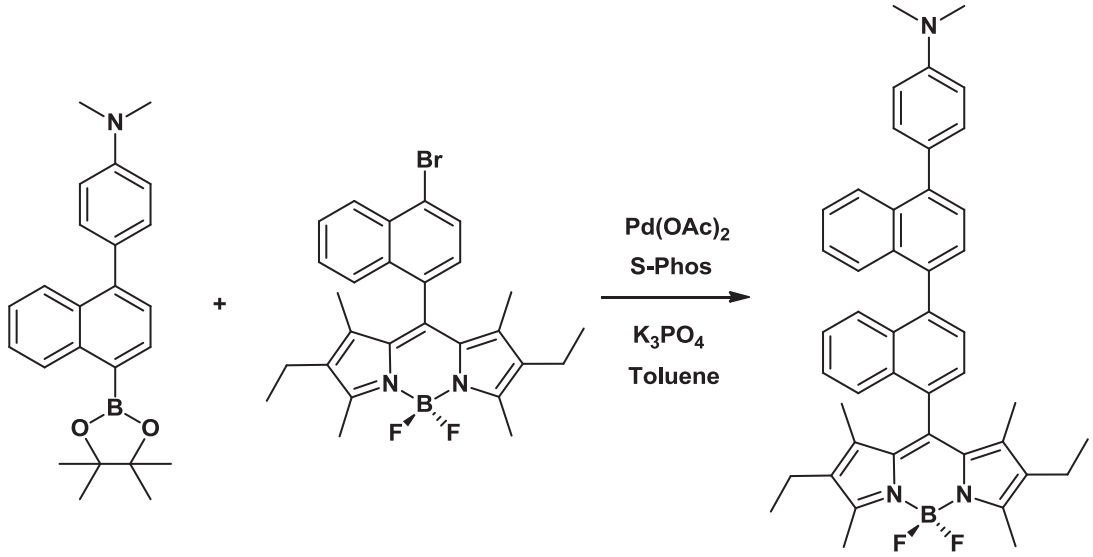

A flame dried Schlenk flask was charged with $PdCl_2(PPh_3)_2$ (0.0015g, 0.002 mmol, 8 mol%), 1-(dimethylaminophenyl)-4-(4,4,5,5-tetramethyl-1, 3, 2-dioxaborolan-2-yl)-naphthalene (0.01g, 0.027 mmol, 1eq) and sodium carbonate (2.0 M) (0.25mL, 3.0eq). Finally, BRNBD (0.02g, 0.04 mmol, 1.5eq) and freshly distilled THF were then added and the resulting mixture was heated at 80˚C for 16 hours with rapid stirring. The reaction mixture, which was red in colour, was then allowed to cool to room temperature and was passed through a short silica plug and the solvent removed to leave a red solid. This was then purified by column chromatography to give a red crystalline solid, **DMANBD** (0.014g, 50% yield).

^{1}H NMR ($CDCl_3$, 300 MHz): δ (ppm) = 8.15 (d, *J* = 9.0 Hz, 1H), 7.94 (d, *J* = 6.0 Hz, 1H), 7.63, (d, *J* = 3.0 Hz, 1H), 7.57 (m, 1H), 7.53 (s, 2H), 7.52 (d, *J* = 3.0 Hz, 1H), 7.43 (m, 3H), 7.32 (m, 3H), 7.18 (d, *J* = 6.0 Hz, 1H), 6.93 (d, *J* = 6.0 Hz, 2H), 3.08 (s, 6H), 2.20 (s, 6H), 2.30 (q, *J* = 6.0 Hz , 4H), 1.23 (s, 3H), 1.16 (s, 3H), 0.99 (m, 6H).

^{13}C NMR ($CDCl_3$, 75 MHz): δ (ppm) = 153.93, 112.33, 140.70, 140.07, 138.62, 138.35, 138.10, 136.51, 133.32, 133.06, 132.98, 132.79, 132.06, 131.40, 130.97, 129.03, 128.22, 127.80, 126.99, 126.76, 126.57, 126.57, 126.31, 126.23, 125.86, 125.75, 125.64, 125.46, 112.33, 40.70, 17.11, 14.68, 12.61, 11.35.

^{11}B NMR (160 MHz, $CDCl_3$) δ = -0.63 ((t, *Jav* = 26.94 Hz).

^{19}F NMR (470 MHz, $CDCl_3$) δ = 145.41 (F_A) ; δ = 145.63 (F_B). J_{AB} = 112 Hz

Acc. mass calculated for $C_{45}H_{44}BF_2N_3$= 676.3677 found 676.3671

Chapter 3

Julolidine Bodipy– A Novel Sensing Donor-Acceptor Dyad

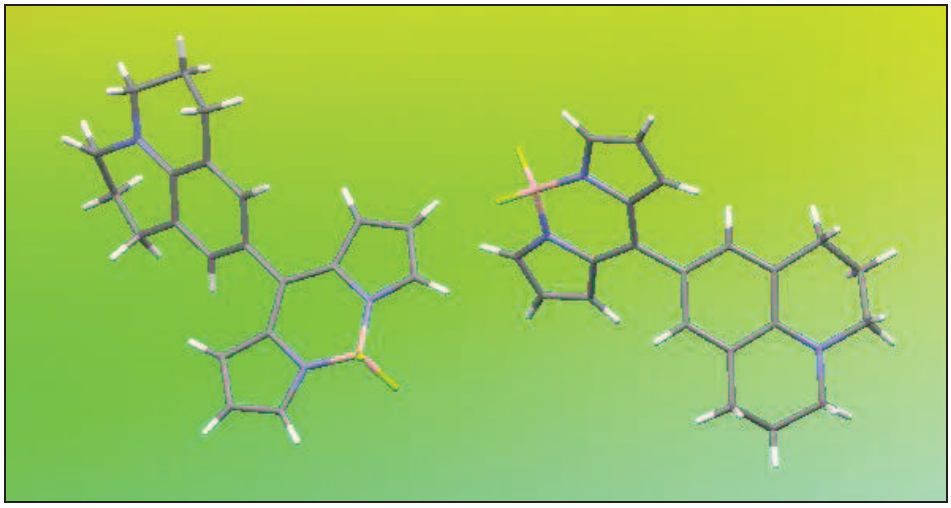

This chapter is entirely based on the design, synthesis and photophysical and electrochemical analysis of the novel dyad **JULBD**, the structure of which is given below. **JUL** = julolidine.

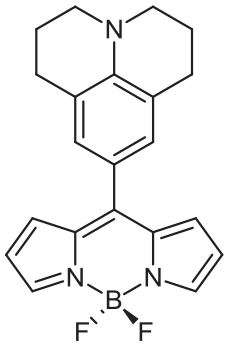

JULBD

*Figure 1 – The structure of **JULBD**.*

Photophysical terms and explanations

In several of the tables of photophysical data included within this chapter, the following symbols are used. For the purpose of clarity they are explained below:

λ_{em}	emission maxima
Δ_{ss}	Stokes Shift
Φ_{fl}	fluorescence quantum yield
τ	lifetime
k_{rad}	radiative rate constant
k_{NR}	non-radiative rate constant

Symbols used in equations (for example in section *3.5.2*) are discussed and defined within each section of the chapter for clarity.

It should be explained that much of the photophysical examination of **JULBD** was carried out in the 'Measurement Laboratory' which is run by Professor Anthony Harriman. The work was done by Master's student Dave Howgego. I would like to acknowledge his diligent and valuable contributions to the work undertaken on **JULBD** which is discussed herein.

3.1 Introduction

3. 1. 1 Molecular sensing and probing devices

Molecular probing and sensing systems are of utmost importance across numerous disciplines. More specifically, fluorescent sensors which are able to detect, quantify or image certain ions or molecules have become essential and ubiquitous tools in science and technology.[1] The uses of fluorescent sensors span a variety of disciplines to include biological imaging[2,3], chemosensing[4] and viscosity analysis and measurement[5,6,7]. The properties associated with bodipy chromophores, namely high fluorescence quantum yields (Φ = 60-90%), high molar absorption coefficients (ε = 40,000-110,000 M^{-1} cm^{-1}) and sharp absorption bands observed (fwhm $\approx$ 25-35 nm) make them the perfect candidates for use within such applications. These favourable properties, in addition to the long excited state lifetimes (1-10 ns), negligible triplet-state formation and a remarkable photostability and a powerful synthetic robustness and adaptability, permit the synthesis of intricately designed sensors which commonly feature in the literature. It is only really since the mid-nineties that bodipy based dyes have received the recognition they deserve as successful candidates in this field, but the growing numbers of research publications and patents reinforce its ever-increasing popularity.

Fluorescent indicators for real time sensing and imaging purposes are crucial tools in the fields of materials- and life-sciences[8, 9,10]. Recently, Gabbai and Lin[11] developed an [^{18}F] radio-labelled version of the bodipy chromophore (denoted [^{18}F]-[2-F^{+}] from hereon in) for use as a positron emission tomography/ fluorescence dual modality imaging agent. Its bio-distribution and clearance was studied in mice, where the probe was found to successfully accumulate in the liver and kidneys. This was revealed via fluorescence imaging of these organs by irradiation at λ = 500 nm and the *ex vivo* microPET and *in vivo* PET studies showed excellent correlations. The group are currently studying the radio-fluorination of bodipy dyes that emit in the near Infra-Red (NIR) region of the electromagnetic spectrum.

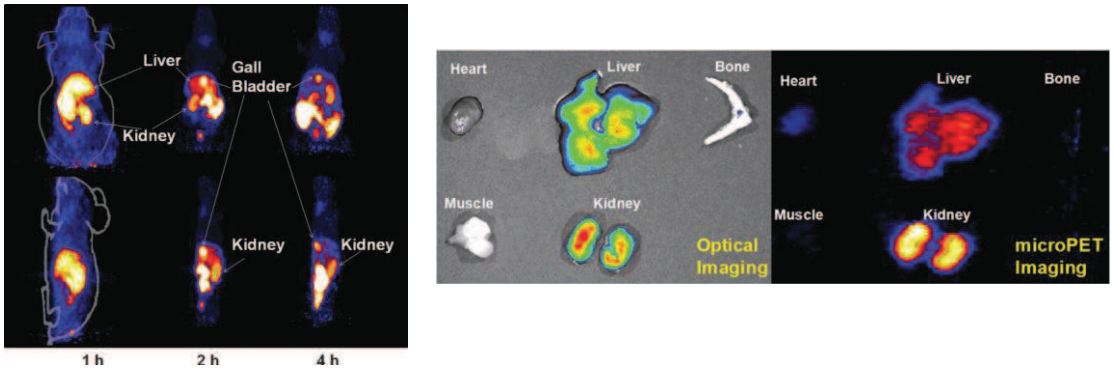

Figure 2[11] – Left: PET images of a mouse injected with the radio-labelled chromophore [^{18}F]-[2-F^{+}] showing that no detectable bone uptake is observed up to 4 hours post injection. Right: Ex vivo fluorescence (left) and microPET (right) imaging of dissected mouse organs.

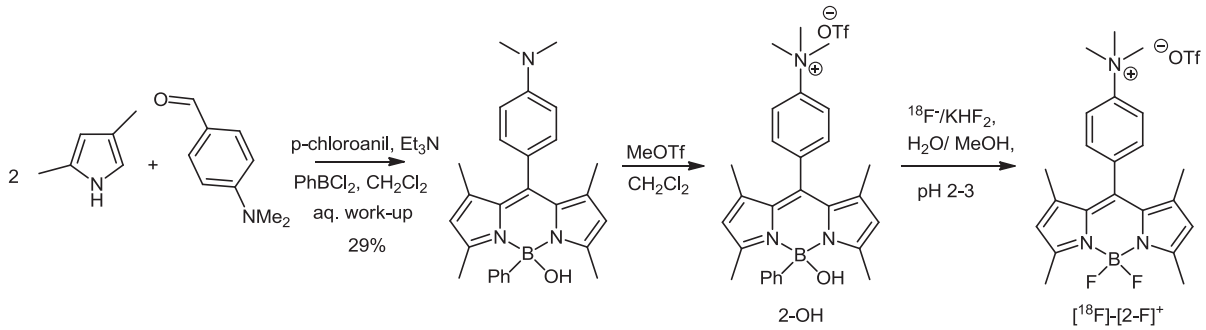

Scheme 1[11] – The synthesis of [^{18}F]-[2-F^{+}] from the bodipy hydroxo derivative.

Species capable of sensing toxic or hazardous ions are also of high importance in modern science. The toxic heavy metal and environmental contaminant, mercury, is dangerous to human life even at low concentrations[12] and can cause serious health concerns such as brain damage[13], DNA damage[14] and various cognitive and motion disorders[15]. It can be transferred via edible fish,[16] as it is easily passed through the food chain as organometallic mercury. This occurs following the transformation of mercury from its elemental or inorganic form by anaerobic organisms. Systems able to detect such species are therefore of pivotal importance and much emphasis has been placed in recent years on the design and synthesis of fluorescent mercuric ion sensors[17]. An elegant example is the near IR emitting chemosensor generated by Atilgan *et al.*[18] in which a large hypsochromic shift (approx. 90 nm) can be observed

in both the absorption and emission spectrum upon co-ordination of Hg^{2+} into the macrocyclic moiety appended to the phenyl rings branching via alkene mediated conjugation from the 5' and 3' position on the bodipy.

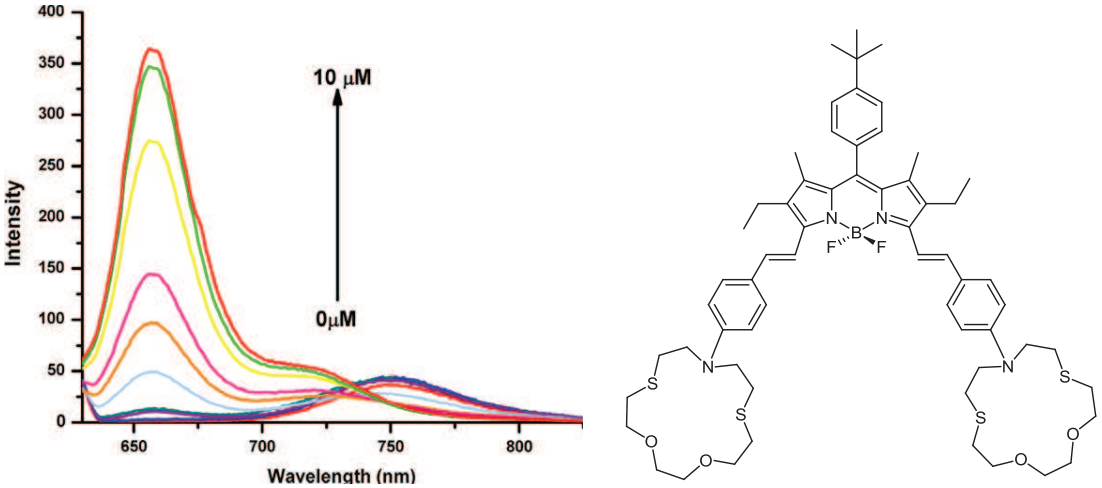

Figure 3[18] – Left: An emission spectrum of the chemosensor designed by Atilgan et al. at increasing concentrations of Hg^{2+} in THF. Right: the structure of the chemosensor.

3.1.2 Molecular rotors

Molecular rotors have enjoyed success across an extensive variety of scientific disciplines[19,20,21,22,23,24.] They are described in the literature as fluorescent molecules that form twisted intramolecular charge transfer (TICT) states[25] upon photoexcitation. Such systems therefore exhibit two competing de-excitation pathways: fluorescence emission and non-radiative de-excitation from the TICT state[26].

Viscosity is a significant physical parameter in determining the diffusion rate of species in biological systems. Molecular rotors are often incorporated into such work, due to the fact that TICT formation is viscosity dependent. As aforementioned, the intramolecular rotation or twisting exhibited by fluorescent molecular rotors leads to non-radiative decay from the excited state back to the ground state. The rotation or twisting observed is slowed down in a viscous environment, which restricts access to the non-radiative decay pathway. This leads to an increase in the quantum yield and lifetime of fluorescence. Molecular rotors are therefore rapidly emerging as novel biosensors for both local and bulk microviscosity[17] offering real-time response and high spatial resolution.

Molecular rotors offer many advantages over environment sensitive probes, for example, they can be used independent of the polarity of the environment. This is due to the fact that emission intensity is influenced by the viscosity, whereas polarity changes are reflected in a small shift of the peak emission wavelength.[27,28] Furthermore, fluorescence-based viscosity measurements can be taken with fluid volumes as minimal as 100 microlitres, and theoretically, fluorescence measurements take sub-second acquisition times.

Over recent years, promising developments have been made incorporating bodipy into fluorescent molecular rotors. These largely operate on the premise of hindered intramolecular rotation. For example, Lindsey *et al.*[29] published work indicating that both the fluorescence lifetime and quantum yield of the S_1 excited state for 8-phenyl bodipy or 8-(4-*tert*-butylphenyl) bodipy were significantly smaller than those measured for more hindered analogues. These slightly bulkier systems possessed either a mesityl or an o-tolyl substituent at the 8 position. The group suggested that free rotation of the 8-aryl moiety would lead to higher fluorescence quantum yield and lifetime values by reducing the non-radiative decay of the S_1 state.

3.1.3 Charge transfer mechanisms in organic dyads

Charge transfer (CT) in donor-acceptor systems is associated with various physical phenomena including optical CT electronic transitions[30], highly directional dipole moments[31], long-range electron transfer[32], twisted intermediate states[33], magnetic ordering[34] and solvatochromism[35]. Research carried out investigating charge transfer processes has a long history and there are numerous publications[36,37,38,39,40,41,42] proposing the theoretical reasoning behind a large number of CT mechanisms, reactivities and rates. Charge transfer rates can be affected by various quantum phenomena to include nuclear tunnelling, quantum interference and curve crossing and a number of theories have been proposed, incorporating these factors. In this chapter, investigations into the charge transfer processes occurring within **JULBD** are carried out using absorption spectroscopy and Marcus theory and the dependencies observed upon solvent polarity are discussed. The subsequent chapter will address the properties of the system in a different manner, looking into the observed NMR chemical shifts to probe the electronic environment at each carbon atom in **JULBD**.

3.2 Design and Synthesis

The design of the novel dyad, **JULBD**, was formulated from the desire to generate a molecular rotor with both excellent sensing capabilities and the ability to emit fluorescence via an on/off mechanism in the manner of a molecular switch. It is known that 9-(dicyanovinyl)-julolidine (abbreviated to DCVJ from hereon in) possesses a powerful probing ability, due to the availability of the lone pair on the julolidine nitrogen to donation.

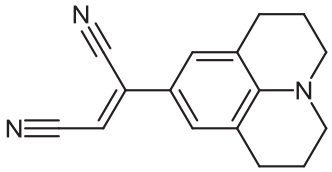

Figure 4 - 9-(Dicyanovinyl)-julolidine (DCVJ), a commercially available molecular rotor. The intramolecular charge transfer takes place between the julolidine nitrogen atom as electron donor and the electron accepting nitrile group.

The julolidine unit was therefore incorporated into the design of our system, whilst the bodipy fluorophore accounted for the fluorescent nature of the probe. A 'push-pull' type architecture was envisaged. Here, the bodipy moiety acts as the electron acceptor, whilst the nitrogen atom with its lone pair plays the role of electron donor. The aryl moiety of the julolidine residue forms the π-conjugated bridge connecting the two. This type of system is by no means uncommon[43,44,45] and in recent years much work has been undertaken to further investigate the optical[46,47] and redox[48] and photophysical[49] properties of push-pull chromophores of this nature.

The synthetic strategy employed in order to achieve the target dyad is highlighted in *Scheme 2.*

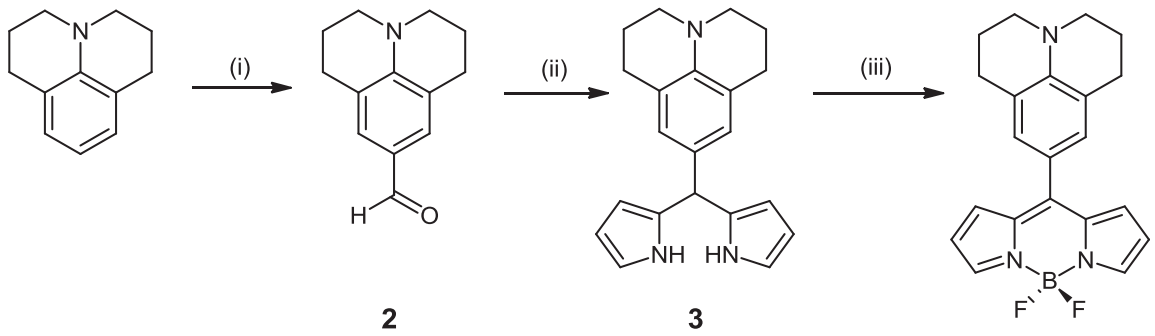

Scheme 2 – Reagents and conditions: (i) $POCl_3$, DMF, 90°C, 3 hrs, (ii) pyrrole, TFA, DCM, RT (iii) DDQ, N,N'-diisopropylethylamine, $BF_3.Et_2O$, RT.

The first step followed the Vilsmeier-Haack protocol in order to add the aldehyde functionality to the commercially available julolidine starting material. This reaction proceeded readily to give julolidine-9-carboxaldehyde (**2**) in 75% yield following an aqueous basic work-up and column chromatography on silica gel. Compound **2** was then condensed with pyrrole in the presence of a catalytic quantity of TFA in order to generate the dipyrromethane[50,51]. It should be mentioned here that pyrrole is used in this synthesis as both solvent and reagent and the excess pyrrole is recycled following its removal from the system by vacuum distillation. After work-up, the crude material was purified by column chromatography on basic alumina to generate julolidine dipyrromethane (**3**) in 30% yield.

The final reaction initially involved an oxidation step facilitated by DDQ to afford removal of the *meso* proton at the dipyrrin core, which was then followed by a subsequent addition of the base, N,N-diisopropylethylamine. The base served to abstract the pyrrole protons, prior to the chelation step, which generated the BF_2 unit, completing the indacene core to yield crude **JULBD.** The crude material was then purified by column chromatography on silica gel using DCM/ Petrol (2:1). Pure **JULBD** was isolated in the acceptable yield of 18%.

In order to try and optimize the yields of **3** and of **JULBD**, the final two steps of the synthetic protocol, namely the dipyrromethane and subsequent bodipy formation, were repeated. This was following the synthesis of a substantial stock-pile of julolidine 9-carboxaldehyde. It was revealed in work by Lindsey *et al.,*[52] that TFA may not necessarily be the preferred acid for achieving dipyrromethane formation.

This is due to the fact that it has been proven to cause 'darkening' of the reaction mixture, thought to be caused by a mixture of product decomposition and generation of unwanted side products. The dominant by-products include the N-confused dipyrromethane and also the tripyrrane species. These are both shown in *Figure 5* below. The isomeric N-confused dipyrromethane can be removed by recrystallization, whilst purification by column chromatography should be employed to omit the tripyrrane species.

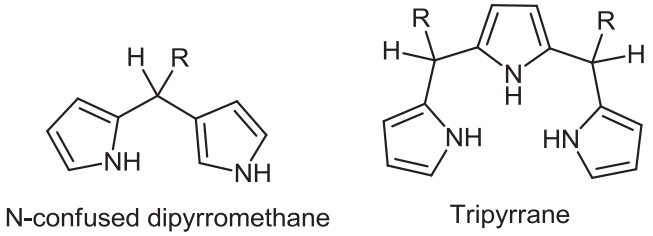

Figure 5 – The α,β-linked 'N-confused' dipyrromethane and tripyrrane side products which can be generated.

In light of this information, two of the Lewis acids which had been previously tested by Lindsey *et al.,* when investigating modifications to traditional dipyrromethane formation, were individually incorporated in the synthetic protocol in the place of TFA. Therefore, a series of small scale test reactions were conducted, which permitted investigation as to whether or not the 30% yield gained could be ameliorated. Indium chloride and boron trifluoride diethyl etherate were both tested, the former of which had celebrated the most success in the tests undertaken by Lindsey *et al*. Due to previous successes within the group using column chromatography purification for these species[53] on basic alumina, this was again carried out when testing $InCl_3$ and $BF_3.Et_2O$. Unfortunately in each case, an inferior yield (18% and 17% for each acid respectively) of compound **3** was gained. Although the yields were low, it was observed that the reaction seemed to proceed with less 'darkening' of the reaction mixture as documented by Lindsey *et al*.

In spite of the lack of success using $InCl_3$ to generate compound **3**, the synthesis of nitrophenyl dipyrromethane discussed within the following chapter was tested with TFA in the first instance and then with indium chloride. In the case of this reaction, an

improved yield of 18 % was observed using the latter, whilst trifluoroacetic acid catalysis generated a slightly more modest 15 % yield of dipyrromethane. It is evident from these observed yields that Brønsted acid catalysis is required to successfully generate julolidine dipyrromethane (**3**) whilst in the case of the nitro-derivative (denoted **5** in Chapter 4), the Lewis acid was marginally more successful.

3.3 Characterisation and Structure Confirmation

A full range of structural tools were used to analyse **JULBD** and its precursor julolidine dipyrromethane (**3**) including mass spectrometry, ^{1}H, ^{13}C, ^{19}F, ^{11}B NMR spectroscopy, elemental analysis and X-ray crystallography.

3.3.1 NMR Spectroscopy

3.3.1.1 Julolidine dipyrromethane

The proton and carbon NMR spectra corresponding to julolidine dipyrromethane (**3**) are shown below (*Figure 6*).

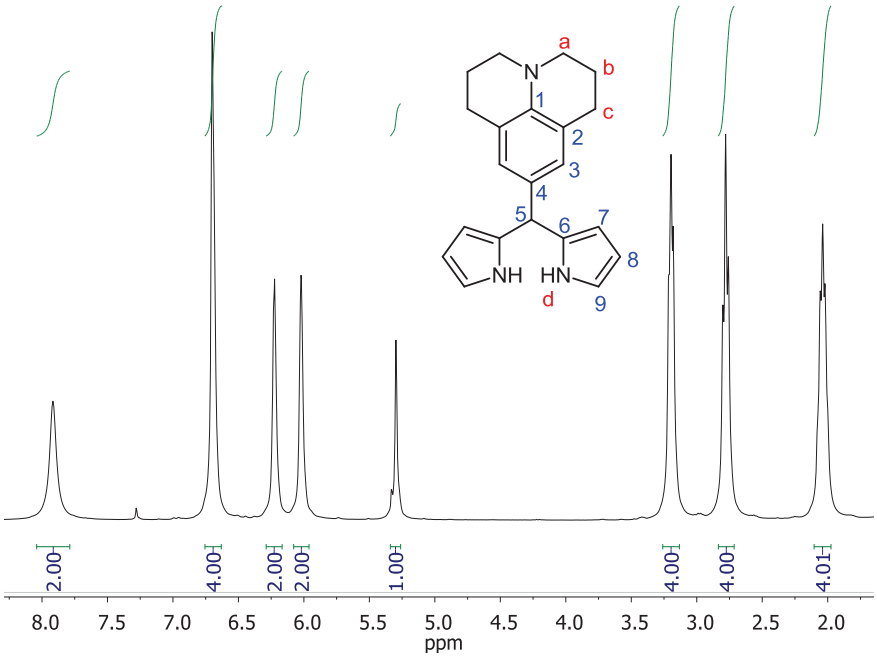

*Figure 6 – The ^{1}H NMR spectrum of julolidine dipyrromethane (**3**) recorded in $CDCl_3$ at 25°C.*

Chemical shift (ppm)	**Intensity (no. of H Atoms)**	**Multiplicity**	**Coupling constant (*J*/ Hz)**	**Assignment**
7.90	2	br s	N/A	d
6.68	4	s and d*	N/A	3 and 9
6.20	2	s	N/A	7
6.00	2	s	N/A	8
5.28	1	s	N/A	5
3.18	4	t	6.0	a
2.76	4	t	6.0	c
2.02	4	m	N/A	b

*Table 1 – The ^{1}H NMR peak assignment for julolidine dipyrromethane (**3**).*

**Although the peak at δ 6.68 has the appearance of a broadened singlet, it is in fact an overlapping singlet (proton set 3) and doublet (proton set 9, coupling to 8), both of which resonate at the same location in the spectrum.*

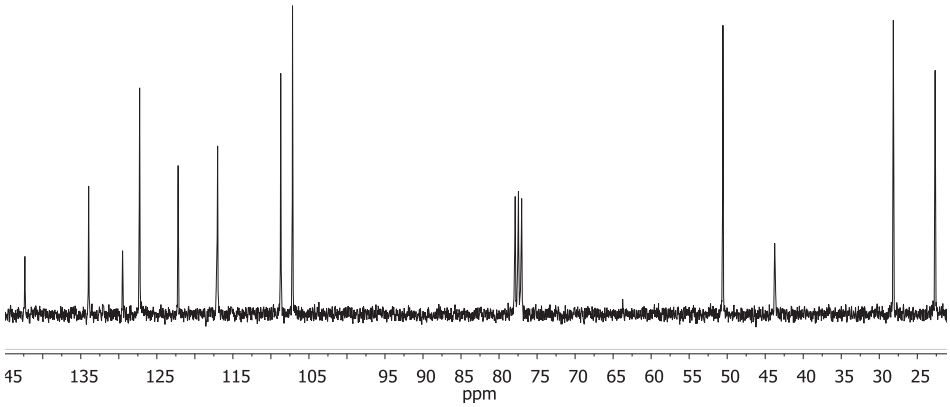

*Figure 7 – The ^{13}C NMR spectrum of julolidine dipyrromethane (**3**) recorded in $CDCl_3$ at 25°C.*

Chemical shift	Carbon atom assignment		Chemical shift	Carbon atom assignment
141.9	1		108.3	8
133.5	6		106.7	7
129.1	4		50.1	a
126.8	3		43.3	5
121.8	2		27.7	c
116.6	9		22.2	b

*Table 2 – ^{13}C NMR peak assignment for julolidine dipyrromethane (**3**) recorded in $CDCl_3$ at RT.*

3.3.1.2 JULBD

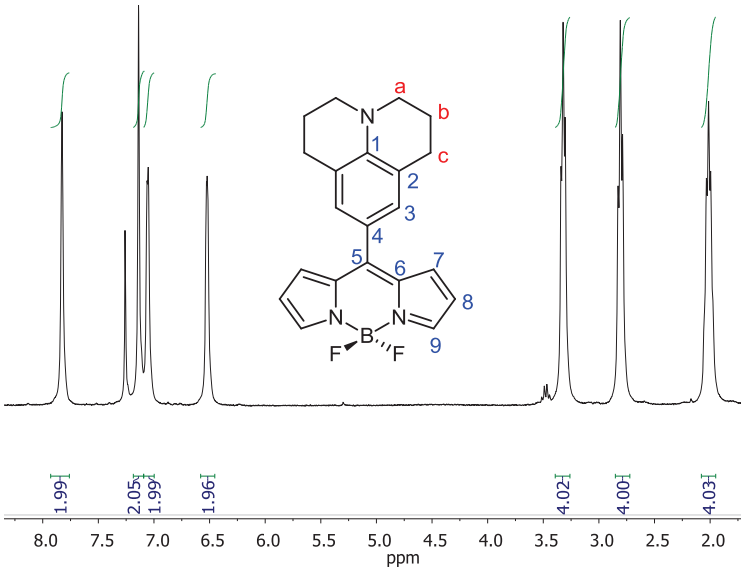

*Figure 8 – The ^{1}H NMR spectrum of **JULBD** recorded in $CDCl_3$ at 25°C.*

Chemical shift (ppm)	Intensity (no. of H Atoms)	Multiplicity	Coupling constant (*J*/ Hz)	Assignment
7.83	2	d	4.0	9
7.14	2	s	N/A	3
7.06	2	s	N/A	7
6.52	2	dd	4.0; 1.9	8
3.32	4	t	6.0	a
2.81	4	t	6.0	c
2.01	4	m	N/A	b

*Table 3 – The ^{1}H NMR peak assignment for **JULBD**.*

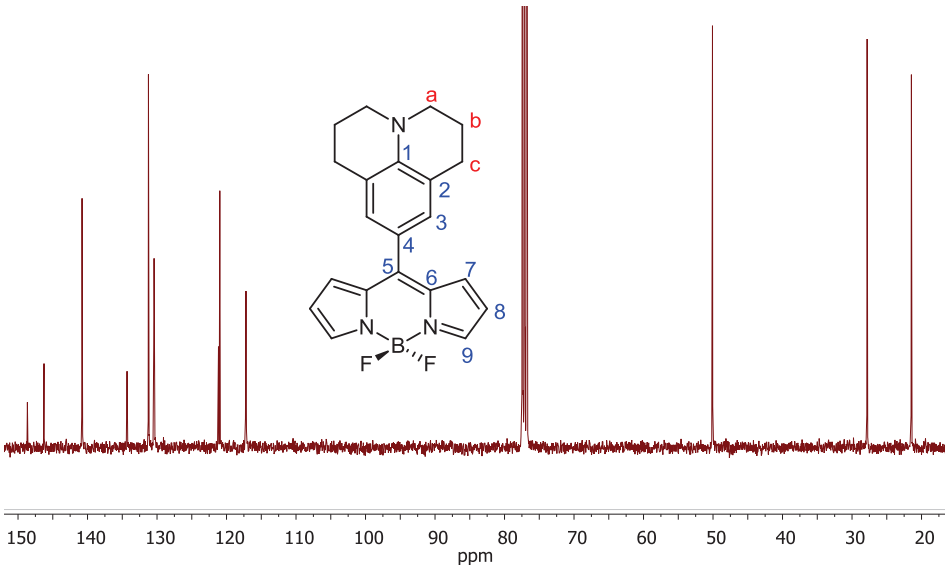

*Figure 9 – The ^{13}C NMR spectrum of **JULBD** recorded in $CDCl_3$ at 25°C.*

Using two dimensional spectra, a full assignment of the proton and carbon atoms in **JULBD** could be made. Techniques which aid spectroscopic assignment by generating correlated spectra are extremely useful and must not be overlooked. The types of correlated spectra that will be used within this thesis are the following:

- COrrelated SpectroscopY, denoted **COSY** from hereon in, is a two dimensional experiment which indicates all the spin-spin coupled protons in a single spectrum. The two proton spectra are plotted orthogonally on discrete

axes. The peaks which are mutually spin-spin coupled are indicated by cross peaks. These are symmetrically situated about the diagonal.

- Heteronuclear Multiple Quantum Coherence (abbreviated to **HMQC**) is a technique which allows a correlation to be made between the proton and carbon spectra. It is also known as ^{1}H-^{13}C COSY. The technique uses a pulse sequence in which a delay time is set to ½ *J*, where *J* is the value of the one bond ^{13}C-^{1}H coupling constant[54]. This generates a correlation between ^{13}C and the proton to which it is directly attached (i.e. a one bond correlation).
- Heteronuclear Multiple Bond Connectivity (**HMBC**) is a second technique whereby the time delay in the pulse sequence is set to correspond to ½ *J*, where *J* is in the region of 10 Hz (a delay of around 50 ms). It is also known as long range ^{1}H-^{13}C COSY. Since many ^{1}H-C-^{13}C (two bond) and ^{1}H-C-C-^{13}C (three bond) coupling constants are rather similar in value and lie in the range 2-20 Hz, then ^{13}C chemical shifts are now correlated with the chemical shifts of those protons separated from them by two or three bonds.
- A **NOESY** (Nuclear Overhauser Effect SpectroscopY) spectrum refers to a two dimensional spectrum which records all the proton-proton NOE's present in a molecule in one single experiment. Each orthogonal axis displays the proton chemical shifts with the normal spectrum appearing on the diagonal. This time however, the cross-peaks indicate those protons that are close in space. In other words, a NOESY displays evidence of through-space rather than through-bond interactions.

The subsequent chapter is concerned with the elucidation of intramolecular charge transfer mechanisms within **JULBD** as revealed via ^{13}C NMR chemical shifts. In order to study this effect, a full carbon and proton assignment was made. The details of this assignment and the spectra used are given below for **JULBD**. The data applicable to the other dyads prepared for comparative purposes is detailed and analysed in Chapter 4.

Some limited assignment of carbon and proton resonances can be located in prior publications on bodipy dyes, thus comparison with literature data was made in order to confirm consistency with the interpretations made[55]. The proton resonances were

the first to be assigned, commencing with those associated with the aromatic and dipyrrin groups by their chemical shifts, coupling patterns and cross-correlations in the corresponding HMQC and COSY spectra. The only distinctive aryl singlet present in **JULBD** is that at δ 7.14 ppm, and this can be assigned to proton set 3. The most downfield doublet, located at 7.83 ppm, can be deemed to be proton 9 due to its characteristic chemical shift which is well known in the literature[56,57]. The locations of 7 and 8 are also known and the assignment of these four protons (3, 7, 8 and 9) permitted identification of the corresponding carbon atoms in the HMQC spectrum, shown in *Figures 10 and 11* by careful analysis of the correlations displayed. The quaternary carbons were also identified through their lack of cross peaks.

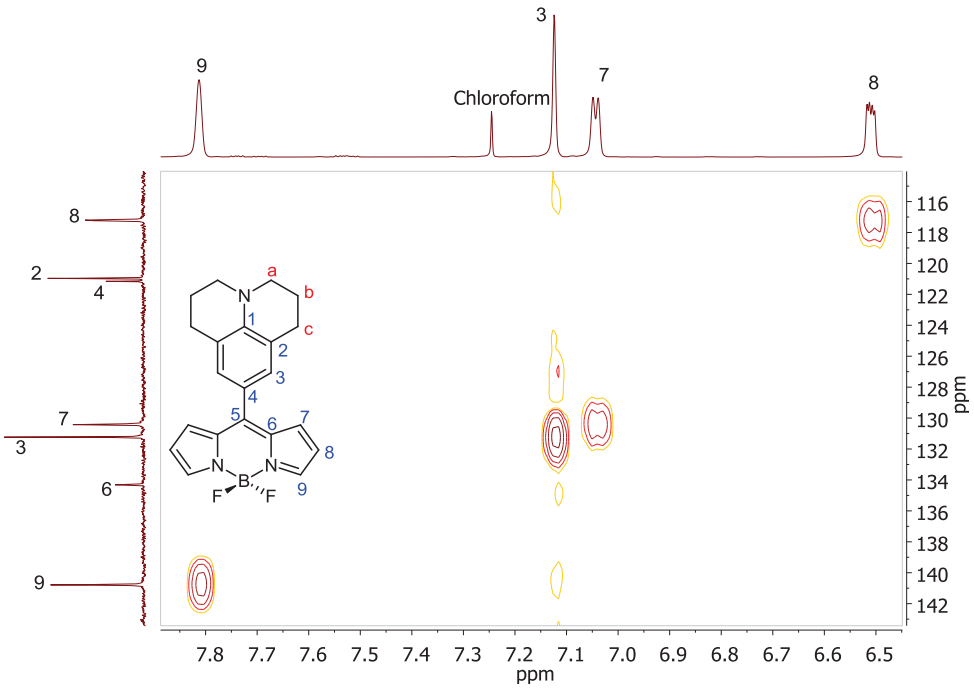

*Figure 10 – A partial HMQC spectrum of **JULBD** showing the aromatic region - recorded in $CDCl_3$ at 25°C.*

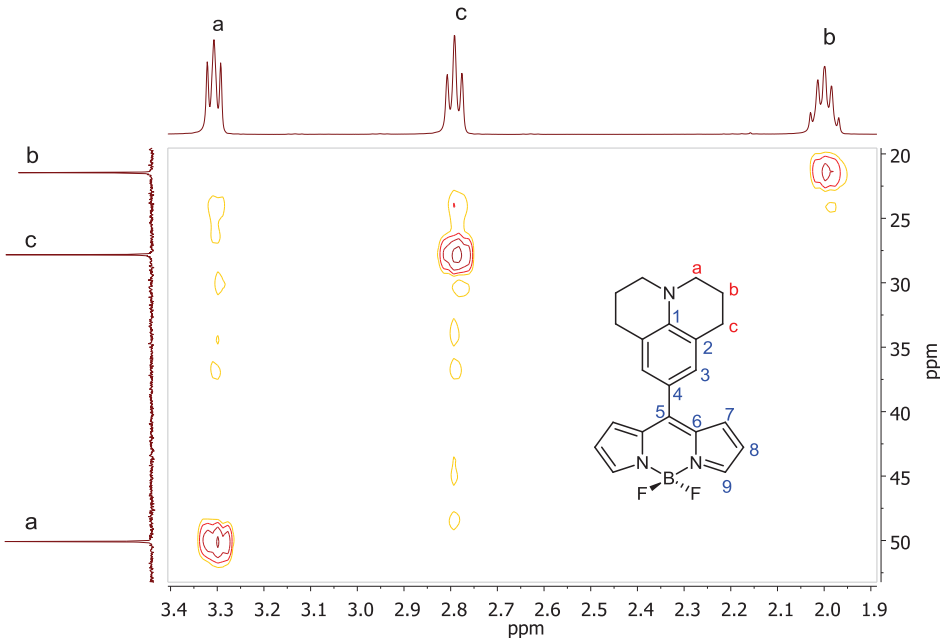

*Figure 11– A partial HMQC spectrum of **JULBD** showing the aliphatic region - recorded in $CDCl_3$ at 25°C.*

The HMBC spectrum, shown in *Figure 12* to *Figure 15* was then addressed, with the first carbon to be confirmed being carbon 9. This had already been identified using the HMQC *(Figures 10* and *11)* from the initial proton assignment and the identity of this carbon was further confirmed by the presence of strong spin-spin ^{3}J and ^{2}J couplings to protons 7 and 8, respectively. Proton 7 shows a strong correlation to the quaternary carbon at δ 134.2 ppm and this was found therefore to be carbon 6. The identity of 6 was also further reinforced by an evident spin-spin coupling to proton 9 via the nitrogen atom. The signals associated with the julolidine unit were then identified in order to eliminate them from the analysis. The identity of carbon 3 has also been established, thus carbon 2 was easily assigned due to its ^{3}J coupling to proton b and ^{2}J coupling to proton c. Carbon 1 was identified in a similar manner as ^{3}J couplings to protons 3 and c were clearly observed in the HMBC spectrum (shown in *Figure 12* to *Figure 15*). Another carbon atom also showed spin-spin coupling to proton 3 and this was assigned to be carbon 5 with the final quaternary carbon being assigned as carbon 4.

This assignment procedure was also repeated for **NITBD** and **PHBD** to be discussed within the following chapter.

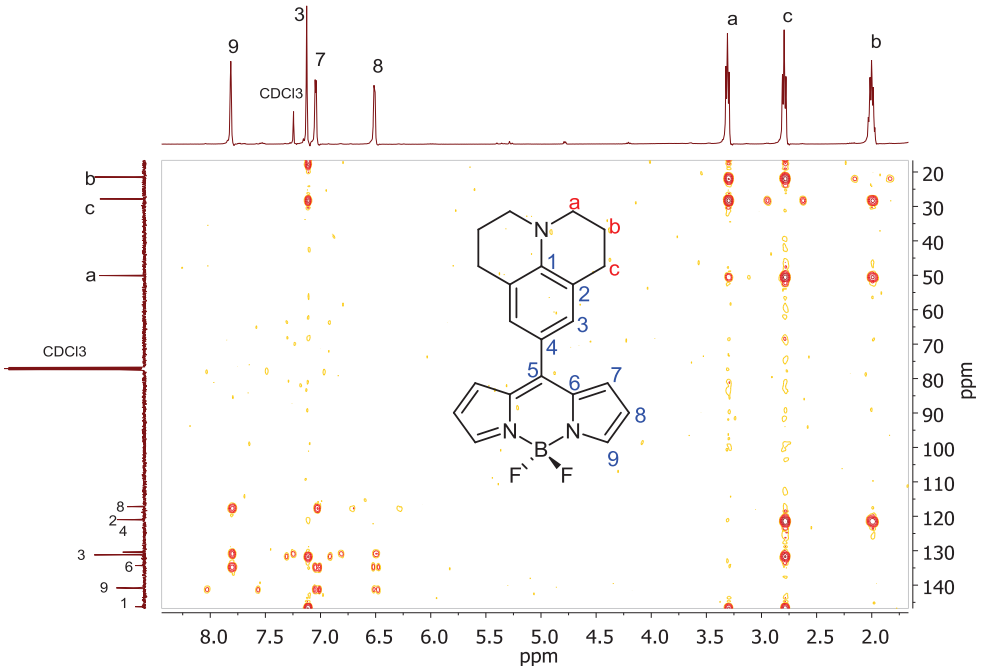

*Figure 12 – The HMBC spectrum of **JULBD** in $CDCl_3$ at 25 ^oC.*

Correlations will be displayed in more detail by expansions of various regions of the spectrum and annotations included to improve the clarity and perception.

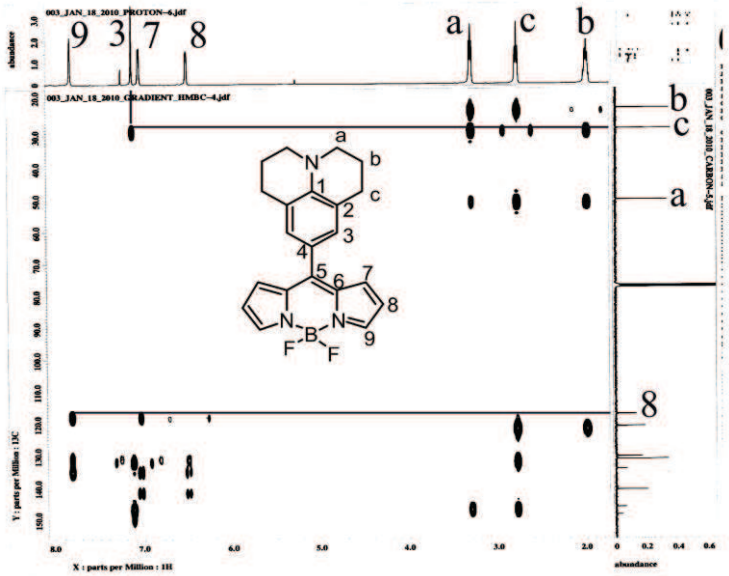

*Figure 13 – An HMBC spectrum of **JULBD** in $CDCl_3$ showing the proton to carbon correlations and partial assignments. Only proton 3 is shown to couple to carbon c whilst protons 9 and 7 both display a correlation with carbon 8.*

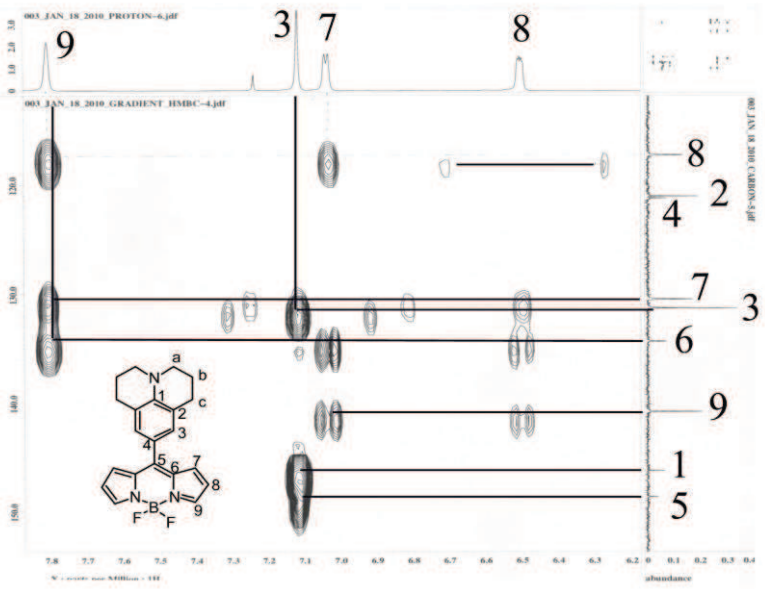

*Figure 14 – Expansion of the HMBC spectrum of **JULBD** in $CDCl_3$ showing the proton to carbon correlations and assignments.*

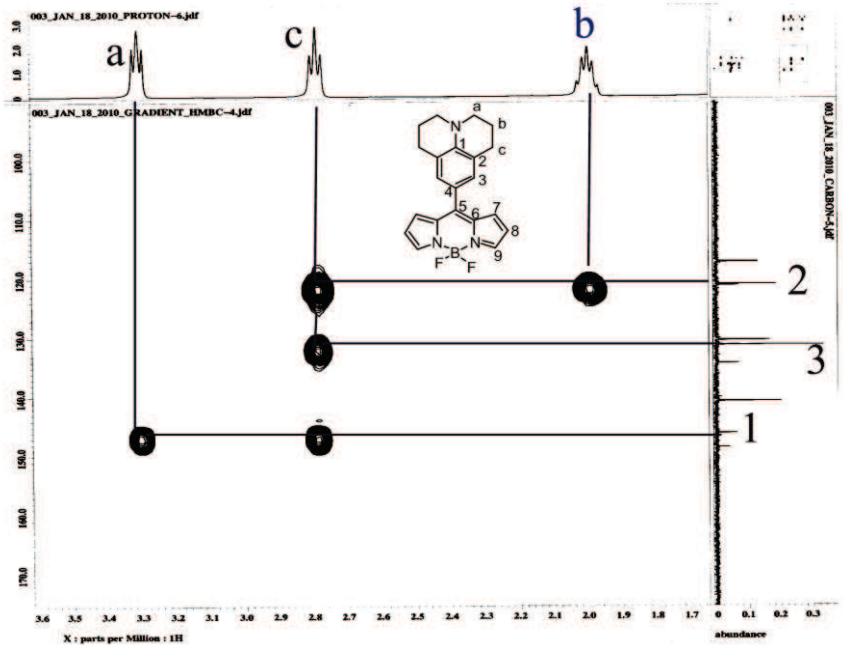

*Figure 15 - Partial HMBC spectrum for **JULBD** in $CDCl_3$ showing the proton to carbon correlations and assignments. Carbons 1, 2 and 3 all display a correlation to proton c, whilst only carbon 2 correlates with proton b as carbons 1 and 3 are too distant. Carbon 1 uniquely shows a correlation with proton a, for the same reason.*

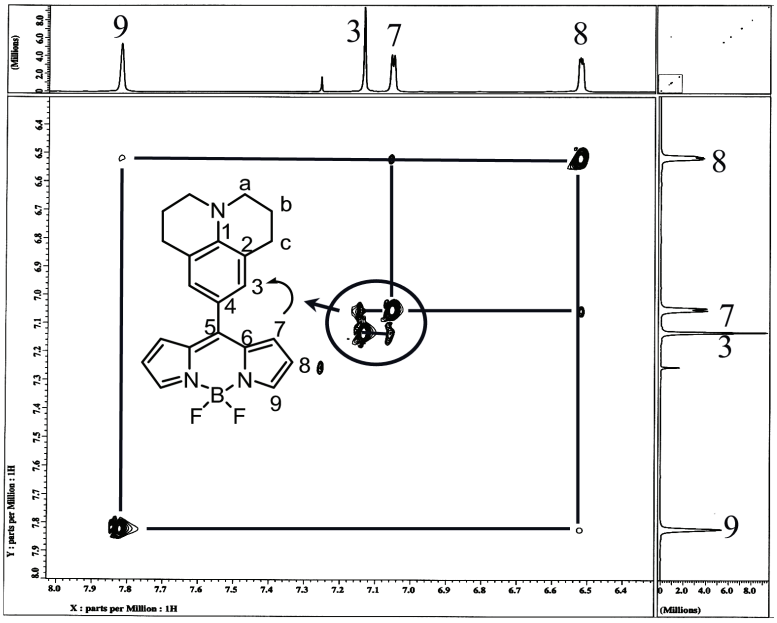

*Figure 16 - NOESY spectrum for **JULBD** in $CDCl_3$. This spectrum displays the NOE between H_7 and H_3 and thus confirms the proton assignments.*

Chemical shift	Carbon atom assignment		Chemical shift	Carbon atom assignment
148.5	5		121.1	4
146.5	1		120.9	2
140.7	9		117.1	8
134.2	6		50.0	a
131.1	3		27.7	c
130.3	7		21.4	b

*Table 4 – ^{13}C NMR peak assignment for **JULBD** recorded in $CDCl_3$ at RT.*

3.3.2 Crystal structure data analysis

Diffraction quality samples of crystalline **JULBD** were obtained by slow diffusion of petrol into a vial of a saturated solution of the compound in dichloromethane.

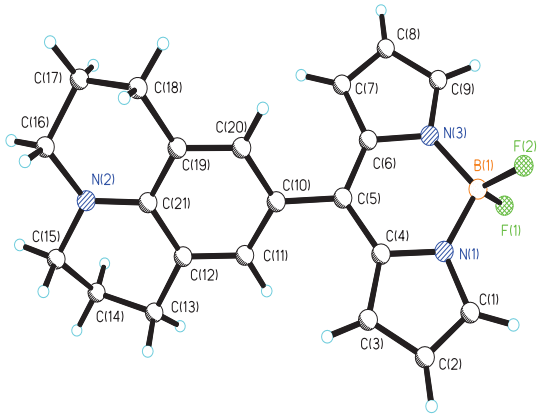

*Figure 17 – The atom labelled crystal structure of **JULBD**.*

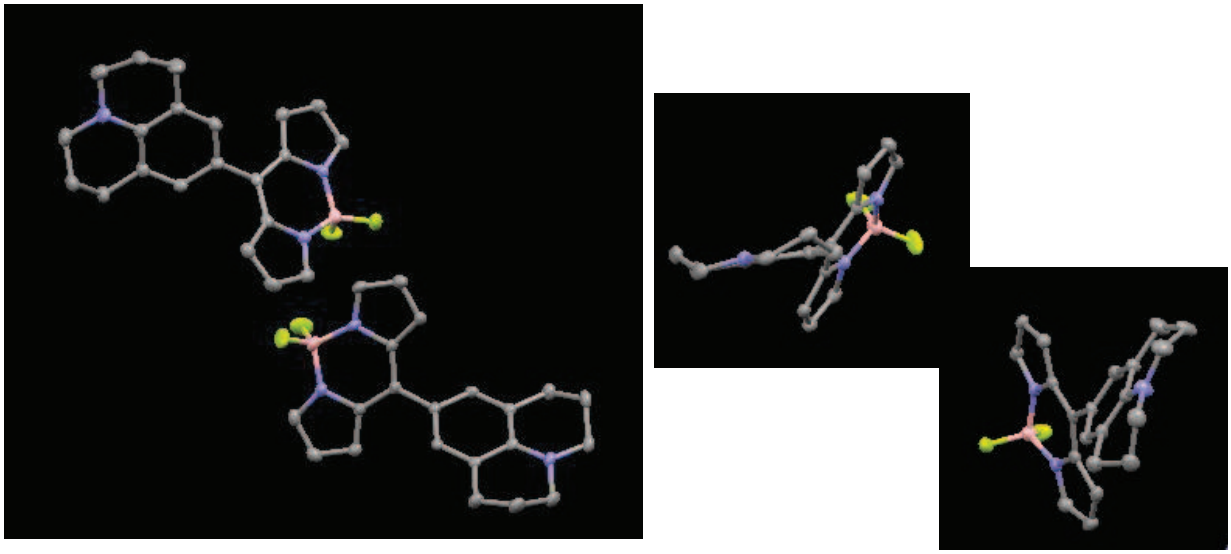

*Figure 18 – Left: Ellipsoid style crystal structure diagram of **JULBD**. Right: Puckering of the aliphatic rings of julolidine observed in the structure.*

It can be seen from the structures (*Figure 18*, right) that puckering occurs in the cyclohexane ring moieties of julolidine, which reduces ring-strain within the system. Furthermore, a structural motif commonly observed in crystalline structures of bodipy systems can be seen – namely the head-to-tail conformation adopted by units of the chromophore.

3.4 The electrochemical properties of JULBD

An examination into the electrochemical behaviour of **JULBD** was carried out in CH_2Cl_2 (0.2 M TBATFB) by cyclic voltammetry.

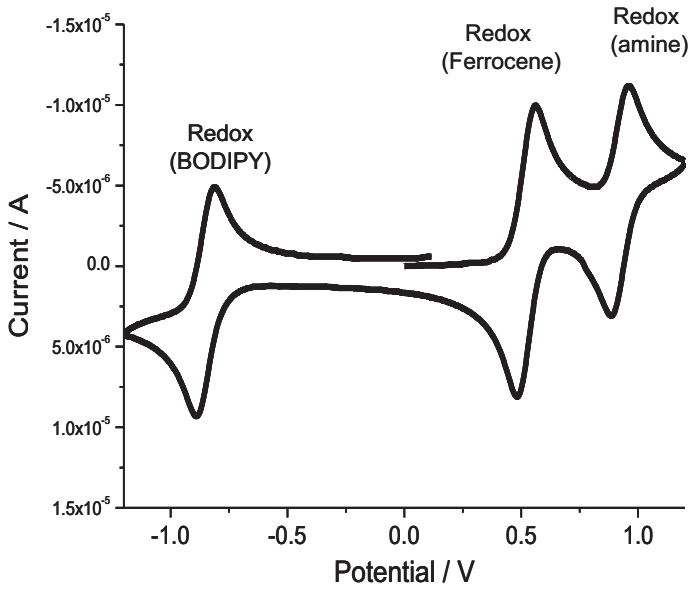

*Figure 19 – An annotated cyclic voltammagram recorded of **JULBD** in DCM (0.2M TBATFB).*

The cyclic voltammagram for **JULBD** can be interpreted in terms of the known electrochemical behaviour of isolated bodipy[58]. It can be seen that quasi-reversible one electron oxidation and reduction processes are observed for both the bodipy and the amine moiety in **JULBD**. However, when the second cyclic voltammagram was recorded over a wider potential window (*Figure 20*, below), oxidation of the amine in the julolidine component of the molecule becomes irreversible. This indicates that at higher oxidation potentials, unexpected processes are occurring at the electrode surface, for example, a type of unusual or unexpected side reaction or some variety of radical decay.

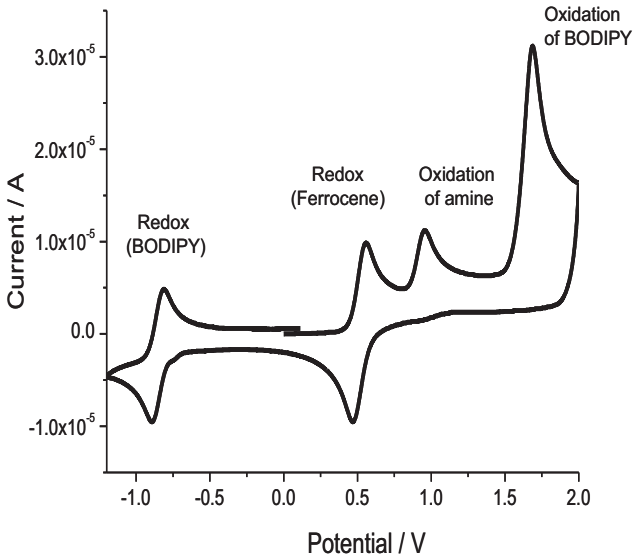

*Figure 20 – A second cyclic voltammagram recorded of **JULBD** under the same parameters over a higher potential range.*

3.5. Photochemical studies

The absorption and fluorescence profiles of **JULBD** proved to be extremely interesting, displaying characteristics which had not been remarked upon previously in chromophores of this nature. The dominating features will now be discussed.

3.5.1 Absorption spectroscopy and data

In **JULBD** it was envisaged that the lone pair on the nitrogen atom of the julolidine unit could be donated to a second species (a proton or metal ion for example) which would inherently 'switch on' the fluorescence signal. This fluorescence would otherwise be quenched through donation of the lone pair in question into the bodipy core via an intramolecular charge transfer process. This premise was tested on a small scale using low-level techniques. To a series of vials containing **JULBD** dissolved in acetonitrile, aliquots of various compounds possessing labile protons were added. In each case, the solution turned yellow from deep blue, indicating a change in the electronic structure of **JULBD**. This was perceived to be protonation of the nitrogen atom, switching on the fluorescence in the system which was otherwise being quenched by the occurrence of an intramolecular charge transfer mechanism. This was confirmed by recording a very basic absorption profile, in which disappearance of the charge transfer band at around λ= 600 nm occurs.

3.5.1.1 Solvent polarity studies

The absorption spectra of **JULBD** in a range of solvents of varying polarity are shown in *Figure 21*. The sets of absorption data recorded are compiled in *Table 6*.

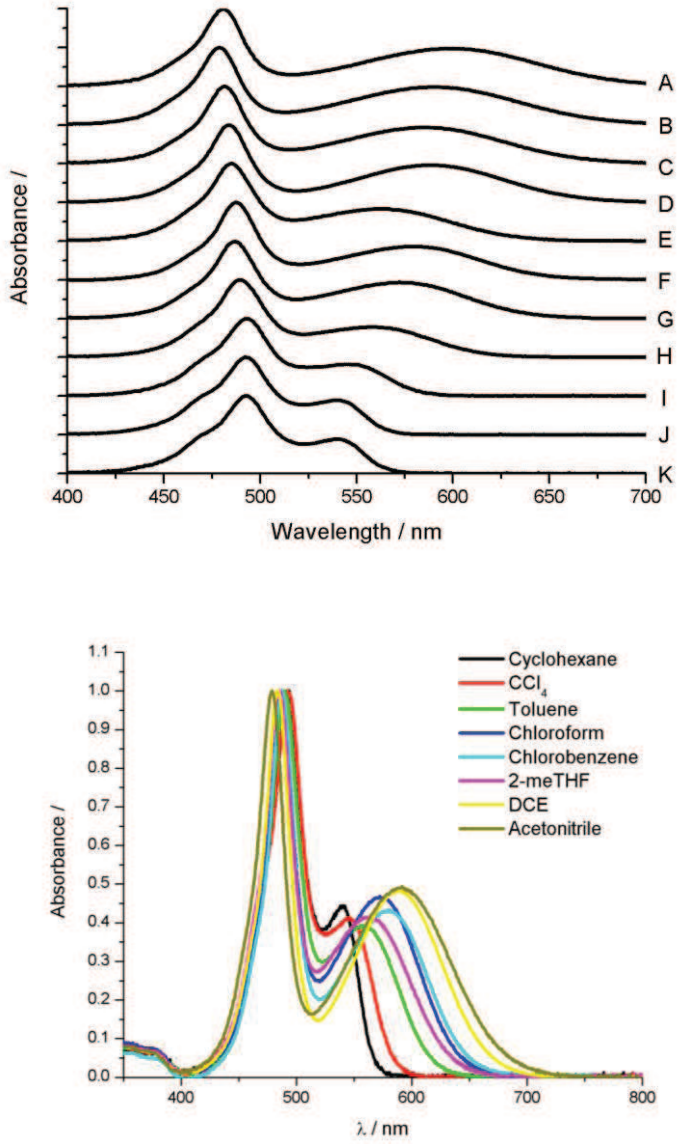

*Figure 21 – Top and bottom: absorption profiles of **JULBD** in a range of solvents of differing polarity.*

Sample	Solvent	Dielectric constant
A	Propylene carbonate	64.40
B	Acetonitrile	35.94
C	Butyronitrile	24.83
D	DCE	10.42
E	Methyl-THF	6.97
F	Chlorobenzene	5.40
G	Chloroform	4.81
H	Toluene	2.38
I	Carbon tetrachloride	2.24
J	Methyl cyclohexane	2.02
K	Cyclohexane	2.02

*Table 5 – The solvents in which the absorption profiles of **JULBD** displayed above were recorded.*

It can be seen that each of the samples displays a typical sharp bodipy absorption band between 479 nm in acetonitrile and 493 nm in cyclohexane. This can be attributed to the 0-0 band of the strong S_0-S_1 transition (assigned "BD" in *Table 6*). The slight overall hypsochromic shift with increase in solvent polarity is consistent with the general behaviour of bodipy chromophores[59] and reflects the polarisability of the solvent. The term dipolarity or polarisability,[60] refers to the ability of the solvent to stabilize a charge or a dipole by virtue of its dielectric effect[61,62].

Similarly, a weak, broad absorption band centred at 325nm (not shown in *Figure 21*) is typical of bodipy systems of this nature. It can be attributed to the S_0-S_2 transition and is not appreciably affected by the polarity of the solvent. The distinctive broad, bell-shaped shoulder on the short wavelength side of the 0-0 band has the makings of a charge-transfer band. It is assigned as "CT" in *Table 6* and is present even in the lowest polarity solvents tested, a feature that has not been previously reported in bodipy chromophores.

The charge transfer band displays a pronounced bathochromic shift with increasing solvent polarity. This ranges from 540 nm in the relatively non-polar cyclohexane through to 592 nm in acetonitrile. The ratio of band intensities remains fairly constant throughout the solvent series, whilst the solvatochromic shift increases steadily. The only exception to this is 2-methyltetrahydrofuran and is most probably the result of a specific solvent effect.

Solvent	ε /	λ_{CT} / **nm**	λ_{BD} / **nm**	**Band ratio** /	**FWHM$_{CT}$** / **cm^{-1}**	**FWHM$_{BD}$** / **cm^{-1}**	$\lambda_S{}^a$ / **cm^{-1}**
Cyclohexane	2.02	540	493	2.2	949.5	1028	97.2
CCl_4	2.24	545	492	2.4	1358	1081	284
Toluene	2.38	558	489	2.3	1713	1063	695
Chloroform	4.81	572	487	2.2	2110	1017	1148
Chlorobenzene	5.40	580	487	2.3	2328	969.3	1374
2-MeTHF	6.97	561	485	2.4	2383	1051	790
Dichloroethane	10.4	590	484	2.3	2392	953.4	1667
Acetonitrile	36.0	592	479	2.0	2682	1012	1723

*Table 6 – Spectroscopic absorption data and photophysical parameters recorded for **JULBD** in a range of solvents.*

Glossary of terms used in Table 6

λ_{CT} = absorption maxima of charge transfer

λ_{BD} = absorption maxima of bodipy

λs = solvent reorganisation energy

ε = dielectric constant

FWHM = full width at half maximum – these values were obtained by separately fitting each peak to the minimum number of Gaussian shaped bands required to gain a sound representation of the spectrum.

Excimers (excited state dimers) and other small aggregating units have also been reported to exhibit broad, bell-shaped bands in their absorption spectra. In order to investigate the true origin of the broadness observed in the **JULBD** absorption profile, a concentration dependence experiment was carried out. Absorption spectra were recorded for discrete sets of increasingly dilute solutions of **JULBD** in cyclohexane and in acetonitrile. A straight-line dependence of the intensity of absorption bands (both CT and BD) upon concentration confirms that the system fully adheres to the Beer-Lambert law[63] in both solvents tested. A constant peak intensity ratio also implies that the broad band observed in each solvent is not the result of an aggregate. It can therefore be deduced that the bands are due to a direct photo-induced transition to the charge-transfer state.

3.5.2 Potential Energy Model and Marcus Theory

In the 1950's, Marcus developed the first fundamental quantitative description of electron transfer reactions in solution[64,65]. This theory was based originally on investigations of "self exchange reactions" and "cross reactions"[66] of metal ions. However, the general concept could also be applied to intramolecular electron transfer processes in inorganic and organic mixed valance species[67].

The theories and models proposed by Marcus remain the cornerstone on which many more sophisticated models of electron transfer have been based.[68] In spite of its formal simplicity, Marcus theory has also been proven to take into account the decisive factors affecting the rate of charge transfer[69]. It can still be widely applied to both homogeneous and heterogeneous electron transfer reactions and will be used to describe the charge transfer processes occurring in **JULBD**.

It can be seen from the two discrete bands present in the absorption spectrum of **JULBD**, that excitation of the ground state molecule can lead to direct population of two separate excited states. One of these is the partially charge-separated state. This

can be described as $^{+\delta}$J-B$^{\delta-}$, whilst the second is the locally excited state (J-B*). This is another factor which supports the notion that **JULBD** demonstrates appreciable charge transfer character.

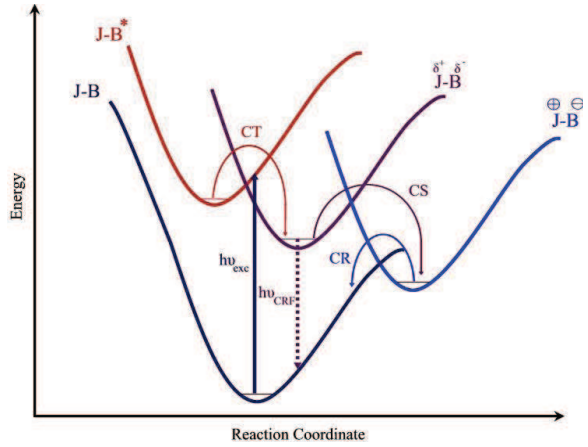

*Figure 22 – A potential energy diagram for photoexcitation of **JULBD** and subsequent intramolecular charge transfer and fluorescence processes. $h\upsilon_{exc}$ = energy for excitation, $h\upsilon_{CRF}$ = energy of charge recombination fluorescence, CR = charge recombination, CS = charge separation, CT = charge transfer.*

Upon formation of the locally excited state, the molecule undergoes rapid decay to the exciplex. This process occurs on a much more rapid timescale than radiative decay from the locally excited state. The pathway is accompanied by a change in electron density distribution by way of a charge-transfer mechanism. This can be described in terms of Marcus Theory[70]. The main features concerned with this theorem are covered in the equation below:

$$k_{ET} = \frac{2\pi}{\hbar}\left(\frac{V_{DA}^2}{\sqrt{4\pi\lambda k_B T}}\right)\exp\left(\frac{-\left(\Delta G^0 + \lambda\right)^2}{4\lambda k_B T}\right)$$

Equation 1 – The principal features of Marcus Theory expressed as an equation.

Some of the symbols present in *Equation 1* above will now be defined for clarity. The term λ is the reorganisation energy. This can be thought of as the energy it would take to force the reactants to possess the same nuclear configuration as the products without charge-transfer occurring. In our system it is the energy needed to force the locally excited state molecules of **JULBD** to have the same nuclear configuration as those in $^{+\delta}$J-B$^{\delta-}$. It is the sum of both the solvent- and nuclear- internal reorganisation

energies. The former can be attributed to the change of orientation polarization of the solvent, whilst the latter represents the change of molecular structure (for example variation in bond lengths and bond angles) of the donor and the acceptor.

$\Delta G°$ is the free energy change between the reactants and the products, a term which vanishes if the donor and acceptor are chemically equivalent. k_{ET} and $k_B T$ are the electron transfer rate and the thermal energy respectively (k_B representing the Boltzmann constant here). $\hbar$ is the Dirac constant. This is a physical constant which is common-place in Quantum mechanics and is equal to h/(2π) where h refers to Planck's constant. V_{DA} is the electronic coupling matrix element by which the coupling between donor and acceptor is related at orbital contact, V_0, to the distance between them (d) by way of an attenuation factor (μ). This is shown in *equation 10* (below).

$$V_{DA} + V_0 \exp(-\mu d)$$

Equation 10 – The electronic communication between donor and acceptor is related at orbital contact to their separation distance, taking into account the resistivity of the bridge (μ).

When designing and synthesising donor-acceptor dyads, knowledge of V_{DA} is of great importance as it permits rational design of novel bridging moieties to be incorporated into such species. Furthermore, a much improved understanding of the role of the bridge in electron exchange processes[71,72,73] can be gained. According to super-exchange theory, the electronic matrix coupling element will reduce exponentially with increasing distance between donor and acceptor[74].

ΔG^0 is the change in Gibbs free energy which accompanies the charge transfer process. Within a classical treatment, the diabatic free energy surfaces J-B* and $^{+\delta}$J-B$^{\delta-}$ are parabolas with identical λ (reorganisation energy) values.

Hence it follows by a simple algebraic analysis that $\Delta G^{\ddagger}$ can be calculated by *Equation 11* below:

$$\Delta G^{\mp} = \frac{\left(\Delta G^{0} + \lambda\right)^{2}}{4\lambda}$$

Equation 11- The quadratic dependence of the change in free energy of activation on ΔG^{0} and λ as predicted by Marcus theory.

The motivation to calculate diabatic potentials often occurs when the Born Oppenheimer approximation does not hold, or is not justified for the molecular system under study. The diabatic picture can be used to extract qualitative insight and predictions about energy landscapes. The diabatic free energy surfaces for electron transfer reactions can be calculated from first principals using Marcus Theory[75,76].

By *Equation 11*, the parabolic relationship between the driving force for reaction and charge transfer rate is divided into three specific regions. As the thermodynamic driving force increases whilst still below the value of –λ, the rate of charge transfer will show a progressive increase. This is referred to as the 'normal region' and reaches a maximum when $\Delta G^{0} = -\lambda$, at which point the rate becomes activation-less. As the driving force is increased beyond $-\lambda$, the rate begins to decrease in the 'inverted region'[77,78].

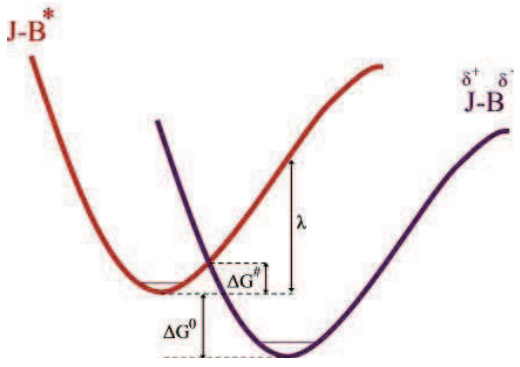

Figure 23 – A potential energy diagram detailing the key aspects of Marcus Theory.

When ΔG^{0} and –λ are similar, this results in rapid charge transfer from J-B* to form the $^{+\delta}$J-B$^{\delta-}$ state. The latter state exhibits charge recombination fluorescence in non-polar solvents. It should also be noted that a further charge separation process can

occur to form the fully charge separated state, $^{+}$J-B^{-}. Thus, radiative decay from this state is a forbidden process and only via activated charge recombination, can the molecule return to the ground state. This takes place within the Marcus inverted region. The $^{+}$J-B^{-} state is highly sensitive to changes in solvent polarity. In very non-polar solvents, its free energy is above that of the $^{+\delta}$J-B$^{\delta-}$ state (*Figure 22*) and charge separation is thermodynamically unfavourable, which leads to emission from the exciplex. In spite of this, the charges on the molecule are stabilised even in low polarity solvents. This diminishes the free energy of the radical pair below that of the $^{+\delta}$J-B$^{\delta-}$ state and creates a preference for charge separation over charge-recombination fluorescence. The way in which competition could be established between charge separation and charge recombination fluorescence over a very narrow polarity range, suggests that **JULBD** may be used as a polarity sensitive probe.

3.5.3 Fluorescence spectroscopy and data

3.5.3.1 Solvent dependence studies

Steady state and time-resolved fluorescence spectra of **JULBD** were obtained in a range of solvents. The data obtained is collected in *Table 7*.

Solvent	λ_{em} [a] / nm	Δ_{SS} / cm^{-1}	FWHM / cm^{-1}	ϕ_{fl} [b] / %	τ [c] / ns	k_{RAD} / s^{-1}	k_{NR} / s^{-1}
Cyclohexane	570	856.91	1008	100	3.3	3.04x10^{8}	0
CCl_4	590	1530.7	1676	47	1.4	7.14x10^{8}	3.79 x10^{8}
Toluene	655	2654.0	1009	7.0	1.7	5.88x10^{7}	5.47 x10^{8}
Chloroform	715	3481.2	1020	0.1	0.76	1.32x10^{6}	1.31 x10^{9}
Chlorobenzene	725	3448.3	1133	0.2	0.67	1.49x10^{9}	1.49 x10^{9}
2-MeTHF	745	4402.5	1018	0.08[d]	0.94	1.06x10^{5}	1.06 x10^{9}

[a] λ_{max} derived from corrected emission spectra, excitation wavelength 450 nm. [b] Luminescence quantum yields measured against cresyl violet in BuCN as a standard[79] with excitation at 460 nm. [c] Fluorescence lifetimes excitation at 505 nm. [d] Minimum measureable fluorescence limit.

*Table 7 – Spectroscopic fluorescence spectral data and photophysical parameters recorded for **JULBD** in a range of solvents at 295K.*

The fluorescence studies undertaken indicate that luminescence yields also show a pronounced dependence upon solvent polarity. To reinforce this, it can be seen that a very small increase in solvent dielectric constant results in a huge reduction in quantum yield. For example, an increase in ε of just 4.95, results in a 1250-fold reduction in quantum yield from unity in cyclohexane, to 0.08 in 2-methyltetrahydrofuran. Furthermore, **JULBD** is considered to be non-fluorescent in dichloromethane and more polar solvents due to the pronounced stabilisation of the charge separated state by highly polar solvents.

3.5.3.2 Temperature dependence of emission

In order to investigate the effect of temperature on the fluorescence properties of **JULBD**, the emission spectra of a series of samples dissolved in a range of solvents were obtained at 77K. As to be expected, **JULBD** is fluorescent in non-polar methyl cyclohexane (ε = 2.024) at room temperature. However, it was observed that the emission profile appears altered and the fluorescence intensity much diminished at very low temperature. One can attribute this to a specific solvent effect which relates to the properties of solvents upon cooling. For example, methyl cyclohexane can form an ice rather than an optically transparent glass when cooled below its freezing point. Conversely, **JULBD** was non-fluorescent in higher polarity solvents such as propylene carbonate, ethanol, and butyronitrile at room temperature. However, in all three solvent systems, the molecule was seen to recover its emissive properties at very low temperature. It was suggested that this effect was observed as a result of the dramatic variation in liquid physical properties upon cooling. It has been established that the solvent polarity in the liquid state increases with decreasing temperature[80,81,82,83,84,85,86,87,88,89.] This is due to the increase in density until the vitrification point is reached. At this point, the dielectric constant drops remarkably and a glass is formed. This glass is effectively non-polar.

To further investigate this hypothesis, a more rigorous dependence test was set up whereby the emissive properties of **JULBD** were quantitatively recorded in two separate polar solvents over a broad range of temperatures. The results of the experiment conducted in butyronitrile are displayed in *Figure 24*.

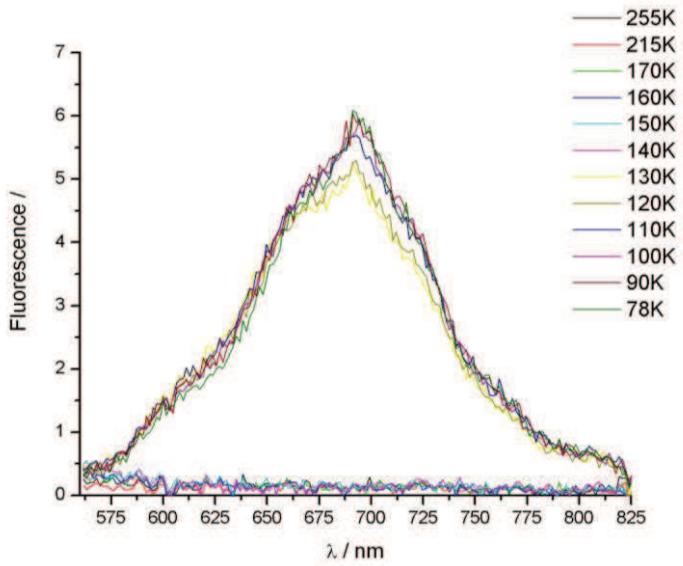

*Figure 24 – Emission spectra recorded of **JULBD** in butyronitrile solution from 255-78 K. The Excitation wavelength here was 470 nm.*

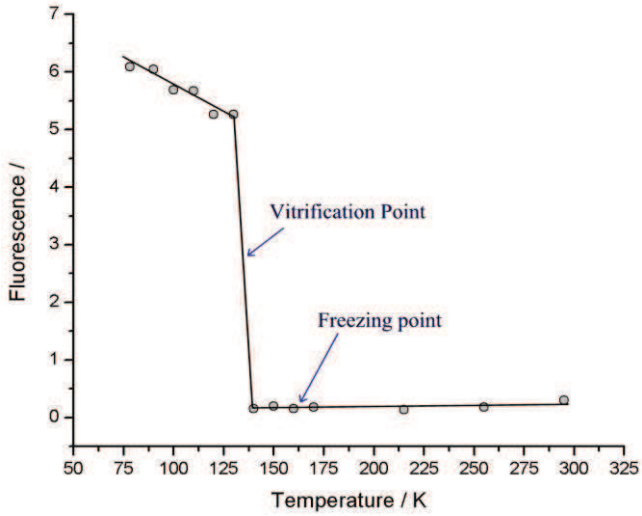

*Figure 25 – Fluorescence intensity at emission maximum (691 nm) for **JULBD** in BuCN at various temperatures.*

It can be seen that a pronounced change in fluorescence intensity is observed between 130-140 K. This transition occurs approximately 30 degrees below the freezing point of BuCN (161 K) and marks the beginning of the so-called glass region.

This observation supports the previous prediction that the charge transfer state (where the fluorescence originates) is stabilised by polar environments and is occupied uniquely upon vitrification. At this point, the polarity of the surroundings drops and fluorescence is subsequently switched on. This study implies that **JULBD** could also be used as a detector for solvent vitrification behaviour.

3.5.3.3 Fluorescence Titration

One manner by which a more qualitative grasp can be gained of the effect of polarity on the fluorescent properties of a system, is by carrying out a titration experiment. Samples of equal overall concentration of solute were prepared in solutions of steadily increasing mole fractions of dichloroethane in cyclohexane and ethanol in cyclohexane. The emission spectra at each mole fraction for the dichloroethane experiment are displayed below in *Figure 26*.

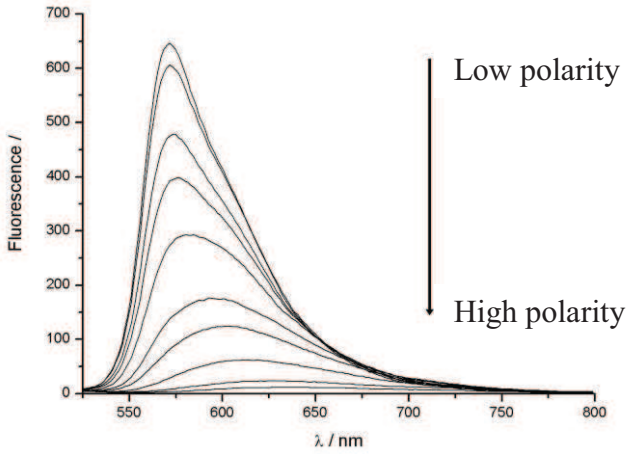

*Figure 26 – Emission spectra recorded for **JULBD** in dichloroethane: cyclohexane mixtures of varying mole fractions. Excitation wavelength = 470 nm.*

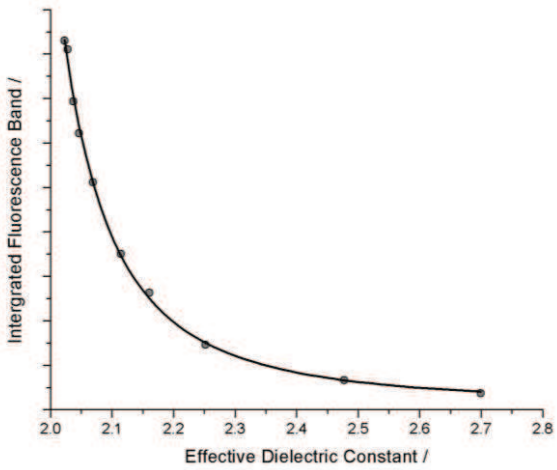

Figure 27 – Calibration curve showing predicted fluorescent intensity at different solvent dielectric constants.

Making the assumption that the dielectric constant is a linear function of the mole fraction, the results gained can be used to generate a calibration curve. Using this information, **JULBD** can be used to measure the precise polarity of a medium. An application of such a probe would be to monitor the progress of a chemical reaction in which there are subtle polarity variations between the reactants and the products

3.6 Concluding remarks and future studies

Investigation and research into the subject area of chemosensing devices and molecular rotors has lead to the successful design and synthesis of **JULBD**. The spectral properties of this dyad have been found to exhibit a significant and pronounced dependence on solvent polarity. This includes the presence of a prominent charge transfer band, which prevails even in low polarity solvents. This feature has not been observed previously in chromophores of this nature and suggests that the charge transfer capabilities of this system are more substantial than initially predicted. Results obtained from polarity dependence experiments provided a discrete range over which the intensity of charge-recombination fluorescence is systematically reduced It can be deduced therefore that **JULBD** is a suitable system for utilisation as a polarity sensitive probe. This was also confirmed when the charge transfer capabilities of the system were related to Marcus theory. The photophysical properties of **JULBD** were analysed via a series of potential energy diagrams. These results suggested that competition can be established between charge separation and charge recombination fluorescence over a narrow polarity range, a surprising find due to the thermodynamically unfavourable nature of charge separation when the free energy of the fully charge separated state of **JULBD** is above that of the partially charge separated state.

Results obtained from temperature-dependence studies carried out in high polarity solvents in which the system is non-emissive have indicated that fluorescence can be ‘switched on’ upon formation of a glass. This provides a second possible application for **JULBD**, as a detector for solvent vitrification behaviour.

An additional use of **JULBD** is in the field of biological imaging and last year, a University based Neuroscience laboratory used **JULBD** to image the stomatogastric ganglion (STG) of a brown crab (*cancer pagarus*).

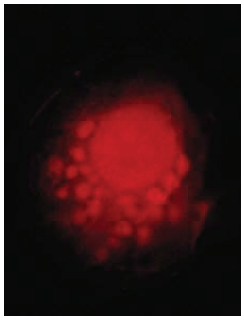

*Figure 28 – The image generated following incorporation of **JULBD** into the ganglion of a brown crab.*

It is thought that with the use of ultra-fast transient absorption spectroscopy, further information may be gained which will allow a more substantial elucidation of the charge separation and recombination processes occurring within the dyad. It is hoped that this work may be carried out by a future member of the MPL.

3.7 References

[1] Boens, N.; Leen, V.; Dahaen, W. *Chem. Soc. Rev*. **2012**, *41*, 1130.
[2] Zhao, W.; Carreira, E. M. *Chem –Eur. J*. **2006**, *12*, 7254.
[3] Lee, J.-S.; Kang, N. Y.; Kim, Y. K.; Samanta, A.; Feng, S.; Kim, H. K.; Vendrell, M.; Park, J. H. Chang, Y.-T. *J. Am. Chem. Soc*. **2009**, *131*, 10037.
[4] (a) Rurack, K.; Kollmannsberger, M.; Resch-Genger, U.; Daub, J. *J. Am. Chem. Soc*. **2000**, *122*, 968. (b) Rurack, K.; Kollmannsberger, M.; Daub, J. *Angew. Chem. Int. Ed.* **2001**, *40*, 385. (c) Turfan, B.; Akkaya, E. U. *Org. Lett*. **2002**, *4*, 2857. (d) Gee, K. R.; Rukavishnikov, A.; Rothe, A. *Comb. Chem. High Throughput Screening.* **2003**, *6*, 363. (e) Goze, C.; Ulrich,G.; Charbonnière, L.; Cesario, M.; Prangé, T.; Ziessel, R. *Chem.-Eur. J.* **2003**, *9*, 3748. (f) Cha, N. R.; Moon, S. Y.; Chang, S.-K. *Tetrahedron Lett*. **2003**, *44*, 8265. (g) Moon, S. Y.; Cha, N. R.; Kim, Y. H.; Chang, S.-K. *J. Org.Chem.* **2004**, *69*, 181. (h) Gabe, Y.; Urano, Y.; Kikuchi, K.; Kojima,H.; Nagano, T. *J. Am. Chem. Soc.* **2004**, *126*, 3357. (i) Coskun, A.; Akkaya, E. U. *Tetrahedron Lett.* **2004**, *45*, 4947. (j) Baruah, M.; Qin, W.; Basariæ,N.; De Borggaeve, W. M.; Boens, N. *J. Org. Chem.* **2005**, *70*, 4152. (k) Yamada, K.; Nomura, Y.; Citterio, D.; Iwasawa, N.; Suzuki, K. *J. Am. Chem. Soc.* **2005**, *127*, 6956. (l) Coskun, A.; Akkaya, E. U. *J. Am. Chem. Soc.* **2005**, *127*, 10464 (m) Martin, V. V.; Rothe, A.; Gee, K. R. *Bioorg. Med. Chem. Lett*. **2005**, *15*, 1851-1855.
[5] Alamiry, M. A. H.; Benniston, A. C.; Copley, G.; Elliott, K. J.; Harriman, A.; Stewart, B.; Zhi, Y. G. *Chem. Mater*-, **2008**, *20*, 4024.
[6] Yin, X.; Li, Y.; Zhu, Y.; Jing, X.; Li, Y.; Zhu, D. *Dalton Trans*, **2010**, *39*, 9929.
[7] Kuimova, M. K.; Yahioglu, G.; Levitt, J. A.; Suhling, K. *J. Am. Chem. Soc*. **2008**, *130*, 6672.
[8] Desvergne, J. –P; Czarnik, A. W. *Chemosensors of Ion and Molecule Recognition*, Kluwer, Dordrecht, 1997.
[9] De Silva, A. P.; Gunaratne, H. Q. N.; Gunnlaugsson, T.; Huxley, A. J. M.; McCoy, C. P.; Rademacher, J. T.; Rice, T. E. *Chem. Rev*. **1997**, *97*, 1515.
[10] Valeur, B. *Molecular Fluorescence Principals*, Wiley-VCH, Weinheim, 2002.
[11] Lin, Z.; Lin, T.-P.; Shuanglong L.; Huang, C. W.; Hudnall, T. W.; Gabbai, F. P.; Conti, P. S. *Chem. Commun*, **2011**, *47*, 9324.
[12] Fitzgerald, W. F.; Lamborg, C. H.; Hammerschmidt, C. R. *Chem. Rev*. **2007**, *107*, 641. (b) Harris, H. H.; Pickering. I. J.; George, G. N. *Science*, **2003**, *301*, 1203. (c) *Chem. Rev*, **2008**, *108*, 3443. (d) Renzoni, A.; Zino, F.; Franchi, E. *Environ. Res. Sect., A*. **1998**, *77*, 68.
[13] Chapman, L. A.; Chan, M. H. *Toxicology*. **1999**, *132*, 167.
[14] Tchounwou, P. B.; Avensu, W. K.; Ninashvili, N.; Sutton, D. *Environ. Toxicol*. **2003**, *18*, 149.
[15] Takeuchi, T.; Morikawa, N.; Matsumoto, H.; Shiraishi, Y. *Acta Neuropathol*, **1962**, *2*, 40.
[16] a) Boening, D. W. *Chemosphere*, **2000**, *40*, 1335 (b) Trudel, M.; Rasmussen, J. B. Environ. Sci. Technol. **1997**, *31*, 1716. (c) Clarkson, T. W. J. *Trace Elem. Exp. Med*. **1998**, *11*, 303. (d) Frodello, J. P.; Romeo, M.; Viale, D. *Environ. Pollut*, **2000**, *108*, 447.
[17] (a) Rurack, K.; Kollmnnsberger, M.; Resch-Genger, U.; Daub, J. *J. Am. Chem. Soc*. **2000**, *122*, 968 (b) Yuan, M.; Li, Y.; Li, J.; Li. C.; Liu, X.; Ly, J.; Xu, J.; Liu, H.; Wang, S.; Zhu, D. *Org. Lett,* **2007**, *9*, 2313. (c) Wang, J. B.; Qian, X. H. *Org. Lett*. **2006**, *8,* 3721 (d) Coskun, A.; Akkaya, E. U. *J. Am. Chem. Soc*. **2006**, *128*, 14474.
[18] Atilgan, S.; Kutuk, I.; Ozdemir, T. *Tetrahedron Letters*. **2010**, *51*, 892.
[19] Haidekker, M. A.; Tsai, A. G.; Brady, T.; Stevens, H. Y.; Frangos, J. A.; Theodorakis, E.; Intaglietta, M. *Am. J. Physiol; Heart Circ. Physiol*. **2002**, *282*, 1609.
[20] Paul, A.; Samanta, A. *J. Phys. Chem. B*. **2008**, *112*, 16626.
[21] Mennucci, B.; Cappelli, C.; Guido, C. A.; Cammi, R.; Tomasi, J.; *J. Phys. Chem. A*. **2009**, *113*, 3009.
[22] Zhu, L. L.; Li, X.; Ji, F. Y.; Ma, X, Wang, Q. C, Tian, H. *Langmuir*. **2009**, *25*, 3482.
[23] Kuimova, M. K.; Botchway, S. W.; Parker, A. W.; Balaz, M.; Collins, H. A.; Anderson, H. L.; Suhling, K.; Ogilby, P. R. *Nat. Chem*. **2009**, *1*, 69.
[24] Shao, J.; Ji, S.; Li, X.; Zhao, J.; Zhuo, F.; Guo, H. *Eur. J. Org. Chem*, **2011**, *76*, 6100
[25] Rotkiewicz, K.; Grellmann, K. H.; Grabowski, Z. R. *Chem. Phys. Lett*, **1973**, *19*, 315.
[26] Haidekker, M. A.; Theodorakis, E. A. *Org. Biomol. Chem*. **2007**, *5*, 1669.
[27] Loutfy, R. O.; Law, K. Y. *J. Phys. Chem*. **1980**, *84*, 2803.
[28] Haidekker, M. A.; Brady, T. P.; Lichlyter, D and Theodorakis, E. A. *Bioorg. Chem*. **2005**, *33*, 415.
[29] Kee, H. L.; Kirmaier, C.; Yu. L.; Thamyongkit, P.; Youngblood, W. J.; Calder, M. E.; Ramos, L.; Noll, B. C.; Bocian, D. F.; Scheidt, W. R.; Birge, R. R.; Lindsey, J. S.; Holten, D. *J. Phys. Chem. B*. **2005**, *109*, 20433.

[30] (a) Rosokha, S. V.; Kochi, J. K. *J. Am. Chem. Soc*. **2007**, *129*, 828. (b) Launay, J. –P. *Chem. Soc. Rev.* **2001**, *30*, 386-397 (c) Demandis, K. D.; Hartshorn, C. M.; Meyer, T. J. *Chem. Rev*. **2001**, *101*, 2655. (d) Hush, N. S.; Reimers, J. R. *Co-ord. Chem. Rev*. **1998**, *177*, 37.
[31] (a) Oh, D. H.; Sano, M.; Boxer, S. G. *J. Am. Chem. Soc.* **1991**, *113*, 6880; b) Stiegman, A. E.; Graham, E.; Perry, K. J.; Khundkar, L. R.; Cheng, L. –T.; Perry, J. W. *J. Am.Chem. Soc.* **1991**, *113*, 7658; c) Baumann, W.; Bischof, H.; Fröhling, J. –C.; Brittinger, C.; Rettig, W.; Rotkiewicz, K. J.; *Photochem. Photobiol. A: Chem.* **1992**, *64*, 49.
[32] (a) Shuster, G. B. Acc. *Chem. Rev*. **2000**, *33*, 253. (b) Wasielewski, M. R. *Chem. Rev*. **1992**, *92*, 435.
[33] Grabowski, Z. R.; Rotkiewicz, K.; Rettig, W. *Chem. Rev*. **2003**, *103*, 3899.
[34] (a) Lappas, K..; Prassides, K.; Vavekis, D.; Arcon, R.; Blinc, P.; Cevc, A.; Amato, R.; Feyerherm, F.; Gygax, N.; Schenck, A. *Science.* **1995**, *267*, 1799; b) Sato, T.; Yamabe, T.; Tanaka, K. *Phys. Rev.* **1997**, *56*, 307.
[35]a) Sep, W. J.; Verhoeven, J. W.; de Boer, Th. J. *Tetrahedron.* **1975**, *31*, 1065; b) Reichardt, C. *Chem. Soc. Rev.* **1992**, *21*, 147; c) Létard, J. –F.; Lapouyade, R.; Rettig, W. *J. Am. Chem. Soc.* **1993**, *115*, 2441; d) Fromherz, P. *J. Phys. Chem.* **1995**, *99*, 7188 e) Laage, D.; Thompson, W. H.; Blanchard-Desce, M.; Hynes, J. T. *J. Phys. Chem. A.* **2003**, *107*, 6032; f) Reichardt, C. *Chem. Rev.* **1994**, *94*, 2319.
[36] Marcus, R. A.; Sutin, N.; *Biochem. Biophys. Acta*, **1985**, *811*, 265.
[37] Hanggi, P.; Talkner, P.; Borkovec, M. *Rev. Mod. Phys*. **1990**, *62*, 251.
[38] Hartmann, L.; Goychuk, I.; Hänggi, P. *J. Chem. Phys*. **2000**, *113*, 11159.
[39] Barzykin, A. V.; Frantsuzov, P. A.; Seki, K.; Tachiya, M. *Adv. Chem. Phys*, **2002**, *123*, 511.
[40] Levich, V. G. *Adv. Electrochem. Electrochem. Eng.* **1965**, *4*, 249
[41] Garg, A.; Onuchic, J. N.; Ambegaokar, V. *J. Chem. Phys*. **1985**, *83*, 4491.
[42] Zhao, Y.; Liang, W-Z. *Chem. Soc. Rev*. **2012**, *41*, 1075.
[43] Jones, G.; Jackson, W. R.; Kanoktanaporn, S.; Bergmark, W. R. *Photochem. Photobiol.* **1985**, *42*, 477.
[44] Kessler, M. A.; Wolfbeis, O. S. *Spectrochim. Acta*. **1991**, 47A, 187.
[45] Anstead, G. M.; Carlson, G.E.; Kym, P. R.; Hwang, K. J.; Katzellenbogen, J. A. *Photochem. Biol.* **1993**, *58*, 785.
[46] Enjalbert, Q.; Racaud, A.; Lemoine, J.; Redon, S.; Menaf Ayhan, M.; Andraud, C.; Chambert, S.; Bretonniere, Y.; Loison, C.; Antoine, R.; Dugourd, P. *J. Phys. Chem. B*. **2012**, *116*, 841.
[47] Plaquet, A.; Champagne, B.; Kulhánek, J. Bureš, F.; Bogdan. E.; Castet, F.; Ducasse, L.; Rodriguez, V. *Chem. Phys. Chem*. **2011**, *12*, 3245
[48] Raposo, M. M. M.; Castro, M. C. R.; Belsley, M.; Fonseca, A. M. C. *Dyes and Pigments*. **2011**, *91*, 454.
[49] Sarma, M.; Chatterjee, T.; Ghanta, S.; Das, S. K. *J. Org, Chem*. **2012**, *77*, 432.
[50] Lee, C, -H.; Lindsey, J. S. *Tetrahedron*, **1994**, *50*, 11427.
[51] Gryko, D.; Lindsey, J. S. *J. Org. Chem*. **2000**, *65*, 2249.
[52] Laha, J. K.; Dhanalekshmi, S.; Taniguchi, M.; Abroise, A.; Lindsey, J. S. *Org. Proc. Res. Dev*. **2003**, *7*, 799.
[53] The scaleability of the dipyrromethane formation reaction was improved using column chromatography techniques followed by distillation as documented within the following publications (a) Brückner, C.; Sternberg, E. D.; Boyle, R. W.; Dolphin,D.; *Chem. Commun*. **1997**, 1689. (b) Boyle, R. W.; Brückner, C.; Posakony, J.; James, B. R.; Dolphin,D. *Org, Synth*. **1998**, *76*, 287. (c).; Brückner, C.; Posakony, J.; Johnson, C. K.; Boyle, R. W.; James, B. R.; Dolphin,D. *Porphyrins Phthalocyanines*. **1998**, *2*, 455. (d) Littler, B. J.; Miller, M. A.; Hung, C-H.; Wagner, R. W.; O'Shea, D. F.; Boyle, P. D.; Lindsey, J. S. *J. Org. Chem*. **1999**, *64*, 1391.
[54] Williams, D. H and Fleming, I. *Spectroscopic Methods in Organic Chemistry*, McGraw-Hill, New York, 1995**.**
[55] Schmidt, E. Y.; Trofimor, B. A.; Mikhaleva, A. I.; Zorina, N. V.; Protzuk, N. I.; Petruchenko, K. B.; Ushakov, I. A.; Dvorko, M. Y.; Méallet-Renault, R.; Clavier, G.; Vu, T. T.; Tran, H. T. T.; Pansu, R. B. *Chem-Eur J*. **2009**, *15*, 5823.
[56] Schmitt, A.; Hinkeldey, B.; Wild, M.; Jung, G.; *J. Fluoresc*. **2009**, *19*, 755.
[57] Tram, K.; Yan, H.; Jenkins, H. A.; Vassiliev, S.; Bruce, D. *Dyes Pigm*. **2009**, *82*, 392.
[58] Ziessel, R.; Goze, C.; Ulrich, G.; Céario, M.; Retailleau, P.; Harriman, A.; Rostron, J. P. *Chem. Eur. J*. **2005**, *11*, 7366.
[59] Qin, W.; Rohand, T.; Baruah, M.; Stefan, A.; Van Der Auweraer, M.; Dehaen, W.; Boens, N. *Chem. Phys. Lett.* **2006,** *420*, 562.

[60] For recent publications on the topic please refer to Catalán, J.; Reichardt, C. *J. Phys. Chem. A*. **2012**, *116*, 4726-4734 and Madeira, P. P; Bessa, A; Alvares-Ribeiro L; Aires-Barros M. R; Reis, C. A; Rodrigues, A E; Zaslavsky BY. *J. Chromatogr A*. **2012**, *1229*, 38.
[61] Reichardt, C.; Welton, T. *Solvents and Solvent Effects in Organic Chemistry*. Wiley-VCH, Weinheim. 2011.
[62] A solvent dipolarity scale can be established – or details and a list of SP and SdP values for 163 solvents please refer to reference 393b within the book *Solvents and Solvent Effects in Organic Chemistry*. Reichardt, C.; Welton, T., Wiley-VCH, Weinheim.. 2011
[63] Atkins, P.; de Paula, J. *Atkins' Physical Chemistry*. 7th ed.; Oxford University Press: 2002; p 491.
[64] Marcus , R. A. *J. Chem. Phys*. **1956**, *24*, 966.
[65] Marcus, R. A. *Rev. Mod. Phys*. **1993**, *65*, 599.
[66] Wieghardt, K. *Chem. Unserer Zeit*. **1979**, *13*, 118.
[67] Lambert, C.; Heckmann, A. *Angew. Chem. Int. Ed*. **2012**, *51*, 326.
[68] Vos, J, G.; Forster, R. J.; Keyes, T. E. *Interfacial Supramolecular Assemblies*, Wiley and Sons Ltd, 2003.
[69] Paneth, P.; Dybala-Defratyka, A. *Kinetics and Dynamics: from Nano- to Bio- scale,* Springer, New York, 2010.
[70] Marcus, R. A.; Sutin, N. *Biochimica et Biophysica Acta – Reviews on Bioenergetics*. **1985**, *811*, 265.
[71] Borchardt, A.; Fuchicello, A.; Kilway, K. V.; Baldridge, K. K.; Siegel, J. S. *J. Am. Chem. Soc*, **1992**, *114*, 1921.
[72] (a) Sygula, A.; Rabideau, P. W. *J. Am. Chem. Soc*. **1999**, *121*, 7800. (b) Sygula, A.; Rabideau, P. W. *J. Am. Chem. Soc*. **2000**, *122*, 6323.
[73] (a) Rabideau, P. W.; Marcinov, Z.; Sygula, R.; Sygula, A. *Tetrahedron Lett*. **1993**, *34*, 6351 (b) Zhou, Z. *J. Phys. Org, Chem*. **1995**, *8,* 103.
[74] Janata, J.; Gendell, J.; Ling, C. Y.; Barth, W.; Backes, L.; Mark, H. B. Jr.; R. G. Lawton. *J. Am. Chem. Soc.* **1967**, *89*, 3053
[75] Marcus, R. A.; Sutin, N. *Biochim. Biophys. Acta*. **1985**, *881*, 265.
[76] For a review see D. Chandler in *Classical and Quantum Dynamics in condensed phase simulation,* edited by B. J. Berne, G. Ciccotti and D. F. Coker. World Scientific, Singapore. 1998.
[77] Suppan, P. *Top. Curr. Chem*. **1992**, *163,* 95.
[78] (a) Grampp, G. *Angew. Chem*. **1993**, *105*, 724 (b) Grampp, G. *Angew. Chem. Int. Ed*, **1993**, *32*, 691.
[79] Isak, S. J.; Eyring, E. M. *J. Phys. Chem.*. **1992,** *96*, 1738.
[80] Suppan, P. *J. Photochem. Photobiol. A*. **1990**, *50*, 293.
[81] Reichardt, C. *Solvents and Solvent Effects in Organic Chemistry*, 2nd ed.; VCH: Weinheim, 1988, and references therein.
[82] Dimroth, K.; Reichardt, C.; Schweig, A. *Justus Liebigs Ann. Chem.* **1963**, *669*, 95.
[83] Kawski, A.; Kolakowski, W. *Acta Phys. Pol.* **1966**, *29*, 177.
[84] Reichardt, C.; Harbusch, E.; Müller, R. In *Advances in Solution Chemistry*; Bertini, I., Lunazzi, L., Dei, A., Eds.; Plenum: New York, 1981; pp 275-293
[85] Suppan, P.; Tsiamis, C. *J. Chem. Soc., Faraday Trans. 2*. **1981**, *77*, 1553
[86] Hagan, T.; Pilloud, D.; Suppan, P. *Chem. Phys. Lett.* **1987**, *139*, 499.
[87] Ghoneim, N.; Rohner, Y.; Suppan, P. *Faraday Discuss. Chem. Soc.***1988**, *86*, 295.
[88] Linert, W.; Jameson, R. F. *J. Chem. Soc., Perkin Trans.* **1993**, *2,* 1415.
[89] Streck, C.; Richert, R. *Ber. Bunsen-Ges. Phys. Chem.* **1994**, *98*, 619.

Chapter 4

Elucidating Charge Transfer in the Ground State using NMR Spectroscopy

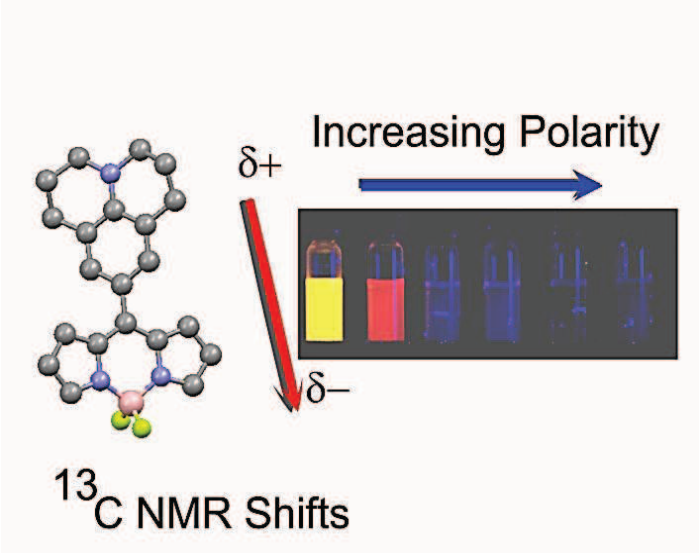

The work within this chapter forms the basis of the following publication: Benniston, A.; Clift, S.; Harriman, A. *Journal of Molecular Structure*. **2011**, *985*, 346.

The structures and names of the bodipy compounds to be discussed within this chapter are given in *Figure 1*. The nomenclatures used are as follows: BD = bodipy, JUL = julolidine, NIT = 4-nitrophenyl, PH = phenyl.

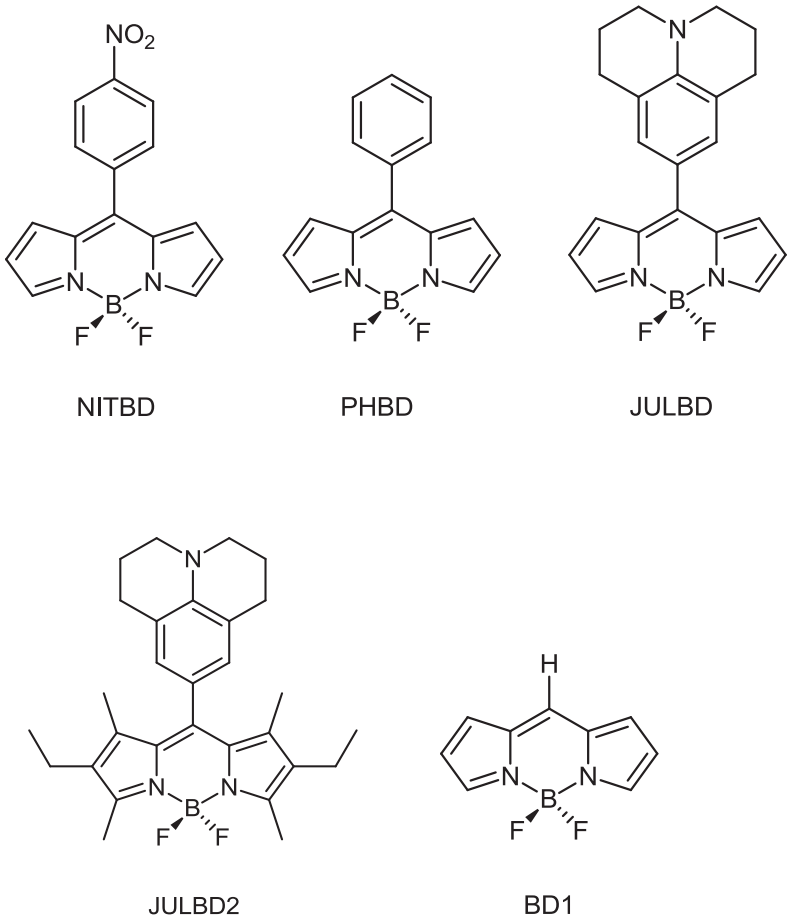

Figure 1 – The structures and naming scheme for the bodipy compounds discussed in Chapter 4.

Computational Chemistry abbreviations explained

A small portion of this chapter addresses quantum chemical calculations and several computational protocols are mentioned. For clarity, the abbrevations used are indexed below (*Table 1*) with their full names and a brief explanation of their meaning:

Abbreviation	Full name	Explanation
AM1	Austin Model 1	A semi-empirical method developed by Dewar and co-workers[1] in 1985. Approximates two electron integrals and uses a modified expression for nuclear-nuclear core repulsion.
PM3	Parametric method number 3	Developed by James Stewart, this semi-empirical method uses a Hamiltonian similar to the AM1 Hamiltonian but with a different parameterization strategy. This model is widely used for rapid estimation of molecular properties and includes many elements, even transition metals.
MNDO	Modified Neglect of Diatomic Overlap	Another semi-empirical method - developed by Dewar and Thiel[2] in 1977 which parameterizes one-centre two-electron integrals based on spectroscopic data for isolated atoms.
HF	Hartree-Fock	An Ab initio method based on the optimization of spin orbitals to give the lowest possible energy.
DFT	Density Functional Theory	First developed by Walter Kohn and Pierre Hohenberg[3] in 1964 – determination of the properties of multi-electron systems using electron density functionals.
B3LYP	Becke 3-Parameter Lee-Yang-Parr	A combination of Hartree-Fock theory and local density functional theory devised by Axel D. Becke in 1993[4].
STO-3G	Slater Type Orbital -3 Gaussians	The minimal basis set – each basis function is a combination of three Gaussians which simulates a Slater Type orbital.
3-21 G		A split basis set which has more functions for valance orbitals than for core orbitals
6-31 G		A polarisation basis set which includes d-type basis functions for 2nd row elements and therefore permits more accurate rendering of π bonds.
6-31 G*		To the 6-31 G basis set are added either six d-type (Li to Ca) or ten f-type (Sc to Zn) Cartesian-Gaussian polarization functions.

Table 1- The computational models and basis sets used mentioned within this chapter and in the publication.

4.1 Introduction

This chapter focusses largely upon the use of NMR spectroscopy to elucidate, and further understand intramolecular charge transfer interactions within the dyad **JULBD**. The interest in carrying out such a study stems from observations surrounding the charge transfer capabilities of the dyad, the synthesis and characterisation of which was addressed within the previous chapter. It was noticed from the absorption profiles recorded, that the ground state compound displayed significant charge transfer character in solvents of varying polarity.

This chapter is also concerned with the synthesis and characterisation of further control dyads used in the study, where the dipole moment changes either in magnitude or direction. These were achieved by replacing the julolidine residue with either a phenylene group (to generate **PHBD**) or the electron withdrawing 4-nitrobenzene (**NITBD**).

NMR spectroscopy is an invaluable tool by which to observe the effects of ground state charge transfer[5]. Direct evidence of electronic density distributions in organic systems can be generated from observed chemical shifts[6]. When such systems are perturbed, for example, by solvent-induced charge transfer effects, certain chemical shift changes are likely to evolve.[7] One way in which these changes can be studied, is via the generation and subsequent analysis of NMR spectra of the charge transfer system in question. These spectra should be recorded in various solvents of disparate polarity. Any changes in chemical shift values observed can then be correlated with the polarity of the solvent. In order to conduct this experiment coherently, numerous parameters must be established and other interfering effects discounted.

In order to avoid any ambiguity which may arise when studying solvent effects in this manner, an empirical model should be employed for the solvent polarity scale. Several such examples exist and have been applied successfully in spectroscopic studies similar to that documented within this chapter. For example, changes in the ^{13}C NMR spectra of iodoalkanes observed in Lewis base solvents[8]. Solvent polarity function models include Reichardt's E_NT parameter[9], Gutmann's donor number[10] or Taft and Kamlet's β and π parameters[11].

Prior work[12] on merocyanine-type dyes (which feature within applications including optoelectronics[13,14], non-linear optics[15] and information recording devices[16,17,18]) has also addressed the influence of solvent polarity on ^{13}C NMR chemical shifts. These species show strong ground state charge transfer and inherent zwitterionic character in the polymethine backbone. For example, the triarylmethane dye shown below in *Figure 2* (left) derives its solvatochromism from an intramolecular charge transfer from the donor dimethylamino-phenyl groups to the acceptor barbituric moiety. The spectral behaviour of this compound was found to parallel the solvatochromism exhibited by the related dye (*Figure 2,* below, right) also described within the publication.

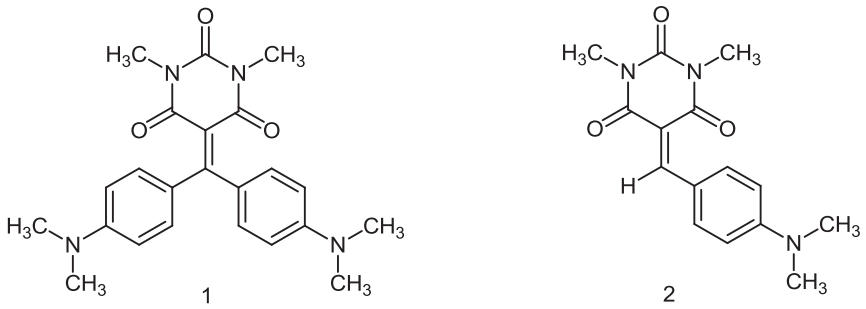

Figure 2 – The solvatochromic merocyanine type dyes[19] synthesised by Rezende et al.

A study of the NMR spectra of these two systems in various solvents was carried out, with chemical shift assignments being made by means of both normal and long-range COSY measurements. Evidence from spectral data, supported by theoretical calculations, highlighted the major structural difference between the two merocyanines; namely, whilst **2** may be described as a typical merocyanine, **1** behaves as an ylid type compound. It possesses a highly polarised C5-C7 bond (see *Figure 3* below) bridging the donor and acceptor moieties.

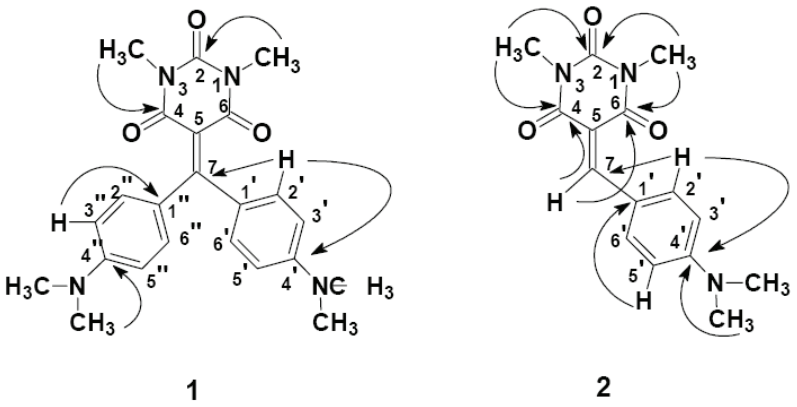

1 2

*Figure 3 – HMBC correlations of compounds **1** and **2**.*

A second NMR study[20] on the electronic structure and solvatochromism of this type of compound revealed a strong correlation between the calculated charges on carbon atoms of the polymethine chain and their ^{13}C NMR chemical shifts. Solvent polarity was also found to exert an influence on bond orders for dyes with positive and negative solvatochromism.

The utility of NMR spectroscopy in probing the electronic environments in diverse system types can clearly be seen.

4.2 Synthesis

The synthetic strategies employed to achieve the two target reference dyads are highlighted in *Scheme 1* below.

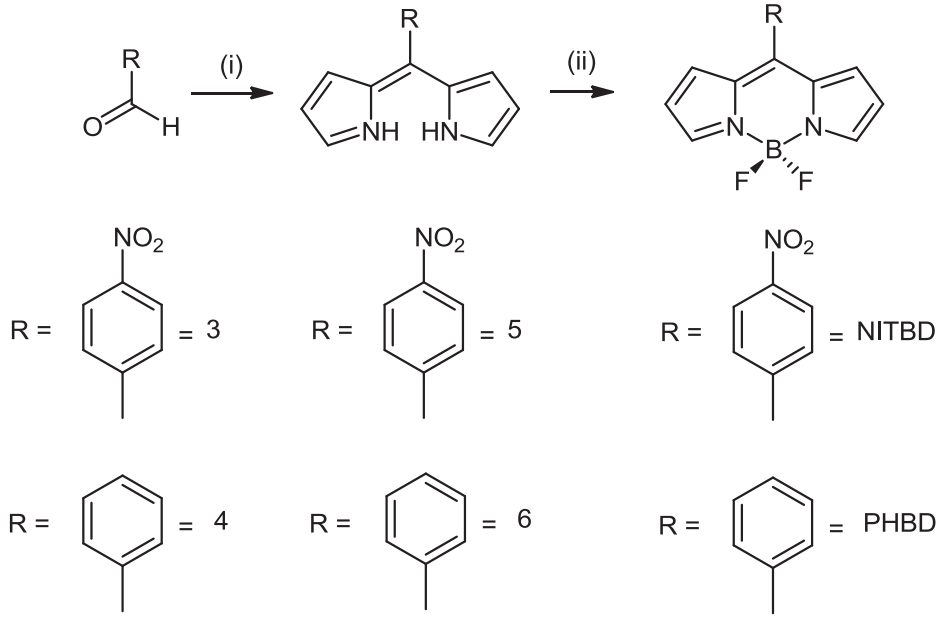

Scheme 1 – Reagents: (i) DCM, TFA, pyrrole (ii) DDQ, N,N-diisopropylethylamine, $BF_3.Et_2O$.

The synthetic route is analogous to that employed in the preparation of **JULBD**, which involves the isolation of the dipyrromethane unit, prior to formation of the bodipy under standard conditions. Both **5** and **6** were isolated in higher yield than julolidine dipyrromethane, which is possibly due to the fact that the aldehyde carbon in both cases is more electrophilic which increases the likelihood of nucleophilic attack at the aldehyde.

The first step of the synthetic route is preparation of the intermediary dipyrromethane from the corresponding commercially available aldehyde. 4-nitrobenzaldehyde was used as the starting material in the synthesis of **NITBD**, whilst **PHBD** was prepared from simple benzaldehyde. In both cases the reaction proceeded cleanly and easily. Whilst **PHBD** was a literature compound, in spite of the dipyrromethane[21] (**6**) having been previously isolated and characterised, **NITBD** was a novel bodipy derivative. Full characterisation was therefore carried out on this dyad.

As an additional study, the relationship between the distribution of electron density and ^{13}C chemical shift was analysed. This was in light of prior work[22] by Palafox *et al.* who showed that for phenothiazine, electron densities on certain carbon atoms are related to the observed experimental chemical shifts. In order to investigate this further, four additional bodipy derivatives were used as control compounds to ascertain the electron density distribution at each dipyrrin carbon atom. The structures of these four compounds are shown below (*Figure 4*).

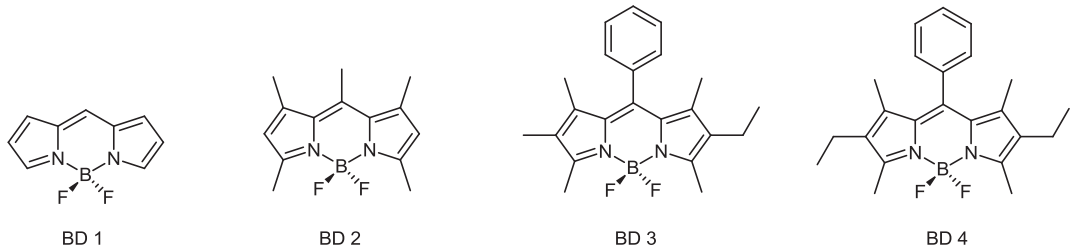

Figure 4 – The series of bodipy based compounds used in the computational calculations.

Samples of **BD2-BD4** were used from starting materials generated by previous group members, while **BD1** had never before been synthesised within the group and was therefore generated specifically for the study.

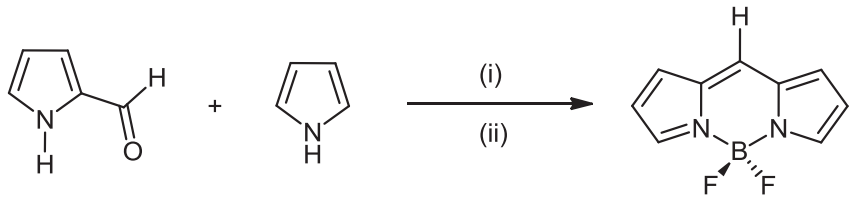

*Scheme 2 – The synthesis of **BD1**[23]. Reagents: (i) TFA, DCM (ii) N,N' diisopropylethylamine, $BF_3.Et_2O$.*

The preparation of **BD1** was a one-pot reaction for which the temperature had to be carefully controlled prior to the addition of each reagent. For example, the system is cooled prior to addition of N,N-diisopropylethylamine and boron trifluoride diethyletherate, and then heated gently (25-30°C) overnight following successful addition. The reaction is believed to proceed via attack of pyrrole on 2-formyl pyrrole, following protonation at the aldehyde oxygen atom by trifluoroacetic acid to increase its susceptibility to nucleophilic attack. Following purification of **BD1** by

column chromatography (using toluene as eluent for the first column and DCM for the second), the compound was isolated in 7% yield (literature yield[23] = 8%). The low yields can be attributed to the fact that several cycles of column chromatography were required to gain the high level of purity required for this compound.

One further compound was also generated but it turned out that it was not required for use in the NMR studies. This was a bodipy analogous to **JULBD** but with the exception of substitution at the indacene core. This was named **JULBD2** and was prepared according to *Scheme 3* below under typical bodipy forming conditions. The aldehyde required in the synthesis had conveniently been prepared previously for the synthesis of juloldine dipyrromethane. It was hoped that further studies would be carried out at a later date comparing the charge transfer capabilities of **JULBD2** with the properties exhibited by original **JULBD**. From first glance it can be assumed that the alkyl substitution at the indacene core which renders the bodipy less electron affinic would slightly destabilise the charge separated state. It is believed that work on this area, such as a photophysical analysis or further NMR studies would provide insight into electron density and charge distribution in **JULBD2**.

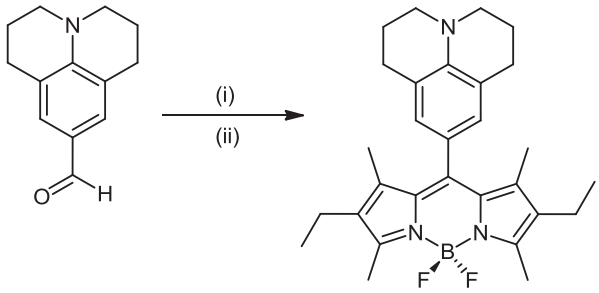

*Scheme 3 – The synthesis of **JULBD2**. Reagents: (i) 2,4-dimethyl-3-ethylpyrrole, TFA, DCM (ii) DDQ, N,N-diisopropylethylamine, $BF_3.Et_2O$.*

4.3 Characterisation and Structure Confirmation

4.3.1 Crystal Structures

The crystal structures of a selection of the compounds (e.g., **NITBD**, **PHBD** and **JULBD2**) discussed within this chapter are given below.

4.3.1.1 NITBD

Crystals of **NITBD** were readily obtained by slow evaporation of diethyl ether into a saturated dichloromethane solution of the compound. Single crystal X-ray diffraction studies indicate that the meso-nitrophenyl ring in the bodipy compound does not lie completely perpendicular to the indacene plane and instead resides in a slightly offset position, with a torsion angle of 124.93° being observed between the carbon atoms C11, C10, C5 and C6. The crystal packing diagram shows how the molecules adopt a head-to-tail packing sequence to allow for maximum interaction of the nitro substituted phenyl ring of each unit.

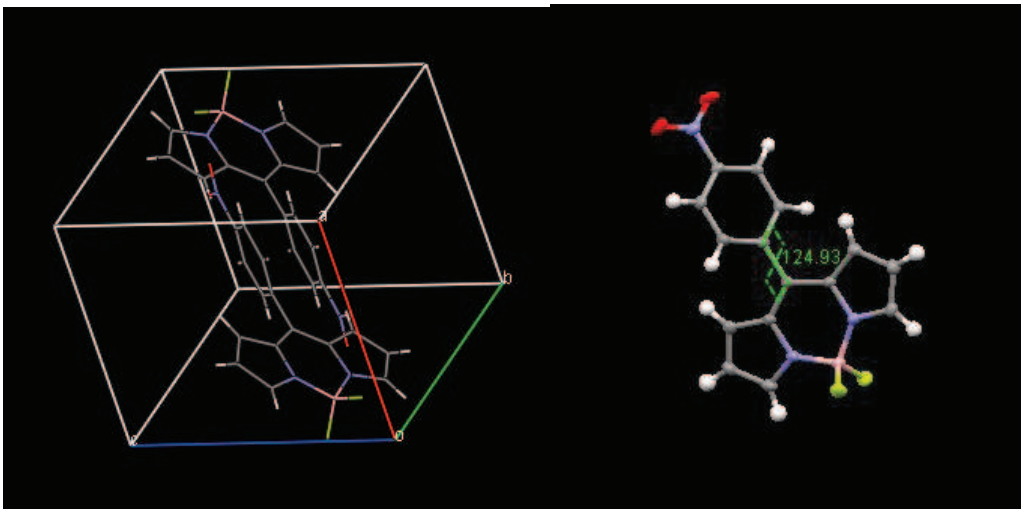

*Figure 5 – Left: The crystal packing arrangement of **NITBD**: carbon (grey), nitrogen (blue), oxygen (red), boron (pink), fluorine (green). Right: the torsion angle in **NITBD**.*

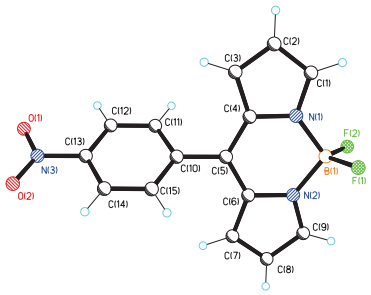

*Figure 6 - The atom labelled crystal structure of **NITBD**.*

4.3.1.2 PHBD

Crystals of **PHBD** were obtained by slow evaporation of petrol into a saturated dichloromethane solution of the compound.

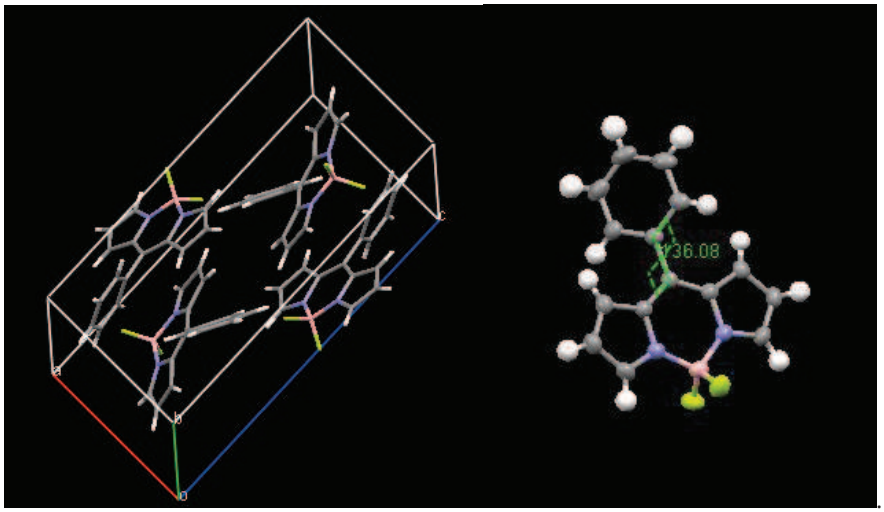

*Figure 7 – The crystal packing arrangement of **PHBD**: carbon (grey), nitrogen (blue), oxygen (red), boron (pink), fluorine (green).*

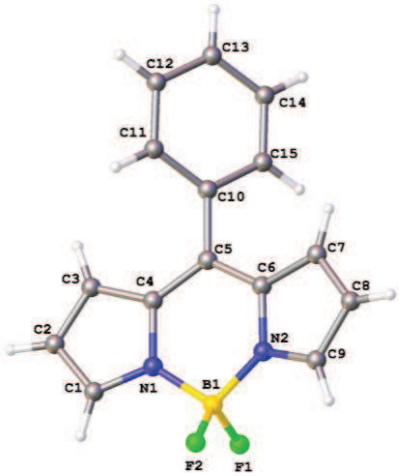

*Figure 8 – The atom labelled crystal structure of **PHBD**.*

Single crystal X-ray diffraction studies indicate that in **PHBD**, as in **NITBD**, the meso-phenyl ring does not lie completely perpendicular to the indacene plane. Instead it resides in an offset position, with a torsion angle of 136.08° being observed between the carbon atoms C15, C10, C5 and C4.

4.3.1.3 JULBD2

Crystals of the indacene core substituted compound **JULBD2** were also obtained by slow evaporation of diethyl ether into a saturated dichloromethane solution of the compound. In this compound, single crystal X-ray diffraction studies indicate that a torsion angle of 100.09° is observed between the carbon atoms C28, C18, C5 and C4. For the equivalent atoms in **JULBD** the torsion angle was observed to be 128.02° (please refer to *Figure 11*).

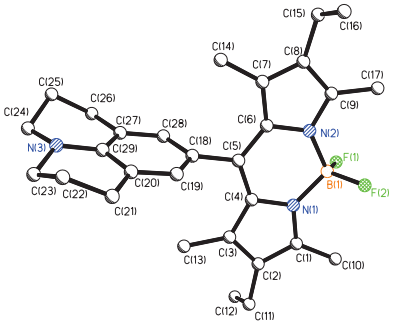

*Figure 9 - The atom labelled crystal structure of **JULBD2**.*

This means that a greater degree of orthogonality could be seen between the julolidine moiety and the indacene core in **JULBD** when compared to **JULBD2**. It is very likely that the julolidine moiety in **JULBD2** will experience a steric hindrance effect from the methyl groups in the 1 and 7 positions.

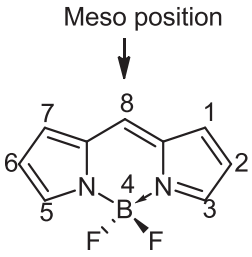

Figure 10 - The structure and numbering scheme of bodipy.

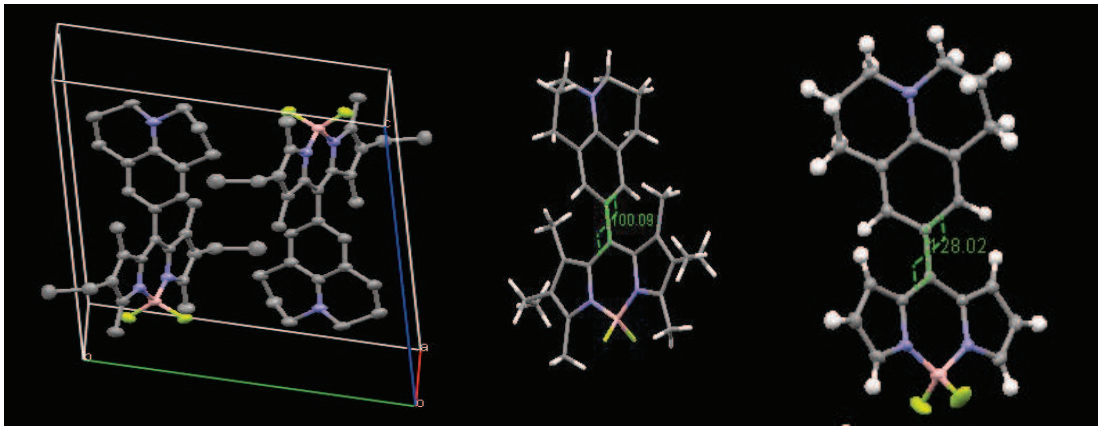

*Figure 11 – Far left: The crystal packing arrangement of **JULBD2**: carbon (grey), nitrogen (blue), boron (pink), fluorine (green). Middle: torsion angle in **JULBD2**. Far right: the larger torsion angle observed in **JULBD**.*

The crystal packing diagram below *(Figure 12)* indicates how the molecules adopt a head-to-tail packing sequence to allow for maximum interaction of the phenyl ring of each julolidine unit.

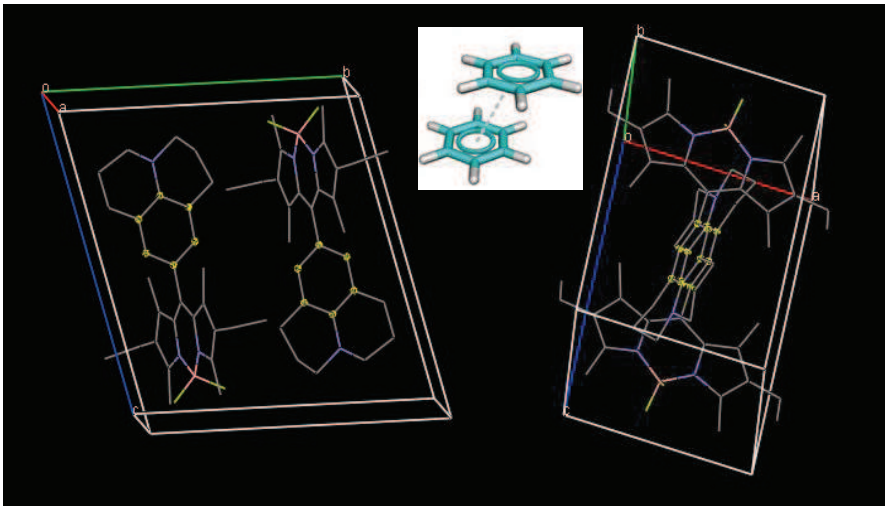

Figure 12 – The crystal packing diagram indicating how the phenyl rings stack, leading to maximal interaction. Insert: an image[24] showing typical π-stacking interactions.

4.4 NMR spectroscopic data

^{1}H, ^{13}C, ^{19}F and ^{11}B NMR spectra were recorded for **NITBD**, **PHBD**, **BD1** and **JULBD2**. The carbon spectra of all but the latter were recorded in a range of solvents

of disparate polarity for use in the NMR study. Proton and carbon spectra of **BD2-BD4** were also recorded and can be located in the supplementary data section of the publication.

4.4.1 NITBD

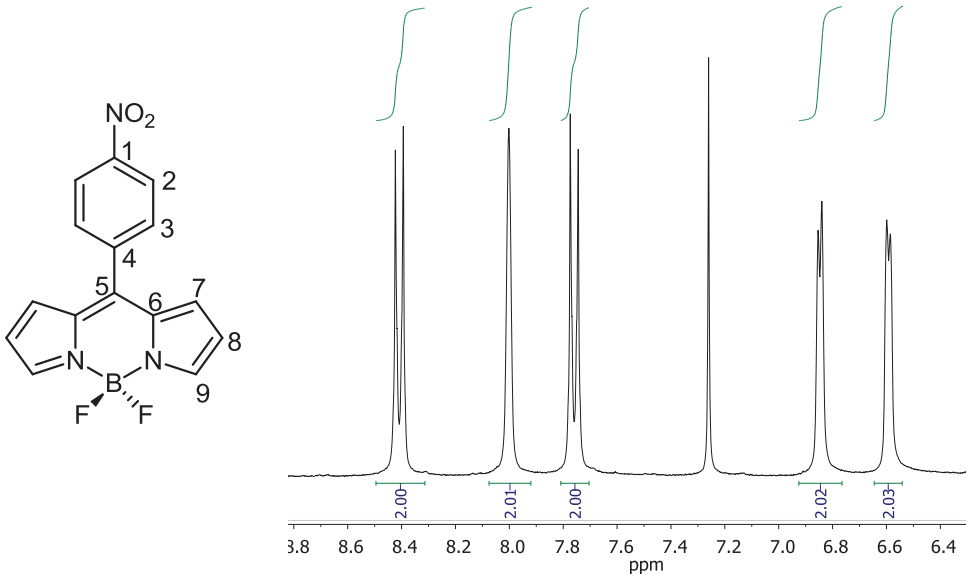

*Figure 13 – The aromatic region of the ^{1}H NMR spectrum for **NITBD** in $CDCl_3$ at RT.*

Chemical shift (ppm)	Intensity (no. of H Atoms)	Multiplicity	Coupling constant (*J*/ Hz)	Assignment
8.41	2	d	8.8	2
8.00	2	s	N/A	9
7.76	2	d	8.8	3
6.85	2	d	4.0	7
6.59	2	d	4.0	8

*Table 2 – The ^{1}H NMR peak assignment for **NITBD**.*

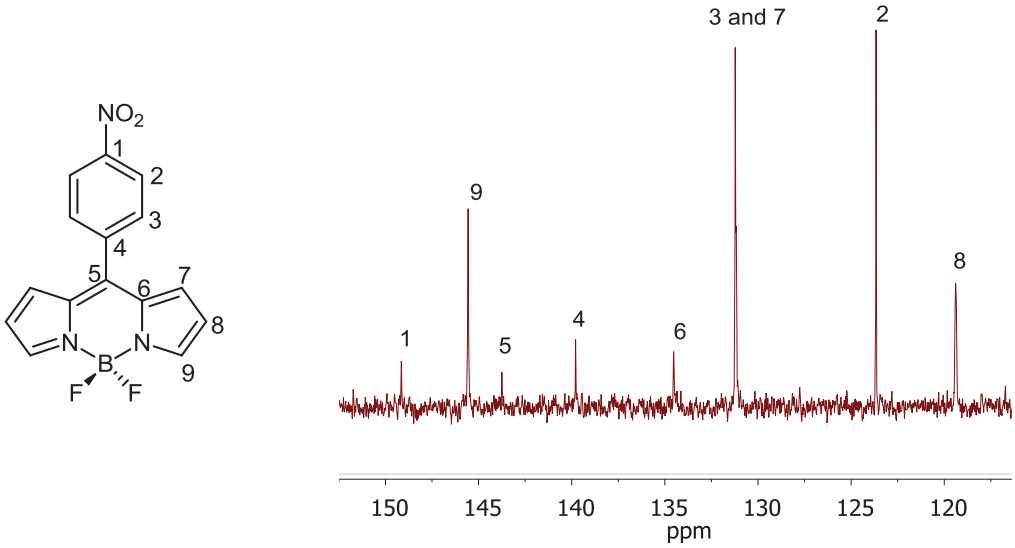

*Figure 14 – ^{13}C NMR spectrum of **NITBD** in $CDCl_3$ at RT.*

Chemical shift (δ)	Carbon assignment	Chemical shift (δ) (Continued)	Carbon assignment
149.1	1	131.2	7
145.6	9	131.2	3
143.8	5	123.7	2
139.8	4	119.4	8
134.5	6		

*Table 3 – ^{13}C Chemical shifts for **NITBD** recorded in $CDCl_3$ at RT.*

4.4.2 PHBD

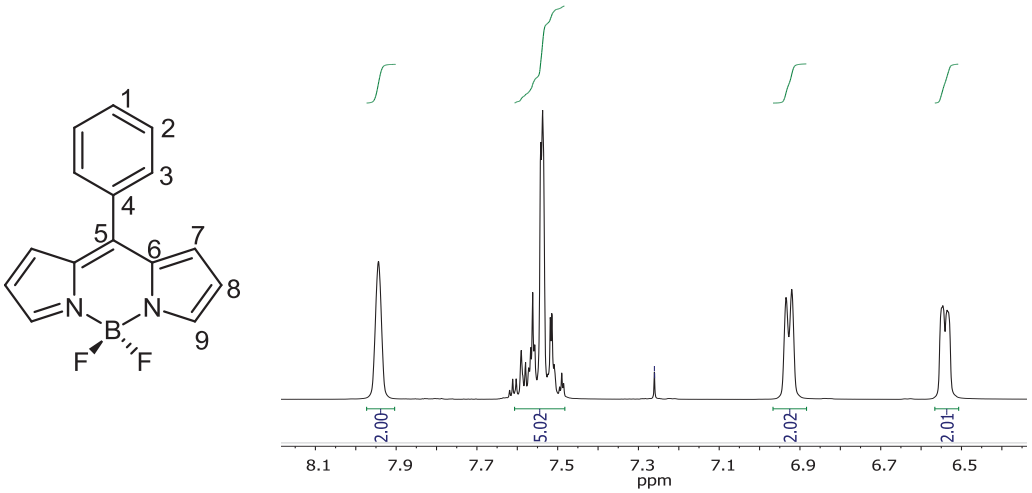

*Figure 15 – The aromatic region of the ^{1}H NMR spectrum of **PHBD** in $CDCl_3$ at RT.*

The most downfield shifted proton set at δ 7.94 corresponds to those adjacent to the nitrogen atom of the indacene core, i.e., in the 3 and 5 position according to the typical bodipy numbering scheme (9 on the structure). Meanwhile, the most downfield shifted doublet situated at δ 6.93 ppm corresponds to the protons in the 1 and 7 position (protons 7). The remaining doublet at δ 6.54 ppm can be attributed to the protons in the 2 and 6 position (protons 8). The five protons situated on the phenyl ring resonate as a multiplet with a complex appearance.

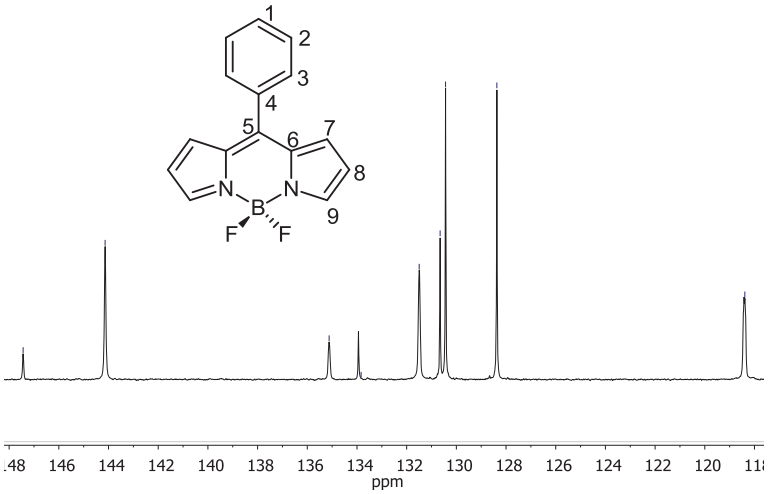

*Figure 16 – ^{13}C NMR spectrum of **PHBD** in $CDCl_3$ at RT.*

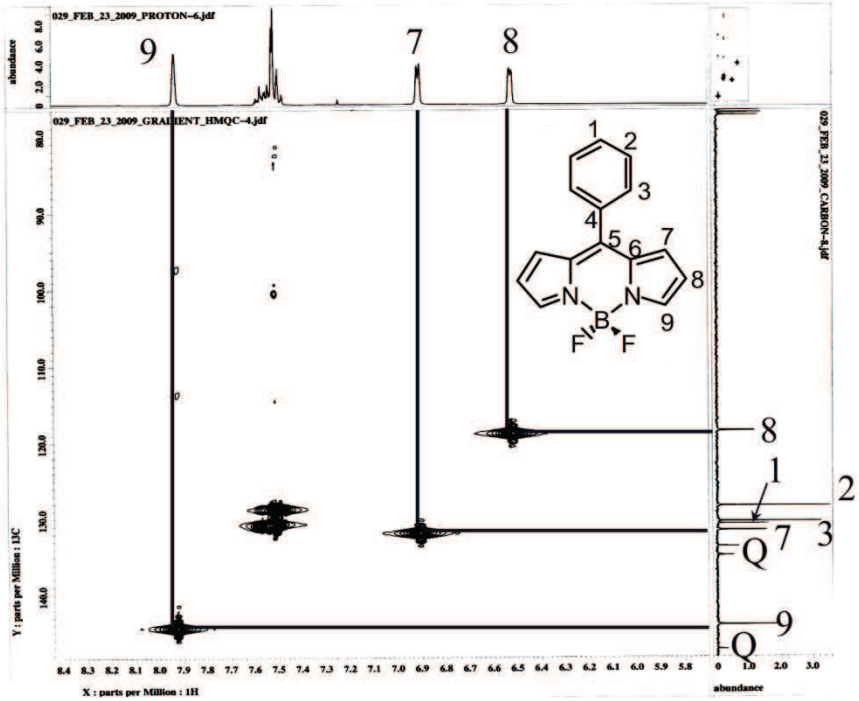

*Figure 17 – HMQC spectrum of **PHBD** in $CDCl_3$ at RT showing the proton to carbon correlations.*

An annotated HMQC spectrum of the molecule is shown above (*Figure 17*) and shows the carbon and proton assignment. Carbons 4, 5 and 6 are quaternary carbons and are denoted Q on the diagram. The other carbon atoms have been assigned using a combination of literature chemical shift values and observations taken from the other spectra for the remaining dyads in the series.

Chemical shift (ppm)	**Intensity (no. of H Atoms)**	**Multiplicity**	**Coupling constant (*J*/ Hz)**	**Assignment**
7.94	2	s	N/A	9
7.54	5	m	N/A	Phenyl ring protons
6.93	2	d	3.7	7
6.54	2	d	3.7	8

*Table 4 – The ^{1}H NMR peak assignment for **PHBD**.*

In order to determine the identity of quaternary carbon atoms 4, 5 and 6, an HMBC spectrum was recorded and is shown below (*Figure 18*). Carbon 6 was assigned first as correlations were observed between this carbon atom and protons 7, 8 and 9. This peak could only correspond to carbon 6 as carbon 5 is too many bonds away from both proton 8 and proton 9 to reasonably display a correlation and carbon 4 is too distant from all of these protons. The remaining two peaks corresponding to carbons 4 and 5 both display a correlation with the multiplet at δ 7.54 corresponding to the phenyl protons. It has already been seen that in **JULBD** and **NITBD**, carbon 5 appears downfield of 4 which was also confirmed by a low-level peak assignment prediction. Thus, carbon 5 was assigned as the most downfield peak in the carbon spectrum, at δ 147.3 ppm.

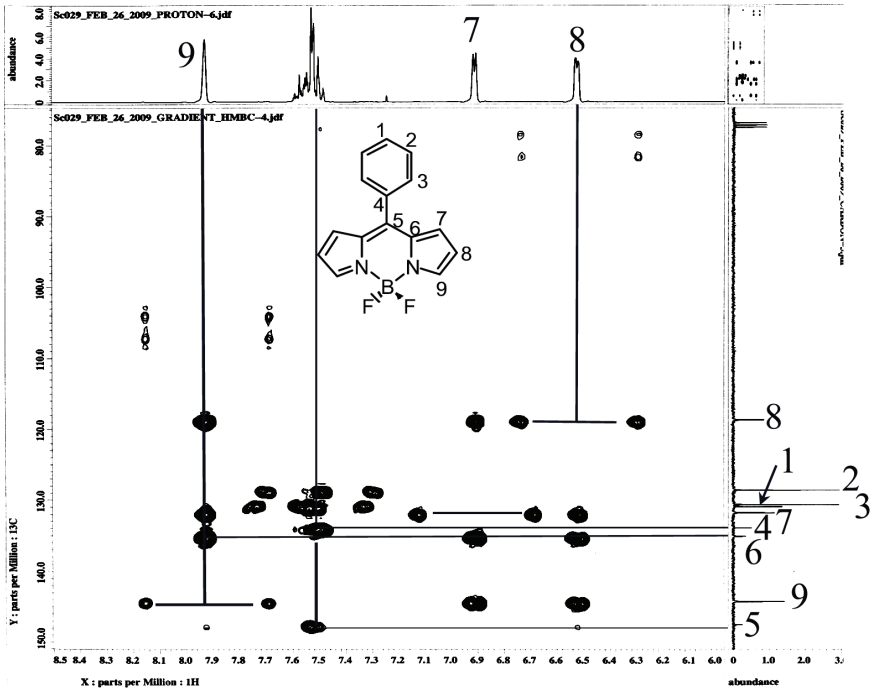

*Figure 18 – HMBC spectrum of **PHBD** recorded in $CDCl_3$ at RT.*

Chemical shift (δ)	Carbon assignment	Chemical shift (δ) (Continued)	Carbon assignment
147.3	5	130.7	1
144.0	9	130.4	3
134.8	6	128.4	2
133.6	4	118.5	8
131.5	7		

*Table 5 – ^{13}C chemical shift assignment for **PHBD** in $CDCl_3$ at RT.*

4.4.3 JULBD2

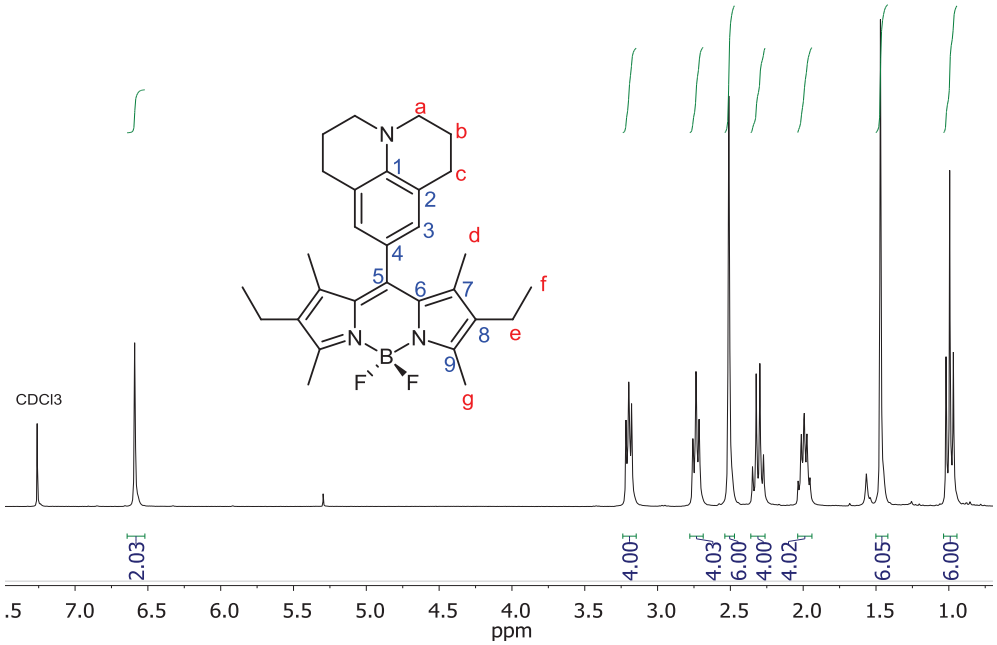

*Figure 19 – ^{1}H NMR spectrum of **JULBD2** in $CDCl_3$ at RT.*

Chemical shift (ppm)	Intensity (no. of H Atoms)	Multiplicity	Coupling constant (*J*/ Hz)	Assignment
6.59	2	s	N/A	3
3.20	4	t	5.5	a
2.74	4	t	5.5	c
2.51	6	s	N/A	g
2.31	4	q	7.5	e
1.99	4	m	N/A	b
1.47	6	s	N/A	d
0.99	6	t	7.5	f

*Table 6 - ^{1}H NMR peak assignment for **JULBD2**.*

The peaks corresponding to the protons on the cyclohexane ring moiety of julolidine can be instantly assigned as their positions are known from the **JULBD** assignment. The locations of the peaks corresponding to the methyl and ethyl groups of the indacene core substitution are also well known from a previous assignment. Similarly, the protons attached to carbon set 3 are simply assigned due to the unique singlet in

the aromatic region which can only correspond to these protons. The HMQC spectrum can now be considered to assign the non-quaternary carbon atoms.

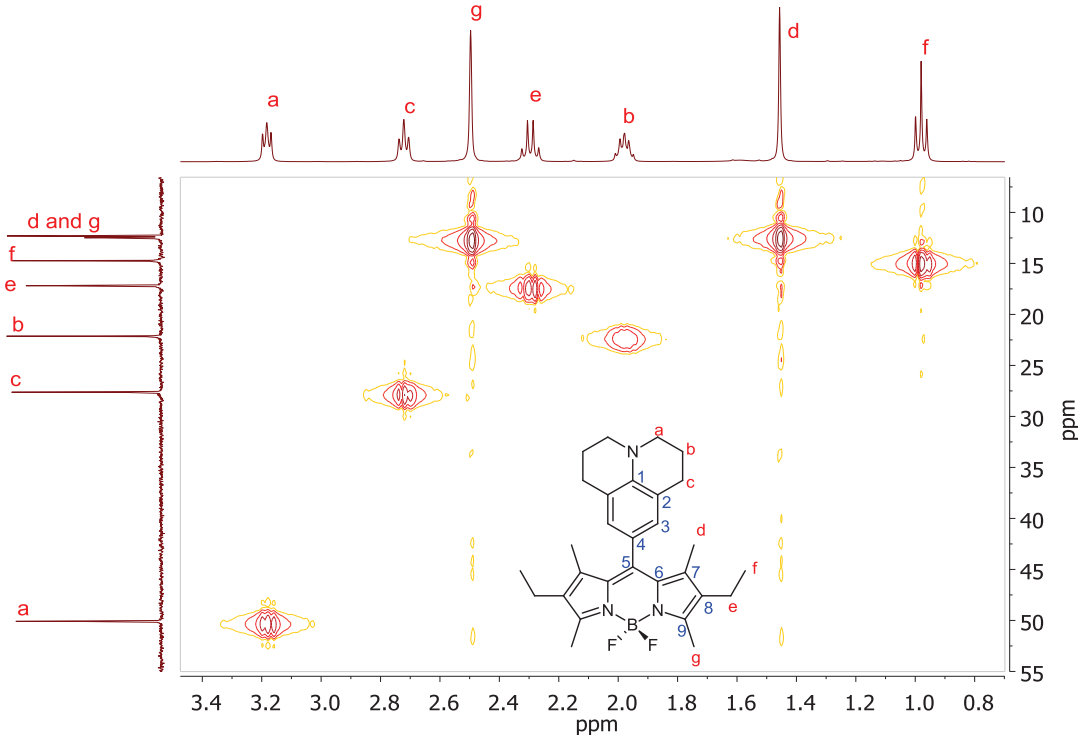

*Figure 20 – HMQC NMR spectrum of **JULBD2** in $CDCl_3$ at RT.*

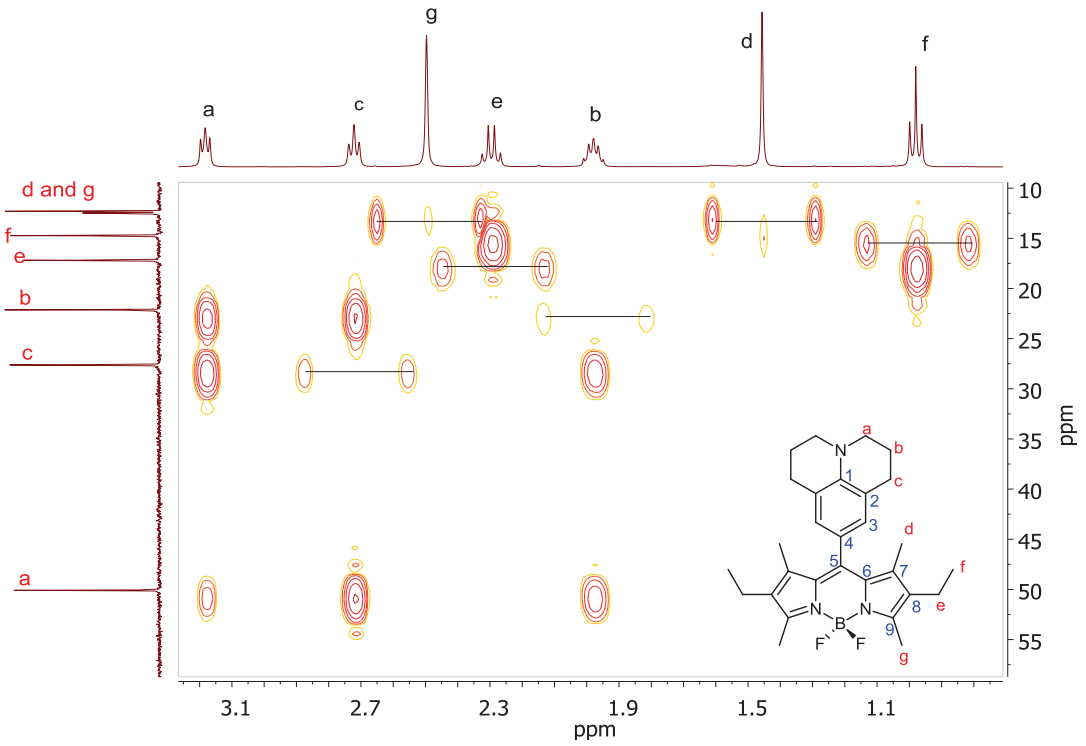

*Figure 21 – HMBC spectrum of **JULBD2** in $CDCl_3$ at RT.*

The *J* correlations in the HMBC spectrum in *Figure 21* are highlighted by the annotated lines. These allow a direct correlation to be seen between several connected proton and carbon atoms and permits the assignment of carbons b, c, d, e, f and g.

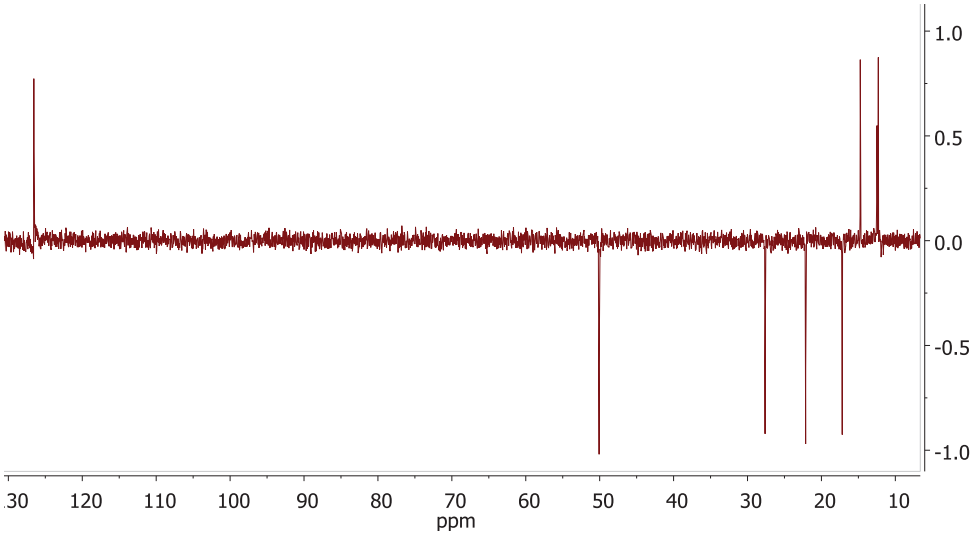

Figure 22 – Selective view of the DEPT-135 spectrum for ***JULBD 2*** *recorded in* $CDCl_3$ *at RT.*

The DEPT-135 technique produces a spectrum in which signals corresponding to CH and CH_3 groups appear in a different phase from those generated by CH_2 groups. In *Figure 22*, it can be seen that the peaks at δ12.21, 12.39 (these two peaks appear extremely close together in the spectrum above) and δ14.64 in the aliphatic region of the spectrum, in addition to the peak at δ126.47 in the aromatic region are in the opposite phase to the remainder of the peaks. Due to the fact that the peak at δ126.47 was instantly assigned to be carbon 3 (due to the correlation observed in the HMQC spectrum) and we know this carbon has a single hydrogen atom attached, it can be elucidated that the CH and CH_3 groups point upwards in this spectrum and the CH_2 groups downwards. Thus the peaks in the aliphatic region correspond to carbons D, G and F.

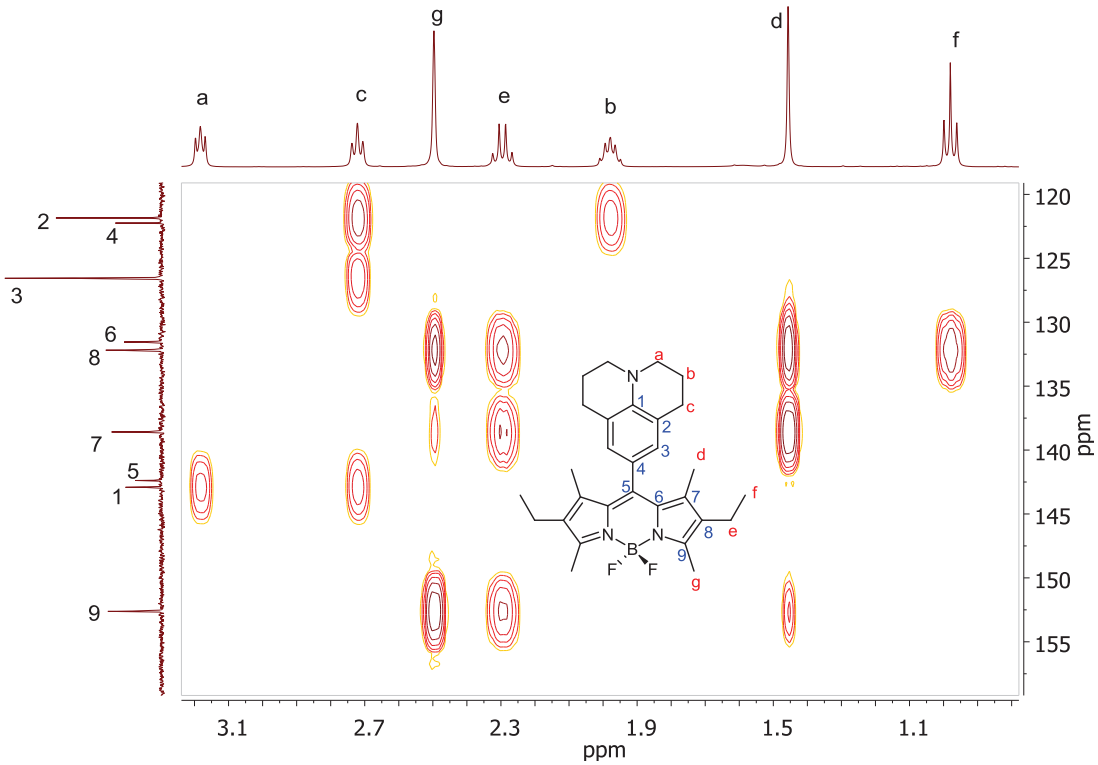

Figure 23 – An extract from the HMBC spectrum recorded of ***JULBD2*** *in $CDCl_3$ at RT, showing the aromatic carbon region and the aliphatic proton peaks.*

From the portion of the HMBC spectrum shown in *Figure 23*, along with a low-level peak prediction programme, the remaining carbon atoms were assigned. Carbon 9 was the first to be located. At this carbon atom, correlations to protons g, e and d were observed, similar to the correlation cross peaks seen at carbons 8 and 7. 8 also shows a correlation to aliphatic proton f.

When looking at carbons 7, 8 and 9, the latter typically resonates in the most downfield position and the peak prediction tool confirmed this. Carbon 8 was also assigned on the basis that it would be more likely to correlate to proton f than either carbon 7 or 9 would, due to its proximal location.

Carbons 1 and 5 possess chemical shift values in very close proximity and the spectrum must be closely examined to determine which of the proximal peaks show correlations to certain protons. Upon expansion of the spectrum, it could be seen that the correlation cross peaks to protons a and c were in line with the slightly more downfield peak, i.e., carbon 1. Carbons 4 and 5 are both the least likely to correlate

with any aliphatic protons, thus the assignment of these two carbons is fitting. The peak prediction tool suggested that carbon 5 should resonate downfield of 4. The carbon atom assigned to be 2 shows correlations with proton sets b and c which certainly fits.

Finally, the assignment of carbons 6 and 1 can be explained. Carbon 6 was assigned on the basis that it is unlikely to show correlations with any protons other than set d. Meanwhile, carbon 1 shows a correlation to aliphatic carbon sets a and c.

Chemical shift	Carbon atom assignment		Chemical shift	Carbon atom assignment
152.53	9		121.75	2
142.82	1		49.99	a
142.29	5		27.53	c
138.49	7		22.04	b
132.09	8		17.09	e
131.45	6		14.64	f
126.47	3		12.39	d and g
122.15	4		12.21	

*Table 7 - ^{13}C NMR peak assignment for **JULBD2** recorded in $CDCl_3$.*

4.5 Investigations into solvent polarity effects

4.5.1 Solvent polarity effects

It is well known that solvent polarity is an integral factor when establishing the level of intramolecular charge transfer in photoactive assemblies of the type discussed within this chapter. Consequently, ^{13}C NMR spectra were recorded for each of **JULBD**, **PHBD** and **NITBD** in a range of deuterated solvents. This was carried out in order to explore the influence of solvent polarity on the electronic environment at carbon atoms throughout the systems. The full results can be acquired from the supporting information section of the publication, whilst the most significant and noteworthy observations are discussed hereon in.

Table 8, below, shows the collected ^{13}C chemical shifts of the three dyads recorded in $CDCl_3$ at 25°C. $\Delta\delta_1$ is defined as δ **JULBD**-δ **PHBD** and $\Delta\delta_2$ as δ **NITBD**-δ **PHBD**.

Carbon no	JULBD	NITBD	PHBD	$\Delta\delta_1$	$\Delta\delta_2$
1	146.5	149.1	130.7	15.4	18.4
2	120.9	123.7	128.4	-7.5	-4.7
3	131.1	131.2	130.4	0.7	0.8
4	121.1	139.8	133.7	-12.7	6.1
5	148.5	143.8	147.3	1.2	-3.5
6	134.2	134.5	134.9	-0.7	-0.4
7	130.3	131.2	131.6	-1.3	-0.4
8	117.1	119.4	118.5	-1.4	0.9
9	140.7	145.6	144.0	-3.3	1.6

Table 8 – ^{13}C NMR chemical shifts (ppm[a]) for the bodipy based derivatives in $CDCl_3$ at 25°C.

[a] Error ± 0.1 ppm

In *Table 9*, the chemical shift differences for carbon atoms 5 and 9 are highlighted. In spite of the limited range of solvents, valuable trends can be observed. For example, the variation of $\Delta\delta_2$ for carbon 9 observed for **NITBD** is essentially insensitive towards solvent polarity changes. In spite of this, there are clear perturbations seen for carbon 5, which is to be expected considering that this is the connector atom. This behaviour can be used to argue that the extent of ground state charge transfer is minimal for the nitro derivative and thus, significant solvent polarity effects are negated. This idea is consistent with the computed dipole moment (the product of the computed quantity of positive or negative charge and the distance between their centroids).

However, noteworthy changes in $\Delta\delta_1$ are observed for **JULBD** at carbons 5 and 9, where variations appear to mirror one another; i.e., an increase for carbon 5 is accompanied by a decrease for carbon 9. The final two columns in *Table 9* are solvent polarity functions. E_NT is representative of Reichardt's E_NT parameter whilst SPP is

the abbreviation used to represent Catalàn's solvent dipolarity/ polarisability function.[25]

Reichardt's E_NT parameter is the normal E_T30 solvent polarity parameter based on the intramolecular CT absorption of a pyridinium-N-phenolate betaine dye. Catalàn's solvent dipolarity/ polarisability (SPP) scale is based on UV-vis measurements of the 2-N,N-dimethyl-7-nitrofluorene/ 2-fluoro-7-nitrofluorene probe/ homomorph pair[1].

Solvent	**$\Delta\delta_1$ (C_5)**	**$\Delta\delta_2$ (C_5)**	**$\Delta\delta_1$ (C_9)**	**$\Delta\delta_2$ (C_9)**	**E_NT^a**	**SPP**
$(CD_3)_2SO$	0.8	-2.9	-4.6	1.1	0.444	1.000
D_8-THF	1.3	-2.9	-3.6	1.2	0.207	0.838
CD_2Cl_2	1.1	-3.8	-3.8	1.2	0.309	0.876
CD_3CN	0.8	-3.2	-4.3	1.2	0.460	0.895
$(CD_3)_2CO$	1.2	-3.0	-4.0	1.2	0.355	0.881
$CDCl_3$	1.2	-3.5	-3.3	1.6	0.259	0.786

*Table 9 – Difference in ^{13}C chemical shifts for selected carbon atoms for **JULBD** and **NITBD** in various deuterated solvents.*
[a] values taken for the protiated solvent[26]

The chemical shift data obtained for **JULBD** was then compared with both the SPP function and Reichardt's E_NT parameter. The modulus of the chemical shift difference, expressed as $|\Delta\delta_1|$ was used for simplification. The plots generated are shown in *Figure 24* below.

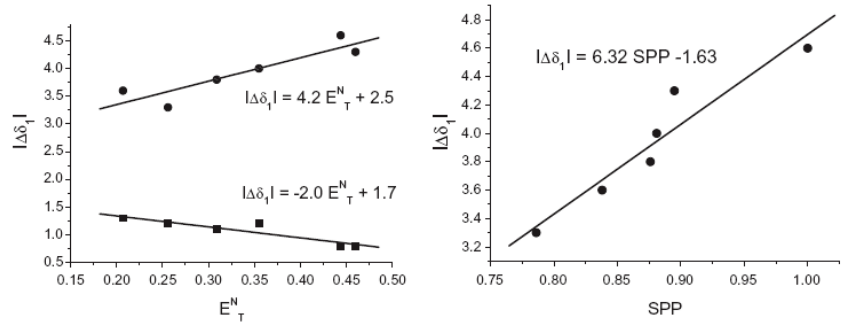

*Figure 24 - $|\Delta\delta_1|$ versus Reichardt's E_NT parameter for **JULBD** (shown left) and $|\Delta\delta_1|$ versus Catalàn's solvent dipolarity/ polarisability function (SPP) for **JULBD** (right). Carbon 9 (●) and carbon 5 (■) linear least squares fit (solid line). The obtained least-squares linear equation to the data points is also shown.*

It should be pointed out that there is an adequate least squares linear correlation for carbon 9 of $|\Delta\delta_1|$ with both SPP and the E_NT parameter. The latter parameter also gave a strong correlation for carbon 5. It can also be observed that the modulus of the gradient for carbon 9 is approximately twice that for carbon 5 (*Figure 24,* left). This result indicates that the carbon alpha to the nitrogen is more susceptible to changes in electron density.

4.5.2 Quantum chemical calculations

It is suggested from the solvent dependent NMR findings, that the distribution of electron density within the dipyrromethene segment is somehow related to individual ^{13}C chemical shift values. This can be backed up by work conducted by Palafox *et al*.[27] The group were able to show that in phenothiazines, (heterocyclic organic compounds known to possess remarkable pharmacological properties[28]) electron densities on certain carbon atoms are related to the experimental chemical shifts.

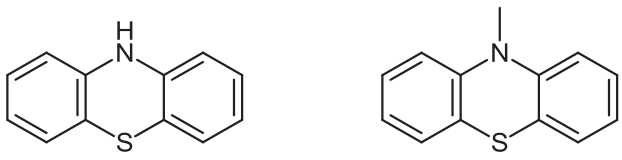

Figure 25 – Phenothiazine (left) and N-methyl phenothiazine (right) studied by Palafox et al.

The group incorporated both semi-empirical and *ab initio* methods and interpreted their NMR findings in terms of the electron densities on the atoms and the stacking solute-solute association in DMSO solution. In general, they found that in both compounds, the experimental chemical shifts agree with their calculated values through their electronic densities. Linear correlations between the two, calculated by Hartree-Fock and B3LYP were established.

In order to determine whether or not a similar correlation was achievable for our range of compounds, high level computational calculations were conducted. These studies were carried out both on the target molecules and in addition to this, on four further bodipy derivatives used as control compounds. These results were included in an attempt to ascertain the electron density distribution at each dipyrrin carbon atom. The structures of these bodipy systems are shown below (*Figure 26*). Whilst **BD1** was prepared for the project, it should be noted that **BD2-BD4** were stored samples prepared previously by former group members.

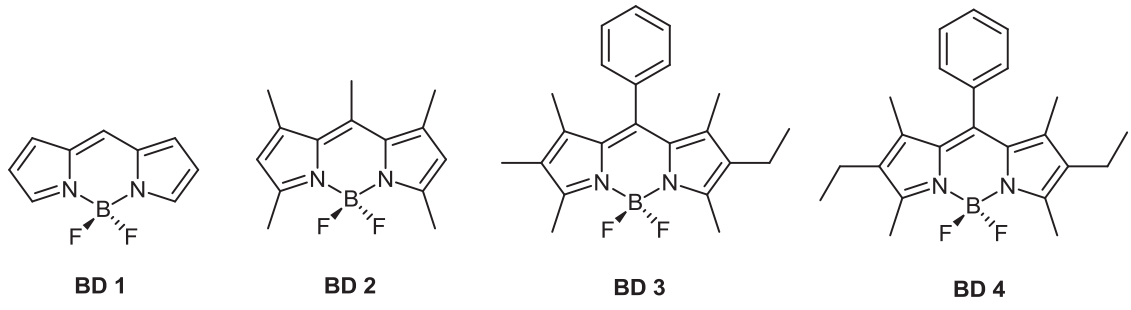

Figure 26 – The additional bodipy based compounds used in the computational calculations.

These supplementary derivatives were considered to be a means of identifying the most appropriate computational protocol. In addition, it would permit testing as to

whether the relationship between the electron charge density and the ^{13}C NMR chemical shift could be applied to a wider range of bodipy compounds.

The carbon assignment for **BD3** is known in the literature[29] and the data for the other three systems was collected in the same way as that for the target compounds. When it came to **BD1** however, complications arose. This was due to the fact that the compound had been prepared and characterised previously[30,31,32] and two conflicting ^{13}C resonance assignments reported. A chemical shift assignment different to that reported within this thesis had also been made for the protons adjacent to the nitrogen atoms. In an attempt to resolve this issue, the sample of **BD1** was subjected to a full $^{1}H/\ ^{13}C$ chemical shift assignment similar to that performed on the target compounds.

In the ^{1}H chemical shift assignments documented in the literature,[6,7,8] the most downfield resonance is taken as proton 7 and proton 9 is at δ 7.18 ppm, a deduction based on the COSY spectrum (*Figure 27*). This spectrum is identical in appearance to that collected using the sample prepared in house. However, the NOESY spectrum provided conflicting information - suggesting instead that the most downfield resonance is proton 9. This is supported by a low-level ^{1}H NMR chemical shift prediction carried out using ChemDraw ULTRA. The apparent long range coupling shown in the COSY spectrum can be attributed to the "W" effect.[33]

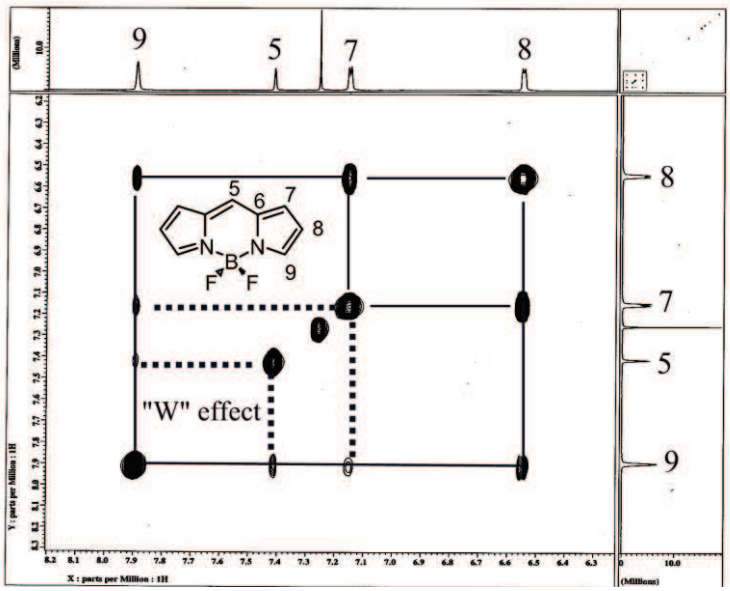

*Figure 27 – COSY spectrum of **BD1** in $CDCl_3$, showing the cross correlations and the apparent long-range ^{5}J "W" effect spin coupling between carbons 5 and 9.*

For the control compounds, partial Mulliken charges were calculated for the energy minimised structures *in vacuo* at several different computational levels, i.e., AM1, PM3, MNDO, HF-321G, HF-631G**, DFT (B3LYP/6-311++G**. Please refer to the glossary at the beginning of the chapter for more details on these terms.

Mulliken charges differ from effective charge in that they are nominal atomic charges determined by Mulliken population analysis[34] -the simplest technique to describe the electron distribution in a molecule[35]. Effective charge and Mulliken charge encapsulate differing aspects of the physics involved, with the former giving more information on the vibrational properties of molecules and hence their chemical bonding. In contrast to this, the Mulliken population analysis yields more information on electron density distributions in systems and is more useful in our study.

The most suitable calculation carried out in this situation was deemed to be the DFT (density functional theory) method. Calculations using HF-321G and HF-631G** also offered Mulliken charge results consistent in sign and nature for the entire bodipy series, whilst some computational theory was less successful.

As an example, when **BD3** is analysed as a control, a linear correlation is observed between the calculated Mulliken charge obtained from the DFT study and the ^{13}C chemical shift for the carbon resonances concerned. It was noted that the Mulliken charge calculated for C6/6a was highly positive and not in keeping with the observed δ value, a trend which was actually observed for calculations made at all levels of theory on each of the bodipy derivatives. In order to overcome this issue, the linear fit shown in *Figure 28* below was plotted for use as a calibration curve with which to correct this over-estimation.

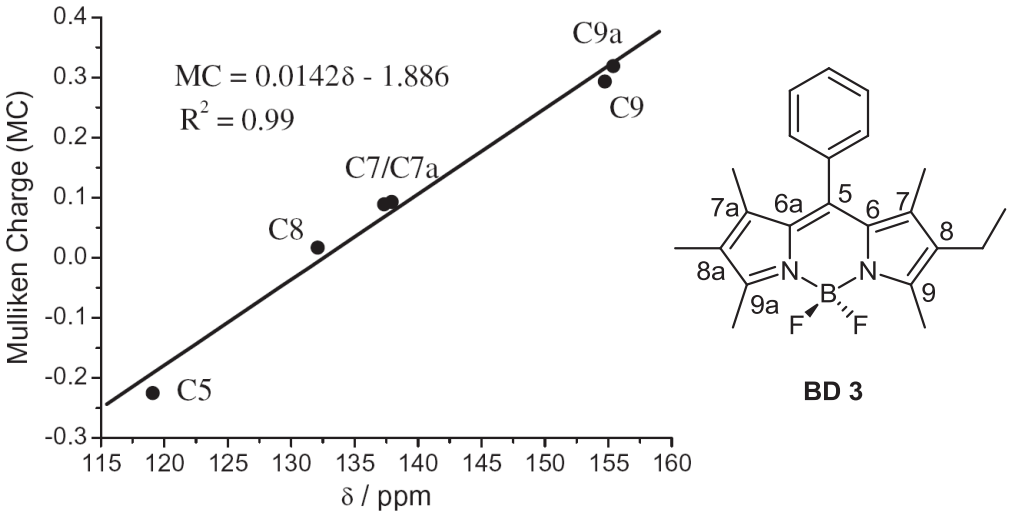

*Figure 28 – Correlation between the Mulliken charge at the carbon atoms and the corresponding chemical shift[36] (δ) measured in $CDCl_3$ for **BD3**.*

A number of similar plots obtained for the other bodipy derivatives studied, also displayed a good linear relationship between Mulliken charge and chemical shift and the slopes and intercepts derived from these plots are collected in *Table 10* below.

Compound	Slope / MC δ^{-1}	Intercept / MC
BD1	0.0122	-1.70
BD2	0.0198	-2.67
BD4	0.0141	-1.89
JULBD	0.0085	-1.17
PHBD	0.0081	-1.12
NITBD	0.0091	-1.40

Table 10 – Calculated parameters from the Mulliken charge versus ^{13}C chemical shift plots for a series of bodipy derivatives.

It must be mentioned however, that although the R^2 (goodness-of-fit) value varies widely through the range of compounds studied, the slopes are extraordinarily similar across the series. It should be taken into account that non-alkylated to fully-alkylated dipyrrin units and non-meso substituted derivatives are all included together. A noteworthy observation is that the slope/ intercept values for **JULBD** and **PHBD** are extremely similar. In addition to this, at a computational level, the electron donating

capability of the julolidine moiety does not appear to seriously affect the electron density distributions in the dipyrrin core. This is in spite of the clear localization of the HOMO on the julolidine and the LUMO on the bodipy core as detailed in *Figure 29*.

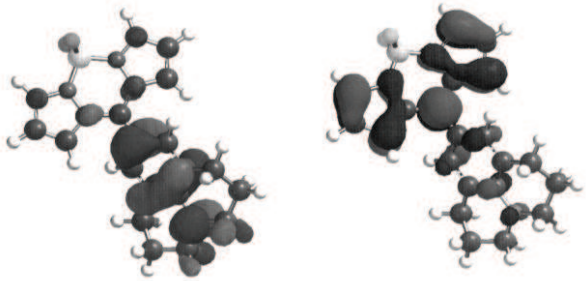

*Figure 29 - Computer generated HOMO (left) and LUMO (right) for **JULBD** in vacuo using the DFT (B3LYP/6-311++G**) method.*

Carbon 5 uniquely appears to be much affected as illustrated by the plot shown in *Figure 30* below. This examines the variation in Mulliken charge with chemical shift when comparing **JULBD** with **PHBD**. In spite of this, it is noticeable that the upfield shifts for carbon 6 to 9 are accompanied by, albeit small, increases in electron density on the carbon atoms.

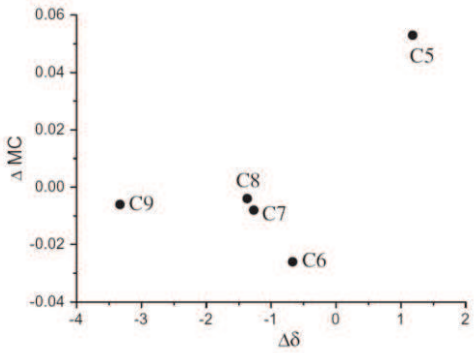

*Figure 30 – The change in Mulliken charge versus change in chemical shift when comparing **JULBD** with **PHBD**.*

4.6 Photophysical Properties

The photophysics of bodipy based systems is a well documented topic in the literature[37]. The absorption profile generated is known to prominently display a broad feature at short wavelength which is associated with the S_0-S_2 electronic transition. In addition to this, a sharper and more intense peak can be located at lower energy and assigned to the S_0-S_1 electronic transition. In the absorption profiles recorded for

PHBD and **NITBD** in acetonitrile (*Figure 31*), the long wavelength absorption band maximum (λ_{BD} = 504 nm) for **NITBD** is slightly red shifted when compared to **PHBD** (λ_{BD} = 497 nm) and a notable increase in the band half width is also seen. In addition, the close resemblance between the two reinforces the fact that ground state charge transfer in **NITBD** is very small.

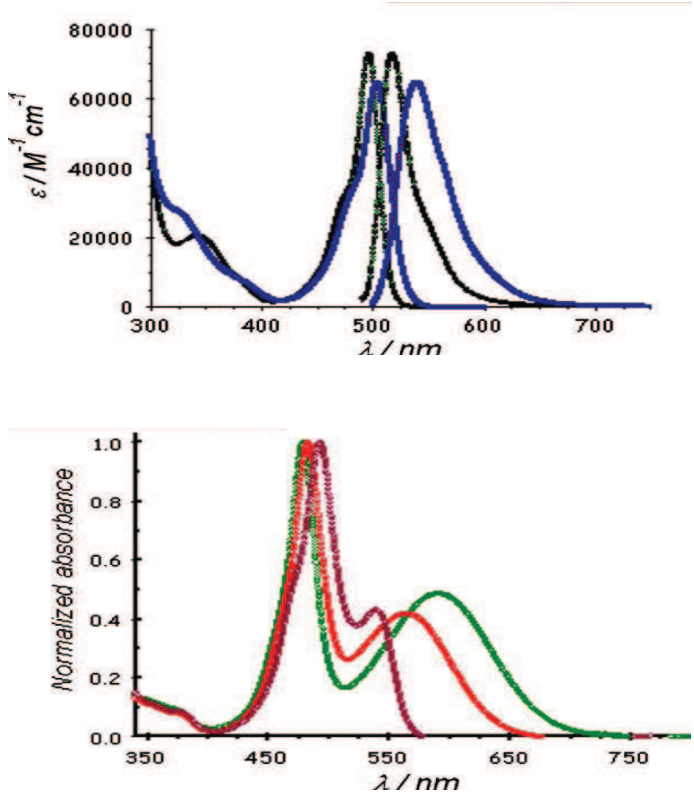

Figure 31 – Top: absorption and normalised fluorescence spectra[38] *recorded for* ***PHBD*** *(green) and* ***NITBD*** *(blue) dyes in CH_3CN solution at RT.*
Bottom: normalised absorption spectra recorded for ***JULBD*** *in cyclohexane (purple), ethyl acetate (red) and acetonitrile (green) at room temperature.*

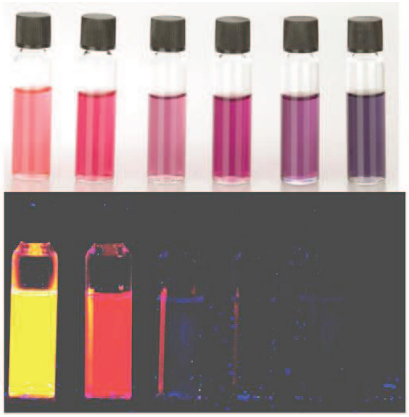

*Figure 32 – Top: Solutions of **JULBD** in CCl_4, di-n-butyl ether, ethyl acetate, DCM, chlorobenzene and butyronitrile (L→R). Bottom: An identical set of solutions under illumination.*

In addition, there is an accompanying reduction in the molar absorption co-efficient at the band maximum – a broadening effect which is also apparent in the fluorescence spectral profile for **NITBD** in acetonitrile (see also *Figure 31*). Here, the fluorescence maxima are located at 518 and 540 nm respectively for **PHBD** and **NITBD**, whilst the quantum yield of fluorescence measured for **PHBD** (MeCN, RT) was found to equal just 0.044 (Φ_F) – a substantially smaller value than those typically recorded for bodipy derivatives. This was believed to be due to the fact that the phenylene ring can freely rotate around the connecting C-C bond, creating a molecular rotor type system in which the fluorescence properties are sensitive to changes in the viscosity of the local environment[39].

The fluorescence quantum yield of **NITBD** is further reduced to 0.027 due to the occurrence of an excited state charge transfer effect in which bodipy acts as donor and the nitrobenzene residue behaves as the acceptor. The extended Stokes Shift observed in acetonitrile for **NITBD** (SS = 1320cm^{-1}) relative to **PHBD** (SS = 815 cm^{-1}) also confirms that this effect is taking place. The computer calculated ground state dipole moments for **JULBD**, **PHBD** and **NITBD** are 8.26 D, 5.46 D and 0.05 D respectively. The small value observed for **NITBD** can be attributed to the opposing effect of electron donation by the phenylene unit and charge transfer towards the nitro group. These two effects seem to almost cancel each other out and is also a likely

explanation as to why the ^{13}C NMR chemical shifts are less heavily influenced by polarity change.

It is immediately apparent that the absorption spectrum for **JULBD** is markedly different than those recorded for the other target compounds. Furthermore, even by eye, there is a very noticeable connection between the colour of the solution and the polarity of the solvent. This is illustrated by the images of the set of solutions shown in *Figure 32*. For example, **JULBD** dissolved in CCl_4 affords a red coloured solution, but when an identical quantity is solubilised in butyronitrile, an intense blue colour is observed. It can also be seen that in the latter solvent, in addition to the typical bodipy based absorption bands, a broad, Gaussian shaped charge transfer band is seen at around λ_{CT} = 600 nm. This position of this band exhibits a strong dependency upon solvent polarity and a blue shift, accompanied by line-narrowing is observed as the solvent polarity decreases.

These findings are grouped together in *Table 11* below:

Solvent	**f_{CT}**	**λ_{CT} (cm^{-1})**	**λ_{BD} (cm^{-1})**	**R[a]**	**SPP[b]**
Cyclohexane	0.065	18,532	20,284	2.32	0.557
CCl_4	0.096	18,349	20,268	2.42	0.632
Bu_2O	0.130	18,342	20,467	2.37	0.652
Et_2O	0.185	18,162	20,600	2.41	0.694
1,4-dioxane	0.165	17,980	20,534	2.50	0.701
Me-THF	0.207	17,775	20,610	2.44	0.717
$CHCl_3$	0.213	17,470	20,542	2.35	0.786
EtOAc	0.216	17,737	20,713	2.39	0.795
Chlorobenzene	0.188	17,259	20,509	2.35	0.824
THF	0.196	17,593	20,627	2.39	0.838
DCM	0.248	17,071	20,661	2.12	0.876
Acetone	0.222	17,271	20,807	2.20	0.881
MeCN	0.285	16,955	20,912	2.05	0.895
BuCN	0.267	17,082	20,764	2.20	0.915
Propylene carbonate	0.272	16,578	20,790	2.06	0.930
DMF	0.288	16,784	20,713	2.16	0.939
DMSO	0.290	16,617	20,653	2.13	1.00

*Table 11 – Photophysical properties derived for **JULBD** in a range of solvents at 20°C.*
a = ratio of intensities at the maxima of the bodipy and CT bands.
b = Catalán's solvent polarity function

There is also an accompanying minor shift in λ_{BD} with solvent polarizability. This has been reported previously for bodipy based dyes by Boens and co-workers[40]. In *Figure 33*, the linear correlation observed between λ_{CT} and Catalàn's solvent polarity function (SPP) is shown. The correlation seen is a strong indicator of the high degree of charge transfer in the ground state for this compound. Interestingly, a linear relationship can be observed between λ_{CT} and $|\Delta\delta|$ for carbons 5 and 9 (*Figure 34*).

This result is further indication that the high level of ground state charge transfer character present in **JULBD** affects the ^{13}C NMR chemical shift values.

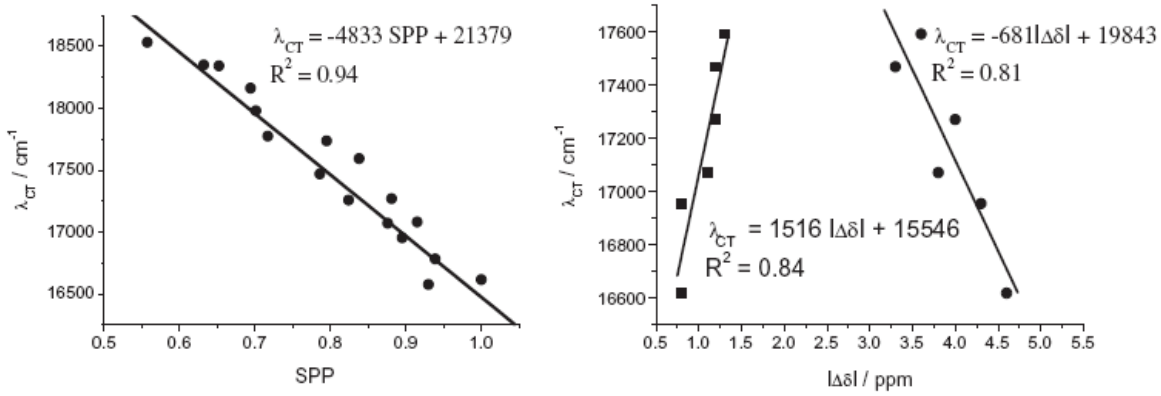

Figure 33 – Left: Correlation between the charge transfer absorption band maximum (λ_{CT}) and Catalán's Solvent polarity function (SPP). Right: Correlation between charge transfer absorption band maximum (λ_{CT}) and change in chemical shift ($|\Delta\delta|$) for carbon 5 (■) and carbon 9 (•). The least squares fit to the data points is also shown in addition to the corresponding equation and goodness of fit.

It can also be seen from *Table 11* on the previous page, that the oscillator strength (f_{CT})[41] for the CT absorption band increases markedly in more polar solvents. In spite of this, the ratio of the intensities at the maxima of bodipy and CT bands does not proceed via a smooth correlation with solvent polarity. Once again, a good linear relationship holds between oscillator strength and SPP with a slope of 0.5 and an intercept of -0.19 being observed. In spite of the fact that when this type of analysis is used, the intercept does not have a real physical meaning, the slope offers an indication of the degree of influence that the solvent exerts over intramolecular charge transfer.

In **JULBD**, fluorescence is observed in non-polar solvents at an intensity which drops swiftly as the solvent polarity increases. It must be said that a highly recognisable characteristic of **JULBD** is the distinctive on/off switching and emission colour change even with very slight variations in solvent polarity. The clear yellow emission found in CCl_4 solution becomes increasingly red in colour in di-n-butyl ether (*Figure 33*) and practically disappears in the other solvents.

4. 7 Conclusion

It has been demonstrated by the studies carried out and detailed within this chapter, that dipyrrin carbon resonances for the strongly coupled donor-acceptor system **JULBD** are susceptible to the local polarity of the solvent.

Comparative methods which minimize problems associated with normal solvent induced chemical shift changes have been used and reasonable correlations observed for carbon chemical shifts to two solvent polarity functions. DFT computational calculations have also proved to be successful in relating the distribution of charge at carbon atoms to ^{13}C chemical shifts for bodipy derivatives. Correlations observed between oscillator strength (f_{CT}) and change in chemical shift (from **JULBD** to **PHBD**) were highly noteworthy, particularly the correlation established for meso carbon 5 shown in *Figure 35* below:

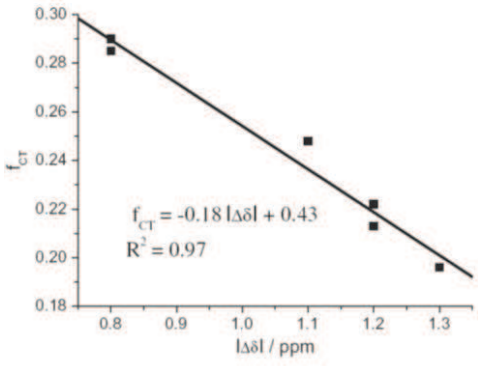

Figure 35 – The correlation observed between the charge transfer oscillator strength and the modulus of the chemical shift change at carbon 5.

This can be attributed to the fact that f_{CT} is directly related to the matrix element of the dipole moment for the charge transfer electronic transition. This makes the correlation particularly feasible, due to the fact that carbon 5 is the connection point for the donor-acceptor subunits. This type of analysis may be applicable on a wider scale than imagined in the first instance and it is fully expected that it will be tested on systems currently being synthesised within the MPL.

It must also be said that the emissive characteristics of **JULBD** and its excited state deactivation are far from straightforward and it is hoped that further studies to be

undertaken on the dyad will reveal more about its fascinating photophysical properties.

4.8 References

[1] Dewar, M. J. S.; Zoebisch, E. G.; Healy, E. F and Stewart, J. J. P. *J. Am. Chem. Soc*, **1985**, *107*, 3902.
[2] Dewar, M. J. S and Thiel, W. *J. Am. Chem. Soc*. **1977**, *99*, 4899-4907.
[3] Kohn, W.; Hohenberg, P. *Physical Review*. **1964**, *136*, 864-871.
[4] Becke, A. D. *J. Chem. Phys*. **1993**, *98,* 1372-1377.
[5] (a) Contreras, R. H.; Llorente, T.; Pagola, G. I.; Bustamante, M. G.; Pasqualini, E. E; Melo, J. I.; Tormena, C. F. *J. Phys. Chem. A*. **2009**, *113*, 9874. (b) Gawinecki, R.; Stanovnik, B.; Valkonen, A.; Kolehmainen, E.; Ósmialowski, B.; Dobosz, R.; Zakrzewska, A. *Struct. Chem*. **2009**, *20*, 655. (c) Moonen, N. N. P.; Pomerantz, W. C.; Gist, R.; Boudon, C.; Gisselbrecht J. –P.; Kawai, T.; Kishioka, A.; Gross, M.; Irie, M.; Diederich, F.; *Chem. Eur. J*. **2005**, *11*, 3325. (d) Neuvonen, H.; Neuvonen, K.; Koch, A.; Kleinpeter, E.; Pasanen, P. *J. Org. Chem*. **2002**, *67*, 6995. (e) Lawrentz, U.; Grahn, W; Lukaszuk, K.; Klein, C.; Wortmann, R.; Feldner, A.; Scherer, D. *Chem. Eur. J*. **2002**, *8*, 1573 (f) Morales, R. G. E.; Leiva, M. A.; *Spectrochim. Acta A*, **1999**, *55*, 1493.
[6] Janjua, N. K.; Ahmed, R. Q. S.; Khan, A. Y.; Subhani, M. M. S.; Iqbal, R. *J. Mol. Struct*. **2009**, *919*, 321.
[7] Saleh, B. A.; Essa, A. H.; Al-Shawi, A. A. O.; Jalbout, A. F. *J. Mol. Struct*. *THEOCHEM*, **2009**, *909*, 107.
[8] Webb, J.A.; Klijin, J. E.; Hill, P. A.; Bennett, J. L.; Goroff, N. S. *J. Org. Chem*. **2004**, *69*, 660.
[9] Reichardt, C. *Solvents and Solvent effects in Organic Chemistry*, second ed., VCH, New York, 1990.
[10] Gutmann, V. *The Donor-Acceptor Approach to Molecular Interactions*, Plenum Press, New York, 1978.
[11] (a) Kamlet, M. J.; Taft, R. W. *J. Am. Chem. Soc*. **1976**, *98*, 377. (b) Taft, R. W.; Abboud, J. –L. M.; Kamlet, M. J. *J. Am. Chem. Soc*. **1981**, *103*, 1080.
[12] Rezende, M. C.; Flores, P.; Guerrero, J.; Villarroel, L. *Spectrochimica Acta. A*, **2004**, *60*, 1637-1640.
[13] Hammam, E.; El-Nahas, A. M. *J. Phys. Chem. A*. **1998**, *102*, 9739.
[14] Wuerthner, F.; Sheng, Y. *Angew. Chem*. **2000**, *112*, 1243.
[15] Ganeev, R. A.; Tugushev, R. I.; Ishchenko, A. A.; Derevyanko, N. A.; Ryasnyansky, A. I.; Usmanov, T. *Appl. Phys. B*, **2003**, *76*, 683.
[16] Nakatsuji, S.; Ogawa, Y.; Takeuchi, S.; Akutsu, H.; Yamada, J.; Naito, A.; Sudo, K.; Yasuoka, N. *J. Chem. Soc. Perkin. Trans*. **2000**, *2*, 1969.
[17] Wuerthner, F.; Yao, S.; Schilling, J.; Wortmann, R.; Redi-Abshiro, M.; Mercher, E.; Gallego-Gomez, F.; Meerholz, K. *J. Am. Chem. Soc*. **2001**, *123*, 2810.
[18] Mishra, A.; Behera, R. K.; Behera, P. K, Mishra, B. K.; Behera, G. B. *Chem. Rev*. **2000**, *100*, 1973.
[19] Rezende, M. C.; Campodonico, P.; Abuin, E.; Kossanyi, J. *Spectrochim. Acta Part A*, **2001**, *57*, 1183-1190.
[20] Kulinich, A. V.; Ishchenko, A. A.; Groth, U. M. *Spectrochimica Acta Part A*. **2007**, *68*, 6-14.
[21] Litter, B. J.; Miller, M. A.; Hung, C-J.; Wagner, R. W.; O'Shea, D. F. *J. Org. Chem*. **1999**, *64*, 4
[22] Palafox, M. A.; Gil, M.; Nunez, J. L.; Tardajos, G. *Int. J. Quantum. Chem*. **2002**, *89*, 147.
[23] Schmitt, A.; Hinkeldey, B.; Wild, M.; Jung, G. *J.Fluoresc.*, **2009**, *19*, 755-758.
[24] http://www.rsc.org/chemistryworld/News/2011/July/08071102.asp
[25] Catalan, J.; Lopez, V.; Perez, P.; Martin-Villamil, R.; Rodriguez, J. G. *Liebigs Ann*. **1995**, *2*, 241.
[26] Webb, J. A.; Klijin, J. E.; Hill, P. A.; Bennett, J. L.; Goroff, N. S. *J. Org. Chem*. **2004**, *69*, 660.
[27] Palafox, M. A.; Gil, M.; Núñez, J. L.; Tardajos, G. *Int. J. Quant. Chem*. **2002**, *89*, 147.
[28] Alkalis, S. A.; Beck, G.; Grätzel, M. *J. Am. Chem. Soc*. **1975***, 97*, 5723. (b) Forrest, I. S.; Carr, C. J.; Usdin, E. Eds. *Phenothiazines and Structurally related Drugs: Advances in Biochemistry and Pharmacology.* Vol. 9; Raven Press: New York, 1974. (c) Hawkins, D.; Pauling, L. *Orthomolecular Psychiatry*; W. H. Freeman, San Francisco, 1973. (d) Henry, B. R.; Kasha, M. *J. Chem. Phys*. **1967**, *47*, 3319.
[29] Xie, X.; Yuan, Y.; Krüger, R.; Bröring, M. *Magn. Reson. Chem*. **2009**, *47*, 1024.
[30] Schmitt, A.; Hinkeldey, B.; Wild, M.; Jung, G. *J. Fluoresc*. **2009**, *19*, 755.
[31] Tram, K.; Yan, H.; Jenkins, H. A.; Vassiliev, S.; Bruce, D. *Dyes Pigm.* **2009**, *82*, 392.
[32] Arroyo, I. J.; Hu, R.; Merino, G.; Tang, B. Z.; Peña-Cabrera, E. *J. Org. Chem*. **2009**, *74*, 5719.
[33] Silverstein, R. M.; Webster, F. X.; *Spectroscopic Identification of Organic Compounds*, sixth ed., John Wiley & Sons, 1998.
[34] Mulliken, R. S. *J. Chem. Phys*. **1955**, *23*, 1833.
[35] Leszczynski, J. *Computational Chemistry:Reviews of Current Trends Volume 2*, World Scientific Publishing Co. Pte. Ltd, MA, USA, 1997.

[36] Chemical shift values are taken from the following reference: Xie, X.; Yuan, Y.; Krüger, R.; Bröring, M.; *Magn. Reson. Chem.* **2007**, *47*, 1024
[37] (a) Benniston, A. C.; Copley, G. *Phys. Chem. Chem. Phys*. **2009**, *11*, 4124. (b) Ziessel, R.; Ulrich, G.; Harriman, A. *New J. Chem.* **2007**, *31*, 496.
[38] An excitation wavelength of 485 nm was used for the emission spectra.
[39]Benniston, A. C.; Harriman, A.; Whittle, V. L.; Zelzer, M. Eur. *J. Org. Chem*. **2010,** *75*, 523.
[40] (a) Rohand, T.; Lycoops, J.; Smout, S.; Braeken, E.; Sliwa, M.; Van der Auweraer, M.; Dehaen, W.; De Borggraeve, W. M.; Boens, N. *Photochem. Photobiol. Sci*. **2007**, *6*, 1061. (b) Qin, W.; Rohand, T.; Baruah, M.; Stefan, A.; Van der Auweraer, M,; Dehaen, W.; Boens, N. *Chem. Phys. Lett*. **2006**, *420*, 562. (c) Qin, W.; Baruah, M.; Van der Auweraer, M.; De Schryver, F. C.; Boens, N. *J. Phys. Chem. A,* **2005**, *109*, 7371. (d) Qin, W.; Baruah, M.; Stefan, A.; Van der Auweraer, M.; Boens, N. *ChemPhysChem*. **2005**, *6*, 2343.
[41] Bakhshiev, N. G.; Gularyan, S. K.; Dobretsov, G. E.; Kirillova, A. Yu.; Svetnichnyĭ, V. *Opt. Spectrosc*. **2007**, *103*, 741.

Chapter 5

The Synthesis of Donor-Spacer-Acceptor Dyads via Modern Methods in Catalysis

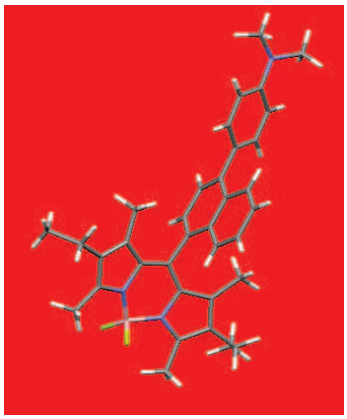

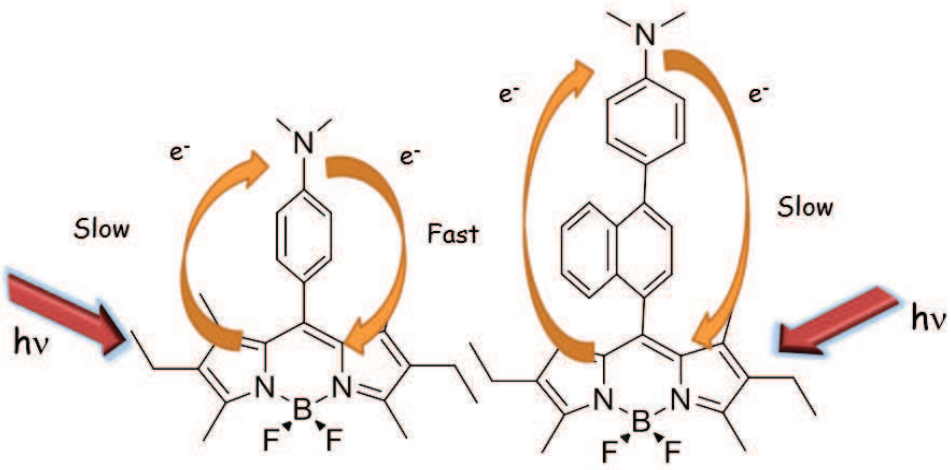

Some of the material featured in this chapter is included in the following publication: Benniston, A. C.; Clift, S. V.; Hagon, J.; Lemmetyinen, H.; Tkachenko, N. V.; Harrington, R. W. *ChemPhysChem*, **2012**, *13*, 3672.

The structures and names of the bodipy compounds to be discussed within this chapter are given below:

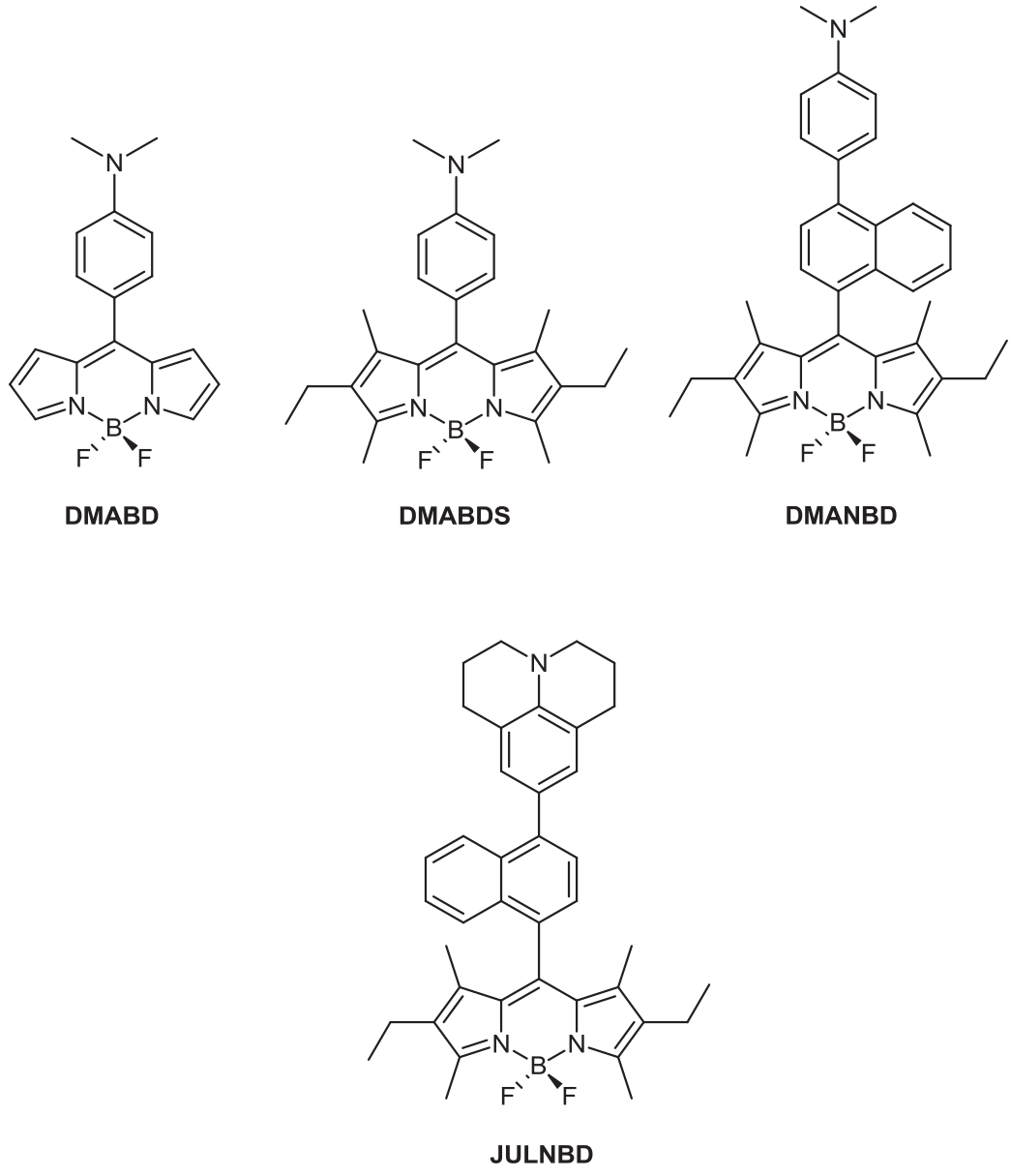

Figure 1 – The bodipy compounds discussed within chapter 5.

5.1 Introduction

5.1.1 Donor-Spacer-Acceptor dyads

A continuous theme which is present throughout this thesis, is the desire to investigate charge transfer in donor-acceptor dyads. An interesting extension to this exploration, is to examine systems which incorporate a spacer, i.e., a bridging moiety that connects the donor unit with its complimentary acceptor. This unit traditionally plays the dual role of being a conduit by which efficient through-bond energy interactions can be promoted and also as a stabilising unit for the maintenance of structural integrity within the assembly[1]. Incorporation of such a unit also allows control of the angles and the distance between donor and acceptor sites which dictate the rate and efficiency of both long-range electron transfer and charge recombination.[2] There has been much interest in recent years concerning photoactive Donor-Spacer-Acceptor systems.[3,4,5] It is known that the strength and degree of electronic coupling between indirectly connected donor-acceptor pairs are sensitive to the conformation[6], length[7] and composition[8] of the spacing moiety in these D-Sp-A dyads. The state of hybridization of carbon bridges can also influence the magnitude of electronic coupling between donor and acceptor.[9]

As aforementioned, the conformation of the bridging moiety is integral to controlling the strength and extent of electronic coupling in such D-Sp-A dyads, an elegant example being the quinone and chlorophyll electron donors and acceptors in photosynthetic reaction centres. These are located at precise orientations and distances in order to encourage efficient and effective charge separation and to hinder charge recombination.[10] Within these systems, the nature of the bridging moiety which links donor and acceptor is deemed to exert a substantial influence over the observed rates of electron transfer.[11] Recently, it has come to light that the handedness of the spacer may also have an effect on the rate of electron transfer. This work will be discussed further in Chapter 6 which addresses the synthesis and characterisation of a binaphthyl-spaced dyad. The species prepared (named **DMABNBD**) can be considered to be a control compound for future work to be carried out within the MPL to investigate the effects induced by chirality on the rate of electron transfer in D-Sp-A dyads.

Within this chapter, the synthesis, characterisation and photochemistry of a series of dyads is discussed. It is hoped that an additional future project will include a thorough photophysical analysis of the species discussed here and also of **DMABNBD**, to compare the effects of increasing the size of the spacer and thus the distance between the *N,N*-dimethylaniline donor and bodipy acceptor.

In order to complete the synthesis of the dyads, many new challenges were embarked upon which had not been previously attempted within the MPL. The most synthetically perplexing step of this particular part of the project was certainly the borylation of julolidine or its brominated counterpart to generate the appropriate coupling partner. Standard methods for the preparation of aryl boronic acids and esters can be harsh and thus incompatible with various functional groups[12]. However, novel techniques have recently emerged[13] which provide a milder route to aryl boronate esters. Within this chapter, a detailed discussion is given of the conditions attempted, including Grignard and organolithiation methods, C-H activation via iridium catalysis and studies incorporating palladium species and novel ligand systems. Due to the utility of aryl boronic acids and esters as key reaction intermediates for the preparation of a wide range of synthetic targets[14], it is hoped that the reaction protocols developed within this chapter will be reproduced by future MPL members.

5.1.2 Carbon-carbon bond formation

Aromatic carbon-carbon bond forming reactions have recently emerged as vitally important methodologies for the preparation of complex organic molecules. Of the numerous coupling procedures presiding over the literature today, the most common are undoubtedly the Suzuki[15,16], Heck[17,18,19] and Sonogashira[20] reactions. Both Negishi[21] and Stille[22] coupling are also increasing in popularity. The former utilises either a nickel or a palladium based catalyst to couple organozinc[23] reagents with various organohalides and was the first procedure which permitted synthesis of unsymmetrical biaryls in high yield. The latter method uses a palladium catalyst to couple stannanes with halides.

Scheme 1[24] which illustrates a general catalytic route is shown below:

m = **Li** (Murahashi); **Mg** (Kumada-Tamao, Corriu); **B** (Suzuki-Miyaura); **Al** (Nozaki-Oshima, Negishi); **Si** (Tamao-Kumada, Hiyama-Hatanaka); **Zn** (Negishi); **Cu** (Normant); **Zr** (Negishi); **Sn** (Stille, Migita-Kosugi).

[M] = Pd, Fe, Ni, Cu, Rh

X = I, Br, Cl, OTf

Scheme 1 – The outline of a general catalytic scheme in which R is an organic moiety, ***m*** *is an element,* ***X*** *is a leaving group and* ***[M]*** *is a metal-based catalyst.*

The standard catalytic cycle described for both the Suzuki and Heck reactions involves a homogenous, molecular palladium catalyst which cycles between the Pd(0) and Pd(II) oxidation states during the course of the catalytic reaction[25]. The two procedures are similar in concept with the exception being that the nucleophile for transmetallation is derived from an aryl boronic acid as opposed to an olefin. The reasoning behind these choices, further mechanistic discussions and the choice of the halide coupling partner to be used will be discussed in greater detail in the following subsection.

With the high commercial availability of many aryl boronic acids, in addition to the fact that standard procedures to generate this type of reagent are well documented in the literature, the Suzuki reaction is preferential in the case of this project. The Stille coupling protocol has the downside of the relatively toxic nature of the stannanes required, whilst the organozinc halides involved in Negishi coupling are less commonly located on a commercial level and in many cases, display only moderate reactivity towards several common organic electrophiles. This is due to the less polar nature of the carbon-zinc bond in comparison to more highly polarised Grignard- and organolithium-species, for example. Amongst the aryl halides, chlorides, with their lower cost and increased compound diversity,[26] are becoming increasingly popular. Noteworthy advances are being made in the development of tailor-made palladium based catalyst systems for the coupling of aryl chlorides[27]. However they remain less reactive and harsher conditions are typically enforced to achieve coupling which can

prove to be detrimental to other species present. Therefore, bromides and iodides which dominate the literature and exhibit higher reactivity[28] will be used preferentially within the synthetic routes devised.

5.2 Synthesis

Scheme 2 and 3 illustrate the initial route designed to accomplish the synthesis of the donor-acceptor dyads discussed within this chapter is given below:

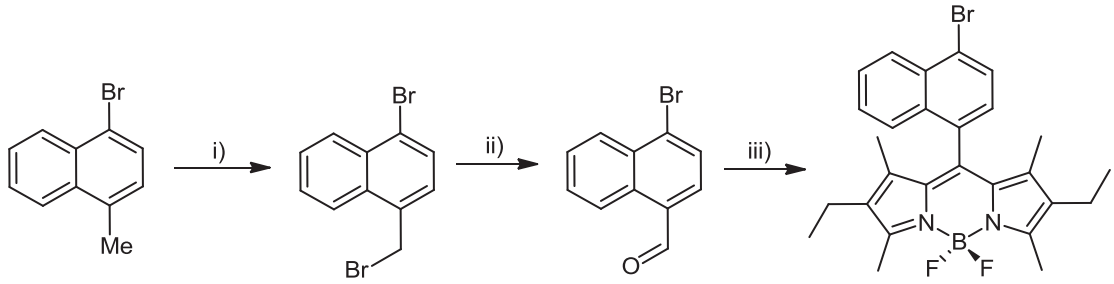

1 **2** **3** **BRNBD**

Reagents: i) N-bromosuccinimide, benzoyl peroxide, CCl_4. ii) DMSO, $NaHCO_3$. iii) DCM, 2,4-dimethyl-3-ethylpyrrole, TFA, DDQ, N,N'-diisopropylethylamine, $BF_3.Et_2O$.

*Scheme 2 – The initially proposed synthetic route to generate **BRNBD**.*

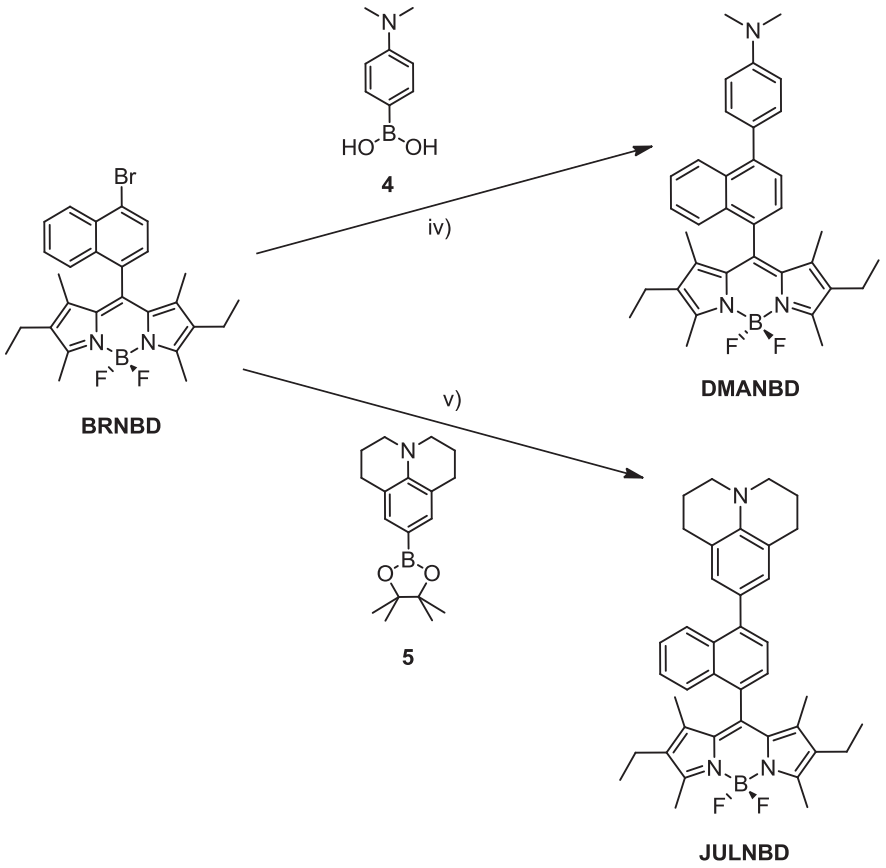

Reagents and conditions: iv) $PdCl_2(PPh_3)_2$, Na_2CO_3 (2.0M), THF, reflux, 24h v) $Pd(PPh_3)_4$, Na_2CO_3 (2.0M), THF, μW, 30mins.

Scheme 3 - Representation of the synthetic route initially devised to achieve the synthesis of ***JULNBD*** *and* ***DMANBD*** *via Suzuki coupling.*

In order to obtain the desired target molecules explored here, various problems were overcome, with the main issue being the synthesis of julolidine boronic ester (compound **5**). This was the component required to generate **JULNBD** via a Suzuki coupling mechanism, appending this unit onto bromonaphthalene substituted bodipy (**BRNBD**). The synthesis of the latter was luckily far more straight forward and involved a 3-step procedure with each synthetic step being well documented in the literature. Furthermore, the starting material, 1-methyl-4-bromonaphthalane (**1**), was commercially available and relatively inexpensive.

The first step was the N-bromosuccinimide and benzoyl peroxide mediated radical bromination of 1-methyl-4-bromonaphthalene, which gave the desired halogenated product (**2**) in a good yield. Carbon tetrachloride was employed initially as solvent, however it was found that when α,α,α-trifluorotoluene, a solvent frequently employed

in radical mediated reactions of this type, replaced the less desirable carbon tetrachloride, the yield was much improved from just 65% to 97%. The product, 1-bromo-4-bromomethylnaphthalene (**2**), was then subjected to a Kornblum reaction[29] whereby it was oxidized to the corresponding aldehyde (**3**) using DMSO and sodium hydrogen carbonate. Again a very high yield was obtained, this time of 90% following column chromatography purification. These two reactions proceeded exceedingly cleanly, with just a very small portion of starting material remaining and no unwanted side products. The final step was generation of the bodipy via the standard synthetic protocol involving aldehyde condensation (1-bromo-4-naphthaldehyde (**3**) in this case) with 2,4-dimethyl, 3-ethyl pyrrole in the presence of TFA followed by oxidation using DDQ to generate the dipyrromethene. Finally, removal of the pyrrole protons was achieved using *N,N*-DIPEA and complexation with boron trifluoride diethyl etherate generated **BRNBD**, in reasonable yield (54%).

In order to create the spaced donor-acceptor dyad, the boronic acid donor counterpart was prepared. It was envisaged that julolidine would again be used as the electron donor due to the success of **JULBD** and the interesting electron donating capabilities of julolidine. Therefore bromination was carried out using NBS in acetonitrile[30] which is outlined in *Scheme 4*.

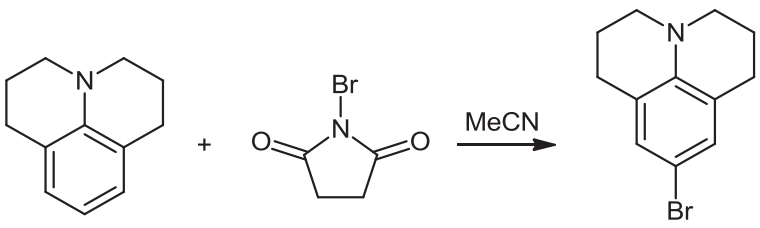

6 **7**

Scheme 4 – The NBS mediated bromination of julolidine.

From the known brominating reagents for aromatic rings,[31] NBS was selected due to the popularity for the electrophilic substitution of aromatic rings[32,33] and the successes encountered by previous group members when using this reagent. Furthermore, bromides typically exhibit higher reactivity than chlorides, for example in the generation of Grignard and organolithium species. 9-bromojulolidine was then purified by column chromatography which removed and recovered all unreacted

julolidine starting material. This could then be used in subsequent reactions. A DCM/ petrol (1:3) mixture was employed as eluent and the desired product was generated in good yield (64%). Subsequent scale-up of this procedure generated a large stockpile of 9-bromojulolidine (**7**) was for use in subsequent manipulations. Unfortunately for a long time, synthesis of julolidine boronic acid was unfruitful. Various literature methods were tested, including much organometallic chemistry such as Grignard reactions and organolithiations.

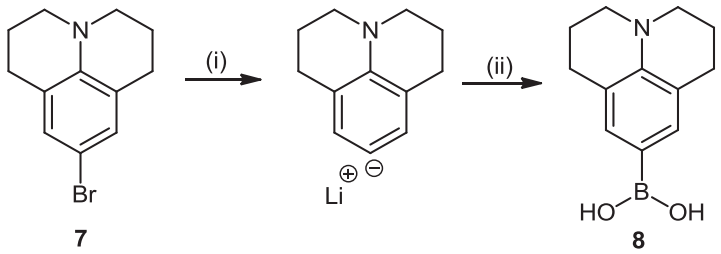

Reagents: (i) THF, -78°, BuLi, (ii) RT, trimethylborate.

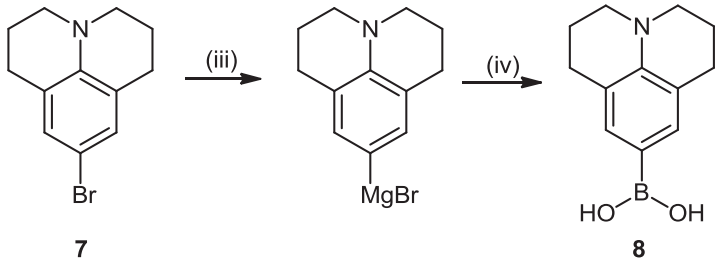

Reagents: (ii) THF, Mg, I_2, Δ, (iv) trimethylborate.
*Scheme 5 – Attempted synthesis of julolidine boronic acid (**8**) via Grignard and organo-lithiation reactions.*

In both cases, the initial debromination/ metallation step was found to proceed successfully but problems arose on completion of the borylation, as it was observed via TLC that much julolidine was regenerated and also that small quantities of bromojulolidine starting material remained. The borylated derivative was absent. Numerous attempts were made to improve the yields but modification of the synthetic protocols by varying solvents, reagents and temperatures proved unsuccessful. Therefore, it was believed that synthesis of the boronic ester as opposed to the acid,

the former of which are notoriously more stable and far simpler to synthesise and store, would be a preferred method to try. The reason that boronic esters were not selected initially over boronic acids was due to the higher volume of publications documenting Suzuki coupling of boronic acids. The fact that our research group had synthesised them previously (meaning that synthetic protocols had been modified and improved) and also that all the reagents required were readily accessible. Luckily, however, esters of this type were becoming increasingly popular for use in this area[34,35] and examples of suitable coupling conditions were far more common than originally anticipated.

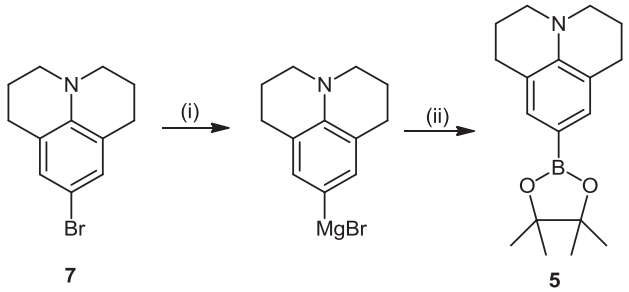

Reagents: (i) THF, Mg, I_2, Δ, (ii) RT, B_2Pin_2.

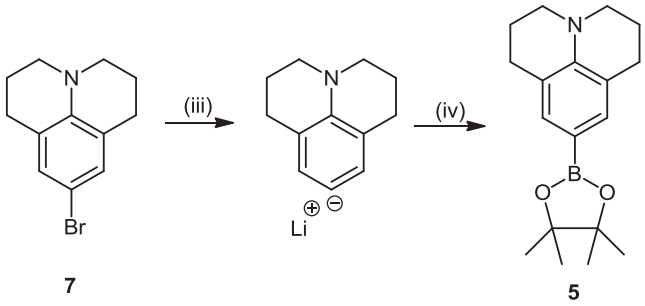

*Scheme 6 – The two protocols devised for the preparation of julolidine boronic ester (compound **5**).*

Reagents: (iii) THF, -78°, ^{t}BuLi, (iv) RT, B_2Pin_2.

Unfortunately, once again the Grignard route proved unsuccessful, with the bispinacolatodiboron (abbreviated to B_2pin_2 henceforth) employed as borylating agent appearing unbound in the crude NMR spectra of the product. Both the ^{1}H NMR spectrum and a TLC of the crude material visibly displayed evidence of residual bromojulolidine and julolidine. However, when tertiary butyllithium in THF was employed, again using B_2pin_2, (via route (ii)), **5** could be isolated in 20% yield (according to *Scheme 6*) following purification by column chromatography on silica gel.

This allowed us to synthesise and isolate a very small quantity of **JULNBD** following the Suzuki coupling reaction of the boronic ester onto the bromonaphthalene substituted bodipy according to *Scheme 3*. However, in order to generate enough material for photophysical investigation, electrochemistry and full characterization, the yields associated with the borylation step had to be improved.

Following a thorough literature search, it was decided that catalytic methods involving palladium and iridium based species would be tested instead. It is only relatively recently that iridium catalysis has been practised to generate boronic ester species of this type via aromatic C-H bond borylation.[36,37] The carbon-hydrogen bond is one of the most fundamental linkages in organic chemistry and activation of this bond offers the possibility of direct introduction of a new functionality. The range of substrates is virtually unlimited[38] and includes polymers, natural products[39] and complex organic systems to name but a few. The versatility of organoboron derivatives in organic synthesis[40,41] renders the activation and subsequent borylation of hydrocarbons highly appealing. When electron donating substituents are used, much success can be observed and C-H activation looked to be a highly promising method.

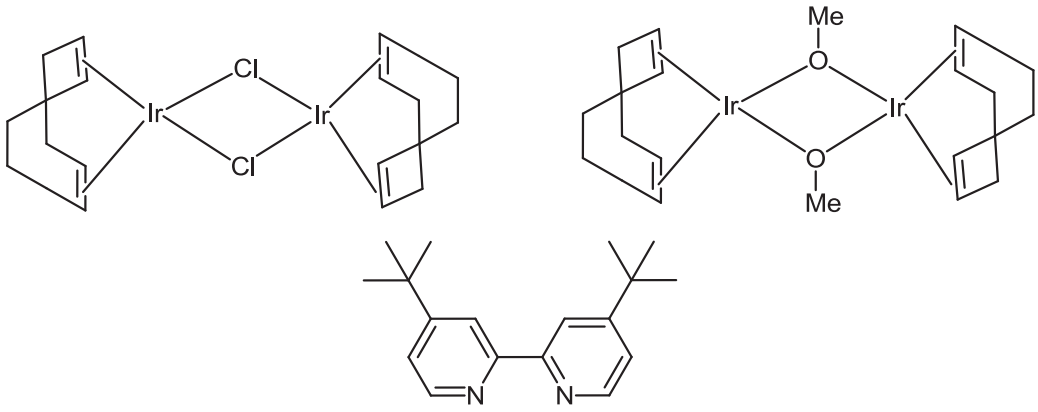

Figure 2 – The structures of the iridium catalysts and ligands discussed.
Clockwise from top left: Bis(1,5-cyclooctadiene)diiridium(I) dichloride, Bis(1,5-cyclooctadiene)diiridium(I) dimethoxide, 4,4'-Di-tert-butyl-2,2'-dipyridyl.

The catalyst employed was $[IrCl(COD)]_2$ and di-tertiarybutylpyridine was used as a ligand (see *Figure 2* for structures). B_2pin_2 was again employed as borylating agent and the solvent used was methyl-tert-butyl-ether (abbreviated to MTBE from hereon

in)[35]. It was found unfortunately that when julolidine was employed as starting material, the desired product did not form and only starting material remained. Therefore, the conditions were altered and $[IrCl(COD)]_2$ (3 mol% with respect to iridium) was used instead, along with 2,2'bipyridine and B_2pin_2. A test reaction was carried out first using one of the starting materials employed by Ishiyama *et al.*[42], α,α,α-trifluorotoluene. The crude reaction mixture was analysed by GC-MS which showed the presence of the borylated product (272 g mol^{-1}) and also a peak corresponding to residual B_2pin_2 (253 g mol^{-1}). ^1H NMR spectroscopy also confirmed the presence of the desired product, but it turned out that the *ortho* substituted isomer had also formed in addition to the *para*-substituted product, in a 1:2 ratio (ortho: para). This was inevitably also a possibility in the synthesis of our desired species.

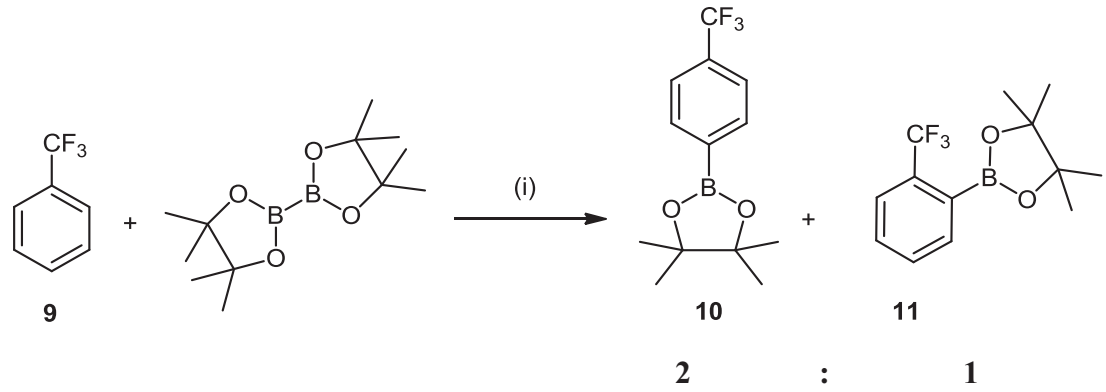

Scheme 7: The borylation of α,α,α-trifluorotoluene.
Reagents: i) $[IrCl(COD)]_2$, 2,2'bipyridine.

Due to the relative success observed during the test reaction, julolidine was then subjected to the same conditions, but it was observed by GC that the percentage conversion to product was extremely low and much starting material remained. The reaction temperature, ligand and solvent were all varied, but to no avail. It was decided therefore that an alternative iridium source should be tested- a methoxy-bridged dimer (compound **13**). Due firstly to its relatively high cost and secondly to the fact that a substantial quantity of [IrCl(COD)] had already been purchased, the desired species was prepared via Scheme 8[43].

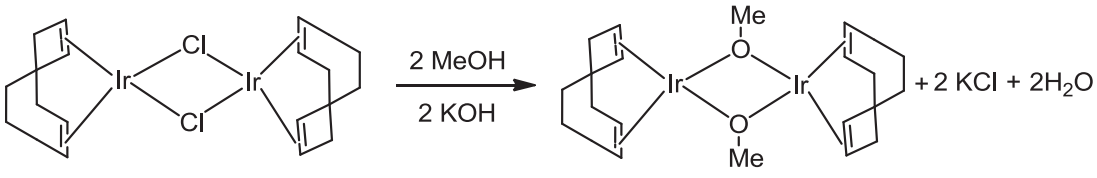

12 **13**

Scheme 8 – Synthesis of the iridium based methoxy-bridged dimer using methanol and potassium hydroxide.

This reaction generated the desired species and a clean ^{1}H NMR spectrum was gained, but unfortunately the product was synthesised in poor yield with much starting material remaining. Therefore, an alternative and equally straight forward synthesis was tested employing sodium methoxide according to *Scheme 9*.

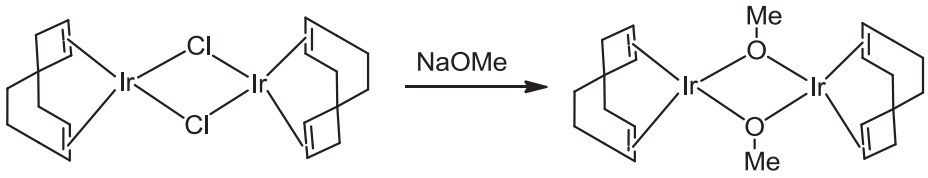

12 **13**

Scheme 9 – Synthesis of the iridium based methoxy-bridged dimer using sodium methoxide.

Again the desired product was generated but in poor yield with much starting material remaining. Thus a third method was tested in which anhydrous sodium carbonate and methanol were used (*Scheme 10*)[44]:

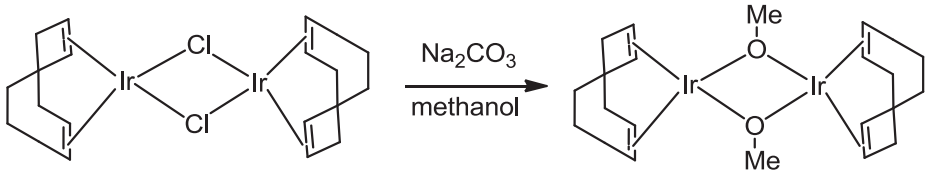

12 **13**

Scheme 10 – Synthesis of the iridium based methoxy-bridged dimer using sodium carbonate and methanol.

This reaction gave the cleanest ^{1}H NMR spectrum and appeared also to give the best conversion to product when the reaction mixture was analysed by GC. Synthesis of

julolidine boronic ester (compound **5**) therefore recommenced employing this catalyst and using microwave irradiation as opposed to conventional heating methods, in-keeping with published work[35]. The ligand used here was 4,4-di-tertbutyl 2,2-dipyridyl and tert-butyl ether was used as solvent. The reaction was heated at 80˚C for one hour. *Scheme 11* summarises this reaction as follows:

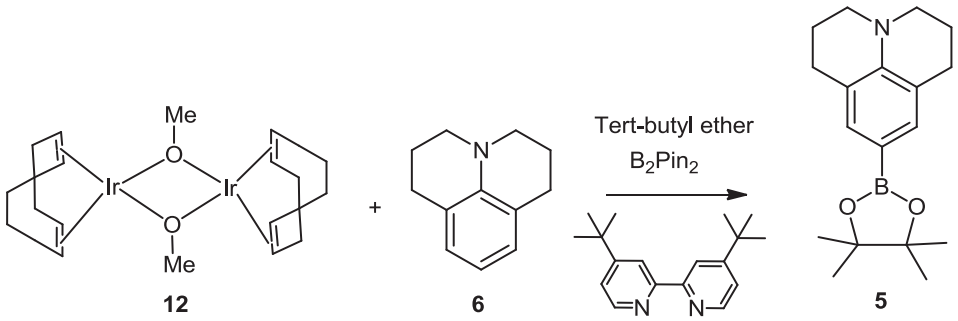

*Scheme 11 - The C-H activation pathway leading to compound **5**, including the iridium based catalytic intermediate.*

The ^{1}H NMR spectrum showed that the reaction had worked but had not gone to completion, thus the synthetic protocol was repeated with a lengthened heating time of 18 hours. This time more product appeared to have been generated, but again it was clear from the integrals in the ^{1}H NMR spectrum that it did not go to completion. The combined crude products were purified by column chromatography. However due to the small scale of each reaction and the low yields, only a very small quantity of boronic ester was isolated, which would prove difficult to proceed with. Therefore, the two options were either to scale-up the reaction or instead, to find an alternative method. Unfortunately upon scale up, an appreciable decrease in the yield was observed and it was decided that a palladium catalysed method might give more successful results.

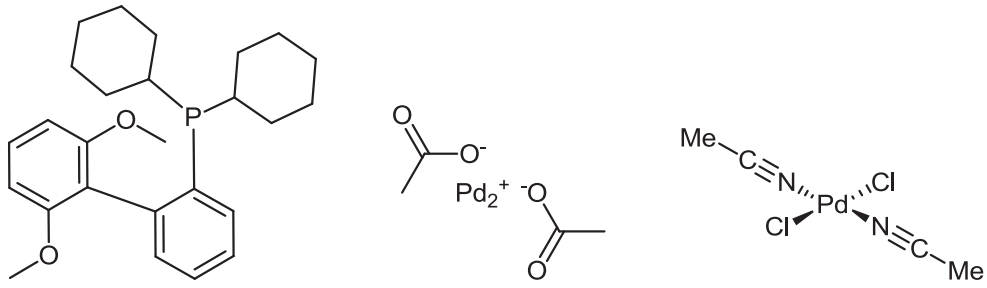

Figure 3 - The palladium catalysts and ligands tested. Left to right: S-phos, Palladium acetate, Bis(acetonitrile)dichloropalladium(II).

The first system tested was based on a communication[45] promoting the use of ionic liquids as an efficient medium for palladium catalysed cross-coupling reactions. 1-Butyl-3-methylimidazolium tetrafluoroborate was used as the solvent and palladium acetate as catalyst with pinacolborane as the boron source. Unfortunately, although the TLC taken indicated product formation, following column chromatography purification, it was evident that the quantity of boronic ester generated was negligible. An alternative catalytic system was therefore developed, also employing palladium acetate, with the ligand 2-dicyclohexylphosphino-2',6'-dimethoxybiphenyl (abbreviated to S-Phos henceforth) and potassium phosphate in 1,4-dioxane[46]. Unfortunately yet again the yields were poor, however upon substitution of palladium acetate with bis(acetonitrile)dichloropalladium(II)[47], an improved conversion was observed and the product was isolated in 40% yield. The method used, developed by Buchwald and Billingsley, also allowed for a lower catalyst loading and shorter reaction times. Suzuki coupling, using microwave irradiation and a traditional tetrakis triphenylphosphosphine palladium (0) catalyst, was then affected to generate further **JULNBD** and the desired product was isolated in good yield following purification by column chromatography.

During the time it took to optimize the julolidine boronic ester synthesis, a second donor-acceptor dyad was prepared using the commercially available dimethylaminophenyl boronic acid as an alternative amine donor. This species was expected to behave slightly differently due to the fact that the dimethylamino- unit was free to rotate about the N-C bond connecting the $N(Me)_2$ group to the aromatic

ring. This molecule was synthesised according to the following scheme and isolated in good yield (70%).

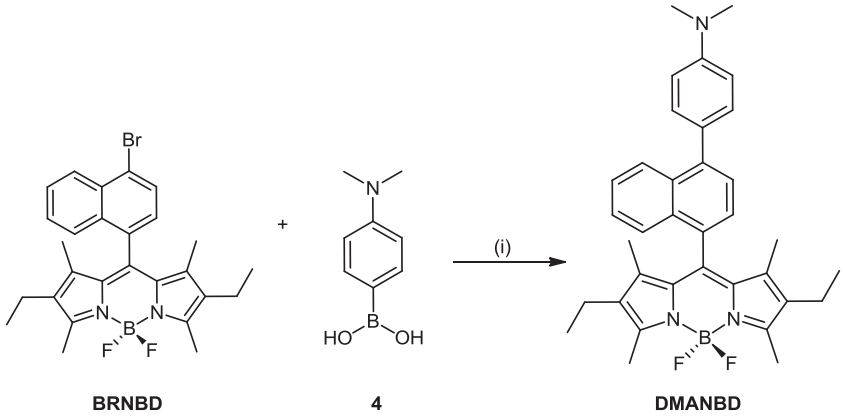

*Scheme 12 - A synthetic method to describe the modified route incorporating the dimethylaminophenyl unit to generate **DMANBD**. Reagents and conditions: i) $PdCl_2(PPh_3)_2$, Na_2CO_3 (2.0M), THF, reflux, 24h.*

The proposed catalytic cycle for the reaction taking place is given below.

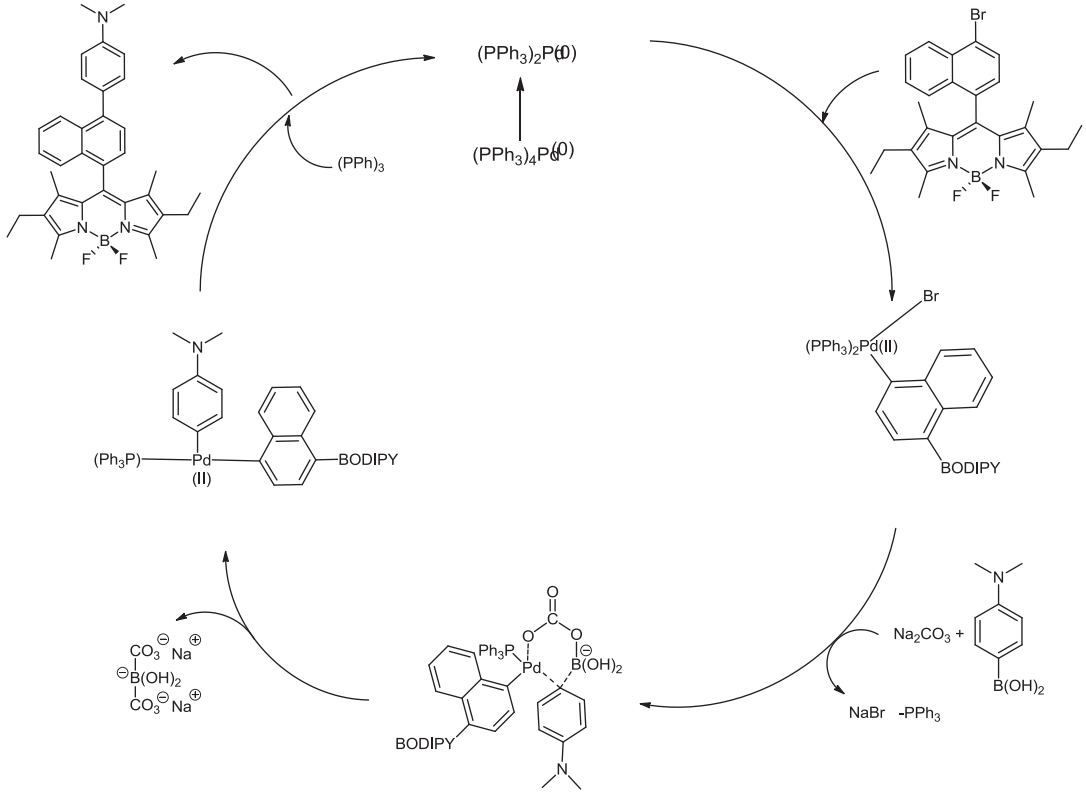

*Figure 4 - A catalytic cycle incorporating the reagents and start materials used for the palladium catalysed Suzuki coupling of **BRNBD** and dimethylaminophenyl boronic acid.*

The cycle highlights the importance of the base involved in Suzuki coupling. It serves to activate the boron atom of the boronic acid by enhancing the polarisation of the organic ligand and thus facilitates the transmetallation process.

In order to compare the effect that the spacer has on the photophysics of the system, the simple un-spaced dyads were synthesised, subjecting the commercially available dimethylaminophenyl-9-carboxaldehyde to standard bodipy forming conditions. Similar to the preparation of **JULBD**, **PHBD** and **NITBD** discussed in Chapter 4, **DMABD** was synthesised via the dipyrromethane which was first purified by column chromatography on basic aluminium oxide, prior to reaction to generate the bodipy.

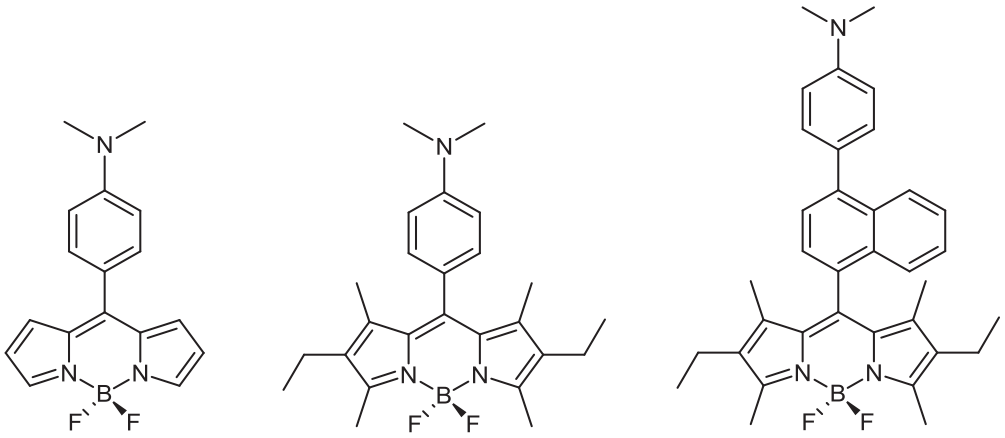

*Figure 5 - The N,N-dimethylaniline substituted bodipy dyad series prepared. (L-R: **DMABD**, **DMABDS**, **DMANBD**.)*

5.3 Crystal Structure Analysis

All three dimethylaniline substituted bodipy molecules readily crystallised to afford X-ray diffraction quality samples. The molecular packing diagram for the crystal structure and atom-labelled molecular structures of all three compounds are given below. For full tables of crystal data and structure refinement please refer to the attached data disc.

5.3.1 DMANBD

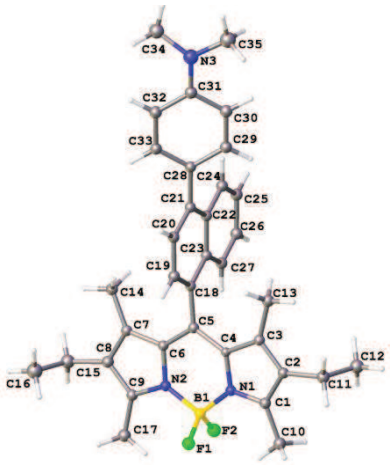

*Figure 6 – The molecular structure of **DMANBD** with atom labelling.*

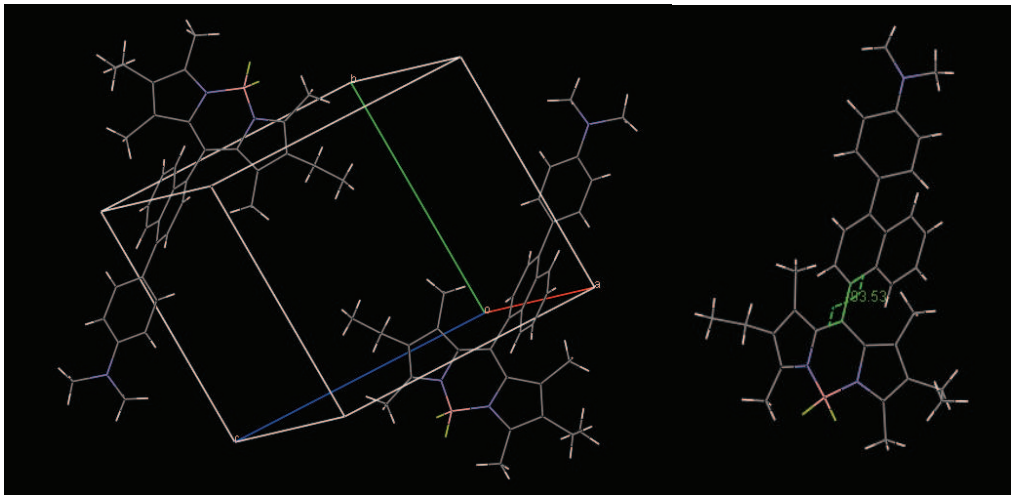

*Figure 7 – Left: Molecular packing in the crystal structure of **DMANBD**: nitrogen (blue), boron (pink), fluorine (green), hydrogen (white). Right: the torsion angle observed between the naphthalene unit and the bodipy framework of 93.53°.*

5.3.2 DMABDS

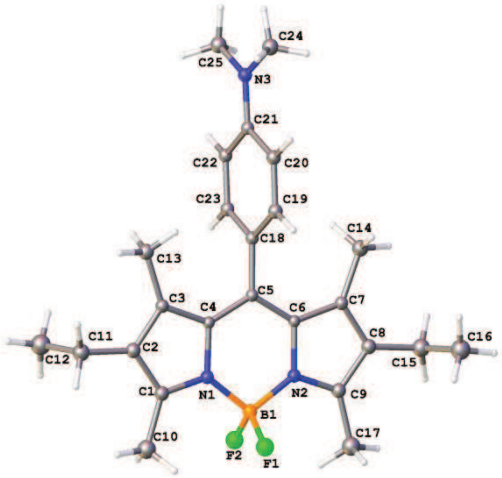

*Figure 8 – The molecular structure of **DMABDS** with atom labelling.*

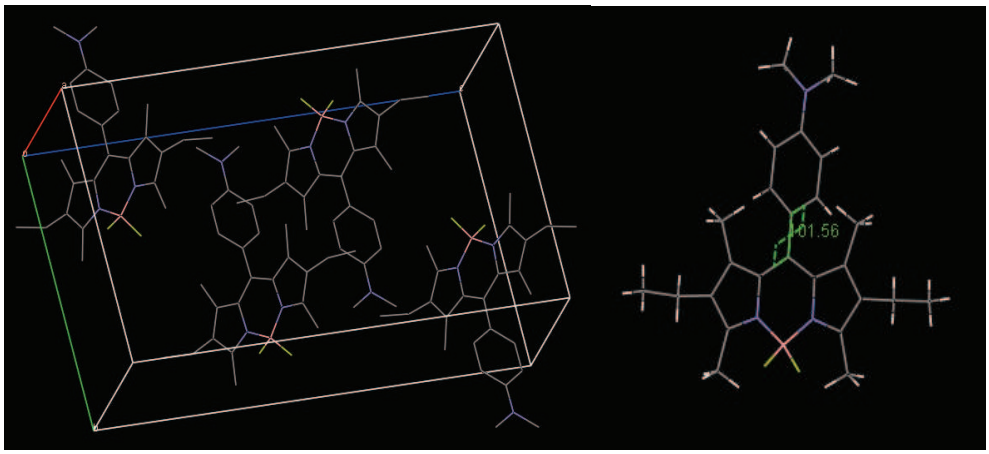

*Figure 9 – Left: The torsion angle calculated for **DMABDS** of 101.56°. Right: Molecular packing in the crystal structure of **DMABDS**: carbon (grey), nitrogen (blue), boron (pink), fluorine (green). The hydrogen atoms have been omitted for clarity.*

It can be seen from both the packing diagram and the molecular structure of **DMABDS**, that the indacene plane and the *N,N*-dimethylaniline unit are almost orthogonal to one another. This is due to the steric constraints imposed by the two 1,7-dimethyl groups. The torsion angle between C4-C5-C18-C19 was calculated to be 101.56°. This is different to the angles observed in **DMANBD** where it can be seen that the naphthalene spacer resides in an almost orthogonal position, whereas the *N,N*-dimethylaniline subunit is less constrained and more in plane with the dipyrrin moiety.

Furthermore, in both dyads the molecular packing diagram shows that the molecules lie parallel to one another in a head to tail orientation. The meso-phenyl ring of the dimethylamino unit of one molecule is almost orthogonal to the indacene core of the second, indicating there are no significant π-π stacking interactions.

From structural determination, it was also possible to obtain an accurate distance between the donor (*N,N*-dimethylaniline) and the acceptor (dipyrrin) groups for both systems. The centre to centre distance, which is indicated in *Figure 10* below, is calculated from the nitrogen atom to a centroid of the middle ring in the dipyrrin core. It can be seen that insertion of the naphthyl spacer results in an approximate 60% increase in distance between the donor and acceptor units.

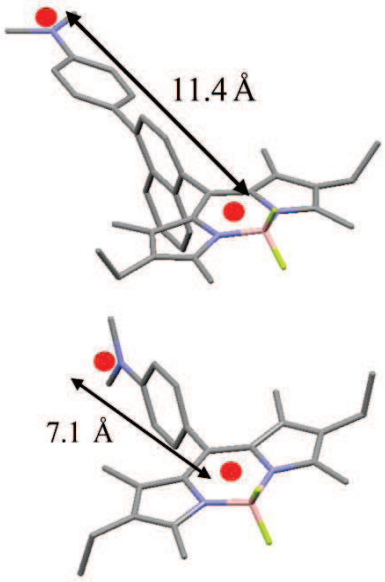

Figure 10 – X-ray structure determined molecular images for ***DMANBD*** *(top) and* ***DMABDS*** *(bottom) with hydrogen atoms omitted for clarity.*

5.3.3 DMABD

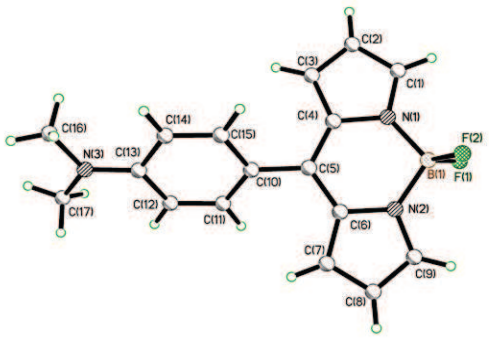

*Figure 11- The molecular structure of **DMABD** with atom labelling.*

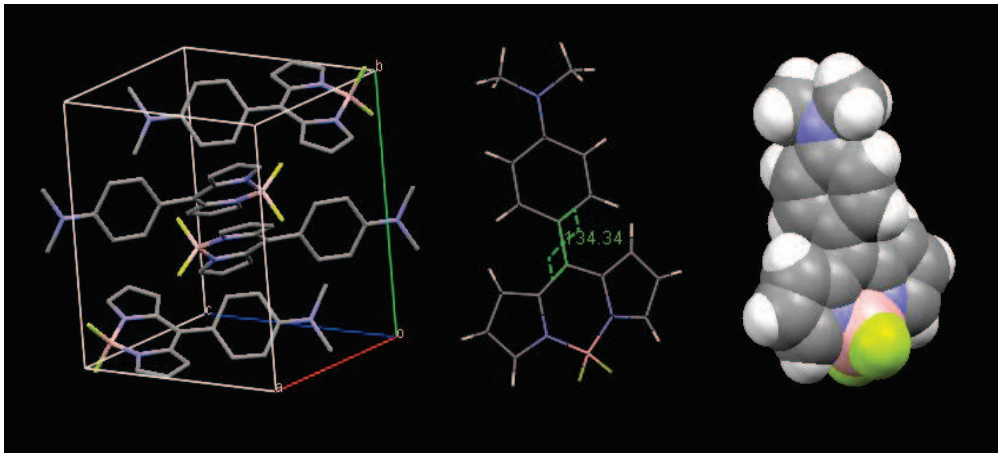

*Figure 12 – Left: Molecular packing in the crystal structure of **DMABD.** Carbon (grey), nitrogen (blue), boron (pink), fluorine (green). The hydrogen atoms have been omitted for clarity. Centre: The torsion angle in **DMABD** of 134.34°. Right: A space-filling diagram of the molecule.*

In all three crystal packing diagrams, a slightly offset head-to-tail centrosymmetric arrangement of the two central molecules can be observed. This is a common motif present in many bodipy derivatives[48].

In all three compounds, the central six membered ring containing B-N1-C4-C5-C6-N2 is almost co-planar with the adjacent 5-membered rings, indicating strong π-electron delocalisation within the indacene plane. The two fluorine atoms in all three compounds occupy apical positions with respect to the mean plane of the indacene ring system. Ball and stick models of **DMANBD** and **DMABDS** developed in Spartan

06 also confirm the orthogonal nature of the phenyl or naphthyl moiety relative to the indacene plane.

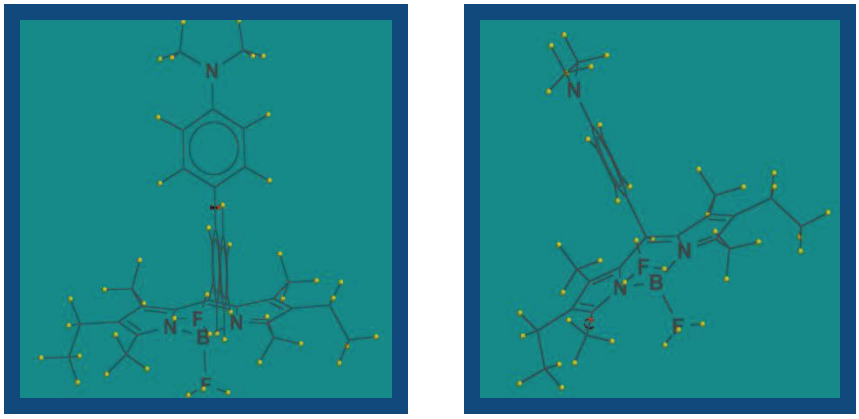

Figure 13 – Molecular models generated using Spartan showing the relative orientation of the indacene plane and the aromatic moiety.

5.4 Molecular Orbital Calculations

The spatial localisation of the HOMO and LUMO for both the dyads were calculated using density functional theory (B3LYP, 6-311G) and Gaussian O3[49]. The representation of the orbitals is shown in *Figure 14*.

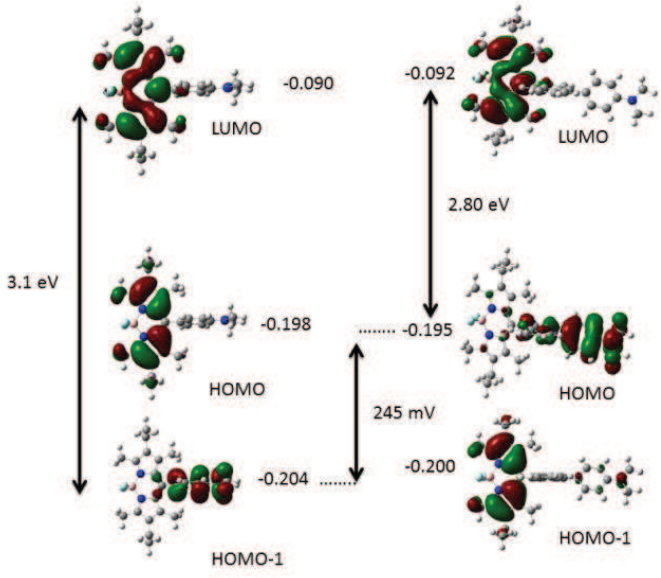

*Figure 14 - Representation of the HOMO-1, HOMO and LUMO for the two dyads (left: **DMABDS** and right: **DMANBD**) as calculated using DFT (B3LYP) and the 6-311G basis set. Energies for orbitals are given in Hartrees.*

In both the *N,N*-dimethylaniline based dyads, the LUMO is localised exclusively on the dipyrromethene unit. The energy of this orbital does not appear to be significantly affected by the nature of the appended aromatic in the meso position. In **DMABDS**, the HOMO is localised on the dipyrromethene moiety, and it is the HOMO-1 that dominates the *N,N*-dimethylaniline group. The difference in energy between the orbitals is small (160 mV).

In comparison, the DFT calculated HOMO for **DMANBD** is localised on the *N,N*-dimethylaniline group and very little electron density resides on the intervening naphthyl unit. The HOMO-1 is localised on the dipyrromethene moiety this time, and once again, a small energy difference between the two orbitals can be observed (136 mV). The variance in ordering of the HOMOs for the two dyads can very likely be attributed to the insertion of the naphthyl group.

In **DMANBD**, the HOMO-LUMO gap of 2.80 eV represents the energy associated with one-electron transfer from the electron donating dimethylamine moiety to the bodipy chromophore. The latter residue is behaving as the electron acceptor here. The similar energy gap for **DMABDS** is 3.10 eV (i.e., HOMO-1 to LUMO). It must be noted that these calculated energy gaps are rather large, since there is no solvation contribution to the stabilisation. However, the general trend of the larger energy gap for **DMABDS** (cf. **DMANBD**) is consistent with the results observed from cyclic voltammagrams which will be discussed later in the chapter.

5.5 NMR spectral data

5.5.1 Fluorine NMR spectra

As previously discussed, typical ^{19}F spectra for bodipy compounds constitute a single quartet due to coupling to ^{11}B ($I = 3/2$, $J \approx 32$ Hz).[50] Often, slight deviation can be seen from this coupling pattern due to the unsymmetrical nature of the appendage present at the *meso* position. ^{19}F spectra for the bodipy derivatives discussed within this chapter are given below in *Figure 15*.

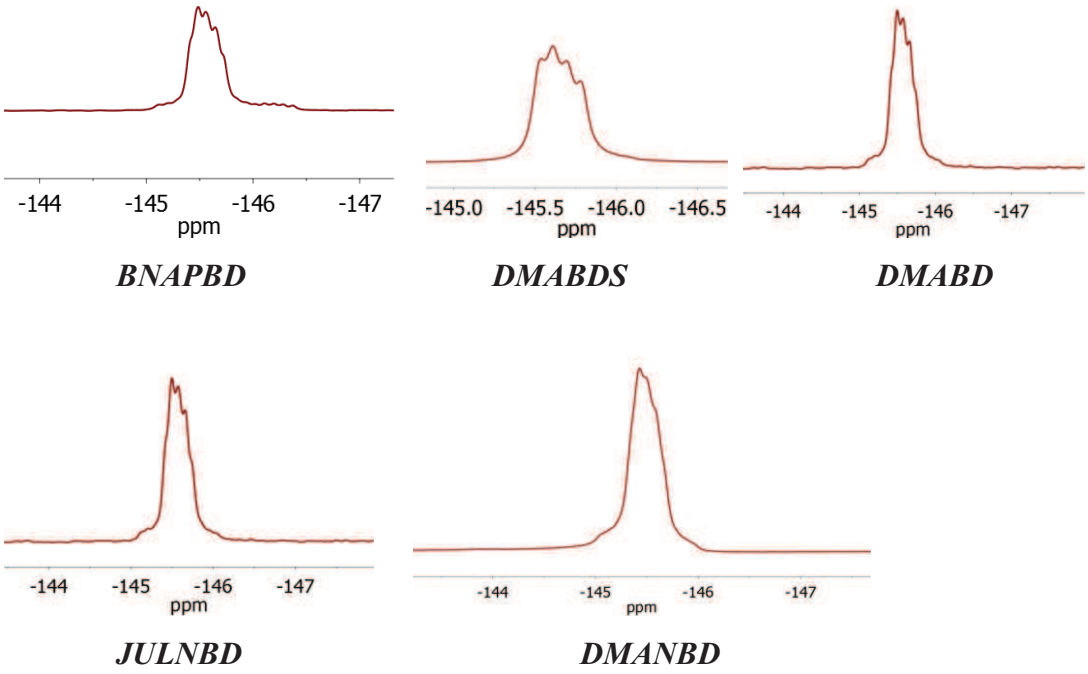

Figure 15 - ^{19}F spectra of the bodipy systems discussed within this chapter.

It can be seen that the fluorine spectra corresponding to **DMABD** and **DMABDS** exclusively display the typical quartet coupling pattern. This is due to the fact that both fluorines are equivalent as all the molecules are symmetrical. In the other spectra, broadening takes place. This is because each other system possesses a different symmetry point group due to the presence of the unsymmetrical spacer. The effect is particularly noticeable in the case of **DMANBD**. For those systems which do not display the characteristic quartet pattern, it is believed that a doublet of quartets is likely to be generated, which is appearing as a broadened peak in the room temperature NMR experiment. The broadening is due to the presence of two inequivalent fluorine atoms which couple both to one another and to boron. This is elucidated further in the following chapter when the binaphthalene spaced *N,N*-dimethylaniline dyad is discussed.

5. 5. 2 Proton NMR spectra

Selected annotated spectra are given below. In order to complete a full proton assignment, 2-dimensional correlated spectra including HMQC, HMBC and COSY methods are used.

The NMR spectra recorded for **DMABDS** will be discussed initially.

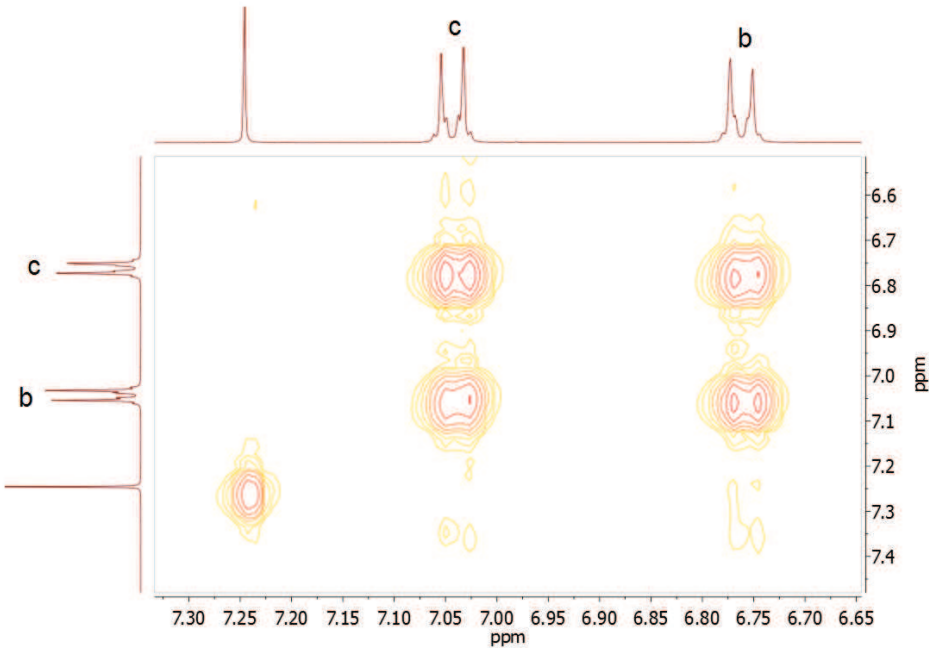

Figure 16 - The aromatic region of the COSY *correlated spectrum of* ***DMABDS*** *in* $CDCl_3$ *at room temperature.*

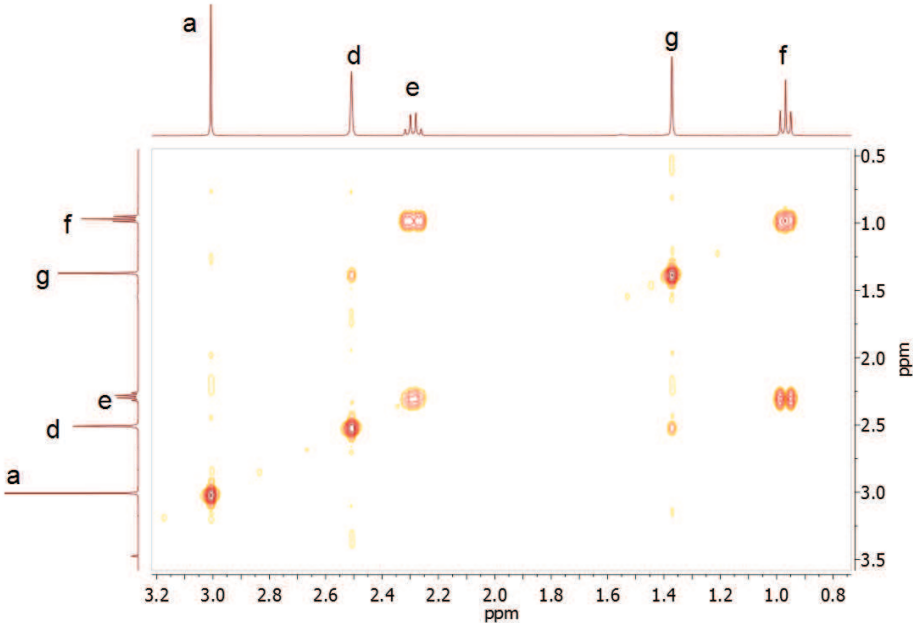

Figure 17 – The aliphatic region of the COSY correlated spectrum of ***DMABDS*** *in* $CDCl_3$ *at room temperature.*

In the aromatic region, a correlation is seen between protons c and b confirming their proximity. In the aliphatic region, a correlation is seen between e and f and a smaller cross peak can be observed connecting d and g.

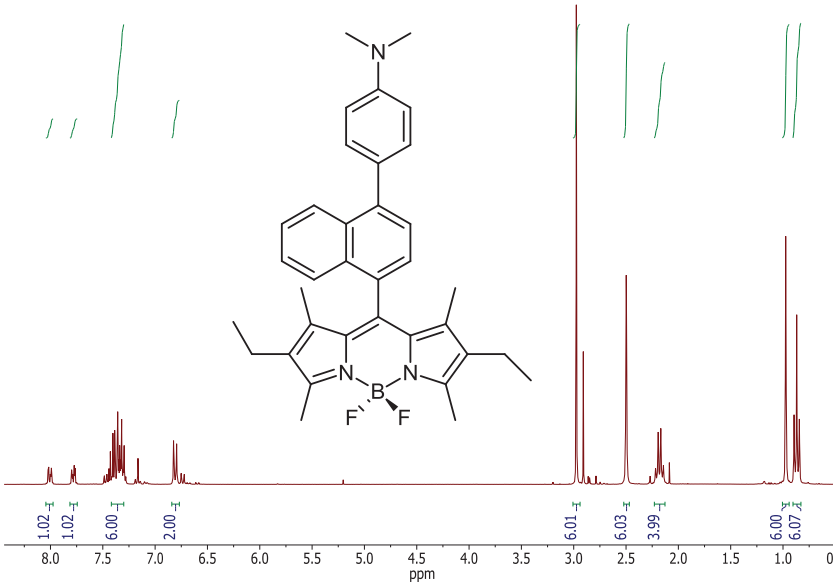

*Figure 18 - A ^{1}H NMR spectrum for **DMABDS** recorded in $CDCl_3$ at room temperature.*

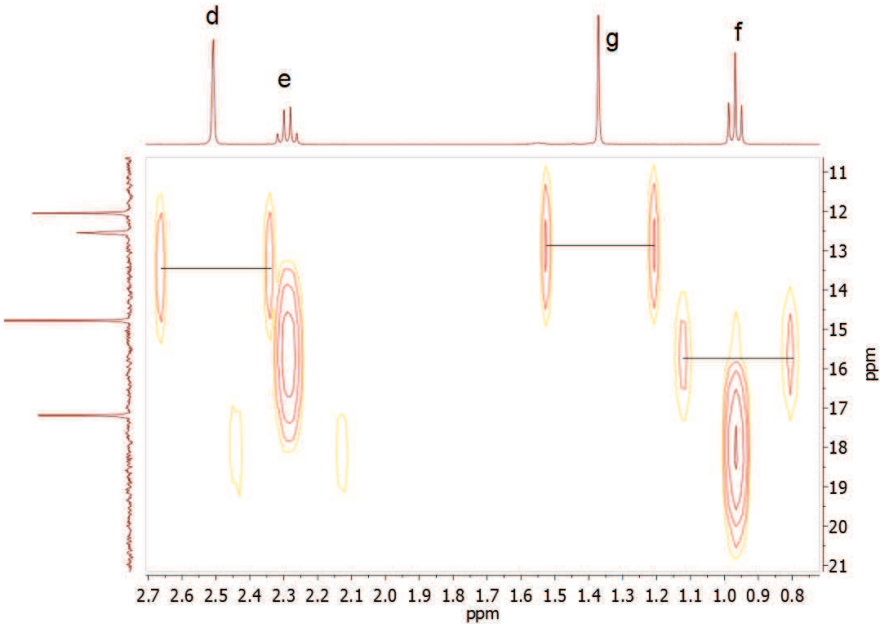

*Figure 19 – An HMBC spectrum of **DMABDS** in $CDCl_3$.*

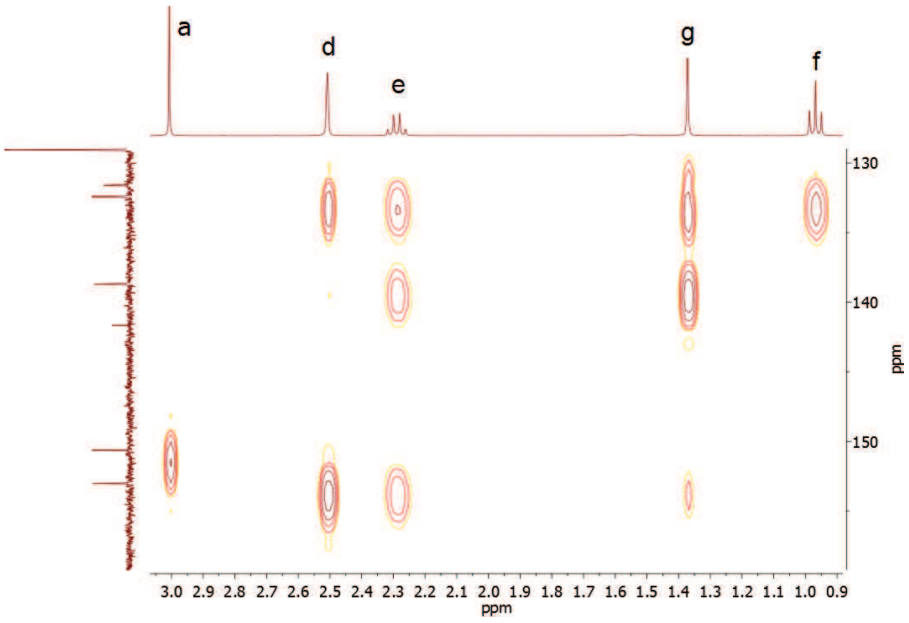

*Figure 20 – An HMBC spectrum showing correlations between aromatic carbon atoms and aliphatic protons of **DMABDS** in $CDCl_3$.*

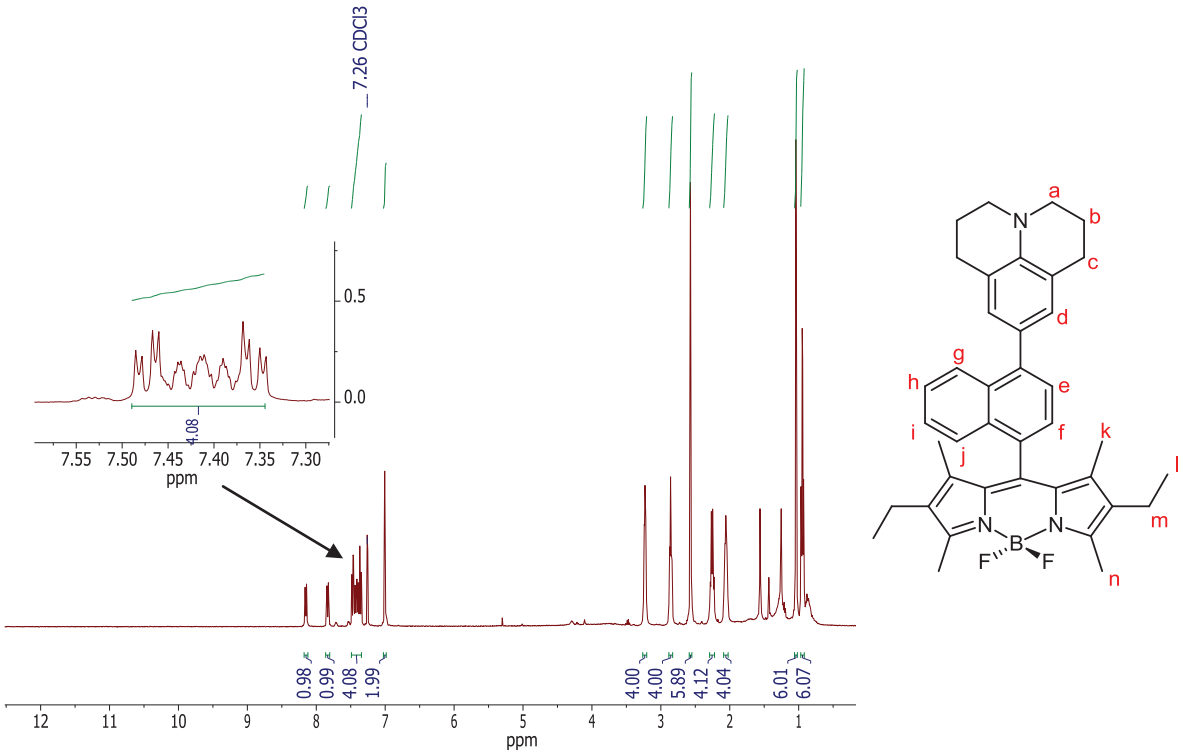

*Figure 21 - An annotated ^1H NMR spectrum of **JULNBD**. The multiplet situated in the region of 7.32 to 7.49 ppm is expanded for clarity.*

Chemical shift (ppm)	Intensity (no. of H Atoms)	Multiplicity	Assignment
8.08	1	d	e and f
7.77	1	d	
7.35	4	m	g, h, i, j
6.94	2	s	d
3.17	4	t	a
2.80	4	t	c
2.50	6	s	n
2.19	4	q	m
2.00	4	m	b
0.97	6	s	k
0.88	6	t	l

*Table 1 – ^{1}H chemical shift assignment for **JULNBD**.*

5.6 Photophysical and electrochemical properties

5.6.1 Electrochemistry

An investigation into the redox behaviour of the *N,N*-dimethylaniline bodipy series was carried out in dry DCM (0.2M TBATFB) by cyclic voltammetry. The working electrode used was glassy carbon whilst a platinum wire was employed as the counter electrode and a silver wire as the reference. The cyclic voltammagrams can largely be interpreted in terms of the known electrochemical behaviour of isolated bodipy[51].

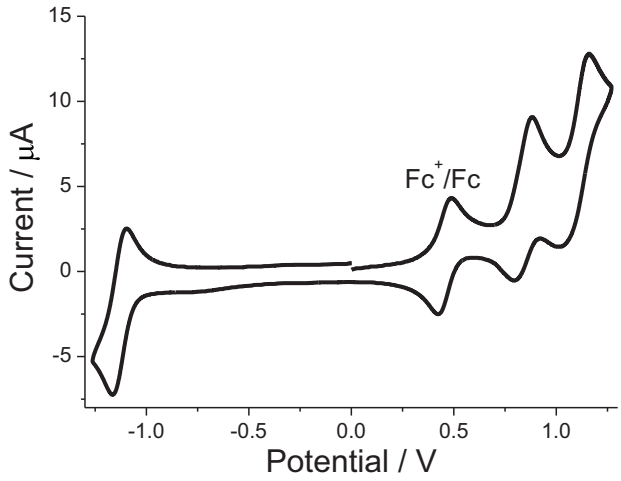

Figure 22 - Cyclic voltammogram recorded for **DMANBD** in dry MeCN (0.2 M TBATFB) at a platinum electrode vs Ag/AgCl. Scan rate = 50 mV s^{-1}.

The oxidative scan segment for the voltammogram of **DMANBD** (*Figure 22*) contains a quasi-reversible one-electron wave at $E_{1/2}$ = +0.84 V (90 mV) vs Ag/AgCl. This wave is associated with oxidation of the amine. Upon further scanning, a second quasi-reversible wave can be observed at $E_{1/2}$ = +1.09 V (140 mV) vs Ag/AgCl. This corresponds to redox of the bodipy site. In the reductive potential window, a one-electron quasi–reversible wave is seen at $E_{1/2}$ = - 1.13 V vs Ag/AgCl and is associated with reduction of the bodipy group. The energy difference (ΔE) between potentials for amine oxidation and reduction of the bodipy is 1.97 V. The solubility of **DMABDS** in MeCN is rather poor and collection of a good quality cyclic voltammogram proved to be difficult. The oxidative scan for **DMABDS** is dominated by two one-electron quasi-reversible waves. These are located at +1.13 V (90 mV) and +1.31 V (190 mV) vs Ag/AgCl. The first wave corresponds to the amine oxidation, whilst the second is oxidation of the bodipy group. The single wave observed at $E_{1/2}$ = - 1.03 V (80 mV) on reductive scanning is again redox at the bodipy site and the corresponding value for ΔE is 2.16 V. It is noted that $\Delta E_{\mathbf{DMABDS}} > \Delta E_{\mathbf{DMANBD}}$. The difference in potentials for oxidation of the amine ($E_{\mathbf{DMABDS}}$-$E_{\mathbf{DMANBD}}$) is 290 mV. It can be seen that the same value from the computational calculation is remarkably similar.

5.6.2 Photophysical studies - Absorption and Fluorescence

Figure 23 presents the electronic absorption spectra for **DMABDS** and **DMANBD** in dilute acetonitrile. The typical sharp strong absorption band associated with the bodipy-centered S_0-S_1 electronic transition is observed at 520 nm in **DMABDS** and 525 nm in **DMANBD**. The small red shift of 5 nm in λ_{ABS} for **DMANBD** can be attributed to the effect of partial conjugation with the naphthyl unit. It can be observed that bodipy-based S_0-S_2 absorption profile for **DMANBD** is much weaker and also obscured by the π-π^* electronic transitions of the naphthyl group.

Extremely weak room temperature fluorescence can be observed from dilute solutions of highly purified samples of **DMABDS** or **DMANBD** in acetonitrile. The emission profiles are reasonable mirror images of the absorption bands and the Stokes' shifts are again typical for Bodipy-like chromophores[52]. Upper limits of fluorescence quantum yields (Φ_{FLU}) for **DMABDS** and **DMANBD** are 0.0003 and 0.002 respectively. Fluorescence lifetimes (τ_s) were too short to be measured by the

conventional time-correlated-single-photon-counting technique. As discussed later, femtosecond up-conversion spectroscopy provided reliable values for τ_s.

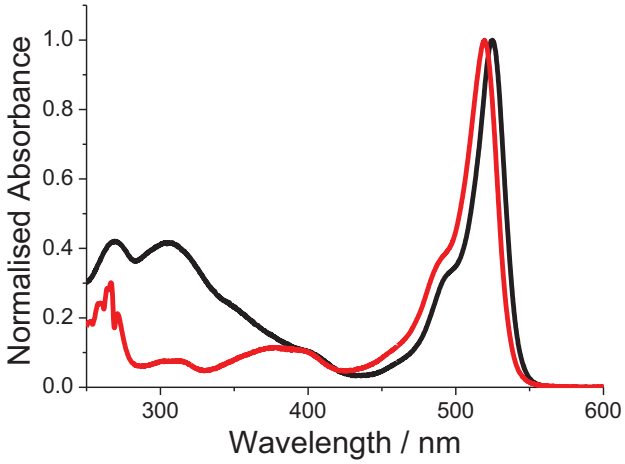

*Figure 23– Room temperature absorption spectra recorded for **DMABDS** (red) and **DMANBD** (black) in dilute acetonitrile.*

5.6.3 Time Resolved Transient Absorption Spectroscopy

This technique was then carried out on the two *N,N*-dimethylaniline systems, **DMABDS** and **DMANBD**. It measures the absorption of a sample at a particular wavelength or wavelength range as a function of time, following excitation by a laser pulse. Transient absorption spectroscopy can be used to rationalise and further elucidate the charge separation and charge recombination mechanisms taking place within photoactive systems. A basic representation of this is featured in the diagram below (*Figure 24*).

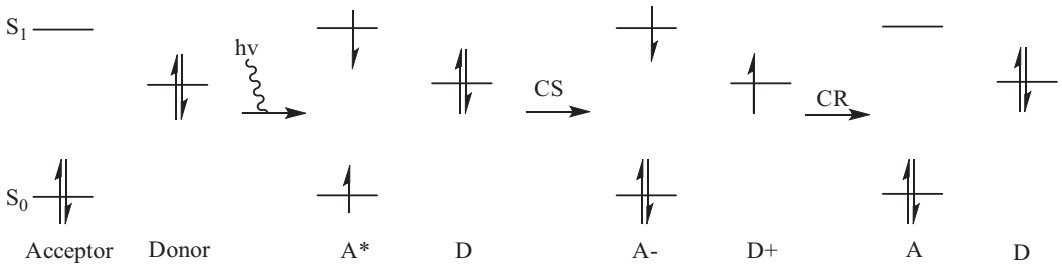

Figure 24 – A diagram to illustrate the mechanism of charge separation and charge recombination within donor-acceptor dyads.

These mechanisms are observed in nature in supramolecular devices such as the photosynthetic reaction centre, in which pigments are arranged in a highly organized manner to execute efficient photon absorption and light harvesting (*Figure 25*)[53,54]. Please refer to the introductory chapter of this thesis for further information on photosynthetic systems.

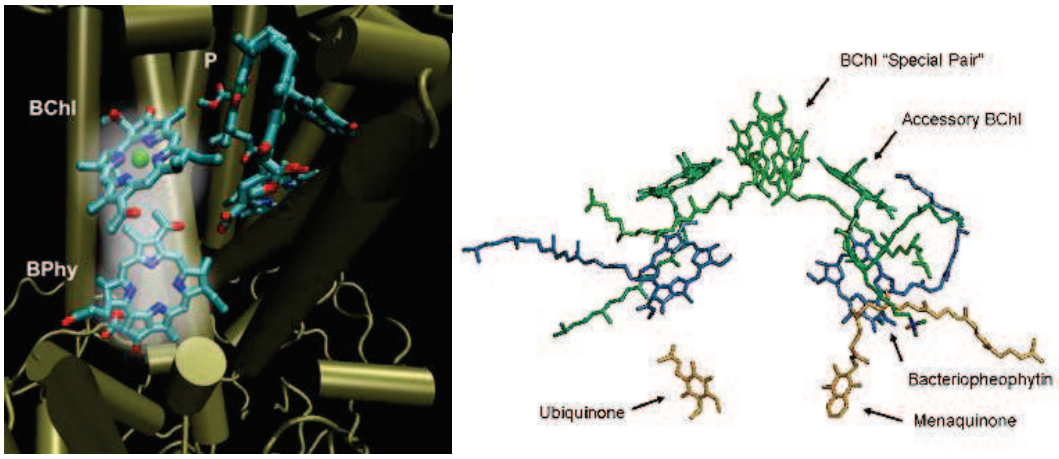

Figure 25 – The images to the left[55] and to the right[56] both display a pigment-protein complex in the photosynthetic reaction centre of a purple bacterium.

In the image above left, the white fog indicates quantum coherence between the excitations of two pigment molecules, Bphy (bacteriopheophytin) and BChI (Bacteriochlorophyll). This promotes efficient energy transfer to the protein[57]. In order to compete with processes which inevitably lead to loss of energy from the system such as internal conversion, intersystem crossing and fluorescence, the electron- and energy-transfer processes which fix the excited state energy in photosynthesis must be executed on an extremely rapid timescale. For example, the process of energy transfer in a photosynthetic membrane occurs over a period of less than 100 femtoseconds to hundreds of picoseconds[58].

In order to investigate these events, ultrafast techniques down to a sub-100 fs resolution must be used. By doing this, energy migration within the system, in addition to the generation of new chemical species (such as charge separated states) can be tracked in real-time. Ultrafast transient absorption spectroscopy can allow us to do this[59].

5.6.4 Results

Results generated from a series of steady-state measurements performed on both dyads indicated efficient excited-state deactivation. In order to further investigate the photophysical properties of the *N,N*-dimethylaniline dyads, femtosecond time-resolved transient absorption experiments were undertaken.

Samples of **DMABDS** and **DMANBD** solubilised in acetonitrile were excited with a 70 femtosecond laser pulse delivered at 385 nm. Around 50-70 time resolved spectra were recorded over a 200-1000 ps time frame depending on the relaxation time of the sample. The data was fitted to generate relaxation time constants and the decay component spectra associated with them. Results of the measurements for **DMABDS** in acetonitrile are given in *Figure 26* below. At an early time delay, a clear bleach effect could be observed at 521 nm and a negative transient absorption in the range of 540-600 nm. Here, virtually no ground state absorption of the sample can be seen. With a time constant of 1.5ps, the negative absorption becomes a transient absorption band with a maximum at around 580 nm. This new feature can be assigned to the bodipy based radical anion[60]. Relaxation can be seen with a time constant of 140 ps. However, after relaxation of the band, some bleaching of the ground state absorption remains, indicating that approximately a quarter of initially excited molecules remain in an excited state.

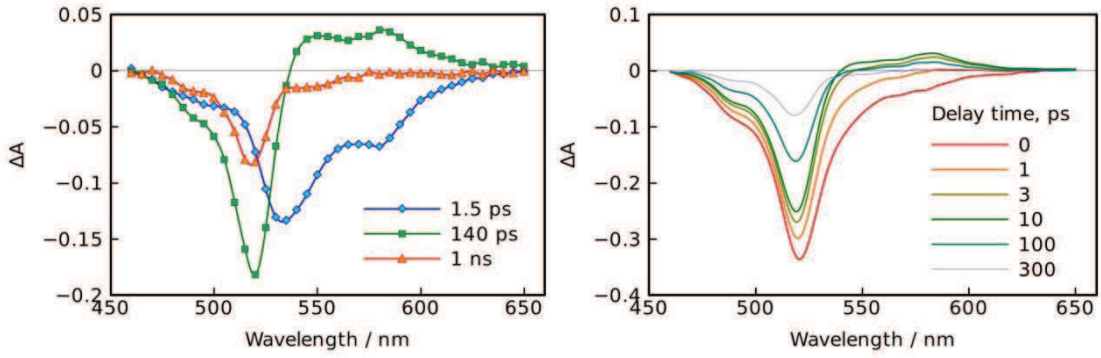

*Figure 26 – Left: Transient absorption decay components obtained from three exponential fit of the pump probe data gained for **DMABDS** in acetonitrile; time constants: 1.5 ps (blue), 140 ps (green) and 1 ns (red). Right: Time resolved transient absorption spectra at a number of delay times obtained after group velocity dispersion compensation; the delay times are indicated in the plot.*

The time profile of the transient absorption evolution at 580 nm in addition to fluorescence decay of the sample measured using up-conversion techniques are presented in *Figure 27*. The strong, almost instant negative absorption at 580 nm becomes positive with the same time constant as the decay of the sample fluorescence. This, along with the fact that the charge separated state is generated from the singlet excited state, suggests that the negative absorption originates from the stimulated emission.

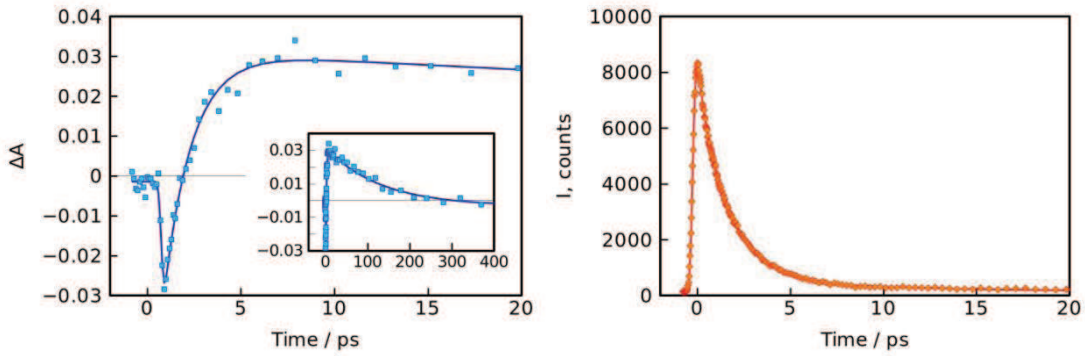

*Figure 27 – Transient absorption time profiles at 580 nm (left) and fluorescence decay at 550 nm (right) recorded of **DMABDS** in MeCN.*

A similar transient absorption experiment was performed with **DMANBD** in MeCN but the results turned out to be harder to analyse. The measurements were repeated in a number of solvents including DMF, THF and toluene. The results of pump probe measurements of **DMANBD** in DMF and comparison of the transient absorption time profile at 580nm with the fluorescence decay are both presented in *Figure 28* below.

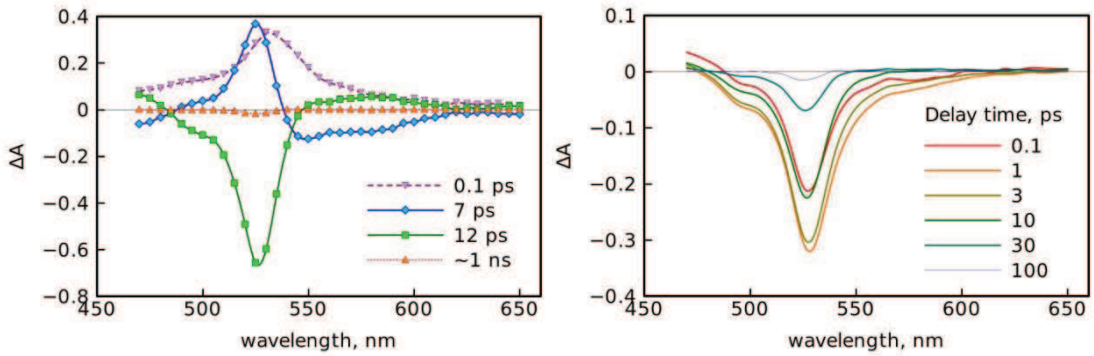

*Figure 28 – Left: Transient absorption decay components obtained from a three exponential fit of pump-probe data of **DMANBD** in DMF. The time constants corresponding to the component spectra are indicated in the plot. Right: Time resolved transient absorption spectra at a number of delay times obtained after group velocity dispersion compensation; again, the delay times are indicated in the plot.*

The transient absorption signal for **DMANBD** decays much more rapidly than that for **DMABDS.** However, it can be seen that the emission decay relaxes more slowly for the naphthalene spaced dyad. At the same time, the number of intermediate states in relaxation of the excited state of **DMANBD** is smaller than for **DMABDS**. A few reactions take place in the same time scale of a few picoseconds which makes quantitative analysis a difficult task. However, the shape of the 12ps component for **DMABDS** is very similar to the 140 ps component for **DMABDS** displaying an absorption band at around 580 nm. This band can be attributed to the charge separated state. The electron transfer takes place from the singlet excited state with time constant close to 7ps. This time constant can be seen in the fluorescence decay plot and also through disappearance of the negative absorption band in the 540-600 nm region of the spectrum. The lifetime of the charge separated state is only 12ps and the small difference in formation and decay time constants renders the band at 580 nm almost invisible. Even so, close inspection of the transient absorption kinetics at 580nm indicates that after simultaneous relaxation of stimulated (negative) absorption and fluorescence, a positive absorption is formed (*Figure 29*).

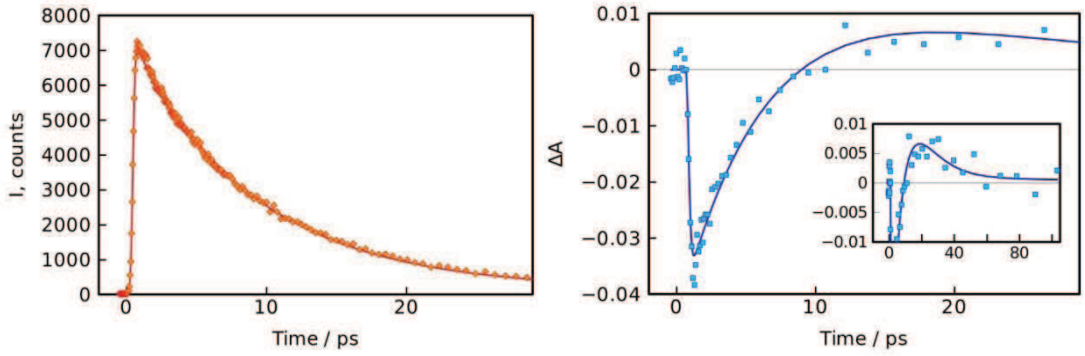

*Figure 29 – Transient absorption time profiles at 580 nm (left) and fluorescence decay at 550 nm (right) of **DMANBD** in DMF.*

Two other differences between the transient absorption profiles for **DMABDS** and **DMANBD** are that for the latter there is a very fast component which can be attributed to internal conversion from the second excited singlet state to the first. This process is extremely fast (0.1 ps) and practically unresolved due to the time resolution of the instrument (of 0.2 ps). There is virtually no long lived component for **DMANBD** which can be explained by the fast charge recombination observed.

In THF, the difference between charge separation and recombination time constants is larger for **DMANBD** and the characteristic bodipy based radical anion band can be seen more clearly. Also, all spectral features of **DMANBD** in acetonitrile, DMF and THF were similar and generally the same conclusions can be made for the transient states formed in all three solvent systems. Unfortunately, comparison of photoinduced reactions in **DMABDS** and **DMANBD** in a broader solvent range was hampered by the poor solubility of the former.

5.7 Interpretation

Based on information gained from cyclic voltammagrams and molecular modelling calculations, a basic model for singlet excited state deactivation for the two dyads can be proposed (*Figure 30*).

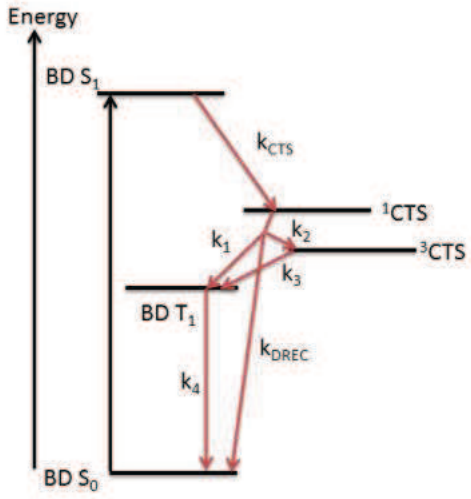

Figure 30 – A simplified energy diagram showing possible contributions to excited state deactivation of the bodipy and the formed charge transfer state.

In polar acetonitrile, the fully formed singlet charge transfer state (^{1}CTS) is situated at around 220 mV (**DMABDS**) and 390 mV (**DMANBD**) below the respective bodipy S_1 states. The Gibb's free energy changes (ΔG_{CT}) for formation of the ^{1}CTS as calculated using *Equation 1* are – 234 meV (**DMABDS**) and – 374 meV (**DMANBD**).

$$\mathbf{\Delta G_{CT} = F(E_D - E_A) - E_{00} + W}$$

Equation 1 – An equation to define the Gibbs free energy changes for formation of the singlet charge transfer state.

In this equation, E_D and E_A are the oxidation and reduction potentials for the donor and acceptor respectively, E_{00} is the mid-point in the crossing of the absorption and fluorescence spectra for the donor (**DMABDS** = 2.34 eV, **DMANBD** = 2.31 eV) and

W is the Coulombic work term. In MeCN these terms for the two dyads are only - 54 meV (**DMABDS**) and - 34 meV (**DMANBD**).

On spin considerations, a lower-lying triplet charge transfer state (^{3}CTS) must also be evaluated. If the energy gap (^{1}CTS-^{3}CTS) is small, then the rate of intersystem crossing (k_2) may be extremely fast[61]. This scenario opens up an efficient pathway to populate the triplet state on the bodipy core (rate = k_3). Direct population of the bodipy triplet state from the ^{1}CTS is another feasible option (rate = k_1), as well as direct restoration of the ground state (rate = k_{DREC}). The value for k_1 is very much dependent on the orientation between the orbitals on the dimethylaniline moiety and the bodipy. In an orthogonal arrangement, the charge transfer process is accompanied by a change in orbital angular momentum which facilitates the necessary spin flip to generate the triplet. Direct recombination from ^{3}CTS to the ground state is a spin-forbidden process and presumably rather slow. Intersystem crossing from the bodipy S_1 to T_1 state is known to be in the order of 10^6 s^{-1}.[27] The energy of the triplet state is around 1.6 eV above the ground state.

The evidence gained from transient absorption profiles suggests that in **DMABDS**, the ^{1}CTS is formed very rapidly (k_{CTS} = 7 x 10^{11} s^{-1}). However, the rate for decay of the ^{1}CTS (second decay component) is considerably slower – around 6.4 x 10^9 s^{-1}. The discrimination between rates for charge separation and charge recombination is extremely good (~100), especially considering the close proximity of the donor to the acceptor. It is worth noting that a similar effect was witnessed for a closely-spaced pyridinium-based bodipy dyad.[62] The value for k_{DREC} is around 5.4 x 10^9 s^{-1} for a driving force (ΔG_{DREC}) of -2.11 eV. This places the electron transfer process well into the Marcus inverted region and the long-lived component in the transient records is assigned to the triplet localised on the bodipy.

In **DMANBD** however, the scenario is rather different and the ^{1}CTS is generated at a much slower rate of around 1.4 x10^{11} s^{-1} and relaxes far more rapidly (~0.8 x 10^{11} s^{-1}), which is to be expected considering the increased distance between donor and acceptor. However, the faster charge recombination requires further analysis and for this we turn to the semi-classic Marcus electron transfer theory. Here, the reorganisation energy can be evaluated from known charge transfer and

recombination rate constants, free energies of the states and also using the assumption that electronic coupling is the same for both reactions[63]. The calculations generate the values of 1.06 and 1.14 eV as the reorganisation energies for **DMABDS** and **DMANBD** respectively, which agrees with the expectation of a higher reorganization energy for **DMANBD** relative to that for **DMABDS.** This is due to the increased charge transfer distance in the naphthalene spaced dyad. The energies can be used to draw a Franck-Condon energy diagram for the two compounds in polar solvent, as illustrated in *Figure 31* below:

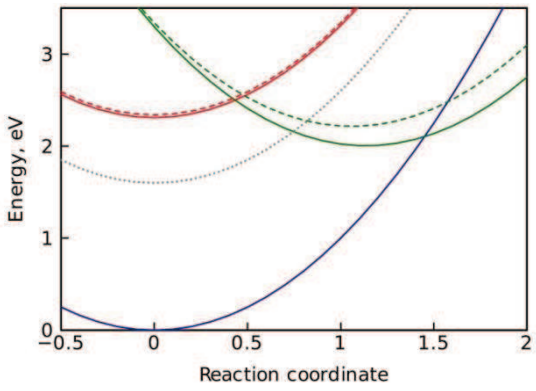

*Figure 31 – A Franck-Condon energy diagram for **DMABDS** (dashed lines) and **DMANBD** (solid lines) in polar solvent. Blue curve – the ground state; red curve – singlet excited state, grey dotted line – triplet state.*

The essential difference in position of the CTS energy profiles is that for **DMANBD** the profile is shifted down (lower free energy of the CTS) and away from the excited state (higher reorganisation energy) relative to that of **DMABDS**.

The potential barrier for the charge separation is smaller for the naphthalene-spaced dyad which could accelerate the electron transfer as compared with **DMABDS.** The distance between the donor and acceptor is larger for **DMANBD**, thus electronic coupling is weaker and the electron transfer rate slows down. The net result is an electron transfer reaction roughly four times slower for **DMANBD**. For the charge recombination, the key factor is the lower potential barrier in the spaced dyad, which is virtually equal to that of charge separation, according to the small difference in the reaction rate constants.

The electronic coupling discussed above can also be estimated for known reaction rate constant and energetics, the free and reorganization energies[64]. According to the semi-classic Marcus theory, the couplings are 690 and 25 cm^{-1} for **DMABDS** and **DMANBD** respectively. The values are certainly reasonable and accounting for the difference in donor-acceptor distance between the dyads of 4.3 Å, the expected decrement factor in exponential dependence of the electron transfer rate constant on the distance is 0.8 Å. This is a very reasonable value for phenyl-like linker between the donor and acceptor. The semi classical ET theory is known to overestimate the rate constants in the inverted Marcus regime. In this particular case, both a quantitative and a qualitative picture predicted by the theory explains the differences observed between the two dyads.

It can also be suggested that charge recombination results in triplet localisation on the bodipy. The long lived component in the transient absorption measurements of **DMABDS** is attributed to the triplet state, as is approximately 25% of the bleaching of the ground state absorption. This gives a rate of conversion from CTS to bodipy triplet state of around 2 x 10^9 s^{-1}. The conversion mechanism is relatively complex, one thought is that the CTS changes in multiplicity then relaxation occurs to the lower-lying locally excited triplet state of the bodipy chromophore. The triplet state is virtually non-existent in excitation relaxation of **DMANBD,** due to the fact that conversion to the triplet state competes with the charge recombination which returns the system directly to the ground state. Since the charge recombination is much faster for **DMANBD** than for the unspaced dyad, the relative amount of molecules relaxing via the triplet state is smaller, even if the rate constants for this reaction pathway are identical. Furthermore, the reaction rates for the relaxation via the triplet state are expected to be slower for **DMANBD** than those for **DMABDS** due to the fact that the potential barrier is higher and the electronic coupling is smaller.

5.8 Concluding remarks

This chapter has described the synthesis, characterisation and basic photophysical examination of a novel series of *N,N*-dimethylaniline substituted bodipy dyads. This gave us an insight firstly into the numerous ways by which carbon-carbon bond

formation can be achieved and also, how reactions may be optimised by varying the solvent, ligand and catalyst. Following thorough research into borylation procedures via C-H activation and palladium catalysis (and subsequent modification and adaptation of these methods) it is hoped that future group members will be able to replicate the procedures to develop novel systems of their own quickly and easily. For effective borylation, it has been established that the palladium nitrile catalyst employed under the conditions discussed herein is a successful species, providing higher yields than other palladium derivatives or iridium based compounds.

Additionally, transient absorption profiles recorded for both **DMANBD** and **DMABDS** have provided information about the charge separation and charge recombination processes occurring within the two dyads. It can be concluded that in **DMANBD**, the naphthyl spacer provides a very feasible pathway for supporting formation of the charge transfer state. From the molecular orbital calculations, it appears that the energies of the spacing unit are extremely well suited to promote fast charge recombination.

It is hoped that further similar studies involving these two dyads may permit further elucidation of the mechanistic pathways occurring. In addition to this, the synthesis and characterisation of the next dyad in the series, the *N,N*-dimethylaniline based binaphthalene spaced system, is addressed in the following chapter. The system is itself interesting due to its chiral nature by restricted rotation. The separation distance will increase by around 40 % and k_{CTS} should decrease to approximately 1 $x10^{10}$ s^{-1} assuming a simple exponential decay model. Of course, a secondary consideration is the twist angle (θ) in the binaphthalene, since electron transfer rates are known to be highly dependent on θ[65]. A thorough photophysical analysis is to be carried out on this species and it is hoped that such studies will permit further elucidation of the mechanistic pathways occurring. They should also allow the degree of involvement of the spacing unit to be analysed to a greater extent.

5.9 References

[1] Gilbert, A.; Allen, N. S.; Cox, A.; Cundall, R. B.; Horspool, W. M.; Reid, S. T.; Weedon, A. C. *Photochemistry – Specialist Periodical Reports*, Royal Society of Chemistry, Cambridge, 1995.
[2] (a) Fox, M. A.; Chanon, M. *Photoinduced Electron Transfer*; Elsevier: Amsterdam, 1988. (b) Balzani, V. *Supramolecular Photochemistry*; D. Reidel: Dordrecht, 1987, (c) Gust, D.; Moore, T. A. *Photoinduced Electron Transfer.* Mattay, J., Ed.; Springer: Berlin, 1991: Vol III. (d) Carter, F. L. *Molecular Electronic Devices*; Marcel Dekker; New York, 1987.
[3] Davis, W. B.; Svec, W. A.; Ratner, M. A.; Wasielewski, M. R. *Nature*. **1998**, *396*, 60.
[4] Benniston, A. C.; Harriman, A.; Li, P.; Patel, P. V.; Sams, C. A.. *Chem. Eur. J*. **2008**, *14*, 1710.
[5] Guldi, D. M.; Maggini, M.; Scorrano, G.; Prato, M, *J. Am. Chem. Soc*. **1997**, *199*, 974.
[6] a) Mujika, V, Nitzan, A.; Mao, Y.; Davis, W.; Kemp, M.; Roitberg, A.; Ratner, M. A.. *Adv. Chem. Phys*. **1999**, *107*, 403-429; b) Benniston, A. C.; Harriman, A. *Chem. Soc. Rev*. **2006**, *35*, 169.
[7] a) Davis, W. B.; Ratner, M, A.; Wasielewski, M. R. *Chem. Phys*. **2002**, *281*, 333, b) Nelsen, S. F.; Newton, M. D. *J. Phys. Chem. A*. **2000**, *104*, 10023.
[8] Shephard, M. J.; Paddon-Row, M. N.; Jordan, K. D. *Chem. Phys*. **1993**, *176*, 289.
[9] Benniston, A.; Grosshenny, V.; Harriman, A.; Ziessel, R. *New. J. Chem*. **1997**, *21*, 405.
[10] Diesenhofer, J.; Epp, O.; Miki, K.; Huber, R.; Michel, H. *J. Mol. Biol*. **1984**, *180*, 385.
[11] (a) Larsson, S. *J. Am. Chem. Soc*. **1981**, *103*, 4034. (b) Larson, J. *J. Am. Chem. Soc., Faraday Trans*, 2. **1983**, *79*, 1375. (c) Miller, J. R.; Beitz, J. V.; Huddleston, R. K. *J. Am. Chem. Soc*. **1984**, *106*, 5057.
[12] Hall, D. G. *Structure, Properties and Preparation of Boronic Acid Derivatives*, In, *Boronic Acids: Preparation and Applications in Organic Synthesis and Medicine*; Hall, D. G., Ed.; Weinham, 2005; pp 1-99.
[13] Ishiyama, T.; Miyaura, N. *Chem. Rec*. **2004**, *3*, 271.
[14] Kotha, S.; Lahiri, K.; Kashinath, D. *Tetrahedron*. **2002**, *58*, 9633.
[15] Miyaura, N.; Yamada, K.; Suzuki, A. *Tetrahedron. Lett*. **1979**, 3437.
[16] Miyaura, N.; Suzuki, A. *Chem. Rev*. **1995**, *95*, 2457.
[17] Heck, R. F.; Nolley, J. P. *J. Org. Chem*. **1972**, *37*, 2320.
[18] Mizoroki, T.; Mori, K.; Ozaki, A. *Bull. Chem. Soc. Jpn*. **1973**, *46*, 1505.
[19] Heck, R. F. *Acc. Chem. Res*. **1979**, *12,* 146.
[20] Sonogashira, K.; Tohda, Y.; Hagihara, N. *Tetrahedron. Lett*. **1975**, 4467.
[21] For a review, see: Negishi, E.-i. In *Metal-catalysed Cross Coupling Reactions*; Diederich, F.; Stang, P. J.; Eds.; Wiley-VCH: New York, 1988, Chapter 1.
[22] Stille, J. K. *Angew. Chem. Int. Ed*. **1986**, *25*, 508.
[23] (a) *Organozinc reagents, A Practical Approach*; Knochel, P.; Jones, P.; Eds Oxford, New York, **1999** (b) Erdick, E. *Organozinc reagents in Organic Synthesis*; CRC Press: Boston, 1996.
[24] Miyaura, N. *Cross Coupling Reactions, A Practical Guide*; Springer-Verlag Berlin Heidelberg, 2002.
[25] Phan, N. T. S.; Van der Sluys, M.; Jones, C. W. *Adv. Synth. Catal*. **2006**, *348*, 609.
[26] (a) Grushin, V. V.; Alper, H. *Chem. Rev*. **1994**, *94*, 1047-1062 (b) Grushin, V. V.; Alper, H. In *Activation of Unreacted Bonds and Organic Synthesis*; Murai, S., Ed.; Springer-Verlag: Berlin, 1999; pp 193-226.
[27] Stürmer, R. *Angew. Chem. Int. Ed*. **1999**, *38*, 3307.
[28] The low reactivity of can be primarily attributed to the strength of the C-Cl bond (bond dissociation energies for Ar-X: Cl = 96 kcal/ mol; Br = 81 kcal/ mol; I = 65 kcal/ mol.) Please refer to the book referenced as 26(b).
[29] Kornblum, N.; Powers, J. W; Anderson, G. J.; Jones, W. J.; Larson, H. O.; Levand, O.; Weaver, W. M, *J. Am. Chem. Soc*. **1957**, *79*, 6562.
[30] Carreño, M. C.; García Ruano, J. L.; Sanz, G.; Toledo, M. A.; Urbano, A. *J. Org. Chem*. **1995**, *60*, 5328.
[31] March. J. *Advanced Organic Chemistry: Reactions, Mechanism and Structure*, 4th Ed.; John Wiley and Sons: New York, 1992, pp 531-534 and references cited therein.
[32] Uncatalysed reactions: (a) Buu Hoi, N. P. *Ann*. **1944**, *556*, 1. (b) Djerassi, C. *Chem Rev*. **1948**, *43*, 271. (c) Ross, S. D.; Finkelstein, M.; Petersen, R. C. *J. Am. Chem. Soc*. **1958**, *80*, 4327. (d) Mitchell, R. H.; Lai. Y. H.; Williams, R. V. *J. Org. Chem*. **1979**, *44*, 4733. (e) Coleman, R. S.; Grant, E. B. *J. Am. Chem. Soc*. **1994**, *116*, 8795.
[33] Catalysed reactions: (a) Schmid, H. *Helv. Chim. Acta*. **1946**, *29*, 1144. (b) Konishu, H.; Aritomi, K.; Okano, T.; Kiji, *J. Bull. Chem. Soc. Jpn*. **1989**, *62*, 591. (c) Bovonsombat, P.; Mc Nelis, E. *Synthesis*, **1993**, 237. (d) Paul, V.; Sudalai, A.; Daniel, T.; Srinivasan, K. V. *Tetrahedron Lett*. **1994**, *35*, 7055.
[34] Sato, M.; Miyaura, N.; Suzuki, A. *Chem. Lett*. **1989**, *18*, 1405.

[35] Larouche-Gaulthier, R.; Elford, T. G.; Aggarwal, V. K. *J. Am. Chem. Soc*. **2011**, *133*, 16794.
[36] Harrisson, P.; Morris, J.; Marder, T. B.; Steel, P. G. *Org. Lett*. **2009**, *11*, 3586.
[37] Plenio, H.; Kollhofer, A.; Datta, A. *Chem. Commun*. **2004**, *13*, 1508.
[38] For comprehensive reviews on this topic: (a) Chen, X.; Engle, K. M.; Wang, D-H.; Yu, J-Q. *Angew. Chem*. **2009**, *121*, 5196-5217. (b) Dyker, G. *Angew. Chem. Int. Ed*. **1999**, *38*, 1698. (c) Pfeffer, M.; Ritleng, V. *Chem. Rev*. **2002**, *102*, 1731.
[39] O' Malley, S. J.; Tan, K. L.; Watzke, A.; Bergman, R. G.; Ellman, J. A. *J. Am. Chem. Soc*. **2005**, *127*, 13496.
[40] Pelter, A.; Smith, K.; Brown, H. C. *Borane Reagents*; Academic: London, 1988.
[41] Matteson, D. S. *Stereodirected synthesis with Organoboranes*; Springer: Berlin, 1995.
[42] Ishiyama, T.; Ishida, K.; Miyaura, N.; Anastasi, N. R.; Hartwig, J. F, *J. Am. Chem. Soc*. **2002**, *124*, 390.
[43] Wieghardt, K.; Siebert, H. *Inorganic syntheses*. **1985**, *23*, 126.
[44] Marigo, M.; Marsich, N.; Farnetti, E. *Journal of Molecular Catalysis A- Chemical.* **2002**, *187*, 169.
[45] Wolan, A.; Zaidlewicz, M. *Org. Biomol. Chem*. **2003**, *1*, 3274.
[46] Billingsley, K. L.; Barder, T. E, Buchwald, S. L. *Angew. Chem. Int. Ed.* **2007**, *46*. 5359.
[47] Billingsley, K. L.; Buchwald, S. L, *J. Org. Chem*. **2008**, 73, 5589.
[48]Herradon, B.; Chana, A.; Alonso, M.; Amat-Guerri, F.; Liras, M. A.; Maestro. *J. Mol. Struct*. **2004**, *697*, 29.
[49] Gaussian 03, Frisch, M. J.; Trucks, G. W.; Schlegel, H. B.; Scuseria, G. E.; Robb, M. A.; Cheeseman, J. R.; Montgomery Jr., J. A.; Jr., Vreven, T.; Kudin, K. N.; Burant, J. C.; Millam, J. M.; Iyengar, S. S.; Tomasi, J.; Barone, V.; Mennucci, B.; Cossi, M.; Scalmani, G.; Rega, N.; Petersson, G. A.; Nakatsuji, H.; Hada, M.; Ehara, M.; Toyota, K.; Fukuda, R.; Hasegawa, J.; Ishida, M.; Nakajima, T.; Honda, Y.; Kitao, O.; Nakai, H.; Klene, M.; Li, X.; Knox, J. E.; Hratchian, H. P.; Cross, J. B.; Bakken, V.; Adamo, C.; Jaramillo, J.; Gomperts, R.; Stratmann, R. E.; Yazyev, O.; Austin, A. J.; Cammi, R.; Pomelli, C.; Ochterski, J. W.; Ayala, P. Y.; Morokuma, K.; Voth, G. A.; Salvador, P.; Dannenberg, J. J.; Zakrzewski, V. G.; Dapprich, S.; Daniels, A. D.; Strain, M. C.; Farkas, O.; Malick, D. K.; Rabuck, A. D.; Raghavachari, K.; Foresman, J. B.; Ortiz, J V.; Cui, Q.; Baboul, A. G.; Clifford, S.; Cioslowski, J.; Stefanov, B. B.; Liu, G.; Liashenko, A.; Piskorz, P.; Komaromi, I.; Martin, R. T.; Fox, D. J.; Keith, T.; Al-Laham, M. A.; Peng, C. Y.; Nanayakkara, A.; Challacombe, M.; Gill, C. M. W.; Johnson, B.; Chen, W.; Wong, M. W.; Gonzalez, C.; Pople, J. A. Gaussian, Inc., Wallingford CT, 2004.
[50] Ziessel, R.; Bonardi, L.; Ulrich, G. *Dalton Trans*. **2006**, *23*, 2913.
[51] Ziessel, R.; Goze, C.; Ulrich, G.; Céario, M.; Retailleau, P.; Harriman, A.; Rostron, J. P. *Chem Eur. J*. **2005**, *11*, 7366.
[52] Benniston, A. C.; Copley, G. *Phys. Chem. Chem. Phys*. **2009**, *11*, 4124-4131.
[53] Berera, R.; Van Grondelle, R.; Kennis, J. T. M. *Photosynth Res*, **2009**, *101*, 105-118
[54] Savikhin, S.; Vanamerongen, H.; Kwa, S. L. S.; Van Grondelle, R.; Struve, W. R. *Biophys. J*. **1994**,*66*, 1597.
[55] http://www.lbl.gov/Science-Articles/Archive/sabl/2007/Jul/quantumSecrets.html
[56] http://www.photobiology.info/Yocum-PRC_files/Fig3.gif
[57] Lee, H.; Cheng, Y. C.; Fleming, G. R. *Science*. **2007**, *316*, 1462.
[58] Sundström , V.; Pullerits, T.; Van Grondelle, R, *J. Phys. Chem. B*. **1999**, *102*, 2327.
[59] For early reviews on ultrafast spectroscopy please refer to: (a) Jimenez, R.; Fleming, G. R. *Ultrafast spectroscopy of photosynthetic systems*. In: Amasz, J.; Hoff, A. J (eds) *Biophysical techniques in photosynthesis. Advances in photosynthesis and respiration* (Series ed. Govindjee), vol 3, Springer, Dordrecht, pp 63-73. (b) Groot, M. L.; Van Grondelle, R.; *Femtosecond time-resolved infrared spectroscopy*. In: Aartsma, T. J.; Mataysik (eds) *Biophysical techniques in photosynthesis, volume II. Advances in photosynthesis and respiration*, vol 28. Springer, Dordrecht. 2008. pp 191-200 (c) Zigmantas, D.; Read, E. L.; Fleming, G. R. *Non-linear femtosecond optical spectroscopy in photosynthesis*. In: Aartsma, T. J.; Matysik, J. (ed) *Biophysical techniques in photosynthesis, volume II. Advances in photosynthesis and respiration*, vol 26. Springer, Dordrecht. **2008**. pp 201-222
[60] Hattori, S.; Ohkubo, K.; Urano, Y.; Sunhara, H.; Nagano, T.; Wada, Y.; Tkachenko, N. V.; Lemmetyinen.; Fukuzumi, S. *J. Phys. Chem. B*. **2005**, *109*, 15368.
[61] Verhoeven, J. W. *J. Photochem. Photobiol*. **2006**, *7*, 40.
[62] Harriman, A.; Mallon, L. J.; Ullrich, G.; Ziessel, R. *ChemPhysChem*. **2007**, *8*, 1207.
[63] Benniston, A. C.; Hagon, J.; He, X.; Lemmetyinen, H.; Tkachenko, N. V.; Clegg, W.; Harrington, R. W. *Phys. Chem. Chem. Phys*. **2012**, *14*, 3194.

[64] Isosomppi, M.; Tkachenko, N. V.; Efimov, H.; Vahasalo, H.; Jukola, J.; Vainiotalo, P.; Lemmetyinen, *Chem. Phys. Lett.* **2006**, *430*, 36.
[65] Benniston, A. C.; Harriman, A. *Chem. Soc. Rev*. **2006***, 35,* 167.

Chapter 6

Alternative methods for bodipy synthesis and the preparation of a binaphthalene-spaced dyad.

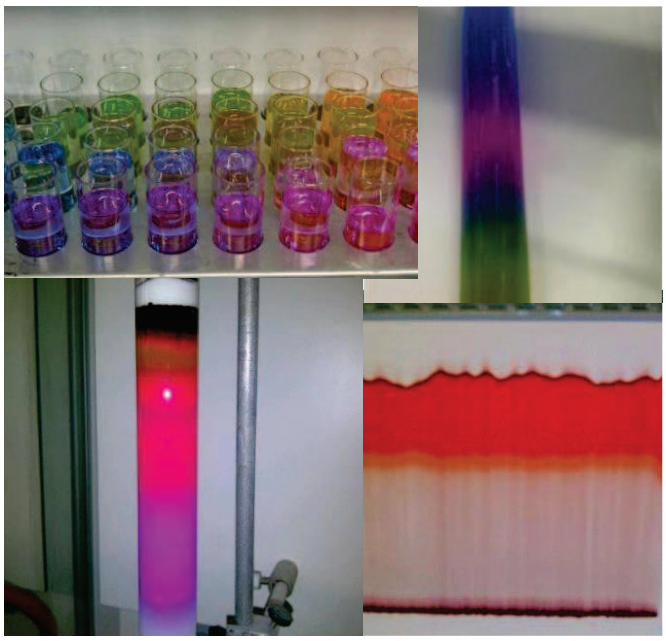

The structures and names of the bodipy compounds to be discussed within this chapter are given in *Figure 1*. The nomenclatures used are as follows: BR = bromine, N = naphthalene, BD = bodipy, TOL = toluene, PH = phenyl, DMA = dimethylaminophenyl and BN = binaphthalene, H = hydrogen.

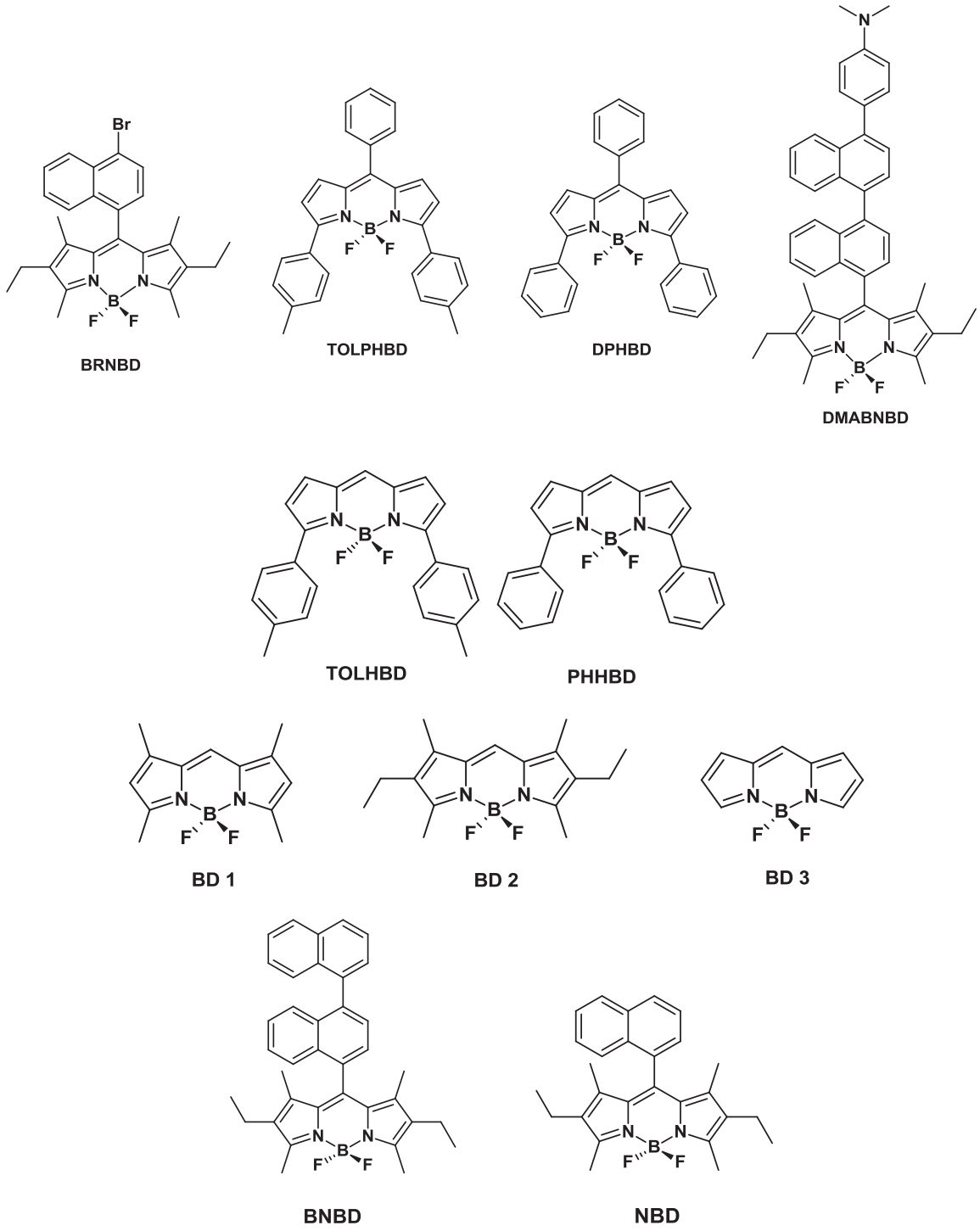

Figure 1 – The bodipy compounds discussed within chapter 6 and their naming.

6.1 Introduction

6.1.1 The bridging unit

As briefly discussed within the previous chapter, future projects to be carried out within the MPL will involve investigation into changes observed in electron transfer dynamics upon incorporation of chiral bridging units into donor-acceptor dyads. For comparative studies and in order to generate a reference compound and complete the series of dimethylaminophenyl derivatives, the final project undertaken is the synthesis of a novel binaphthalene-spaced bodipy dyad. The strapping unit is omitted in order that the spacer moiety can gyrate freely. As aforementioned, incorporating a bridging unit between donor and acceptor in molecular assemblies permits control of the angles and the distance between the two sites. This in turn governs both the efficiency and the rate of long-range electron transfer and charge recombination processes[1]

Work by Rikken *et al.* exploring the issue of magneto-chiral anisotropy[i] using macroscopic electrodes manipulated to generate helical wires, suggests that "the electrical resistance of any chiral conductor should depend linearly both on the external magnetic field and the current through the conductor and on its handedness." Investigating such theories on a molecular scale proved to be a fascinating concept and a pair of novel D-Sp-A dyads, incorporating inherently chiral tethered spacer units was recently developed within the MPL[ii]. The spacer comprised a strapped 2,2'-dialkoxybiphenyl moiety connecting two metal-terpyridine units (ruthenium(II) or osmium(II) bis-2,2':6',2"-terpyridine), with the torsion angle between the two phenyl rings and the internal flexibility being directly modulated by the length of the strap.

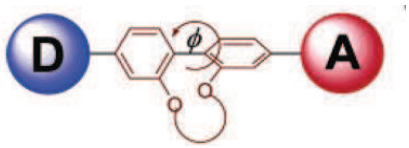

Figure 2 - The change in torsion angle (ϕ) that can be generated by permitting varying degrees of twisting through modification of chain length in an alkoxy- strap.

Applications of such strapped donor-acceptor dyads include optical materials and electronic switches. In the case of the latter, the importance of the tunnelling of electrons through π and σ bonds must be evaluated. In the tethered biphenyl linked

Ru-Os complexes discussed, this was accomplished by comparison of the magnitude of the matrix coupling element, V_{DA}, of both perpendicular and parallel geometries of a 2,2'-dialkoxybiphenyl unit. V_{DA} is related to electron tunnelling through the potential barrier between donor and acceptor and shows an exponential dependence upon the distance between the two moieties, if this barrier is more or less uniform:

$$\mathbf{V_{DA} \alpha \exp[-\gamma R]}$$

where γ is the parameter characterizing electron tunnelling.

However, when a heterogeneous medium exists between donor and acceptor, V_{DA} depends upon the arrangement of particles located between the two and therefore in such bridged species, the particles in question effectively permit a route via which electrons can 'tunnel' by using unoccupied electronic levels.[4]

Over the past decade, numerous theoretical[4] and experimental[5] studies have investigated how the geometry of the spacer unit can determine the magnitude of V_{DA}. Common spacing units incorporated into such dyads include aryls, alkynyls and allyls with simple alkyls also being used but less commonly so. Electron transfer along aromatic units such as polyphenylenes[6] demonstrates increased efficiency in comparison with hydrocarbon chains.[7] Of the aryls, naphthyl and binaphthyl are frequently incorporated units and were the choice moieties for the work discussed within this chapter. This was largely due to the fact that the protocols for resolution are much more firmly established with binaphthyls than for biphenyl species, and the control compound should be as similar as possible to the strapped derivative to be prepared.

6.1.2 Alternative methods of synthesising bodipy systems

This chapter also focuses upon an alternative method of synthesising meso-hydrogen bodipy systems. Since the initial synthesis of the fluorophore by Alfred Triebs and co-workers in 1968,[8] numerous alternative synthetic routes have been developed, facilitating the preparation of fascinating novel systems. Today, the two most popular methods for generating bodipy complexes, namely the acid chloride and aldehyde methods, are based upon the synthetic route employed by Triebs. The slight

modifications and fine-tuning of the syntheses over the years have led to substantial and dramatic improvements in the observed yields. The commercial availability of the starting materials plays a crucial role in the selection of the method to be used, with the corresponding aldehyde typically being far easier to locate than the acyl chloride derivative. The lower reactivity of the former also increases the range of substrates which can be used, as for example, aryl chlorides are too reactive for use with unsubstituted pyrrole.[9]

A recent publication[10] by Burgess and Wu described the preparation of several H-meso bodipy compounds, in which pyrrole derivatives were treated with phosphorus oxychloride, generating the dipyrromethenium cation intermediate. This was then reacted further to give the corresponding bodipy. The mechanism proposed for dipyrromethene formation is given in *Figure 3*. The reaction was followed by ^{1}H, ^{31}P and ^{13}C NMR spectroscopies and continuous UV measurements.

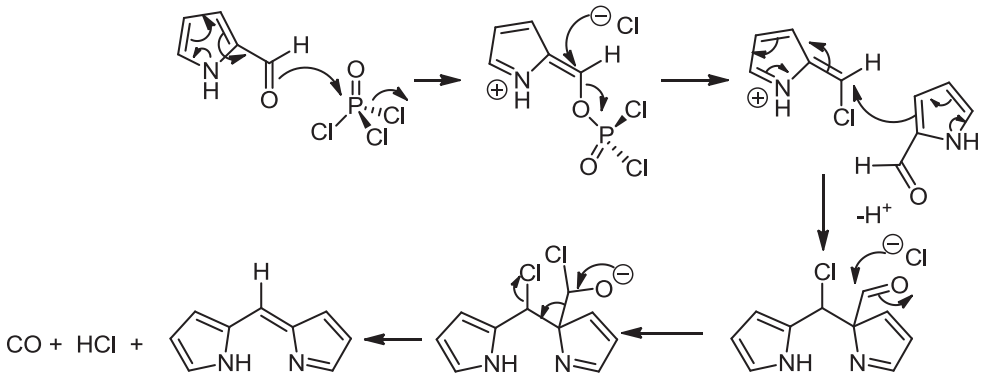

Figure 3 – The mechanism for dipyrromethene formation incorporating phosphorus oxychloride.

Discussed within this Chapter, is a proposed method of bodipy synthesis based upon the ability of the commonly employed reagent/ solvent formamide to undergo protonation in the presence of TFA. The final step is the proposed elimination of ammonium to generate the dipyrromethene unit. This gave promising results using a series of commercially available pyrrole derivatives, and further research is currently underway to improve upon both the yields gained and the range of pyrroles tested.

6.2 Synthesis

6.2.1 Attempted preparation of DMABNBD

In order to complete this project, several synthetic routes were proposed in order to generate the desired product, **DMABNBD**. The initial synthetic strategy designed and attempted is outlined in *Scheme 1*.

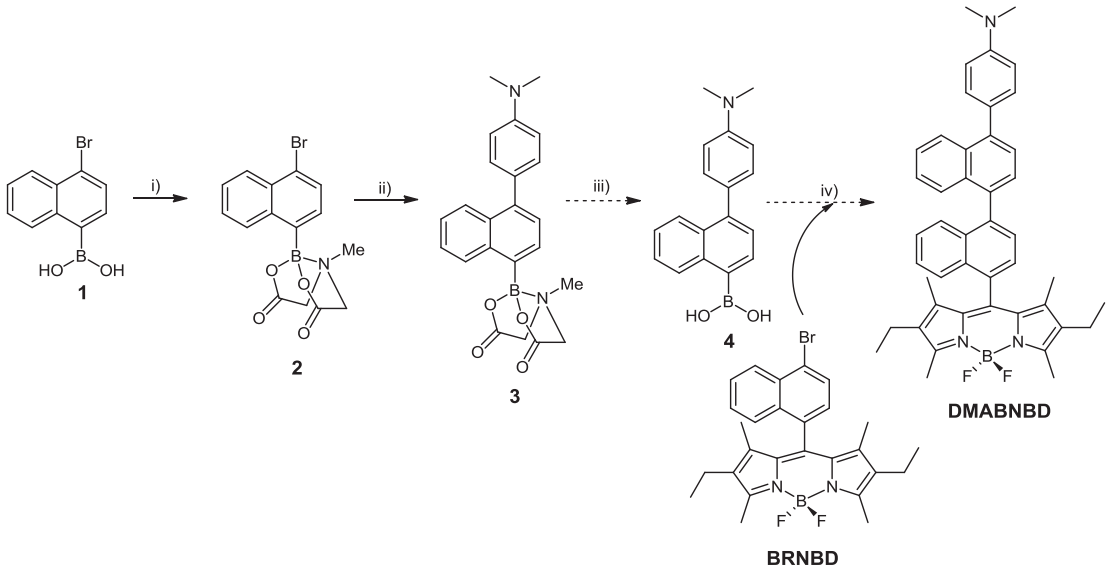

Scheme 1 - The initial synthetic strategy designed and attempted to prepare **DMABNBD**.

Reagents: i) N-Methyliminodiacetic acid, DMSO/ toluene (1:10), Dean-Stark ii) Dimethylaminophenylboronic acid, Na_2CO_3 (2.0M), $PdCl_2(PPh_3)_2$, THF, reflux iii) NaOH iv) Na_2CO_3 (2.0M), $PdCl_2(PPh_3)_2$, THF, reflux.

This synthetic route was very much dependent upon the success of a novel protecting group to allow a coupling reaction to take place at one location, whilst protecting the second reactive functionality. Thus, the first step of the synthesis was protection of the commercially available 4-bromo-1-naphthalene boronic acid (**1**) with *N*-methyliminodiacetic acid (abbreviated to MIDA) to generate the boronic acid surrogate **2**. [11] This is a current and convenient method of protecting the boronic acid functionality in a molecule which also contains another 'active' group at a different position. Elegant syntheses can be carried out using the MIDA boronate platform[12]. Here, it meant that reaction (e.g., Suzuki coupling) could be achieved at this 'active' position (a bromine atom in this case) without interference with the boronic acid

functionality. The protecting group can be removed quickly and easily by stirring in a solution of sodium hydroxide. This protection reaction was successfully achieved in 90% yield using DMSO/ toluene as solvent and fitting a Dean-Stark trap to remove water. The DMSO was later removed on a Kugelrohr. One problem encountered, however, was that even after the sample was heated in a small tube under high vacuum, a small quantity of residual DMSO remained. The next step of the synthesis involved a Suzuki coupling and although it is not uncommon to carry out a reaction of this type in DMSO, it was found that a complex mixture of products was generated. None of the isolated products appeared to be the desired material. The reaction was also repeated omitting the work up step and instead, the Suzuki coupling reagents were added to the degasssed solvent mixture. Unfortunately, again this proved to be unsuccessful and left only unreacted starting materials. An alternative reaction pathway was therefore devised according to *Scheme 2*.

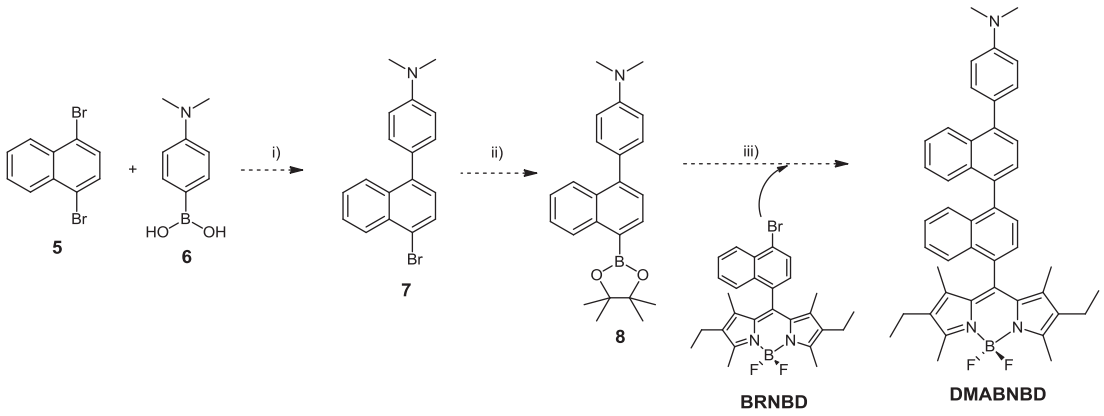

Scheme 2 – The second synthetic route devised towards **DMABNBD**.
Reagents: i) $PdCl_2(PPh_3)_2$, Na_2CO_3 (2.0M), THF, reflux ii) $PdCl_2(CH_3CN)_2$, S-Phos, NEt_3, pinacolborane, dioxane, 80˚C iii) $PdCl_2(PPh_3)_2$, Na_2CO_3 (2.0M), THF, reflux.

The first step attempted involved coupling of 1,4-dibromonaphthalene (**5**) with dimethylaminophenyl boronic acid (**6**) in a 1:1 ratio. It was hoped that addition of the dimethylaminophenyl unit would deactivate the ring to attack at the second bromine atom, ensuring monosubstitution. This would then permit conversion of the second bromine atom to a boronic ester using the coupling conditions developed for the synthesis of julolidine boronic acid discussed in the previous chapter. Finally,

coupling of this compound with **BRNBD** would be affected to generate the desired doubly-spaced compound.

After thorough research on the area, a catalytic system studied and developed by Buchwald *et al.*[13] was tested on the commercially available components, 1-bromonaphthalane (**9**) and naphthalene boronic acid (**10**) (*Scheme 3*). The coupled product, 1,1'-binaphthyl (**11**), was isolated in good yield (60%) proving that this type of system could successfully couple naphthalene-based substrates. To confirm that this method could be used in conjunction with bodipy compounds, the previously synthesised bromonaphthalene bodipy was coupled with naphthalene boronic acid (*Scheme 4*) to generate the corresponding binaphthalene derivative in good yield (52%). In both cases ^{1}H NMR spectra and GC analysis confirmed the purity of the two compounds.

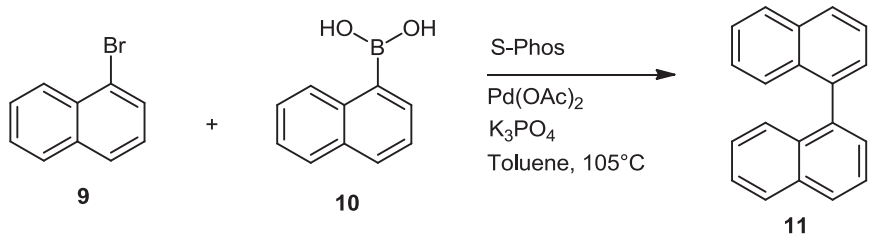

Scheme 3 – The synthesis of 1,1'-binaphthyl via Suzuki coupling.

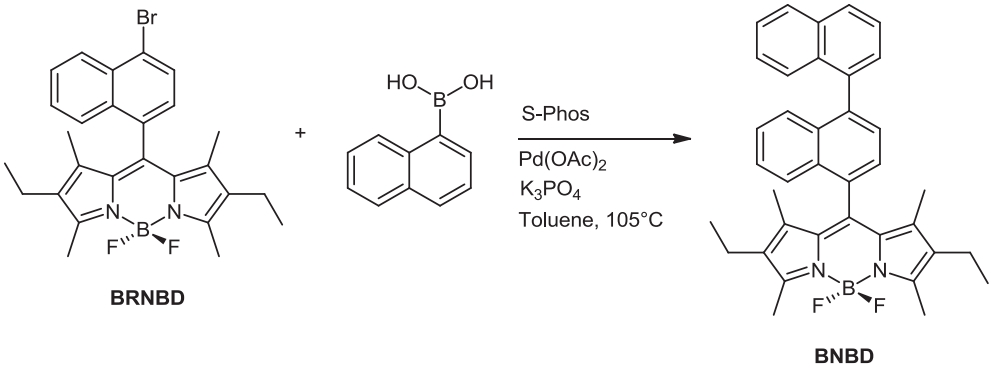

*Scheme 4 – The coupling of **BRNBD** and 1-naphthalene boronic acid under Suzuki conditions.*

Unfortunately in the case of the 1,4-dibrominated (**5**) starting material (*Scheme 2*) it was observed by GC that the quantity of desired product formed in this synthesis was negligible, and both the GC spectrum and TLC analysis showed that much starting

material remained. This reaction was repeated numerous times altering the base and solvent but to no avail. Therefore, an alternative method was tested.

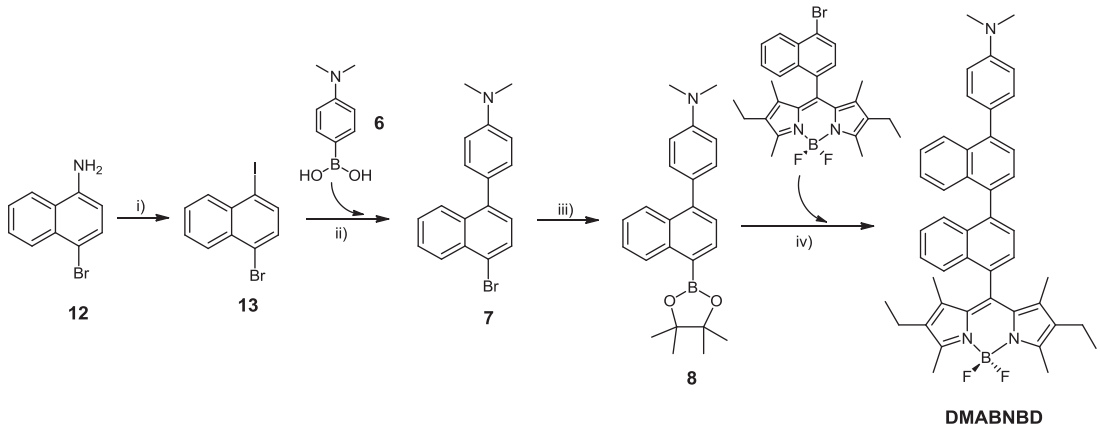

Scheme 5 – The final successful synthetic route devised for preparation of **DMABNBD**.

Reagents and Conditions: i) HCl, $NaNO_2$, 0˚C, KI ii) $PdCl_2(PPh_3)_2$, Na_2CO_3 (2.0 M), THF, reflux iii) $PdCl_2(CH_3CN)_2$, S-Phos, NEt_3, Pinacolborane, dioxane, 80˚C. i) $PdCl_2(PPh_3)_2$, Na_2CO_3 (2.0M), THF, reflux.

This final method required 1-iodo-4-bromonaphthalene (**13**) which was synthesised in high yield via a method[14] developed within the MPL from compound **12**. This new synthetic route was inspired by work carried out by Pratap *et al.,*[15] which involved selective coupling at an iodo group in the presence of a bromine atom at the ortho position. It was hoped that the method could also be applied to iodinated aromatic systems possessing a para bromine atom, as both the catalyst (tetrakis triphenyl phosphine palladium (0)) and the base (sodium carbonate) used by the Pratap group are cheap and readily available.

The Suzuki coupling of bromo-4-iodonaphthalene (**13**) with dimethylaminophenyl boronic acid (**6**) was tested using three different palladium catalysts. S-Phos in conjunction with the palladium acetate catalyst was tested first which gave the desired product. However, it was noticed that yields were improved greatly (99%) when simple tetrakis triphenylphosphine palladium(0) or dichlorobis(triphenylphosphine) palladium(0) were used as the catalyst in THF/water as solvent. It is thought that the addition of water to fully solubilise the base could be important in gaining a good yield in this reaction.

Compound **7** was then converted into the boronic ester (**8**) under those conditions previously discussed within Chapter 5 which uses pinacolborane as the borylating agent and a palladium nitrile-based catalyst. The product was synthesised easily and cleanly but unfortunately the yields were very low (~10%). In spite of this, the reaction was repeated and enough material isolated to continue onto the next step which was the appendage of the bodipy unit. Again, sodium carbonate (2.0 M) and $PdCl_2(PPh_3)_2$ were used and coupling was achieved with ease. Purification by silica gel chromatography (DCM: petrol (1:1)) to remove unreacted **BRNBD** gave the pure product which was fully characterised.

6.3 Alternative Synthesis of Meso-bodipy Derivatives

6.3.1 Novel strategies and new findings

Whilst researching possible synthetic routes, which could be developed in order to prepare the binaphthalene spaced product, a novel and convenient method of synthesising bodipy compounds was encountered. This strategy was developed from the desire to generate the bodipy framework with a halogen atom (bromine or iodine) in the meso position. This would provide a suitable counterpart to affect Suzuki coupling of boronic-acid or -ester derivatives at this site. It was therefore planned that the meso amino substituted bodipy (**AMBD**) would be synthesised. This would then be subjected to a one pot procedure by which this amine would be converted to the diazonium salt and finally substituted to incorporate the halogen (*Scheme 6*). For this, the conditions developed by Dr. S. Mitchell and used later to synthesise 1-bromo-4-iodonaphthalene from 1-amino-4-bromonaphthalene could be used.

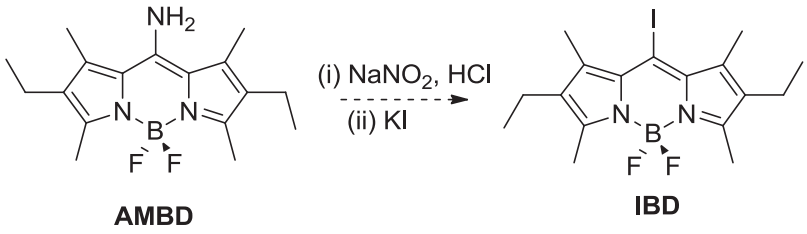

Scheme 6- Synthesis of meso-iodo bodipy from the amino counterpart.

Synthesis of this type of directly functionalised meso-bromo or –amino bodipy had not been carried out previously in our group and was not a well documented procedure in the literature. One known method by which meso-anilino bodipy derivatives can be prepared involves preparation of thiomethyl substituted bodipy followed by a subsequent amination reaction[16] as detailed in *Scheme 7*.

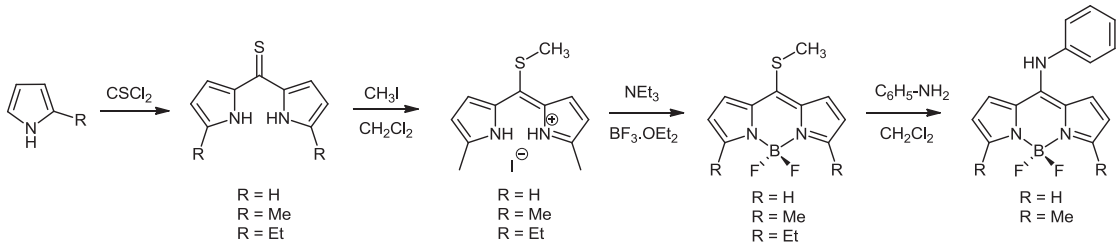

Scheme 7[26] *- The synthetic route developed by Goud et al. which proceeds via the thiomethyl substituted dipyrromethenium salt.*

However, this was a slightly unappealing route due to the highly toxic nature of the thiophosgene starting material. It should be noted that earlier this year, several amino bodipy derivatives were generated via this method[17], including 8-amino bodipy using ammonium acetate (*Scheme 8*).

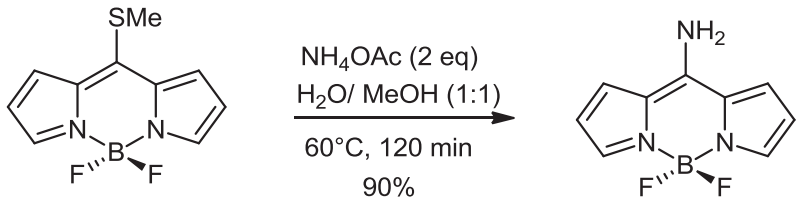

Scheme 8 – Synthesis of 8-amino bodipy from the thio-methyl substituted starting material.

One reagent that was considered to possess the ability to deliver the amino group was formamide; a cheaply and commercially available reagent commonly used as a solvent in organic synthesis. It was hoped that the aldehyde would react in the traditional way to generate the desired bodipy under standard conditions. However, it was seen when the reaction was carried out, that the resulting species generated was in fact not the amino substituted product, but a simple H-meso bodipy in good yield. It was believed, therefore, that the formamide had been protonated at the NH_2 to

generate a good leaving group (ammonium) in accordance with the mechanism shown in *Figure 4*.

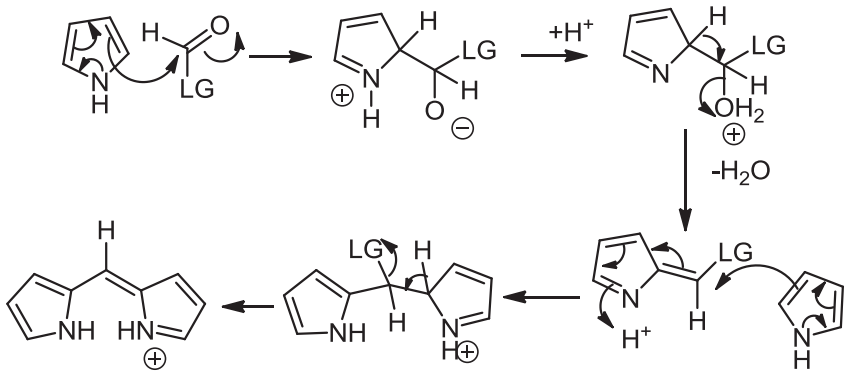

Figure 4 –The proposed mechanism which takes place to generate the dipyrromethenium cation.

It can be elucidated from the mechanism detailed in *Figure 4*, that DDQ is no longer required when this method is used, which immediately removes one step from the synthesis. Overall, this would save time since a bodipy forming reaction is typically stirred overnight following DDQ addition.

Immediately, potential was seen for the generation of H-meso bodipy frameworks using various types of pyrrole derivatives. Whilst investigating reactions, by testing commercially available pyrroles, it was considered that perhaps protection of the amide functionality in formamide may prevent the loss of ammonium, meaning that the desired meso substituted amine could still be generated. Suitable protecting groups for formamide were considered. One option, for which the starting reagent was cheaply available and which is stable to acidic conditions (i.e., it would not be removed upon addition of the trifluoroacetic acid) was methoxybenzyl chloride. This reagent was refluxed with formamide in ethanol overnight, but this method was found to yield 1-(ethoxymethyl)-4-methoxybenzene; i.e., the product of nucleophilic attack of ethanol on methoxybenzyl chloride. It was assumed, therefore, that ethanol is a stronger nucleophile than formamide and an alternative method was tested. This involved simply refluxing methoxybenzyl chloride in a large excess of formamide, which resulted in formation of the desired product in high yield (95%) according to *Scheme 9*.

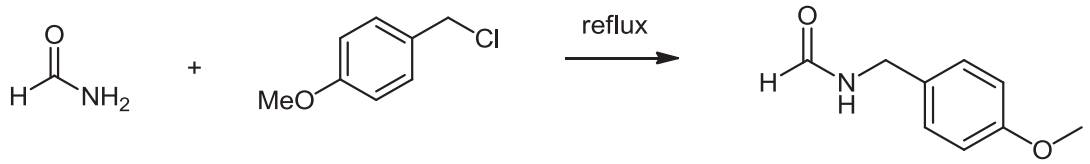

Scheme 9 – The protection of formamide with methoxybenzylchloride to give N-(4-methoxybenzyl)formamide.

However, when the protected species was reacted on to generate the bodipy, again the H-meso substituted species was formed. It was clear that it was going to be more difficult than originally believed to generate the *meso*-halogenated bodipy. Alternative routes were investigated to find a suitable synthetic pathway to the doubly-spaced system. In the meantime, further investigations into using formamide as a bodipy forming reagent were carried out. The table below shows the bodipy species that were prepared using this new method and the corresponding yields. Unfortunately, yields were rather modest at times but this novel synthesis did have the important advantage that the pyrrole used did not require functionalization with an aldehyde group, unlike the higher yielding method developed by Burgess *et al*.

Entry	Pyrrole	Product formed	Yield of desired bodipy(%)
1	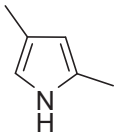	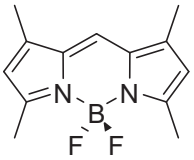	30
2	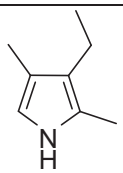	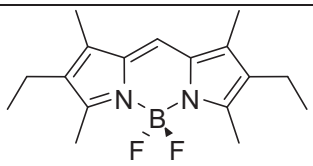	20
3	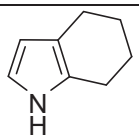	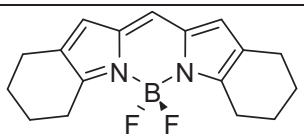 *	~10
4	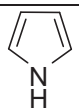	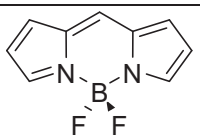	5
5	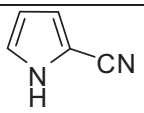	None – entirely starting material	0
6	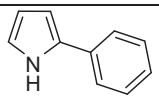	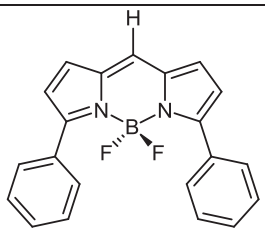	~ 1%
7	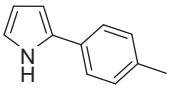	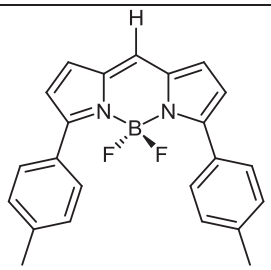	~ 1%
9	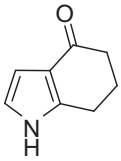	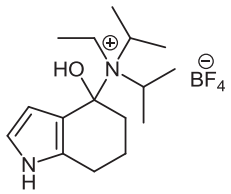	0 – entirely converted to the product shown to the left.

*Table 5 - The pyrrole species tested for their compatibility in the novel 'formamide method' of bodipy synthesis. For those which generated a bodipy, the corresponding yields are quoted. * = please see later in the chapter for an explanation.*

6.3.2 Pyrrole synthesis

Pyrrole is one of the most important simple heterocycles, found in a broad range of natural products and drug molecules and is widespread in nature[18] being the key structural fragment in heme, chlorophyll, numerous secondary metabolites and marine natural products[19]. There are numerous ways of synthesising pyrroles, some of the most common being the multicomponent Hantzsch pyrrole synthesis[20,21,22] based on the reaction between a β-enaminone and a α-haloketone, 1,3-dipolar cycloadditions[23], nucleophillic additions onto nitrile[24,25], carbonyl[26] and amino[27] groups and palladium catalysed methods to synthesise aryl substituted pyrroles. The latter was the method of choice for the synthesis of a small variety of non-commercially available pyrrole derivatives, due to the simplicity of the method and the fact that the starting materials were already available for use in the lab.

Both phenyl[28]- and tolyl-substituted pyrroles were synthesised, with the yields being optimised over several attempts due to the formation of poly-pyrrole during the high temperature reaction. A third pyrrole was also synthesised using a method[29] which proceeds via a nitrovinyl derivative generated by the reaction of an aryl aldehyde with ammonium acetate and nitroethane (acting as reagent and solvent) followed by subsequent reaction of the nitrovinyl species generated with ethyl cyanoisoacetate and DBU in a THF/^{t}BuOH (1:1) mixture. Please refer to *Scheme 10* below. However, this method generates an ethyl ester substituted pyrrole and unfortunately, following reduction with lithium aluminium hydride (sodium borohydride was found not to be a strong enough reducing agent), decomposition occurred on the column. Some starting material was kept and conversion of this into a bodipy was attempted, but complications arose possibly due to unwanted reactions at the ester site, and a complex mixture of products was generated.

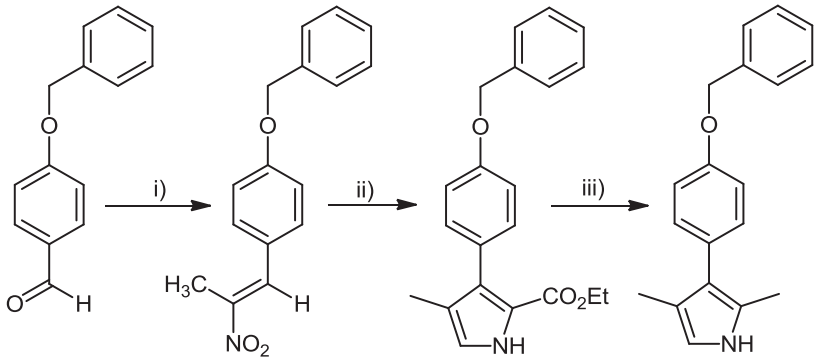

Scheme 10 – Synthesis of a novel aryl substituted pyrrole via literature methods. Reagents: i) nitroethane, ammonium acetate, 60˚C, 14 hrs ii) ethylisocyanoacetate, DBU, ^{t}BuOH: THF (1:1), 60˚C, 14 hrs iii) $NaBH_4$, reflux.

From the table on the previous page (*Figure 5*), it can be seen that the method was limited to activated pyrroles, i.e., those possessing uniquely alkyl substitution, whilst pyrroles with aryl groups directly appended at the 2 position struggled to react at all. In the case of the phenyl- and tolyl- substituted pyrrole, prepared via the palladium catalysed coupling, the characteristic bodipy colour (deep pink for these species) could clearly be seen in the flask and on TLC. But from NMR (^{1}H, ^{19}F, ^{13}C and ^{11}B) spectroscopic studies, it appeared that the yield was negligible. It seemed confusing exactly why these pyrroles did not react, and in order to negate the possibility of there being an issue with the purity of the compounds, they were tested in an alternative bodipy synthesis using benzaldehyde as opposed to formamide. DDQ was incorporated as oxidant according to traditional methods. These formed the meso-phenyl substituted compounds, again in low yield, but this time in a more acceptable quantity. These bodipy derivatives are highly conjugated and unknown in the literature and analysis of the photophysical characteristics of these two compounds could prove to be interesting.

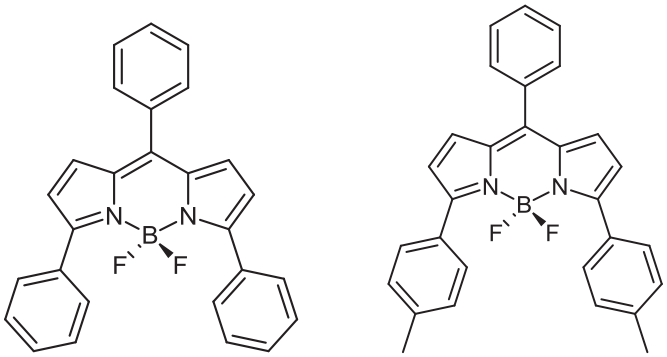

Figure 6 - The meso phenyl substituted bodipy compounds prepared using benzaldehyde via traditional methods.

One reaction, however, generated a confusing bodipy which will be named **BOD-X** from hereon in. This was the reaction of 4,5,6,7-tetrahydro-1H-indole, generated by the reduction of 1,5,6,7-tetrahydro-4H-indol-4-one**.**

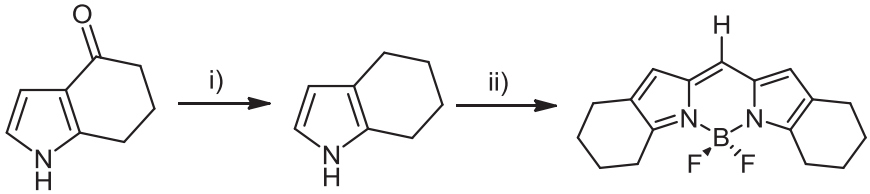

Scheme 11 – The reduction of 1,5,6,7-tetrahydro-4H-indol-4-one followed by the reaction to prepare the desired bodipy using formamide. Reagents and Conditions: i) $NaBH_4$, 2-propanol, 24h, 90˚C, ii) formamide, DCM, TFA, N,N'-DIPEA, $BF_3.Et_2O$. RT.

Although the typical fluorine quartet was present in the product, the spectrum (*Figure 7*) also featured an additional peak at around –55 ppm. The ^{11}B NMR spectrum on the other hand showed the characteristic triplet, although it was slightly upfield of its typical δ = -0.5 to 0.5 ppm location.

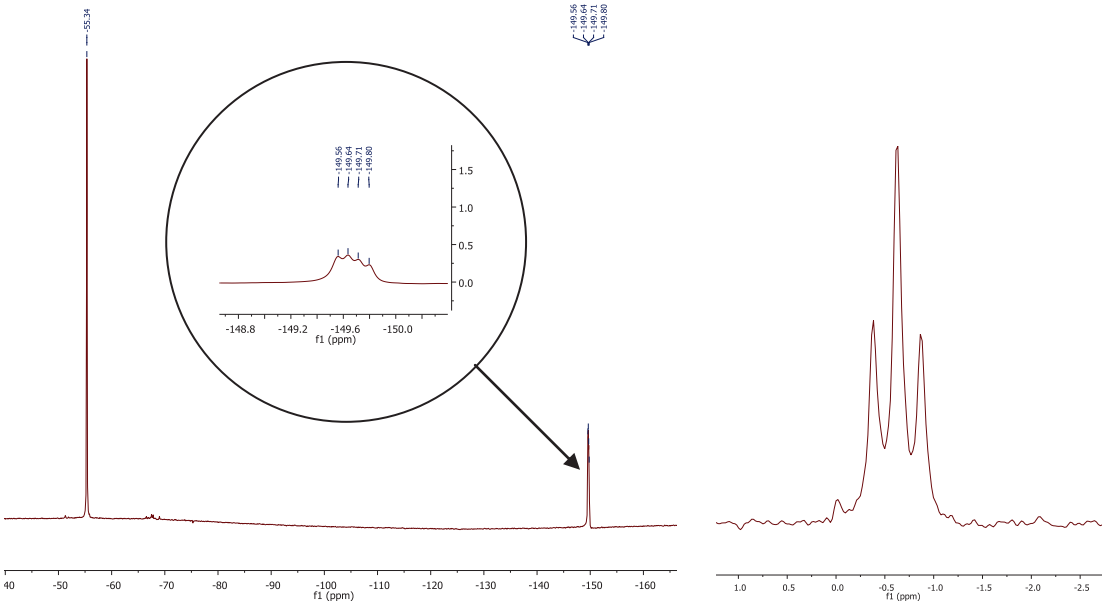

*Figure 7 – The ^{19}F NMR spectrum for **BOD-X** showing the two discrete fluorine peaks (left) and the ^{11}B spectrum displaying the typical triplet multiplicity (right).*

It is difficult to clarify the identity of the second peak with certainty. *Figure 8* shows chemical shifts of common fluorinated derivatives, but the only reagents used in the synthesis in addition to boron trifluoride diethyl etherate (which it cannot be as the chart shows that the BF_3 unit resonates at around -125 ppm) is trifluoroacetic acid. However, the catalytic quantity used, and the fact that this would almost undoubtedly have been neutralised by the amine base, makes this a very unlikely candidate.

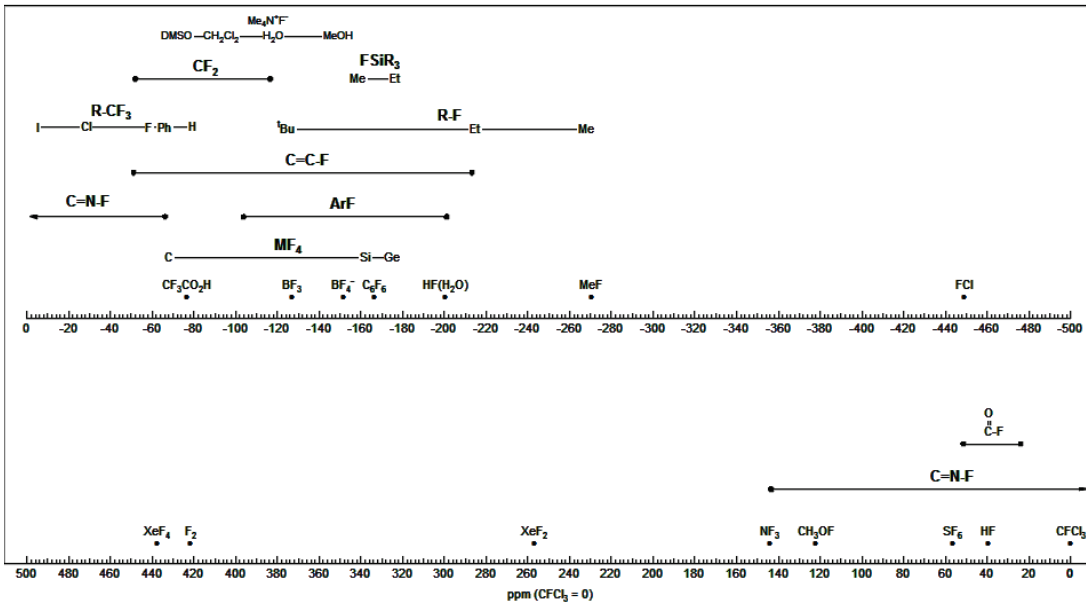

Figure 8- Chemical shifts of common fluorinated derivatives. [30]

In addition, the integration of the ^{1}H NMR spectrum was also inconsistent with the structure of the desired product.

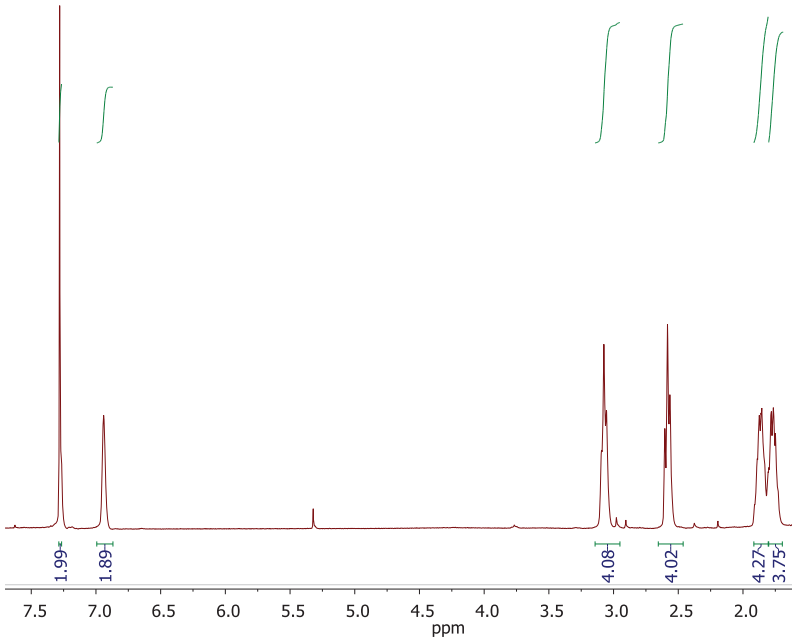

*Figure 9 - Integrated ^{1}H NMR spectrum of **BOD-X** in $CDCl_3$ at room temperature.*

In the ^{1}H NMR spectrum (*Figure 9*), the indole shifts are in the correct location, and the sample was bright pink/ purple in colour, typical of a bodipy compound. However, the proton spectrum had an unusual integration, with the peak which typically corresponds to the bodipy meso hydrogen integrating to two protons instead of one. It is unlikely that the peak, which appears at δ = 6.97 ppm, corresponds to protons on the pyrrole backbone. As seen from the table below, the chemical shift is typical for a bodipy meso hydrogen.

Compound	**^{1}H Chemical shift of meso H (ppm)**
1[20]	6.98
2[20]	6.86
3[31]	6.92
4[20]	7.05

Table 1 – Chemical shift values of meso hydrogens in a selection of bodipy compounds.

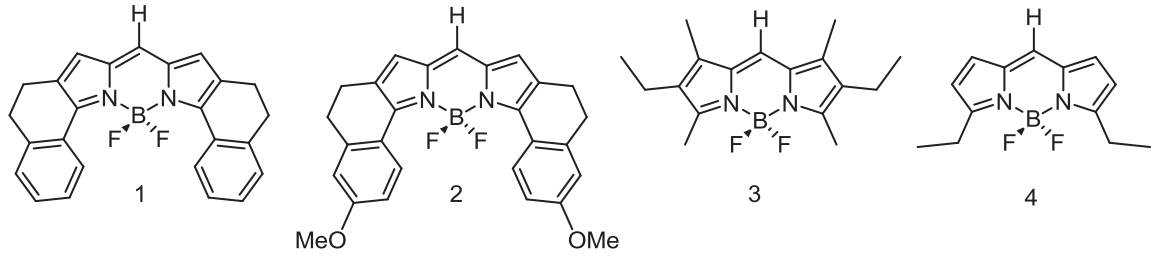

Figure 10 - Various meso-substituted bodipy compounds for which the meso-H chemical shift is known.

A ^{13}C NMR spectrum was also recorded. Due to the scale of the reaction, only a small quantity of product was isolated and the spectrum was therefore recorded on a 500 MHz spectrometer. It can be seen (*Figure 11*) that there are the correct number of carbon atoms, but they are inconsistent with published ^{13}C chemical shifts for this compound:

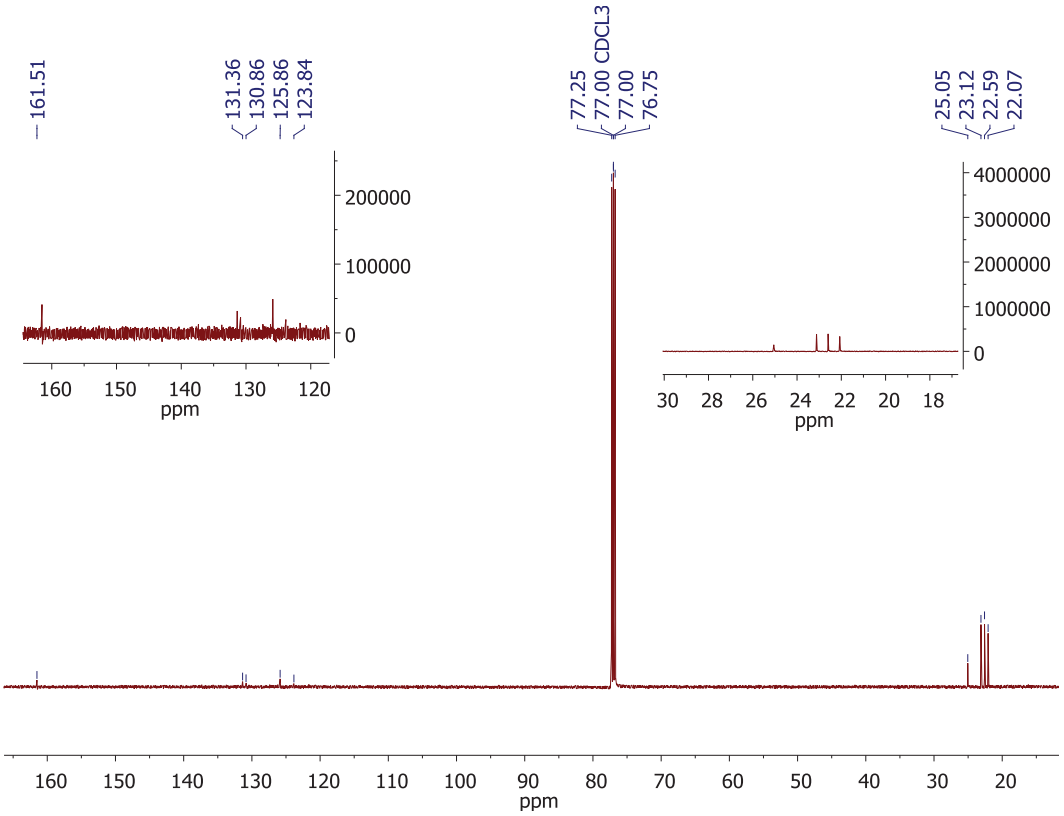

*Figure 11 – A 500 MHz ^{13}C NMR spectrum of **BOD-X** with expansions of the aliphatic and aromatic region (peaks enhanced for clarity).*

^{13}C Chemical shift recorded (aromatic)	^{13}C Literature chemical shift (aromatic)	^{13}C Chemical shift recorded (aliphatic)	^{13}C Literature chemical shift (aliphatic)
161.5	158.0	25.1	24.7
131.4	134.0	23.1	23.1
130.9	129.3	22.6	22.8
125.9	125.9	22.1	22.3
123.8	125.3		

Table 2 – A comparison of the literature[20] chemical shifts and those recorded relative to $CDCl_3$ centred at 77.00 ppm.

Although the literature chemical shifts and those recorded are similar, those corresponding to the aromatic carbons are by no means close enough for the products to be identical. Therefore it can be assumed that a slightly different product was produced. Further investigation is currently underway to further elucidate the structure of this compound.

Disappointingly, the scope of the formamide method is rather limited. After originally discovering the new method, it was believed that it could be used to provide an excellent route to some more unusual bodipy compounds based on purpose designed pyrroles. It is hoped that future work to further elucidate the mechanism of the formamide method (for example by incorporation of deuterium into formamide and monitoring the reaction progress via ^{1}H NMR spectroscopy) may result in unequivocal identification of **BOD-X**. Furthermore, variation of the temperature, solvent and acid used would hopefully also further improve the scope of this method. For example, Lewis acids such as indium chloride or boron trifluoride diethyl etherate could be used preferentially to the commonly used Brønsted acid of TFA. A greater range of pyrrole derivatives could also be generated to prepare diverse libraries of tailor-made H-*meso* bodipys. It is recognised that these compounds are known to possess a high quantum yield of fluorescence which makes them extremely desirable.

6.4 Characterisation and Structure Confirmation

6.4.1 Crystal Structures

The crystal structures of a selection of the compounds discussed within this chapter are given below. **DPHBD**, 1-dimethylaminophenyl-4-bromonaphthalene (**7**) and **DMABNBD** are included.

6.4.1.1 DPHBD

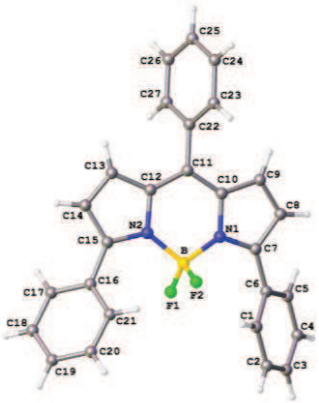

*Figure 11 - the atom labelled crystal structure of **DPHBD***

Crystals of **DPHBD** were readily obtained by slow evaporation of diethyl ether into a saturated dichloromethane solution of the compound. Single crystal X-ray diffraction studies indicate that the meso-phenyl ring in the bodipy compound does not lie completely perpendicular to the indacene plane and instead resides in a slightly offset position, with a torsion angle of 111.12° being observed between the carbon atoms C12, C11, C22 and C23. Similarly, the pyrrole phenyl units exhibit a certain degree of twisting, with torsion angles of 145.06˚ and 131.43˚ respectively being observed between C8, C7, C6, C1 and between C14, C15, C16, C21. The crystal packing diagram shows how the molecules adopt a head-to-tail packing sequence to allow for maximum interaction of the phenyl rings.

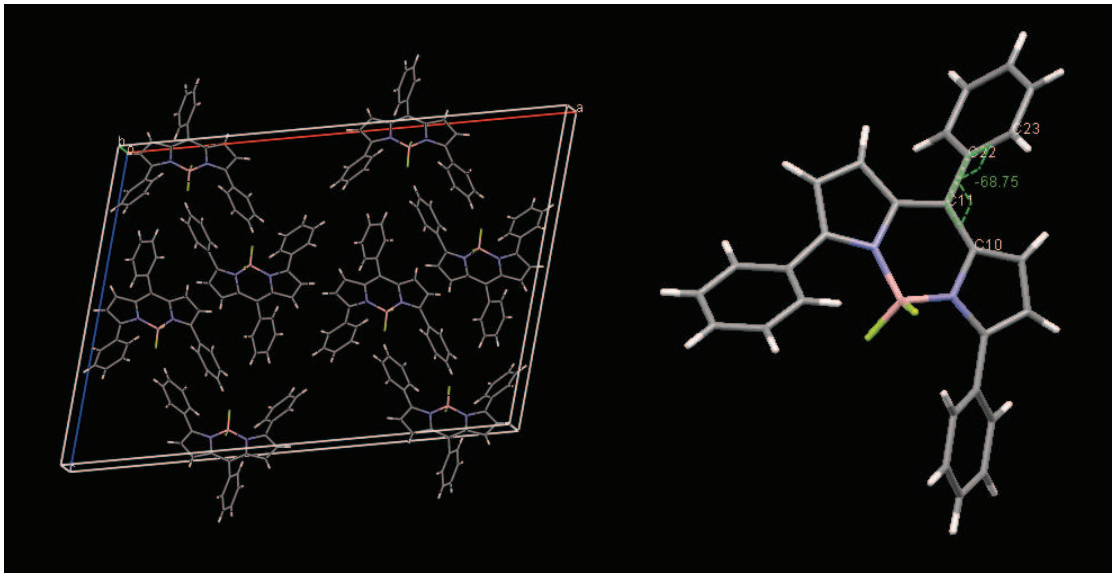

*Figure 12 – Left: The crystal packing arrangement of **DPHBD**: carbon (grey), nitrogen (blue), boron (pink), fluorine (green). Right: torsion angle in **DPHBD** of 68.75°.*

6.4.1.2 1-dimethylaminophenyl-4-bromonaphthalene

Crystallisation of 1-dimethylaminophenyl-4-bromonaphthalene (**7**) was achieved by slow evaporation of petroleum ether into a saturated dichloromethane solution of the compound. Single crystal X-ray diffraction studies indicate again that the phenyl ring lies in a slightly offset position relative to the naphthalene moiety. The torsion angle between C12, C11, C4 and C5 was calculated to be 120.90˚.

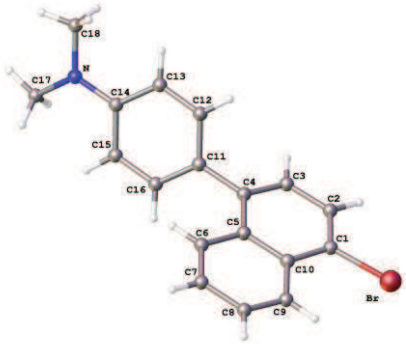

Figure 13 - the atom labelled crystal structure of 1-dimethylaminophenyl-4-bromonaphthalene.

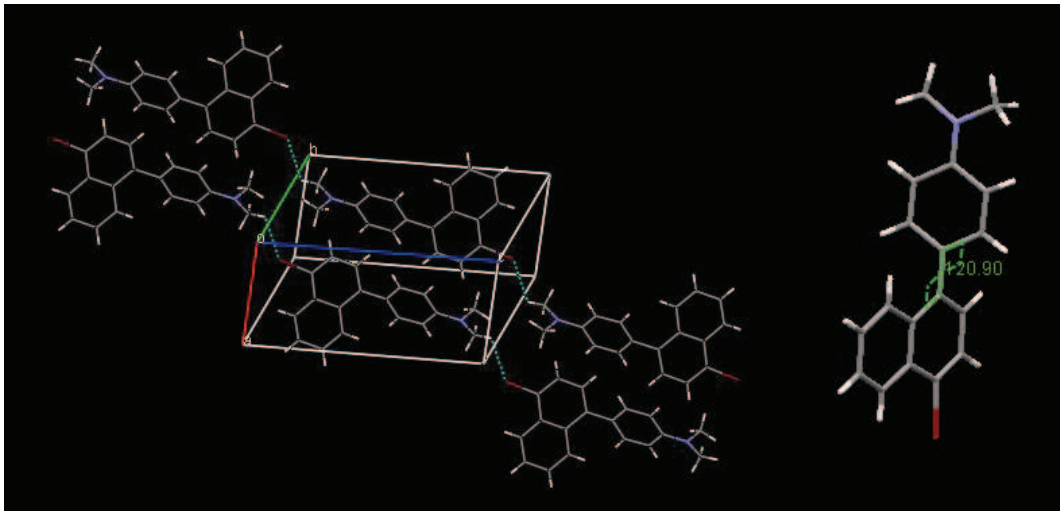

Figure 14 – Left: Molecular packing in the crystal structure of 1-dimethylaminophenyl-4-bromonaphthalene: carbon (grey), nitrogen (blue), bromine (red). Van der Waals interactions between the bromine and methyl hydrogen atoms of the dimethylamino moieties are shown. Right: the torsion angle of 120.90˚.

6.4.2 NMR Spectroscopy

6.4.2.1 Elucidation of ^{19}F spectrum for DMABNBD.

Various fluorine NMR spectra were recorded in $CDCl_3$. The simple ^{19}F NMR spectrum generated initially displayed broadened features, and upon closer inspection, appeared to resemble a possible overlapping doublet of quartets. This can be accounted for by the fact that the two bodipy fluorine atoms are in slightly different environments and therefore inequivalent. The splitting pattern can be attributed to the unsymmetrical nature of the group appended to the meso position, the naphthalene moiety here. The overlap is thought to be occurring due to the proximity of the chemical shift values of the two fluorine atoms relative to their coupling constants. If the spacer was a phenyl ring for example, a simple quartet would be expected, as typically observed in symmetrical bodipy derivatives. However, naphthalene bridged compounds of this type would always be expected to possess a more complex order of symmetry and the spectrum can be described as a second order multiplet. The $^{19}F\{^{11}B\}$ spectrum is shown below:

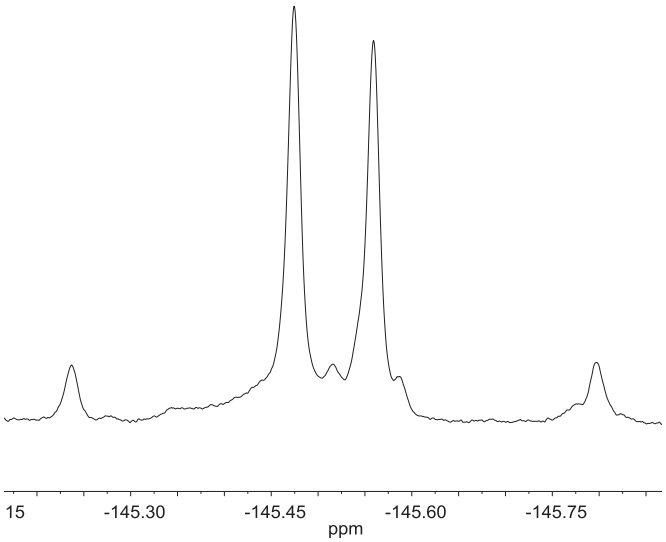

*Figure 15 – $^{19}F\{^{11}B\}$ spectrum of **DMABNBD** in $CDCl_3$* at RT.

All coupling effects related to the ^{11}B nucleus have been removed. The spectrum shows an AB quartet system, meaning that two spin active groups, F_A and F_B, have chemical shifts comparable to J_{AB}. The method by which ν_A and ν_B can be calculated is as follows[32], all chemical shift values have been converted from ppm to Hz:

$\lvert J_{AB} \rvert$	$= (\nu_1-\nu_2)$	$= (\nu_3-\nu_4)$
	= -68351.460 – (-68463.222)	= -68503.054 – (-68615.145)
	= 111.762 Hz	= 112.091 Hz
	= 112 Hz	**=112Hz**

ν_{centre} $= ½ (\nu_2 + \nu_3)$ $= ½ (-68463.222 + (-68503.054))$

$= \mathbf{-68483.138\ Hz}$

$\Delta\nu_{AB}$ $= \sqrt{} (\nu_1-\nu_4)(\nu_2-\nu_3)$ $= \sqrt{}((-68351.460 –(-68615.145))((-68463.222-(-68503.054))$

$= \sqrt{}10503.101$

$\mathbf{= 102.48\ Hz}$

ν_A $= \nu_{centre} + ½\Delta\nu_{AB}$ $= -68483.138 + ½\ 102.48$

$\mathbf{= -68431.898\ Hz}$

ν_B $= \nu_{centre} - \frac{1}{2}\Delta\nu_{AB}$ $= 68483.138 - \frac{1}{2}\ 102.48$ Hz

= -68534.378 Hz

δ_A $= \nu_A$ / MHz $= -68431.898 / 470.62$ Hz

= -145.408

δ_B $= \nu_B$ / MHz $= -68534.378 / 470.62$ Hz

= -145.626

The fluorine spectrum can also be simulated using MestRenova software to further elucidate the splitting pattern observed. This can be done by adding the correct spin groups (two ^{19}F groups (I= ½) and one ^{11}B (I= 3/2)). Unfortunately, this software does not enable us to add the ^{10}B isotope (I = 3) as a forth spin group, so the simulation will not account for the presence of this isotope. δ_A and δ_B as calculated above were inserted into the table. The line widths were approximated from estimation of the peak heights in the recorded (non-simulated) spectrum and the coupling constants were similarly based upon those observed. The spectrum was then recorded on the 500 MHz spectrometer and it can be seen that the simulation has generated a very accurate representation, proving that the effect of the ^{10}B isotope with an abundance of 18.83 % is small.

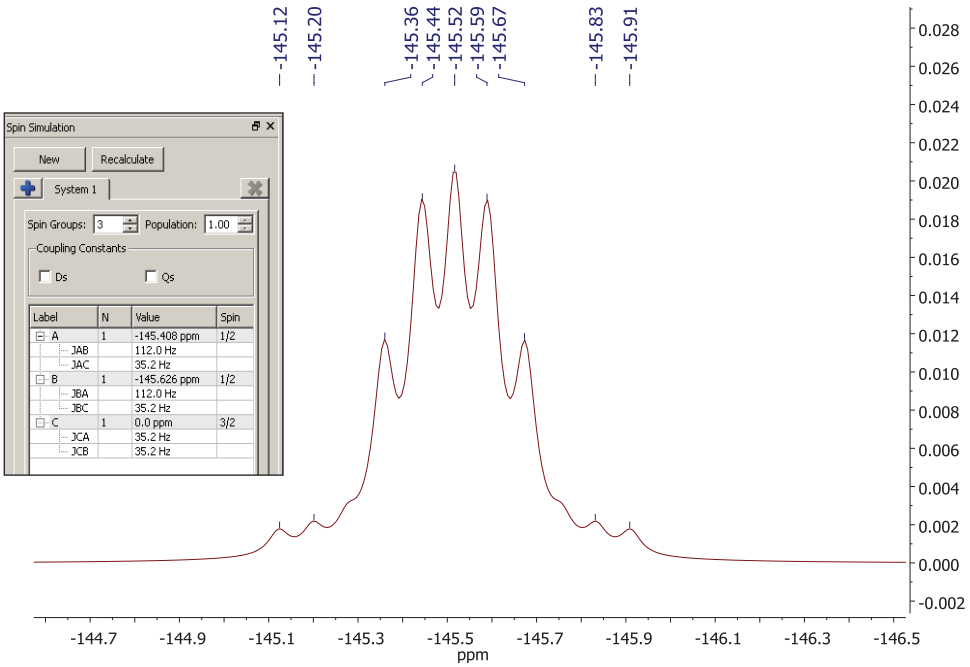

Figure 16 – A spin simulation showing the predicted ^{19}F NMR spectrum calculated using MestReNova software. Insert: The table of parameters used to simulate the spectrum.

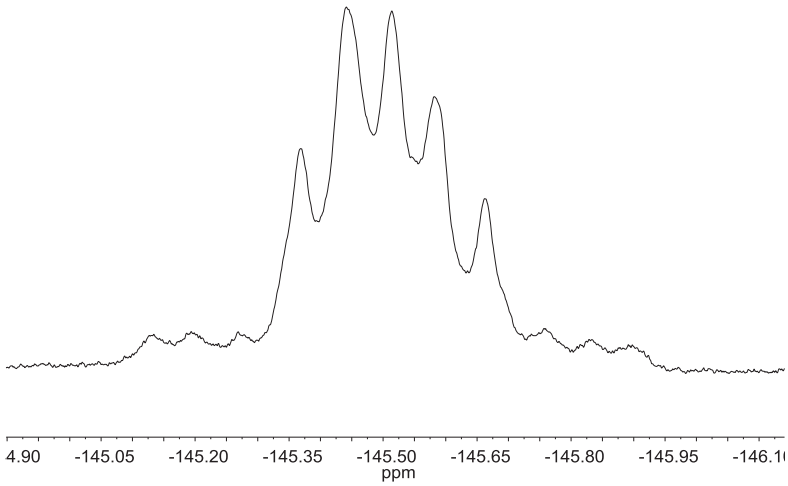

Figure 17 – the ^{19}F spectrum recorded on the 500 MHz spectrometer.

The spin simulation bears a close similarity to the recorded spectrum and it could therefore be deduced that the two fluorine atoms in the bodipy molecule are coupled to each other and have extremely similar chemical shift values.

6.4.2.2 *Interpreted ^{1}H NMR spectra*

The NMR spectra of a selection of the compounds discussed within this chapter are analysed in this section. For **BRNBD** a full analysis is completed and all of the protons and carbons assigned with the exception of one proton set.

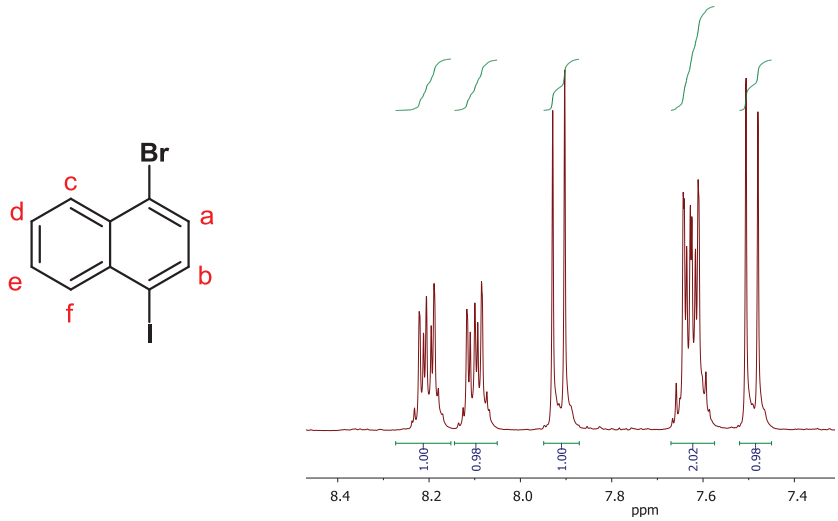

Figure 18 - 400 MHz ^{1}H NMR spectrum for the aromatic region of 1-bromo-4-iodonaphthalene (7) in $CDCl_3$.

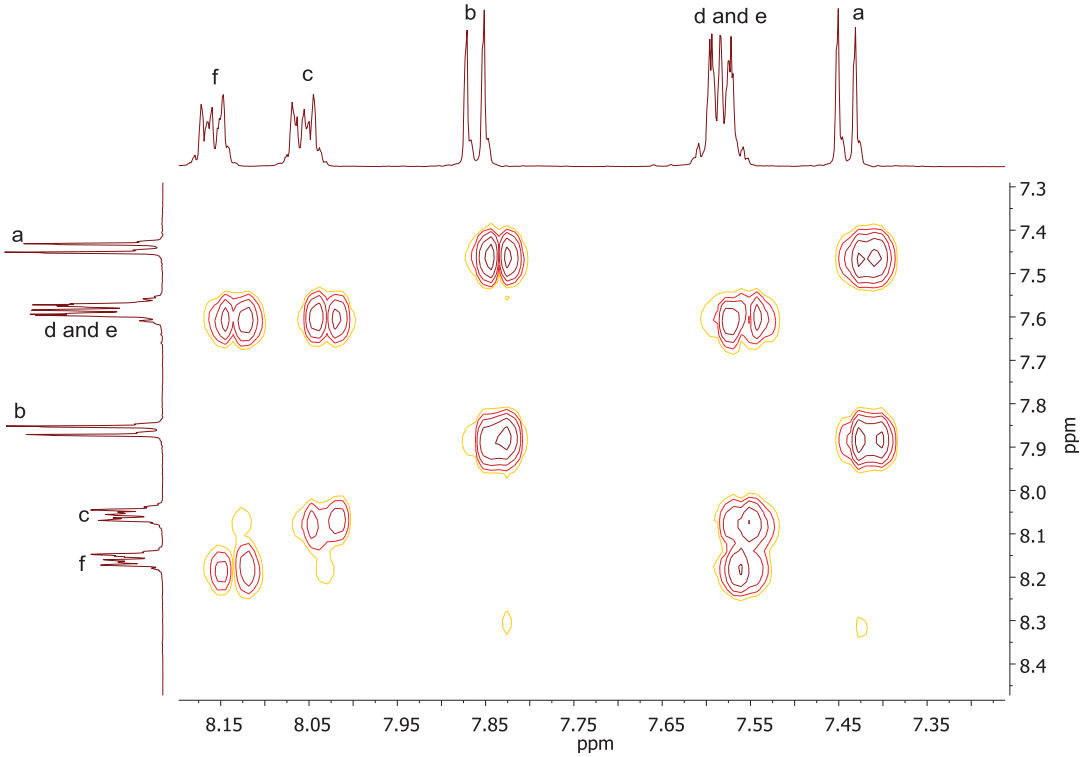

Figure 19 – 400 MHz COSY spectrum of 1-bromo-4-iodonaphthalene in $CDCl_3$.

Chemical shift (ppm)	Intensity (no. of H Atoms)	Multiplicity	Coupling constant (*J*/ Hz)	Assignment
8.2	1	m	N/A	F
8.1	1	m		C
7.9	1	d	7.8	B
7.6	2	m	N/A	D and E
7.4	1	d	7.8	A

Table 3 – The ^{1}H NMR peak assignment for 1-bromo-4-iodonaphthalene.

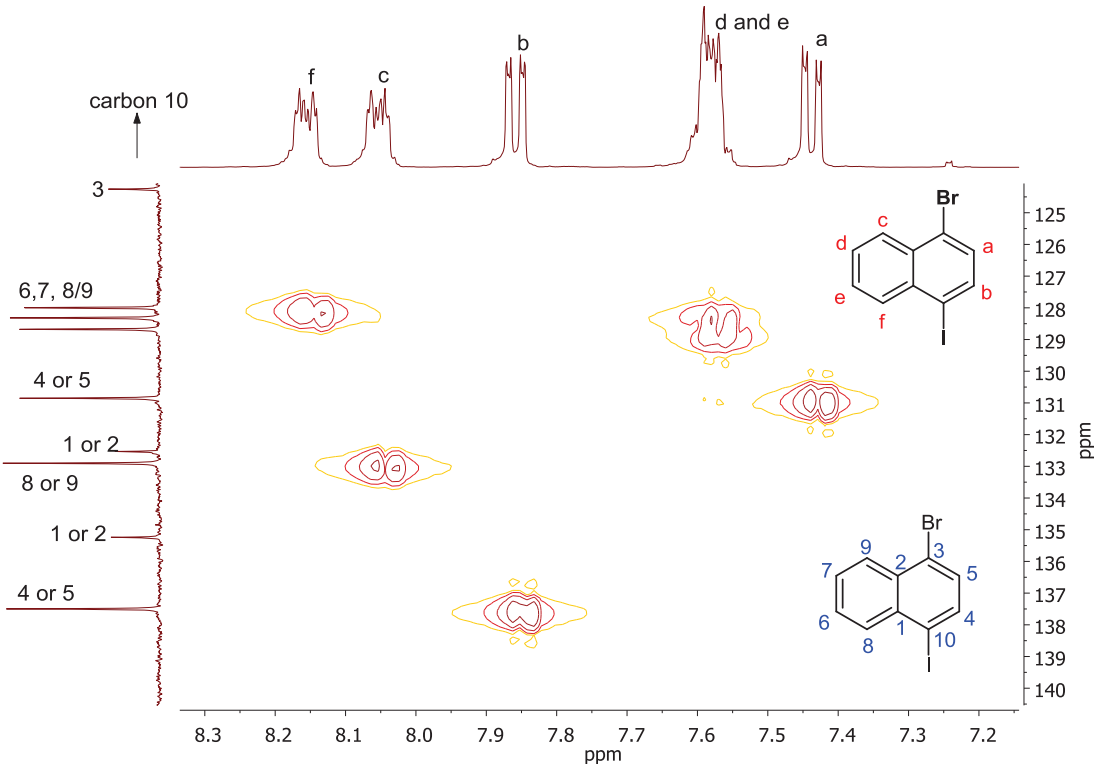

Figure 20 - An HMQC correlation of 1-bromo-4-iodonaphthalene in $CDCl_3$. The proton assignment is given on the structure in red whilst the carbons are shown in blue.

The HMQC can be used to assign the majority of carbon atoms and any ambiguity was resolved by running a simulation of the proton NMR spectrum. This lead to the deduction that proton F is located downfield of C and similarly proton B is downfield of A. It can be seen that carbon 10, to which the iodine atom is attached is up-field shifted relative that to which bromine is attached (carbon 3) and is not included on the spectrum in order to focus on the correlated region of the spectrum more clearly.

Below are a selection of NMR spectra of 1-(dimethylaminophenyl)-4-bromonaphthalene (7).

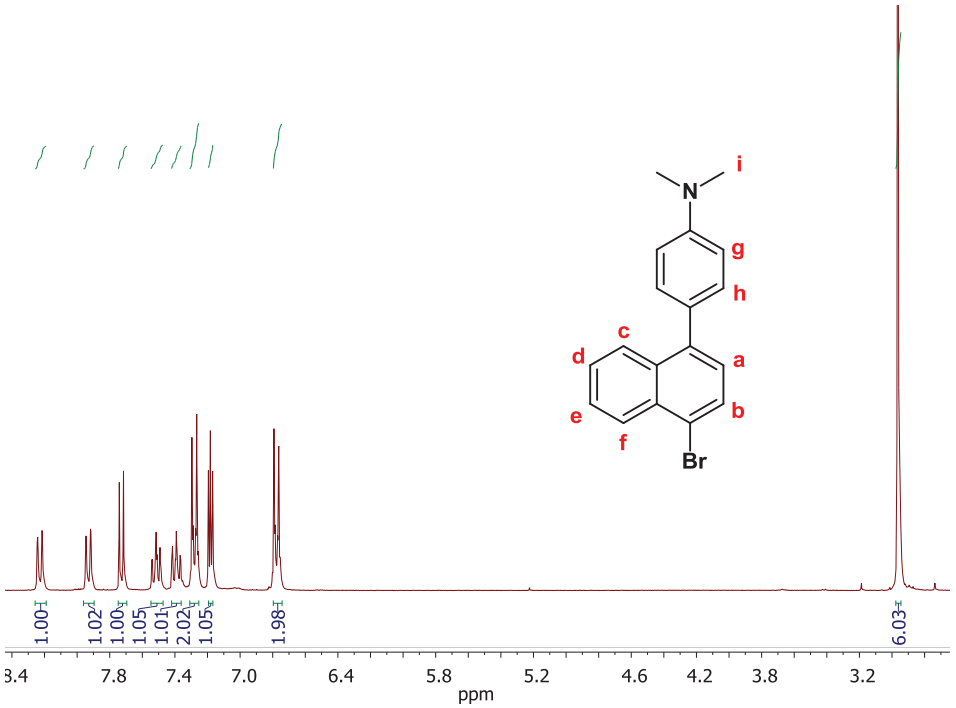

Figure 21- 300 MHz ^{1}H NMR spectrum of 1-(dimethylaminophenyl)-4-bromonaphthalene (7) in $CDCl_3$.

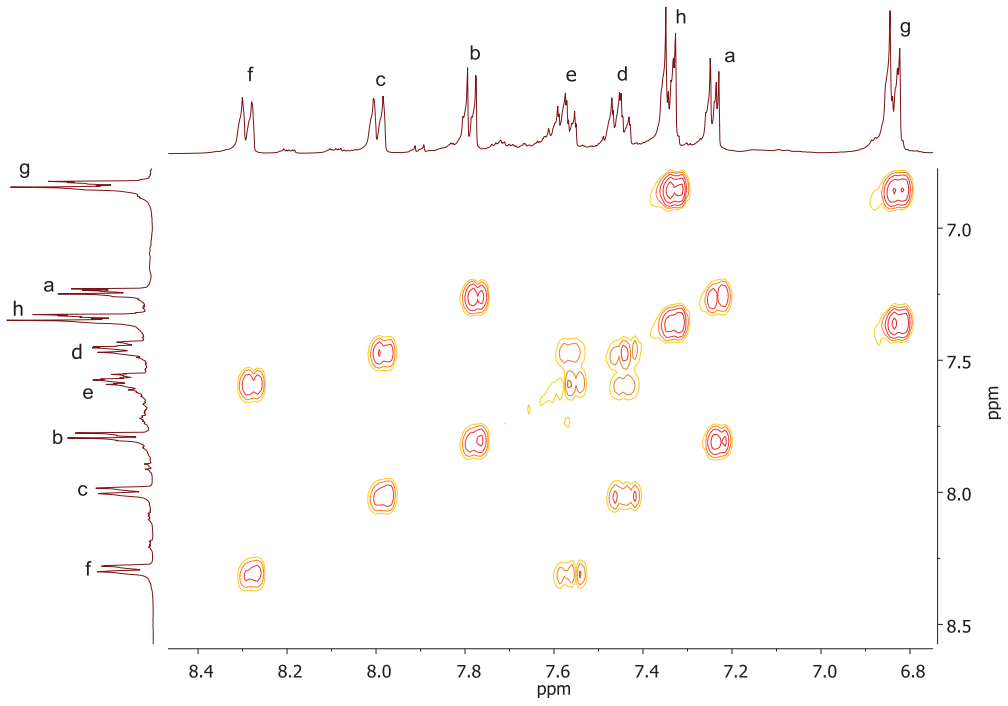

Figure 22 – 400 MHz COSY spectrum of 1-(dimethylaminophenyl)-4-bromonaphthalene in $CDCl_3$.

- This spectrum has a complex aromatic region, consisting of five doublets, two triplets and a multiplet (at approximately δ 7.2 ppm – it has a simplified appearance but when the spectrum is expanded and viewed at increased resolution a multiplet is seen.)
- The pair of doublets which each integrate to two protons, can be assigned to g and h situated on the aromatic ring bearing the dimethylamino group. To deduce which proton is further downfield shifted between g and h, a basic simulation was run. The results predicted h to be further downfield. The remaining three doublets which each integrate to one proton can be assigned to c, f and either a or b, whilst the multiplet is also either a or b. Again, the simulation was analysed, which predicted that b resonates downfield of a.
- When determining the locations of c and f, the simulation was unfortunately less helpful here, as it predicted that the two protons resonate in the same location, which, from the spectrum, is obviously not the case. However, the simulation was able to predict that e resonates downfield of d. These are the two smaller triplets at around δ 7.4 and δ 7.5.
- It can therefore be deduced that f resonates downfield of c due to the correlations observed between f and e and between c and d in the COSY spectrum.
- Although both protons a and b would also be expected to be a doublet, it is thought perhaps that coupling either to the bromine (in the case of b) or to hydrogen h (in the case of a) is also being observed generating a multiplet. A more complex pattern would actually be expected due to the presence of two spin active isotopes of bromine each with an abundance of around 50% (^{79}Br has a natural abundance of 50.54% whilst ^{81}Br has a natural abundance of 49.46%), although a distorted triplet is seen, perhaps this would generate a more complex pattern if a higher frequency spectrometer was to be used.

Chemical shift (to 1 d.p) (ppm)	Intensity (no. of H atoms)	Multiplicity	Assignment
8.2	1	d	f
7.9	1	d	c
7.7	1	d	b
7.5	1	t	e
7.4	1	t	d
7.3	2	d	h (both)
7.2	1	m	a
6.7	2	d	g (both)
2.9	6	s	i

Table 4 – The NMR peak assignment for 1-(dimethylaminophenyl)-4-bromonaphthalene.

Below are a selection of NMR spectra of **BRNBD**.

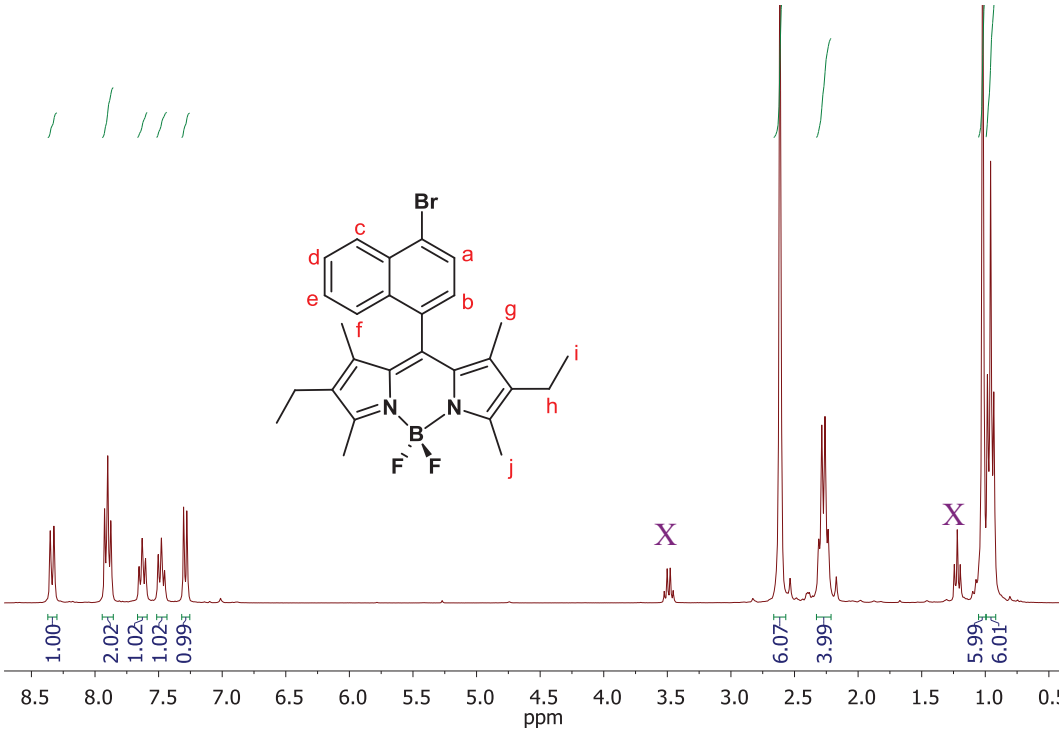

*Figure 23 - 300 MHz ^{1}H NMR of **BRNBD** in $CDCl_3$. X = solvent.*

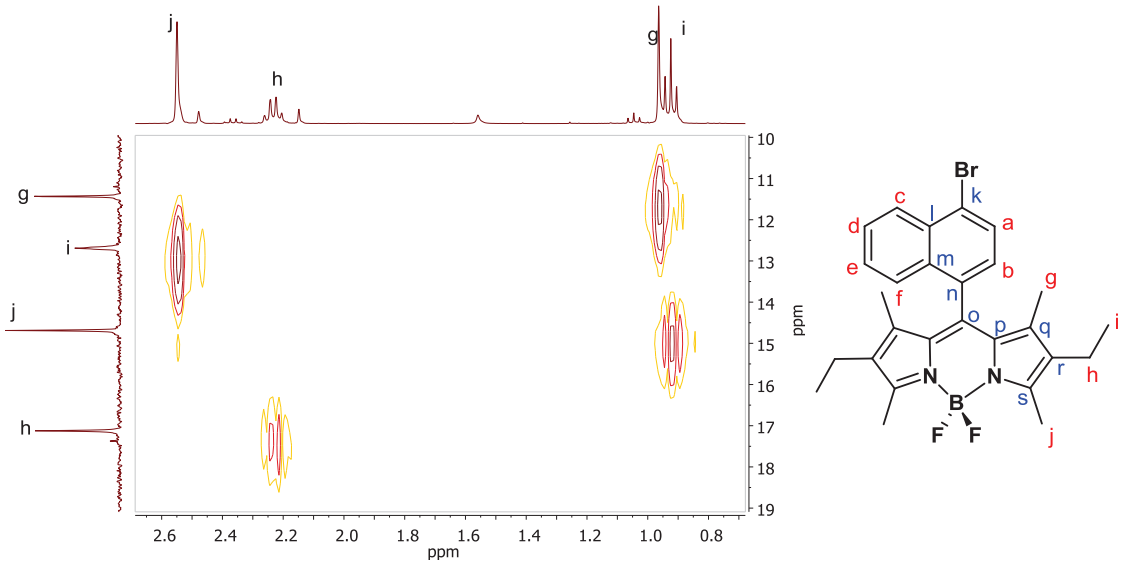

*Figure 24 – Left: The aliphatic region of the 400MHz HMQC correlation for **BRNBD**. Right: An annotated structure illustrating the letters denoted to the carbons and protons to be used throughout this assignment.*

The aliphatic carbon resonances can easily be assigned due to the evident coupling patterns seen in the HMQC (Heteronuclear Multiple Quantum Coherence) spectrum above, with the letters above the peaks being assigned to the carbon atom to which the correspondingly lettered proton set is attached. COSY and HMBC spectra will also be discussed, commencing with the COSY which is featured below.

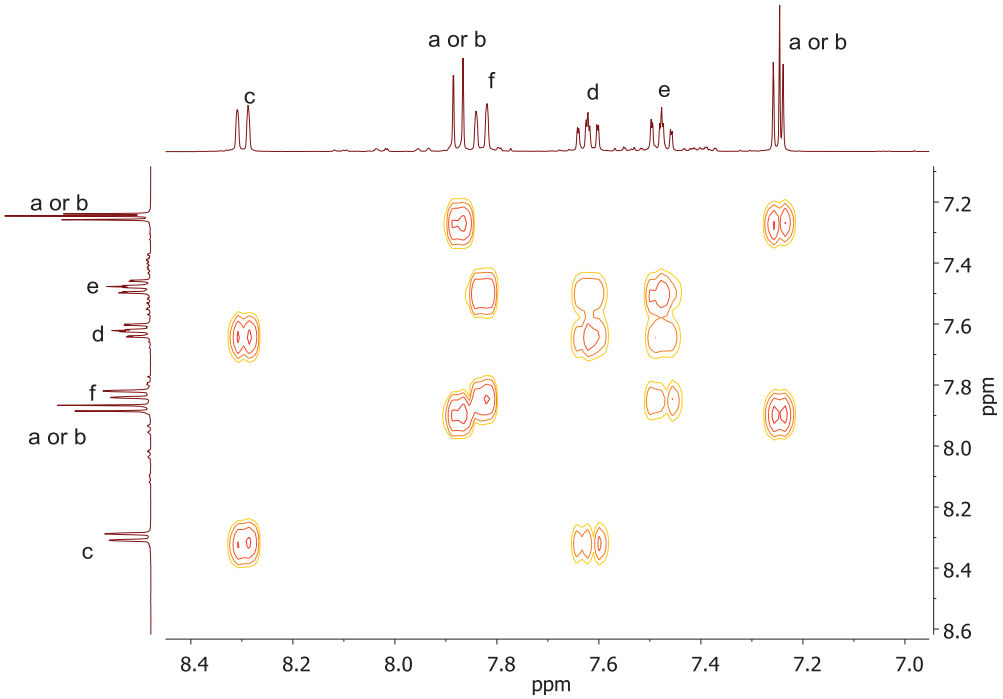

*Figure 25 – An annotated COSY spectrum of the aromatic region of **BRNBD**.*

An initial assignment of protons can be made based on the COSY and HMQC:

Chemical shift (1 dp) (ppm)	**Intensity (no. of H atoms)**	**Multiplicity**	**Coupling constant (*J*/ Hz)**	**Assignment**
8.34	1	d	8.5	c
7.91	1	d*	7.5	a or b
7.89	1	d*	8.5	f
7.64	1	m	N/A	d
7.51	1	m	N/A	e
7.29	1	m	N/A	a or b
2.61	6	s	N/A	j
2.27	4	q	7.5	h
1.02	6	s	N/A	g
0.96	6	t	7.5	i

*Table 5 – An initial proton assignment for **BRNBD**.*

*In the spectra recorded on the 300 MHz machine these two peaks appears as a triplet but in those generated via the 400 MHz machine, two doublets can clearly be seen – please refer to the HMQC which was recorded on 400 MHz spectrometer.

- The two multiplets at δ 7.64 and δ 7.51 can be assigned to protons d and e as these are the only hydrogen atoms which are adjacent to more than one other and these would therefore generate the most complex splitting pattern.
- It can be seen that d and e couple to the doublet at δ 7.82 ppm and also the doublet at δ 8.34. They also couple to each other, reinforcing the assignment. Because a and b are too remote to feasibly show a correlation to d and e, the two doublets aforementioned must correspond to protons f and c.
- In order to assign protons f and c, the HMBC is useful as the most downfield aromatic carbon can instantly be assigned as that *ipso* to the bromine atom on the naphthalene ring, i.e. carbon k. Proton c would show the strongest correlation to k as f is too distant to give a strong enough correlation to display a contour. Therefore, c can be assigned as the most downfield doublet as coupling can be seen to k in the spectrum below. The signal for a and b (which were assigned on

the basis of the 'remaining protons') also show coupling to k which again reinforces our assignment. Although proton a is closer in proximity, from evidence gained so far, it is tricky to distinguish between protons a and b.

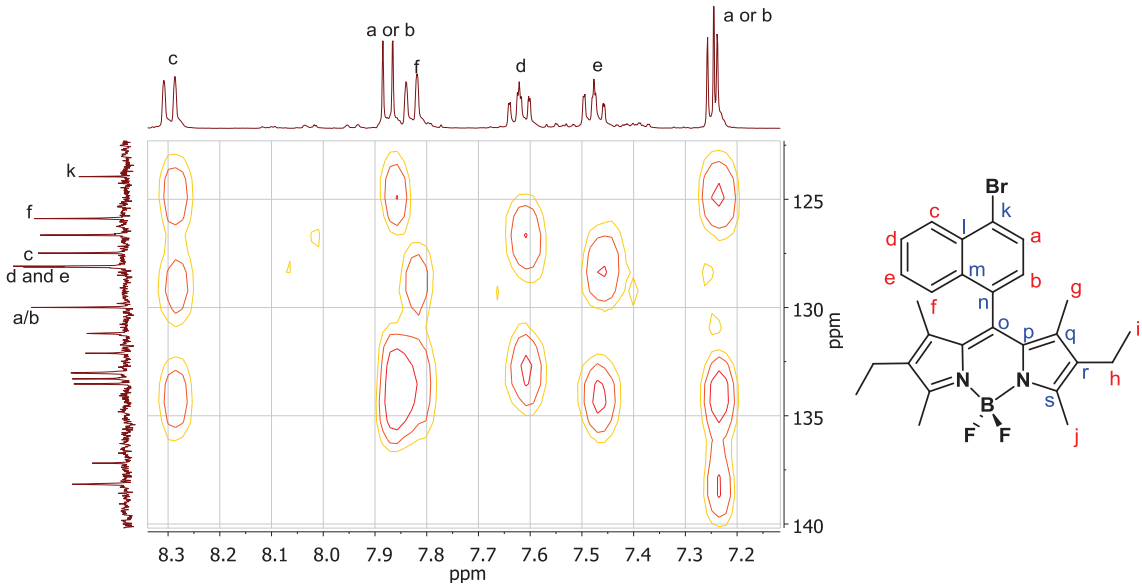

*Figure 26 – HMBC spectrum of the aromatic region of **BRNBD** in $CDCl_3$. The grid is shown here for clarity due to the proximity of the carbon atoms. It can be seen that a slight shift has occurred in the peak positions which has been accounted for when analysing the spectrum.*

The HMQC can now be used to continue to assign the carbon atoms. Previous assignments made using the HMBC spectrum can be carried forward.

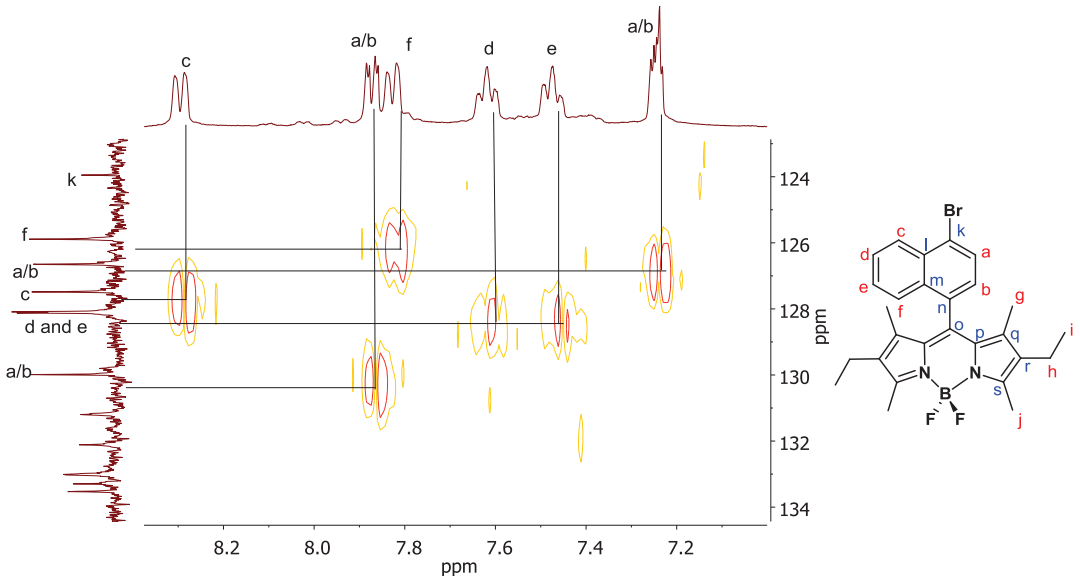

*Figure 27 – An annotated HMQC spectrum of the aromatic region of **BRNBD** with the correlations indicated by the lines.*

- The quaternary carbons l-s however are trickier to assign and the HMQC is no help here.

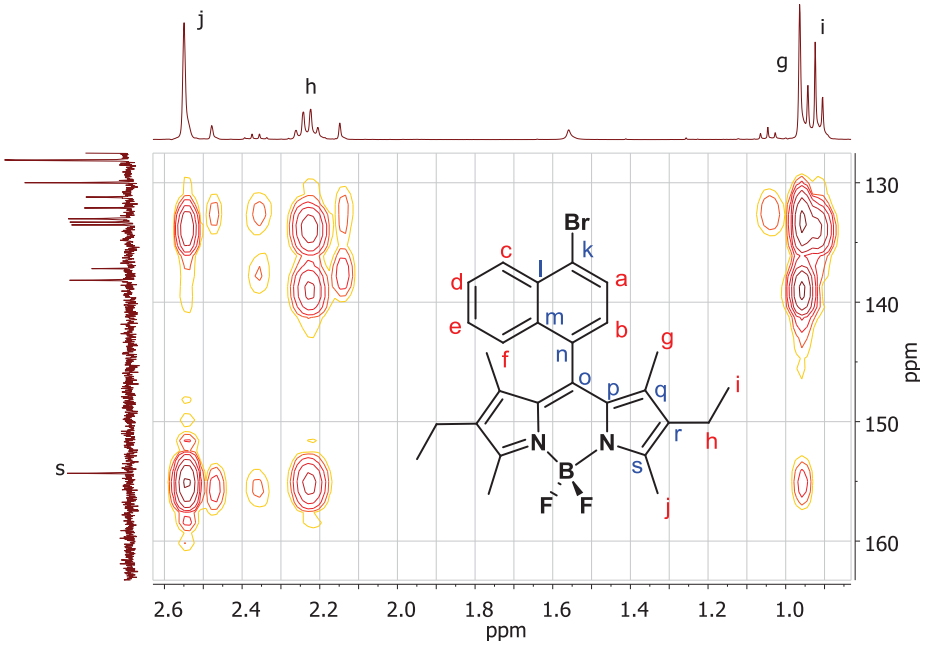

Figure 28 – HMBC: Aliphatic protons showing long range coupling to aromatic carbon atoms, which confirms our assignment of s.

- The aromatic region in the range δ131-140 ppm should be considered next. The only carbon in the region of δ140-160 ppm is carbon s which can be assigned

easily as the chemical shift of this carbon is well known in the literature (*Figure 29*).

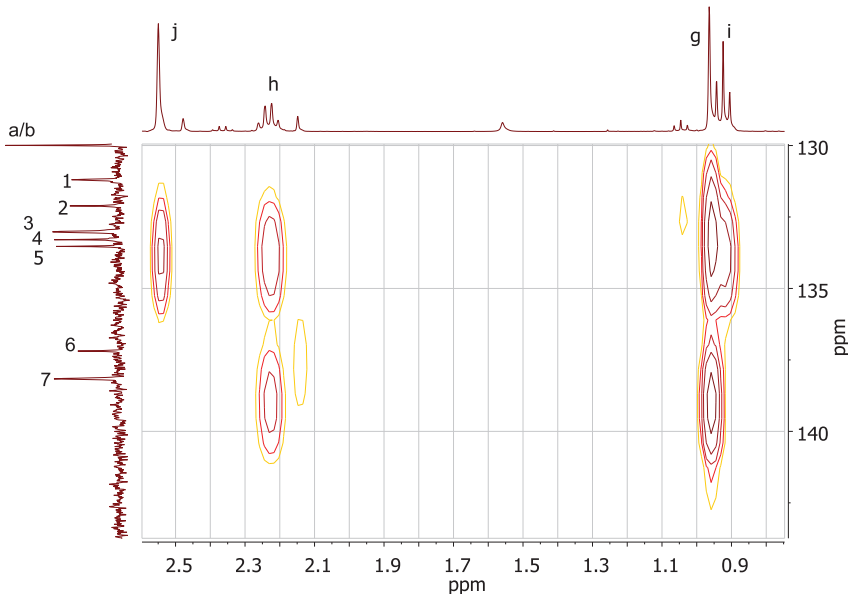

Figure 29 – HMBC: Aliphatic protons showing long range coupling to aromatic carbon atoms. Carbons l-r are labelled 1-7 here, with 7 being the most downfield shifted carbon.

Carbon numbering:

1 -p

2 -l

3 -r

4 -m

5 -o

6 -n

7 -q

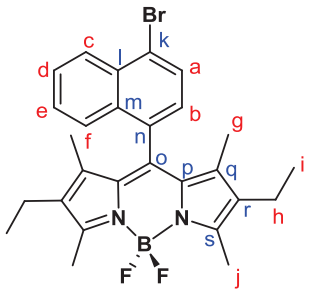

- In the aliphatic proton region, h and g both show correlations with carbon 7 (*Figure 29*). 7 is most likely to be carbon q. Protons j, h and g show correlations with 3. 3 is most likely to be carbon r as s has already been assigned and p and q are a little far from j. No correlations are seen to carbons 1, 2, 5 or 6 by any aliphatic protons.

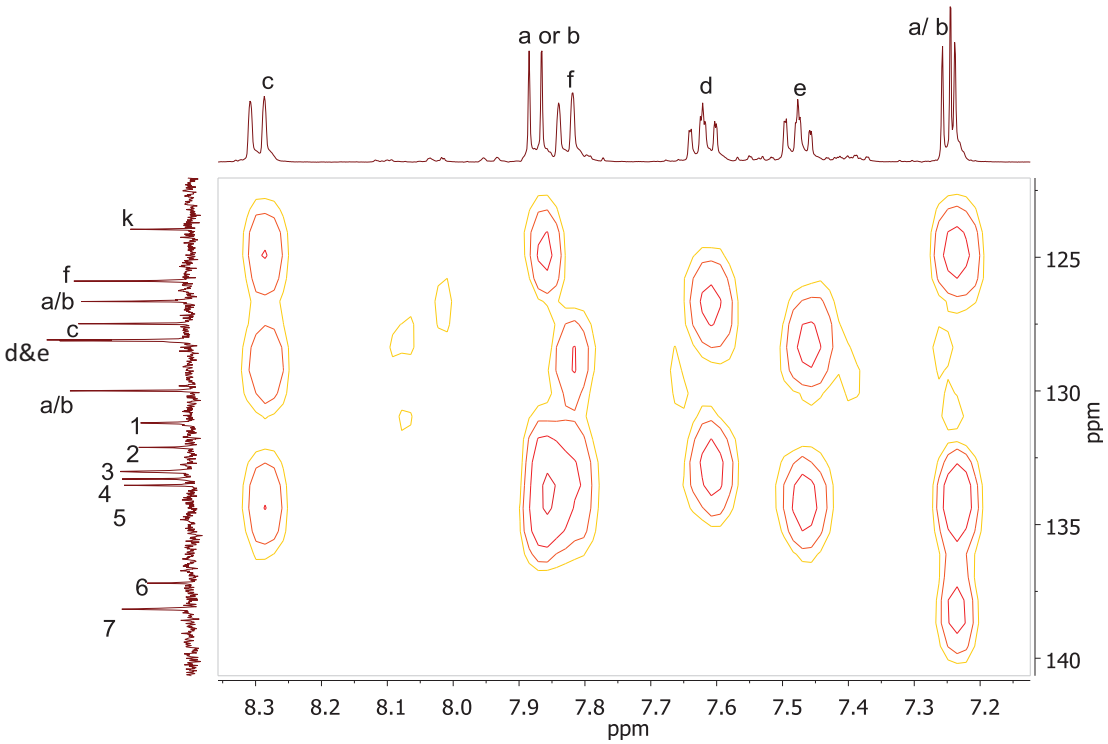

Figure 30 – The aromatic region of the HMBC showing the carbon and proton assignments made so far, along with the numbered carbons to be assigned.

- In the aromatic region of the HMBC, protons a, b and e all appear to couple to carbon 4. Carbon 4 is therefore highly likely to be either l, m or n – probably carbon m which is located either 3 or 4 bonds from all 3 protons. A correlation is seen between proton d and carbon 2. 2 is therefore probably either carbon l or carbon m, although l is more plausible as it is closer in proximity. The more upfield shifted proton which corresponds to either a or b shows a correlation with carbon 6. 6 could be either l, m, n or o. By process of elimination if the other assignment is correct its n or o. Meanwhile, no protons in the aromatic region appear to couple to either 7 (assigned as q- reasonable as no aromatic protons would couple to q), 1 or 5, but the proximity of the contours does make this spectrum tricky to elucidate.

- Therefore the only carbons remaining which require assignment are n or o and p. S and k have already been assigned. The unassigned carbon numbers are 1 and 5 and carbon 6 is still ambiguous. One would expect n to be the furthest downfield shifted and therefore correspond to carbon 6 as electrons are withdrawn from this position into the electron accepting bodipy unit. The other two, o and p are hard to

differentiate but probably correspond to 5 and 1 respectively. This is because p is typically more upfield than o.

Chemical shift (1 dp) (ppm)	**Assignment**	**Chemical shift (1 dp) (ppm)** ***continued***	**Assignment** ***continued***
11.4	**g**	129.8	**a/ b**
12.4	**j**	131.0	**p**
14.4	**i**	131.9	**l**
16.9	**h**	132.8	**r**
123.7	**k**	133.0	**m**
125.6	**f**	133.2	**o**
126.4	**a/b**	136.9	**n**
127.5	**c**	137.8	**q**
127.8	**d and e**	154.1	**s**
127.9			

*Table 6 – The final ^{13}C NMR peak assignment for **BRNBD**.*

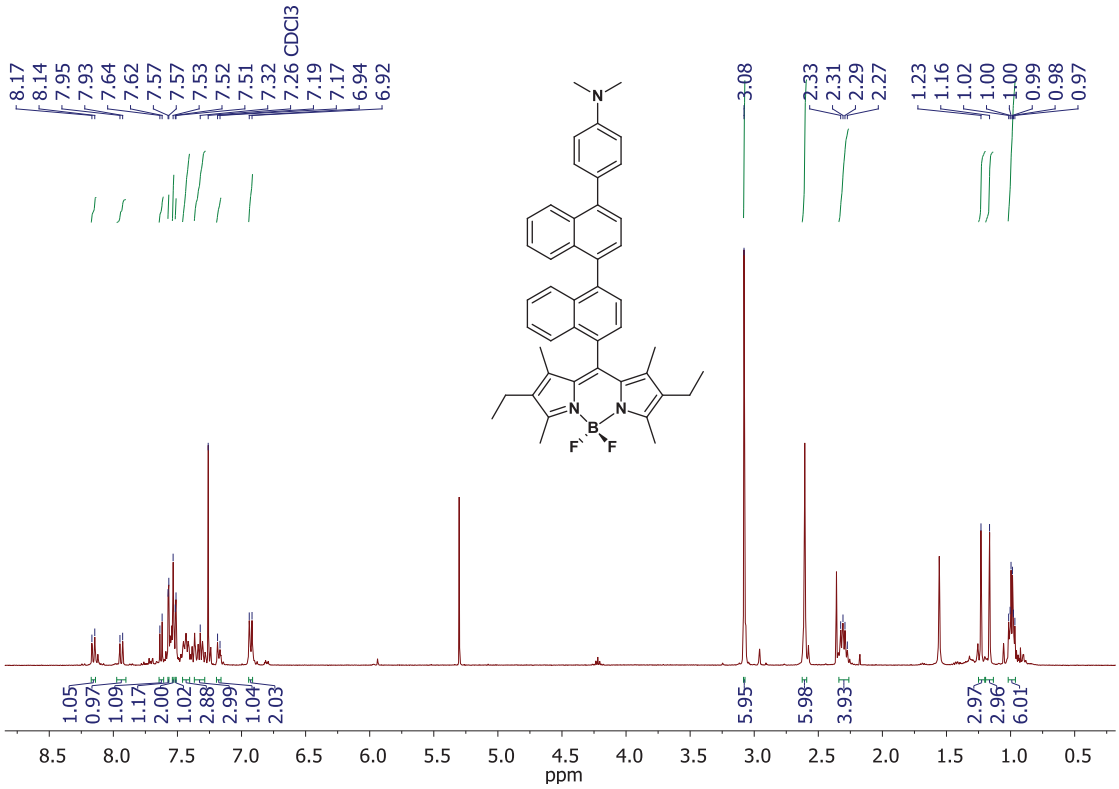

*Figure 31 – ^{1}H NMR spectrum of **DMABNBD** in $CDCl_3$.*

The proton NMR spectrum of **DMABNBD** is shown in *Figure 31*. Interesting features of this NMR include the discrete singlets each integrating to three protons observed at δ1.23 and δ1.16. These correspond to the methyl hydrogen sets on the indacene core closest in proximity to the naphthalene rings. This is a feature unique to this spectrum which was not observed in the proton spectrum of **BRNBD**. Typically these protons resonate as one singlet between 0.9 and 1 ppm.

The complex appearance of the two ethyl CH_3 groups is also a prominent feature of the spectrum. These proton sets generate an unusual splitting pattern which is most likely to be attributed to two overlapping triplets (as each methyl group is split by the adjacent methylene protons). This occurs because each CH_3 unit of the ethyl groups on the indacene core are inequivalent but have extremely similar chemical shift values. A similar splitting pattern can be observed in **BRNBD** (*Figure 33*).

The peak at around δ 2.31 ppm is generated by the methylene protons of the ethyl group. Again, the pattern is slightly more complex than the typical quartet

traditionally observed in the spectrum. This can be attributed to the fact that these protons are diastereotopic and it appears as though a doublet of quartets is generated here. This pattern appears due to splitting of each diastereotopic proton by the adjacent CH_3 group and also by the second methylene proton in the CH_2 unit.

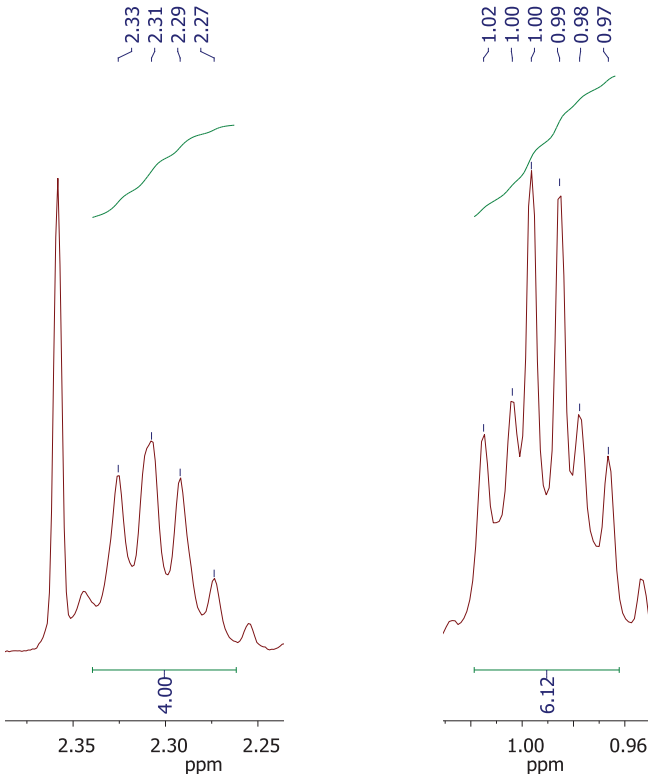

Figure 32 - An expansion of the peaks corresponding to the bodipy ethyl proton sets in ***DMABNBD****.*

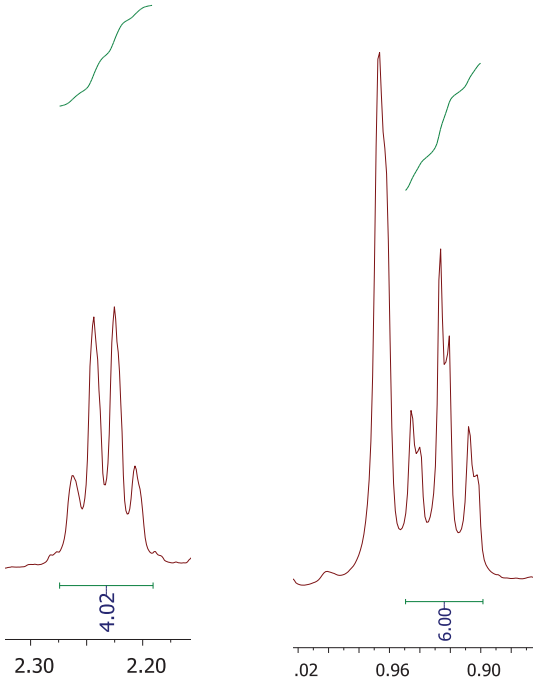

*Figure 33 - An expansion of the peaks corresponding to the bodipy ethyl proton sets in **BRNBD**. The peak corresponding to the methyl proton set nearest the naphthalene ring is also included.*

In **BRNBD** a simple quartet is observed at around δ 2.27 ppm, which corresponds to the two ethyl CH_2 groups on the indacene core of **BRNBD**. This suggests that these two protons do not couple to one another in the manner observed in **DMABNBD** and are not diastereotopic. This suggests that rotation about the carbon-carbon bond linking the indacene core to the bromonaphthalene moiety at the meso position is achieved more easily than it is in **DMABNBD**, perhaps due to the increased length of this bond. Unfortunately at the time of writing this thesis, a crystal structure was not available so the precise bond length could not be calculated. The overlaid pair of triplets observed at around δ0.92 ppm is generated in the same way as that observed in **DMABNBD** although the appearance is somewhat different.

6.4.3 *Mass spectrometry*

A mass spectrum of **DMABNBD** was recorded at the EPSRC National Mass Spectrometry Centre. This shows the theoretical isotope model and the excellent adherence to this data found with the observed results.

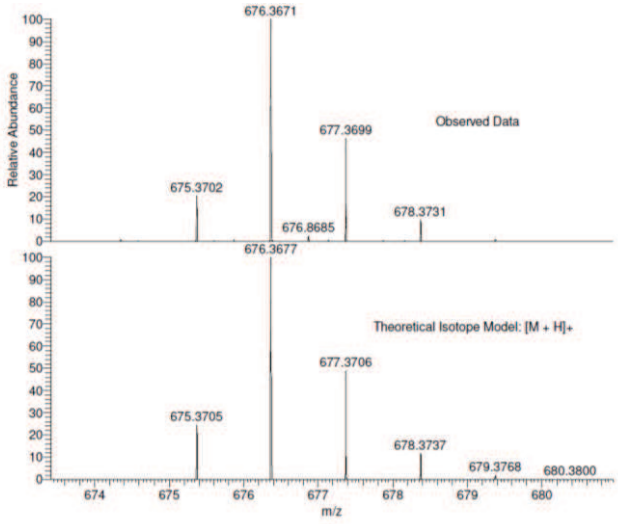

*Figure 34 – Mass spectrometry results for **DMABNBD**.*

6.5 *Photophysical properties*

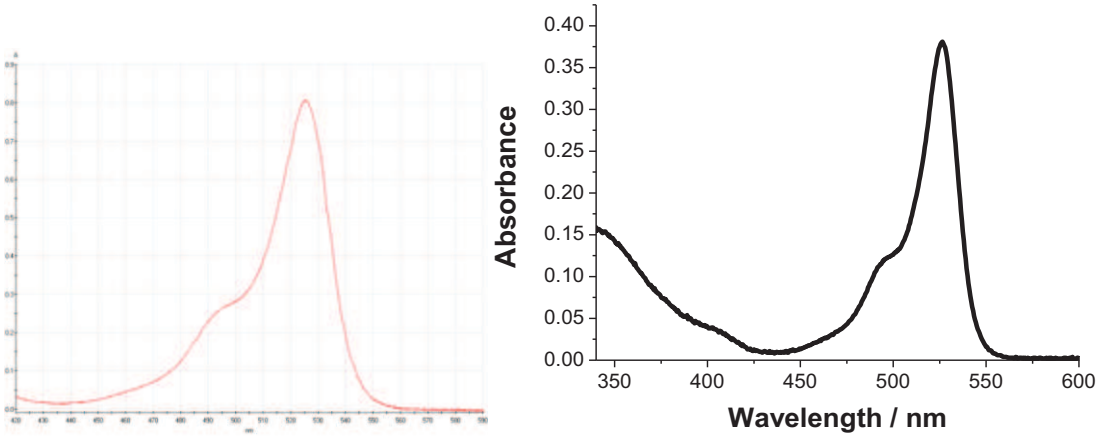

Figure 35 – left: A UV-visible absorption spectrum recorded in dichloromethane. Right: An absorbance spectrum recorded in butyronitrile.

UV spectroscopy was carried out on **DMABNBD** firstly in a dilute dichloromethane solution and secondly in a dilute butyronitrile solution. The left hand spectrum was recorded at 0.1 nm intervals over a wavelength range of 420 to 590 nm with a slow scan rate.

It can be seen from these spectra that **DMABNBD** behaves very much like a standard bodipy compound. A strong, narrow band corresponding to the lowest energy maximum (λ_{abs}) is seen centred at 525-527 nm and can be assigned to the S_0-S_1 electronic transition associated with the bodipy unit. The shoulder on the high energy side at around 495 nm is typical of bodipy compounds carrying uniquely alkyl substituents on the indacene core.

6.6 Concluding remarks and future projects

It is hoped that subsequent studies on the formamide method of bodipy synthesis will provide further insight into mechanistic pathways occurring and how the reaction conditions can be optimized in order to achieve increasingly favourable yields.

A future project to be carried out within the group will concentrate upon the preparation, purification and characterisation of the strapped and inherently chiral set of binaphthalene spaced bodipy D-Sp-A dyads as detailed in the introduction to this chapter. It is hoped that the photochemical analysis to be carried out on the dyad series will provide insight into the photophysics occurring. One particular interest is how charge transfer dynamics can be fine-tuned in order to preserve and stabilise the charge separated state through variation of the matrix coupling element, V_{DA}. The magnitude of V_{DA} will be controlled through optimisation of the energy gaps between orbitals residing on the donor and acceptor. Novel techniques in Time Resolved Raman Spectroscopy could be used more frequently to study how specific molecular motions are coupled to photoinduced charge separation. This technique preserves spatial resolution[33,34] whilst allowing measurements to be generated on a sub pico-second time scale. Furthermore, modern methods and developments in time resolved Electron Paramagnetic Resonance (EPR) spectroscopy can be exploited to investigate charge recombination dynamics on a nanosecond time scale whilst providing significant structural detail.[35]

There are various routes by which the synthesis of the strapped and inherently chiral binaphthalene spaced dyads can be achieved. The pathway initially proposed is outlined below whilst a second method which could be considered, involves separate

iodination[36] of the two enantiomers of binol, (S)-(-)-1,1'-Bi-2-naphthol and (R)-(+)-1,1'-Bi-2-naphthol which are both commercially available. This reduces the length of the synthetic protocol by two steps and generates the iodo species, a more reactive coupling partner than the corresponding brominated derivative.

The first step of the synthesis detailed in *Schemes 9 and 10* involves preparation of the literature compound 4,4'-dibromo-2-2'-dihydroxy-[1,1']binaphthalenyl[37] employing copper chloride hydroxide-TMEDA in an oxygen atmosphere. Attachment of (s)-camphor to the alkoxy groups will permit resolution of the two enatiomers of B-NAP and conversion to the corresponding cyclophane can then be achieved under standard reaction conditions. It should be noted that circular dichroism spectroscopy will be carried out to confirm the enantiopurity at each step, with purity and authenticity of all compounds being confirmed by NMR spectroscopy and mass spectrometry throughout the synthesis.

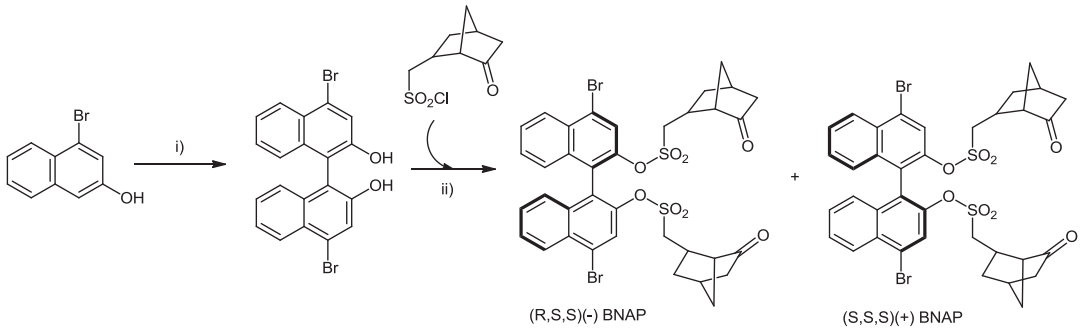

Scheme 9 - Resolution of the two enantiomers of B-NAP using (s)-camphor.
Reagents: i) CuCl(OH)-TMEDA, O_2, DCM; ii) Et_3N, DCM

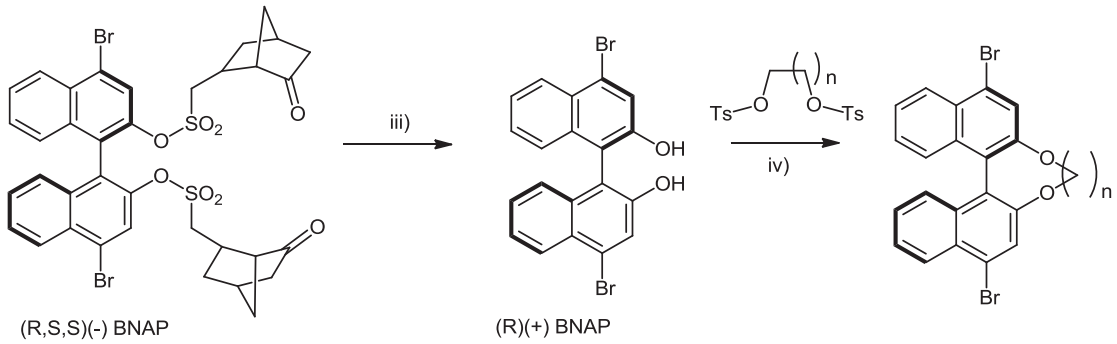

Scheme 10 – Preparation of the enantiopure cyclophane using alkyl tosylates of varying chain length (n=1-4).

Reagents: iii) NaOH, MeOH/ H_2O iv) Cs_2CO_3, acetone

According to *Scheme 11*, the B-NAP cyclophanes will then be coupled onto the boronic ester of julolidine under the appropriate Suzuki conditions as developed and earlier in this chapter. The coupled derivative prepared will then be reacted on to generate the aldehyde by treatment with tributyl tin hydride and carbon monoxide in the presence of a palladium(0) catalyst[38]. This aldehyde is then subjected to standard bodipy forming conditions to generate the desired chiral binaphthalene spaced product.

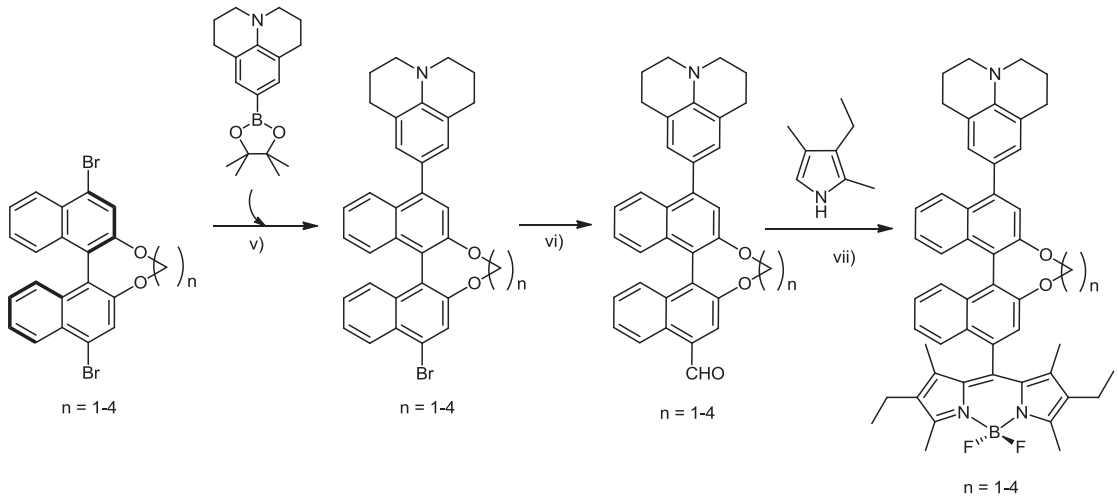

Scheme 11 - Preparation of the strapped bodipy series of varying chain length.
Reagents: v) $PdCl_2(Ph_3)_2$, Na_2CO_3, toluene vi) CO/ Bu_3SnH, Pd(0), vii) 2,4-dimethyl-3-ethylpyrrole, DCM, DDQ, N,N'diisopropylethylamine, $BF_3.Et_2O$.

6.7 References

[i] Rikken, G. L. J. A.; Folling, J.; Wyder, P.; *Phys. Rev. Lett*. **2001**, *87*, 23602.
[ii] Benniston, A. C.; Harriman, A.; Li, P. Y.; Patel, P. V.; Sams, C. A.; *J. Org. Chem*. **2006**, *71*, 3484.
[3] Zhdanov, V. P. *Europhys. Lett*. **2002**, *59*, 681.
[4] (a) Newton, M. D, *Int. J. Quantum Chem*. **2000**, *77*, 255, (b) Naleway, C, A.; Curtiss, L. A.; Miller, J. R. *Chem. Phys*. **1991**, *95*, 8434.
[5] (a) Harriman, A.; Sauvage, J. P.; *Chem. Soc. Rev*. **1996**, *25*, 41; (b) Wasielewski, M. R. *Chem. Rev*. **1992***, 92*, 435; (c) Gust, D.; Moore, T. A.; Moore, A. L.; *Acc. Chem. Res*. **2001**, *34*, 40; (d) Paddon-Row, M. N, *Adv. Phys. Org. Chem*. **2003**, 38, 1; (e) Kim, D.; Osuka, A. *Acc. Chem. Res*. **2004**, *37*, 735; (f) Sessler, J. L.; Sathiosatham, M.; Brown, C. T.; Rhodes, T. A.; Wiederrecht, G. *J. Am. Chem. Soc*. **2001**, *123*, 3655.
[6] (a) Beckers, E. H. A.; Meskers, S. C. J.; Schenning, A. P. H.; Chen, F. W.; Janssen, R. A. J. *J. Phys. Chem. A*. **2004**, *108*, 6933. (b) Ramos, A. M.; Beckers, E. H. A.; Offermans, T.; Meskers, S. C. J.; Janssen, R. A. *J. Phys. Chem. A*. **2004**, *108*, 8201.
[7] Paulson, P. B.; Curtiss, L. A.; Bal, B.; Closs, G. L; Miller, J. R. *J. Am. Chem. Soc.* **1996**, *118*, 378.
[8] Triebs, A.; Kreuzer, F. H. *Liebigs Ann. Chem*. **1968**, *718*, 208.
[9] Loudet, A.; Burgess, K. *Chem. Rev*. **2007**, *107*, 4891.
[10] Wu, L.; Burgess, K, *Chem Commun*. **2008**, *40*, 4933.
[11] Ryo Shintani.; Tamio Hayashi. *Aldrichimica Acta*, **2009**, *42*, 31.
[12] Lee, S. J.; Gray, K. C.; Paek, J. S.; Burke, M. D. *J. Am. Chem. Soc*. **2008**, *130*, 466.
[13] (a) Walker, S. D.; Barder, T. E.; Martinelli, J. R.; Buchwald, S. L. *Angew. Chem. Int. Ed*. **2004**, *43*, 1871. (b) Barder, T. E.; Walker, S. D.; Martinelli, J. R.; Buchwald, S. L. *J. Am. Chem. Soc*, **2005**, *127*, 4685.
[14] Mitchell, S. PhD thesis: "Design and Construction of naphthalene-based architectures for long distance electron exchange." Submitted January 2006.
[15] Pratap, R.; Parrish, D.; Gunda, P.; Venkataraman, D.; Lakshman, M. K. *J. Am. Chem. Soc*. **2009**, *34*, 12240.
[16] Goud, T. V.; Tutar, A.; Biellmann, J.-F. *Tetrahedron*, **2006**, *62*, 5084.
[17] Bañuelos, J.; Martín, V.; Gómez-Durán, C. F. A.; Arroyo Córdoba, I. J.; Peña Cabrera, E.; Garcia-Moreno, I.; Costela, A.; Arbeloa, T. *Chem. Eur. J*. **2011**, *17*, 7261.
[18] Estévez, V.; Villacampa, M.; Menéndez, J. C. *Chem. Soc. Rev*. **2010**, *39*, 4402.
[19]For a summary of the structures of nakamuric acid structures see O' Malley, D. P.; Li, K.; Maue, M.; Zografos, A. L.; Baran, P. S. *J. Am. Chem. Soc*. **2007**, 4762.
[20] Roomi, M. W.; MacDonald, S. F. *Can. J. Chem*. **1970**, *48*, 1689.
[21] (a) Kameswaran, V.; Jiang, B. *Synthesis*. **1997**, *530*; (b) Kaupp, G.; Schemeyers, J.; Kuse, A.; Atfeh, A. *Angew. Chem., Int. Ed*. **1999**, *38*, 2896.
[22] Palacios, F.; Aparicio, D.; de los Santos, J. M.; Vicario, J. *Tetrahedron*. **2001**, *57*, 1961.
[23] For examples refer to: (a) Dhawan, R.; Arndtsen, B. A. *J. Am. Chem. Soc*. **2004**, *126*, 468. (b) Arndsten, B. A. *Chem. –Eur. J*. **2009**, *15*, 302.
[24] Suzuki, D.; Nobe, Y.; Watai, Y.; Tanaka, R.; Takayama, Y.; Sato, F.; Urabe, H. *J. Am. Chem. Soc*. **2005**, *127*, 7474.
[25] Zhang, S.; Sun, X.; Zhang, W. –X.; Xi, Z. *Chem. -Eur. J*. **2009**, *15*, 12608.
[26] Tejedor, D.; González-Cruz, D.; García-Tellado, J.; Marrero-Tellado, J.; López-Rodríguez. *J. Am. Chem. Soc*. **2004**, *126*, 8390.
[27] Naka, H.; Koseki, D.; Kondo, Y. *Adv. Synth. Catal*. **2008**, *350*, 1901.
[28] Sezen, B.; Sames, D. *J. Am. Chem. Soc*. **2003**, *125*, 5274.
[29] Dumoulin, H.; Rault, S.; Robba, M. *J. Heterocyclic Chem*. **1997**, *34*, 13.
[30] Hans Reich, 2011, http://www.chem.wisc.edu/areas/reich/nmr/11-f-data.htm
[31] Falk, H.; Hofer, O.; Lehner, H. *Monatsh. Chem*. **1974**, *105*, 169.
[32] Hans Reich, Chem 606 Structure determination using Spectroscopic methods, 2010, University of Wisconsin. http://www.chem.wisc.edu/areas/reich/chem605/index.htm
[33] Kukura, P.; McCamant, D. W.; Yoon, S.; Wandschneider, D. B.; Mathies, R. A. *Science (Washington, DC)* **2005**, *310*, 1006
[34] McCamant, D. W.; Kukura, P.; Mathies, R. A. *J. Phys. Chem. B*. **2005**, *109*, 10449
[35] Schweiger, A.; Jeschke, G. *Principles of pulsed electron paramagnetic resonance*; Oxford: Oxford, 2001

[36] For a paper offering conditions for iodination of naphthols please refer to Kiran, Y. B.; Konakahara, T.; Sakai, N. *Synthesis*, **2008**, *15*, 2327
[37] Chow, H.-F.; Ng, M-K. *Tetrahedron Asymmetry*, **1996**, *7*, 2251.
[38] (a) Baillargeon, V. P.; Stille, J. K. *J. Am. Chem. Soc*. **1986**, *108*, 452. (b) Pri-Bar, I.; Buchman, O. *J. Org. Chem*. **1984**, *49*, 4009.